NEW YORK CITY DEPARTMENT OF ENVIRONMENTAL PROTECTION
BUREAU OF WATER SUPPLY

Multi-Tiered Water Quality Modeling Program
Annual Status Report

This status report describes work completed by NYCDEP's Multi-Tiered Water Quality Modeling Program during October 2011 – September 2012.

October 31, 2012

Prepared in accordance with Section 5.2 of the July 2007 United States Environmental Protection Agency Filtration Avoidance Determination

Prepared by: Don Pierson, PhD, WWQSR, Water Quality Modeling
Elliot Schneiderman, PhD, WWQSR, Water Quality Modeling
Mark Zion, WWQSR, Water Quality Modeling
David Lounsbury, WWQSR, Water Quality Modeling
Donald Kent, WWQSR, Water Quality Modeling
Adao H. Matonse, City University of New York, Institute for Sustainable Cities
Soni Pradhanang, City University of New York, Institute for Sustainable Cities
Rajith Mukundan, City University of New York, Institute for Sustainable Cities
Yongtai Huang, City University of New York, Institute for Sustainable Cities
Nihar Samal, City University of New York, Institute for Sustainable Cities
Allan Frei, City University of New York, Institute for Sustainable Cities

Table of Contents

1. Introduction

This status report describes work completed for DEP's Multi-Tiered Water Quality Modeling Program during October 2011 – September 2012. The report presents progress on activities discussed in Section 2.4.2 of the New York City's Long-Term Watershed Program (DEP, 2006a). The following activities are reported herein:

- Application of DEP's reservoir, watershed and system models to inform operational decisions during the reporting period (Section 2);

- Model applications and projects related to climate change analyses including analyses of the effects of winter streamflow on eutrophication in Cannonsville Reservoir and turbidity in the Esopus Creek and Ashokan Reservoir and a description of the WRF 4262 project on vulnerability assessment and risk management tools (Section 3);

- Studies related to model development including: a comparison of snowpack models; the development of a possible planning level tool to help identify stream channel erosion sites; examples of the use of newly available gridded data sets for watershed model input; development of empirical rating curves for turbidity load estimation in Esopus Creek; a preliminary test of the CONCEPTS channel evolution model; and an updated calibration of the one-dimensional hydrothermal and water quality reservoir model for Cannonsville Reservoir (Section 4);

- Data analyses that support model development and the understanding of watershed processes including: an analysis of the effects of Tropical Storms Irene and Lee on streamflow in an historical context of extreme hydrologic events; an analysis of the effect of these same events on the reservoirs; a study of the importance of rain-on-snow events in New York State; and an analysis of reservoir stratification and mixing based on high-resolution monitoring data (Section 5);

- Model data acquisition, development and organization (Section 6);

- Collaboration of the Water Quality Modeling Section with other projects and organizations including cooperative arrangements, contracts and proposals. (Section 7); and

- Summary of scientific journal papers and presentations at scientific conferences that the Water Quality Modeling Section has given over the last year (Section8).

2. Use of Models for Support of Operational Decisions

In total, twelve separate turbidity modeling analyses were performed for Kensico, Ashokan and/or Schoharie Reservoirs during the October 2011-September 2012 reporting period. Turbidity model simulations to support operational decisions during the reporting period were almost always related to elevated turbidity that occurred as result of Tropical Storms Irene and Lee during late August and early September 2011. The turbidity generated by these extreme events affected the Catskill and Delaware Systems, and caused alum treatment to be used on the Catskill system water transferred to Kensico Reservoir. The Water Quality Modeling Section performed model simulations to better guide the operations of the system to ensure the delivery of high quality water while minimizing the use of alum. In addition to these model simulations, the Water Quality Modeling Section continued to support development of the Operations Support Tool (OST) through collaboration with DEP's Operations Support Section and the OST contractors.

Simulation Descriptions

Three types of models - reservoir, watershed and system - were used for the simulations during the reporting period. For most of the simulations, LinkRes and its component model 2D reservoir model CEQUAL W2 (DEP, 2004; Cole and Buchak, 1995) was used to simulate turbidity values within the reservoir and aqueduct withdraws. The model has been set up and tested for the Ashokan West Basin, the Ashokan East Basin and the Kensico Reservoir. In addition a number of simulations utilized the current version of the OST which includes the combination of the CEQUAL-W2 models with the OASIS system model (HydroLogics, Inc., 2007; Gannett Flemming and Hazen and Sawyer, 2007).

A "position analysis" strategy was followed for these model runs. Under this strategy, the initial conditions of the reservoir are used as the starting point for the model simulations. Then the model is run for a forecast period which ranges from 1 to 6 months into the future, depending on the simulation goals. For the forecast period, inputs of meteorology and aqueduct water temperature are based on each year in the historical record (1948-2004 for Ashokan and Schoharie model runs and 1987-2004 for Kensico model runs), while initial conditions are set to most recently measured values based on a combination of limnological survey data and in-lake automated buoy measurements. For simulations of Kensico Reservoir, flows and derived turbidity loads are set at fixed values associated with the forecast conditions. With this method, each year represents a separate realization (or trace) of a simulated model outcome. The variability between the traces will result from year to year changes in weather conditions only. This allows for sensitivity analysis of the Kensico effluent based on a series of fixed aqueduct turbidity and flow influent conditions.

In the similar analysis using the OST, the forecasted input flow and turbidity load traces are based on the historical record and are conditioned to recent history. These flows and corresponding turbidity loads are input to the OASIS model, which predicts reservoir storage, water quality and aqueduct flows based on a set of operating rules. In these runs, each trace represents a simulated outcome incorporating both climatic and flow variability of the forecast period. Different operational strategies can be compared by changing the operating rules used by

OASIS. The complete set of positional analysis traces are then be used to develop a statistical probability of potential simulated reservoir storage levels and effluent turbidity.

Table 2.1 lists the turbidity analyses performed during the period. Kensico Reservoir modeling runs were performed in October to aid in determining the proper Catskill and Delaware inflows to Kensico Reservoir that would maintain required Kensico effluent turbidity standards. In December and January, two series of OST runs were performed to better understand the time it would take for Ashokan Reservoir turbidity to decline to more normal levels from the high levels that were created by the tropical events of the late summer. During the winter and spring of 2012 four separate Kensico modeling analyses were performed to better understand both the optimum flows into Kensico and to help determine when and if alum treatment should be concluded. A storm event in late-April caused elevated turbidity in Schoharie Reservoir, and a run of the OST focused on Schoharie Reservoir to gain an understanding of how and when the reservoir turbidity would decline, such that the Shandaken Tunnel could be used without impacting the Esopus Creek. In July another Kensico turbidity modeling run was performed to refine Catskill Aqueduct operations. Finally, a storm event in mid-September 2012 caused elevated turbidity in the Ashokan West Basin. Since the West Basin was already drawn down, the East Basin was largely unaffected by the event. A set of OST model runs was performed to help understand the potential of Ashokan Release Channel usage to reduce turbidity movement from the West Basin to the East Basin of Ashokan. Overall, model runs during this period were effective in helping to determine optimal flow rates that would minimize alum use while continuing to meet water quality standards at the Kensico effluents.

Table 2.1. List of modeling analyses performed during the reporting period including descriptions of each analysis.

Turbidity Modeling Runs October 2011-September 2012

Date	Background	Modeling Description	Results
10/03/2011	Ashokan Reservoir was already impacted by Tropical Storms Irene and Lee when another smaller event caused high turbidity water to move across the dividing weir from Ashokan West Basin to the East Basin. This caused the East Basin Catskill diversion to initially rise to about ~200 NTU. In addition, two plugs of high turbidity water entered Kensico Reservoir during Sep. 29-Oct 1. Turbidity continued to be elevated in the Rondout Reservoir, and turbidity entering Kensico Reservoir at DEL17 was about 3 - 4.5 NTU.	Kensico simulations were run to provide guidance on the Catskill Aqueduct flow rate (with or without stop shutters) to minimize the movement of the turbidity plume in the Catskill arm of Kensico Reservoir to the reservoir effluents. Two flow rates are tested: 50 MGD (minimum with stop shutters) and 275 MGD (minimum w/o stop shutters). In addition, the runs also investigated the potential use of alum on Delaware influent to Kensico Reservoir. The effective turbidity of Delaware influent treated with alum was unknown, so two potential inputs, 1 NTU and 2 NTU were tested. Runs using 4 NTU and 6 NTU input from Delaware were also performed to understand the effects of no alum use.	All model simulations indicated a rapid increase in effluent turbidity as plume of turbidity currently in Kensico reservoir began to influence this reservoir's effluents. Simulations with Catskill flow of 50 MGD show less immediate increase in turbidity at effluents. For the longer term, the optimum mix of the Catskill and Delaware waters was dependent on the difference between alum treated Catskill influent turbidity and Delaware influent turbidity.
10/21/2011	These runs update previous Kensico Reservoir sensitivity simulations that were made in response to the late summer tropical events. At the time of these runs turbidity leaving the Ashokan East Basin via the Catskill Aqueduct was about 50-100 NTU and alum treatment was being applied. In addition, stop shutters were in place and the flow rate from Catskill Aqueduct into Kensico was 250 MGD. Recent surveys show that alum treatment decreased input turbidity (as measured at Kensico limnological survey site 5) to about 3.0 NTU. The Delaware Aqueduct is currently on float mode with turbidity of about 2 NTU.	Kensico reservoir simulations were run to provide refined guidance for a number of operational changes that were to take place, including (1) going off float mode for the Delaware Aqueduct; and (2) removing stop shutters from the Catskill Aqueduct. Three simulations were performed: (1) a simulation of Delaware float mode to understand the effects of not loading Delaware water into Kensico Reservoir; (2) a simulation of routing Delaware water into Kensico and continuing with 250 MGD in Catskill inflow; and (3) a simulation of routing Delaware water into Kensico and removing Catskill stop shutters with a resulting increase of Catskill inflow to 350 MGD.	Simulations of Delaware in float mode versus reservoir mode showed only small differences in effluent turbidity. Increasing Catskill from 250 MGD to 350 MGD showed a small increase in effluent turbidity from about 2.1 NTU to 2.3 NTU.

Turbidity Modeling Runs October 2011-September 2012 (cont'd)			
Date	**Background**	**Modeling Description**	**Results**
12/27/2011	The Tropical Storm Irene and Lee events that occurred in August and September continued to impact the turbidity in the Ashokan Reservoir. Ashokan limnological survey measurements on December 20 indicated turbidity of 55-170 NTU in the West Basin and 22-45 NTU in the East Basin. Alum continued to be used to treat Catskill system water and flow in the Catskill Aqueduct was reduced through the use of stop shutters.	A set of OST simulations including Schoharie and Ashokan Reservoirs was performed to provide an initial estimate of the period of time that Ashokan Reservoir would continue to be impacted by elevated turbidity.	Simulations of Ashokan Reservoir indicated that turbidity would remain elevated in both the East and West Basins for an extended period of time. Model results were highly sensitive to the effective settling rates that the model uses based on partitioning of turbidity into three size classes.
01/06/2012	These runs are a follow-up to the previous runs of 12/27/2011 described above.	A follow-up set of OST simulations were run to provide a comparison of two operational options: (1) turning off the Ashokan Release Channel (ARC) and (2) continuing the Discharge Mitigation Release Channel Protocol with an added program of flushing releases of 600 MGD from the East Basin for 3 days after 14 consecutive days of release from the West Basin.	Under Scenario 1 (ARC off), water was simulated to quickly (about 1-4 weeks) move over the dividing weir from West Basin to the East Basin. The simulated turbidity of this flow was high since there was little time for settling to reduce turbidity in the West Basin Flows under the ARC off scenario were therefore, expected to impact the East Basin turbidity. Under Scenario 2 (alternate ARC use), flow over the dividing weir was delayed and reduced in quantity. This delay generally allowed for more settling of West Basin turbidity and therefore reduced the turbidity in water moving across the dividing weir.

Turbidity Modeling Runs October 2011-September 2012 (cont'd)			
Date	**Background**	**Modeling Description**	**Results**
02/28/2012	Since the tropical events of the fall of 2011, turbidity in Ashokan East Basin had dropped to about 20 NTU. Stop shutters and alum treatment continued to be implemented.	As Ashokan East Basin turbidity continued to decrease, it may be possible within the next few months to end alum use. These Kensico Reservoir simulations were run to provide guidance as to what levels of turbidity could be tolerated as inputs to Kensico Reservoir from the Catskill aqueduct when alum treatment was ended. The tested flow rates were 150, 200 and 250 MGD in the Catskill Aqueduct with aqueduct turbidity of 12, 16 and 20 NTU.-	Results suggested that Kensico effluent turbidities ranging as low as 1.7-2.5 NTU for inputs of 12 NTU and as high as 2.2-3.7 NTU for input turbidity of 20 NTU. Greater flow in the Catskill Aqueduct produced larger effluent turbidity.
03/13/2012	Turbidity in Ashokan East Basin had dropped to about 16 NTU. Stop shutters and alum treatment continued to be implemented.	As Ashokan East Basin turbidity continued to decrease, these Kensico simulations were run to provide guidance as to what levels of turbidity could be tolerated as inputs to Kensico Reservoir from the Catskill Aqueduct when alum treatment was ended. The tested flow rates were 175 and 275 MGD in the Catskill Aqueduct with aqueduct turbidity of 12, 14, 16 and 18 NTU.	Results suggested that Kensico effluent turbidities ranging as low as 1.8-3.0 NTU for input of 12 NTU and as high as 2.3-4.2 NTU for input turbidity of 18 NTU. Greater flow in the Catskill Aqueduct produced larger effluent turbidity.
04/10/2012	Ashokan Reservoir (both basins) had dropped to about 10 NTU. Alum treatment continued to be implemented.	Kensico Reservoir simulations were performed to provide guidance as to what levels of turbidity could be tolerated as inputs to Kensico Reservoir from the Catskill Aqueduct once alum treatment was ended and flow rates were increased. The tested inflow rates were 400, 500 and 600 mgd from the Catskill Aqueduct with aqueduct turbidity of 6, 8, and 10 NTU.	Results suggested that Kensico effluent turbidities ranged as low as 1.8-3.2 NTU for input of 6 NTU and as high as 2.7-5.2 NTU for input turbidity of 10 NTU. Greater flow in the Catskill Aqueduct produced larger effluent turbidity. In addition, the reservoir became thermally stratified during the simulation period. Thermally stratified conditions produced turbidity plumes along the thermocline that reached the vicinity of the effluents.

Turbidity Modeling Runs October 2011-September 2012 (cont'd)			
Date	**Background**	**Modeling Description**	**Results**
04/27/2012	A small event during the previous weekend had elevated turbidity in the Schoharie Reservoir. The elevated turbidity limited the use of the Shandaken Tunnel due to the potential impacts on the Upper Esopus Creek. At the same time the reservoirs were somewhat below normal storage and meteorological forecasts indicated that the weather may continue to be drier than normal. Also due to the previous event, Schoharie Reservoir is currently spilling water to the Schoharie Creek.	The OST was run including water quality for Schoharie Reservoir to provide an estimate of the period of time that it will take Schoharie Reservoir turbidity to reduce such that Shandaken Tunnel usage could be restarted.	The simulations of Schoharie Reservoir indicated that turbidity would remain generally elevated in Shandaken Tunnel over the two month simulation period. The simulations predicted Shandaken Tunnel turbidity levels of: 19-69 NTU on May15; 13-154 NTU on May 30; and 8-54 NTU on June 15. Model results were highly sensitive to the effective turbidity settling rates that were based on partitioning of turbidity into three size classes. In addition, the predicted tunnel turbidity was sensitive to the vertical location of the thermocline relative to the tunnel withdrawal depth. Thermocline predictions were highly variable at this time of year
05/02/2012	Turbidity in Ashokan Reservoir had deceased to about 6-9 NTU. Alum treatment continued to be implemented.	Kensico Reservoir simulations were run to provide guidance as to what levels of turbidity that could be tolerated as inputs to Kensico Reservoir from the Catskill Aqueduct when alum treatment was ended, and aqueduct flows increased. The tested inflow rates are 300, 400, 500 and 600 mgd from the Catskill Aqueduct with aqueduct turbidity of 6, 8 and 10 NTU.	Results suggested that Kensico effluent turbidities could range as low as 1.4-3.1 NTU for input of 6 NTU and as high as 1.8-5.0 NTU for input turbidity of 10 NTU. Greater flow in the Catskill Aqueduct inputs produced larger Kensico effluent turbidity. In addition, thermal stratification of the reservoir intensified during the simulation period. Stratified conditions produced turbidity plumes along the thermocline that might extend close to the effluents.

Turbidity Modeling Runs October 2011-September 2012 (cont'd)

Date	Background	Modeling Description	Results
07/27/2012	There was a low intensity turbidity plume in both the East and West Basins of Ashokan Reservoir. The plume was generally located near or below the thermocline with turbidity ranging from approximately 4-7 NTU. To avoid the higher turbidity, the upper level of the West Basin of Ashokan was being used to divert water to the Catskill Aqueduct. This water was warmer than under normal historical operations. Delivering warmer water to Kensico Reservoir is expected to affect the thermal structure of Kensico and possibly could change the plume dynamics and mixing with Delaware water also being input to Kensico Reservoir.	Kensico Reservoir model simulations were run to better understand the effects the use of warmer water with slightly elevated turbidity from the Catskill Aqueduct influent on the turbidity of Kensico Reservoir effluents. The tested inflow turbidity from Catskill were 4, 6 and 8 NTU with an inflow of 600 MGD These input values were tested with different alternative time series of Catskill influent water temperatures.	With higher water temperature for Catskill influent, the resulting plume of turbidity tended to form with slightly more intensity and closer to the surface within Kensico Reservoir. Since the plume was simulated at a shallow depth above the depth of effluent withdrawal, the simulated effluent turbidity decreased with higher influent temperature.` It was also noted that with a sustained Catskill influent turbidity of 6 NTU or higher automated monitoring should be closely followed to understand to magnitude and location of any turbidity plume that could form.
09/21/2012	As a result of UV plant regulation the Catskill Effluent from Kensico Reservoir was no longer in use. Therefore, all water leaving Kensico Reservoir uses the Delaware Effluent.	The goal of these Kensico reservoir model simulations was to ascertain if the simulated Delaware Effluent turbidity is affected once the Catskill Effluent is turned off. A previous run from October 1 of 2010 was changed from effluent flow of 400 MGD Catskill / 800 MGD Delaware to 0 MGD Catskill / 1200 MGD Delaware.	There was little or no difference in the Delaware Effluent turbidity for the two cases (with and without use of the Catskill Effluent).

Turbidity Modeling Runs October 2011-September 2012 (cont'd)

Date	Background	Modeling Description	Results
09/28/2012	A turbidity event on September 18, 2012 produced a large input of turbidity into the Ashokan and Neversink Reservoirs. In Ashokan the event did not fill the West Basin, but caused a plume of 200-300 NTU water just above the thermocline with values of >30 NTU at other depths. Since West Basin was not filled, the East Basin was only adversely affected to the extent that the dividing weir must stay partially open. In Neversink, a turbidity plume >300 NTU had formed; the Neversink diversion was currently offline; and the diversion was expected to remain offline for the foreseeable future.	An OST simulation was run to provide an estimate of: (a) the period of time that it will take Ashokan Reservoir West Basin turbidity to reach the East Basin, (b) the extent to which the use of the Ashokan Release Channel will change the timing and magnitude of turbidity movement from West to East; (c) the effects of Release Channel use on potential Catskill Aqueduct flow reductions due to turbidity, and (d) the effects of a temporary loss of the Neversink diversion on reservoir storage throughout the system.	In these simulations, use of the release channel under the current protocols marginally delayed the movement of turbid water from the West Basin to the East Basin, however runs performed in October 2012 with more refined (and realistic) operations indicated greater delay and a decrease in the probability of West Basin turbidity moving to the East Basin. Reduction of Catskill Aqueduct flow could be used to reduce Kensico Reservoir turbidity inputs such that alum treatment might be avoided, however, this could require some drawdown in West Branch and Kensico Reservoirs. In about 12% of these simulations either another extreme storm event negatively impacted the Catskill System or a potentially large and unacceptable drawdown of West Branch and/or Kensico Reservoirs was simulated to occur. Later runs of the OST were performed to update these results in October 2012

3. Modeling Applications of Climate Change Impacts

3.1. WRF Project 4262 - Vulnerability Assessment and Risk Management Tools for Climate Change: Assessing Potential Impacts and Identifying Adaptation Options

The WRF Project 4262 – Vulnerability Assessment and Risk Management Tools for Climate Change is utilizing a decision analysis framework to assess water supply vulnerabilities related to climate change and explore potential management adaptations. The project includes a pilot test of the framework for New York City. Project collaborators include researchers from Stockholm Environment Institute, Rand Corporation, Hydrologics, Hazen and Sawyer, DEP, and the National Center for Atmospheric Research (NCAR).

The NYC pilot test is guided by the "XLRM" framework: (Lempert et al., 2003) which structures the analysis of future vulnerability into four main components:

- Exogenous uncertainties ("X") are factors deemed to be beyond human control (e.g. future climate, population, land use, and economic change)
- Levers ("L") are actions or strategies for reducing vulnerability (e.g. operational modifications, capital investments, water conservation programs)
- Relationships ("R") are cause-effect mechanisms (e.g. effect of operational changes on water quality, effect of climate change on reservoir release requirements, effect of water rates on demand, etc.) typically reflected through computer models
- Measures ("M") are performance standards used for ranking the desirability of various scenarios (e.g. percent of days under a drought condition, probability of refill by June 1, frequency of alum treatment events, etc.)

Application of the XLRM framework entails developing future scenarios that combine uncertainties (X) with alternative actions/strategies for reducing vulnerability (L); running these scenarios thru a suite of watershed and reservoir system models that embody key cause-effect relationships (R) between driving (X,L) factors and system performance; and applying system performance metrics (M) as criteria for evaluating effects of uncertain factors and effectiveness of adaptation strategies. Subsequent statistical analyses to formally evaluate adaptation strategies utilize the Robust Decision Making (RDM) decision analysis framework (Groves and Lempert 2007).

Progress has been made to identify the elements of the XLRM components for the NYC pilot test. 145 future climate scenarios derived from 29 GCMs (Global Climate Models), 3 emission scenarios and 2 future periods (2045-2065 and 2081-2100) were developed. From these, a subset of 32 scenarios was selected to cover a range of future conditions that would potentially stress the water supply in relation to drought and turbidity. Climate scenarios were translated into reservoir inflow scenarios using the GWLF watershed model to simulate streamflow driven by alternative meteorology. Three future NYC water system demand scenarios characterized by average annual daily demands of 1120, 1250 and 1450 MGD were developed to represent current demand, projected NYC 2030 demand, and potential higher demand respectively. The combination of these two sets of projections provides a matrix of scenarios to explore the

3.2. Effects of Winter Processes on Reservoir Eutrophication Simulations

The geographic distribution and quantity of lakes are strongly influenced by glacial processes, so that the greatest number of the world's lakes are located in formally glaciated areas particularly in areas the Northern Hemisphere such as the Boreal region (Wetzel, 2001; Lehner and Doll, 2004). These northern locations today, are ones where snow has an important influence of the annual hydrologic cycle, and where the seasonality of the hydrologic and biogeochemical processes regulating nutrient delivery to lakes are influenced by the accumulation and melt of snow. Despite a strong geographic relationship between the distribution of lakes and the occurrence of snow, there is surprisingly little information on the influence of snowmelt hydrology on limnology. One consistent outcome of studies of the effects of climate change on watershed hydrology in the Northeast US is a pronounced shift in the timing of streamflow due to increased winter air temperature and rain, decreased snow, and earlier snowmelt (Burns et al., 2007; Zion et al., 2011)Such a shift in the timing of streamflow, may lead to a greater proportion of the yearly nutrient load being delivered to a lake or reservoir during cold, deeply mixed, and possibly ice covered conditions that would not be expected to be favorable to phytoplankton growth.

Winter streamflow is historically an important component of the annual water budget in the NYC West of Hudson water supply, and the ability to simulate the effects of changing levels of winter streamflow and nutrient loading on reservoir trophic status could be important for simulating present and future variations in reservoir trophic structure. The sensitivity of the two reservoir eutrophication models used by DEP to variations in the seasonality of changing winter nutrient loads had not however been rigorously tested. During 2012 the water quality modeling group undertook an examination of 1) the importance of winter nutrient loads to the annual nutrient load of Cannonsville Reservoir and 2) the sensitivity of the DEP's reservoir eutrophication models to this variability.

Modeling framework

The models used in this investigation were the GWLF VSA watershed model to simulate reservoir inflow and nutrient load, and two versions of a one dimensional reservoir water quality model that focuses on phytoplankton growth and eutrophication (Figure 3.1) GWLF VSA is used to estimate watershed nutrient export. The timing and magnitude of nutrient loading over any given year varies as a function of the daily variations in air temperature and precipitation that drive the model. Yearly variation in the metrological inputs leads to yearly variation in hydrology and nutrient loading, including the proportion of the yearly nutrient load that occurs in the winter. Variations in winter nutrient loads can be examined under contemporary conditions driving the model with measured historical meteorological data or under future conditions by driving the model with air temperature and precipitation data from future climate scenarios. For this study the models shown in Figure 3.1 were driven by both historical data and future climate scenarios.

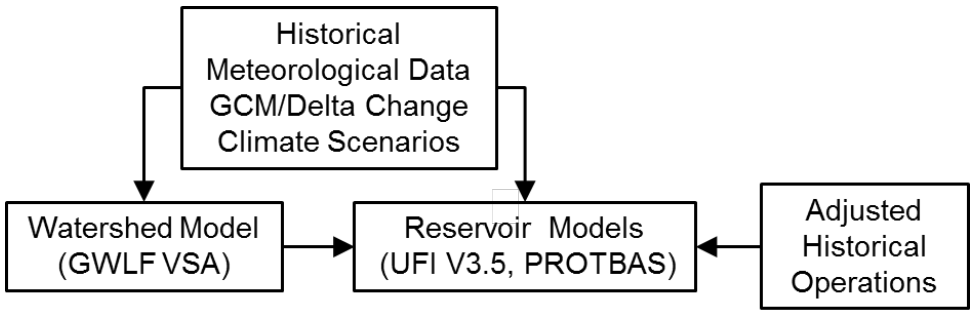

Figure 3.1. Models and data sources used to simulate changes in reservoir phytoplankton and trophic status. Both watershed and reservoir models are driven by daily changes in meteorological data that are either measured or derived from future climate scenarios. Daily variations in reservoir conditions also depend on reservoir operations, which determine reservoir outflow.

The two reservoir water quality models used by DEP are built upon the same one dimensional hydrothermal framework that was developed for DEP by the Upstate Freshwater Institute (Owens, 1998), which simulates the reservoir thermal structure, and the rate of inflow, out flow and vertical exchange between 1 meter vertical cells.

Both models examined here simulate phytoplankton growth as a function of water temperature, light and nutrients. The UFI version 3.5 (UFI V3.5) water quality sub-model is based on the model described by (Doerr et al., 1998). This model has a single phytoplankton component which has a maximum growth rate that varies as a function of temperature and a single rate of light limited growth that occurs below a fixed light threshold. The second model is based on the PROTECH model as developed by (Reynolds et al., 2001), and later modified by (Markensten and Pierson, 2007) and renamed PROTBAS. In PROTBAS, there are 8 major algal functional groups, each of which has distinct allometric characteristics parameterized by the algal surface area, volume and axial length, characteristics that define need for silica and ability to fix nitrogen, and information related to rates of motility and sinking. When comparing these two models, UFI V3.5 has more detailed and realistic algorithms describing the transformations of nutrients and the effects of nutrient concentration on algal growth, while PROTBAS has a better description of the diversity of phytoplankton and the effects of phytoplankton characteristics on growth.

Table 3.1. GCM model used to produce future climate scenarios. For each model scenarios were created for three emission scenarios (A1B, A2, and B1) and two future time periods (2045-2065 and 2081-2100)

GCM	Model Name	Source/Country
CCSM3	Community Earth System Model	NCAR/USA
CNRM-CM3	Global Coupled System model Ver 3	CNRM/France
CSIRO-Mk3.0	CSIRO Mark 3	CSIRO/Australia
ECHO-G	ECHAM4 + HOPE-G	Germany/Korea
GFDL-CM2.0	Geophysical Fluid Dynamic Lab CM2	NOAA/USA
MRI CGCM2.3.2	Meteorological Research Institute CGCM2.3.2	MRI/Japan

Climate Scenarios

Future Climate Scenarios were based on Global Climate Models (GCM) data obtained from the World Climate Research Program's (WCRP's) Coupled Model Intercomparison Project Phase 3 (CMIP3) multi-model dataset. Daily datasets were downloaded for baseline scenario (20C3M) during the period 1960-2000, and three future emission scenarios (A1B, A2 and B1) during two time periods 2045-2065 and 2081-2100, and all data sets were extrapolated to a common model grid and from these future climate scenarios were created using a frequency distribution based change factor methodology proposed by (Anandhi et al., 2011a). For this study GCM/emission scenarios were chosen which contained all the meteorological variables (air temperature, precipitation, solar radiation and wind speed) needed to drive both the watershed and reservoir models in the baseline and two future time periods (Table 3.1).

Results and Discussion

Changes in the seasonality of stream discharge and phosphorus loading, as simulated by GWLF VSA, is illustrated in Figure 3.2. Increased fall-winter precipitation, lower levels of snow accumulation and earlier snowmelt all result in increased winter (Nov-Feb) streamflow, and a somewhat decreased spring (Mar-Apr) runoff period. These results are consistent with many other climate change simulations in areas where snow influences the seasonality of streamflow (Barnett et al., 2005), and also studies of the Catskill region (Burns et al., 2007; Zion et al., 2011), which show a shift in the timing of the spring runoff peak and increased winter levels of streamflow. The Catskill region of New York is an area where the snowpack can play an important role in the yearly hydrologic cycle, but also where the snow accumulation and melt can be highly variable. Consequently, variations in the seasonality of flow, particularly in regards to winter streamflow, are also highly variable, and similar changes in seasonality and variability would also be expected to occur in regards to TDP loading.

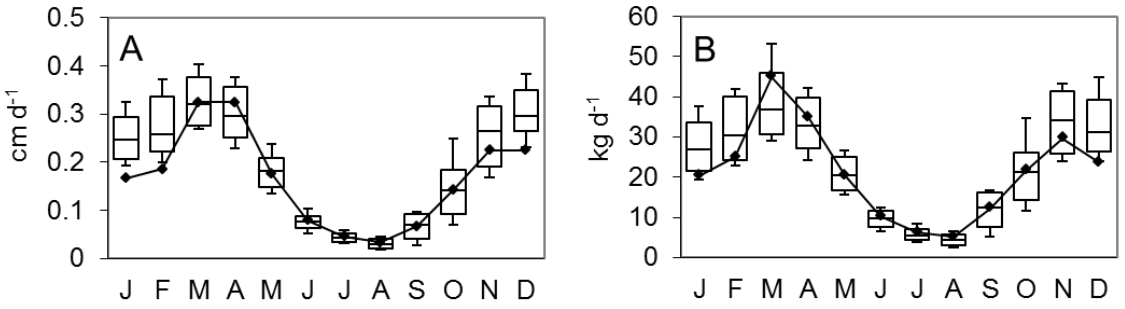

Figure 3.2. Simulated seasonal variation in streamflow (A) and TDP loading (B) under present and future conditions. The line shows the mean daily values for calculated for each month, based on the pooled data from all months in the baseline scenario. Boxplots show the variability of the 36 future scenarios.

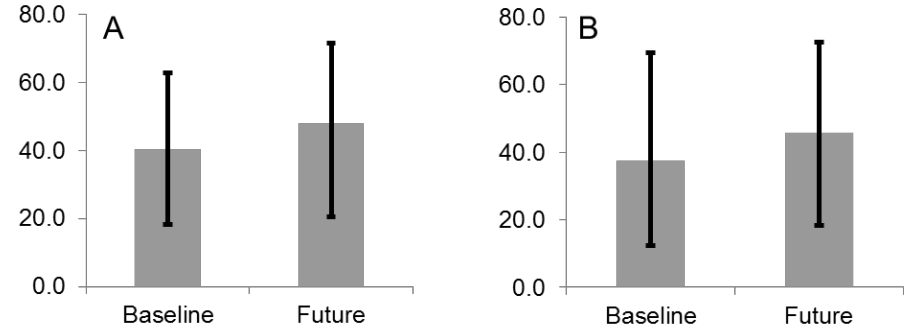

Figure 3.3. The percentage of the total annual streamflow (A) or TDP load (B) that occurred during the winter months (Nov-Feb). Graphs show the median and maximum and minimum of the base line scenario, and the combined results of all future scenarios.

Figure 3.3 shows the proportion of total dissolved phosphorus loading that occurs during the winter months (Nov – Feb) under present baseline conditions and under future conditions based on data from 36 future scenarios. Even under present conditions the importance of the winter months in affecting the annual loads is highly variable. Anywhere from 18% - 63% of the annual streamflow and 12% -70% of the annual TDP load can occur in the winter. With increasing winter flows in the future, there is also an increasing contribution of the winter months to the annual load. Median winter streamflow increases from 40% to 48% of the annual load while the median TDP load increases from 38% to 46%. High levels of variability remain in the future simulations, with anywhere from 20%-72% of the future streamflow, and 18% - 73% of the future TDP load occurring in winter.

Given that phosphorus is the limiting nutrient that regulates phytoplankton biomass in the NYC water supply reservoirs, shifts in the timing of TDP inputs could be expected to impact overall levels of biomass as well as the seasonal patterns of phytoplankton biomass and succession. To examine how climate change will impact reservoir chlorophyll levels, reservoir model simulations were run under baseline conditions and compared to simulations driven by climate scenarios associated with the GCM models in Table 3.1. The results of these simulations are shown in Figure 3.4, using both the UFI 3.5 and PROTBAS water quality models.

Both models show moderate 10-15% increases in mixed layer chlorophyll concentrations for some of the future scenarios and both models also predict that the timing of the spring bloom will move forward by approximately 10-14 days. The somewhat different levels of biomass and different seasonal patterns simulated by the two models are the result of differing assumptions embedding within the two different water quality models. Both models however, produce credible patterns of phytoplankton succession and levels of biomass. The patterns in Figure 3.4 are average seasonal patterns, based on multiple simulation years. Between years there are significant variations in the levels of biomass, as well as the timing and magnitude of the spring peak and fall bloom

We hypothesized that TDP added to the reservoir during winter would be less likely to increase phytoplankton biomass, and that a relationship would exist between the proportion of TDP loading that occurred in the winter and the mean annual mixed layer chlorophyll simulated by our models. Years having a relatively high proportion of winter TDP loading are hypothesized to have less annual biomass. In Figure 3.5 mean annual mixed layer chlorophyll concentration is plotted against the proportion of winter TDP load using data output from both the UFI 3.5 and PROTBAS models. In both cases there is no clear relationship between the average annual chlorophyll concentration and the proportion of winter TDP loading, despite a large range in the proportion of TDP loading that occurs in the winter.

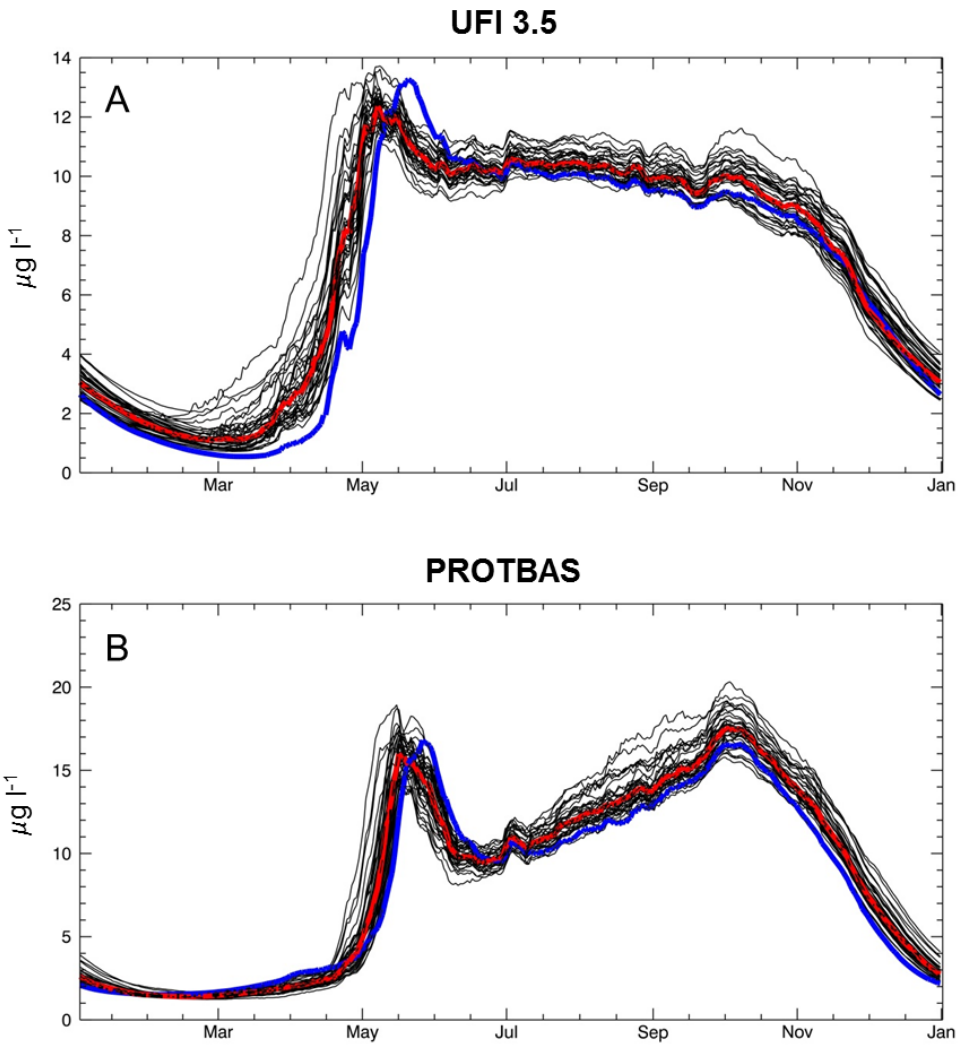

Figure 3.4. Seasonal variations in mixed layer chlorophyll concentration simulated with the UFI 3.5 (A) and PROTBAS (B) models. Each line is the mean daily value of the data from all years in a given scenario. Blue line is the baseline scenario, black lines are associated with each of the 36 future scenarios, and the red line is the median of the future scenarios.

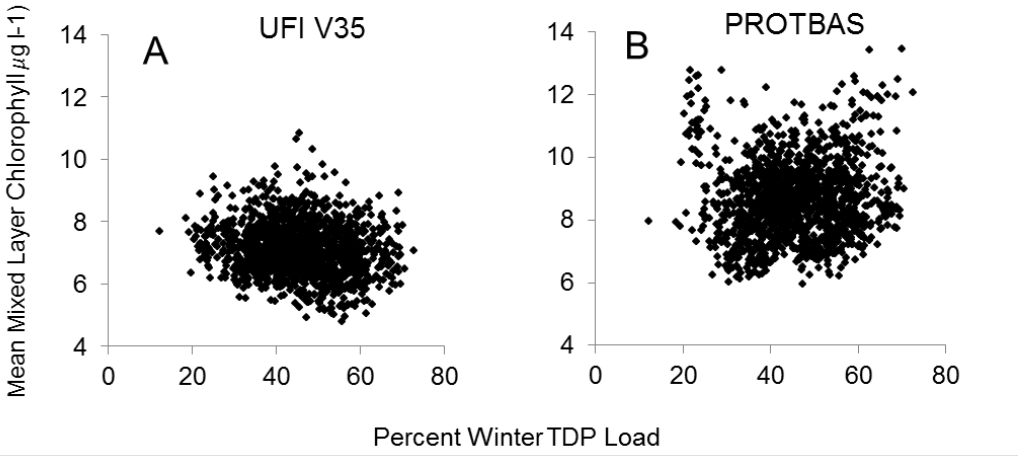

Figure 3.5. The relationship between mean annual mixed layer chlorophyll concentration and the percent of the annual TDP load that occurs in winter (Nov-Feb). Each point is for a single year's data in the baseline and 36 future climate scenarios. The results from UFI V3.5 are shown in A and PROTBAS are shown in B.

In an exercise such as this it is difficult to determine if our hypothesis fails as a result of an incorrect theory, or as a result of the models not correctly representing the lake processes upon which the theory is based. To gain greater insight into model performance, we systematically varied the timing of nutrient input, without changing the amount of annual loading or the meteorological forcing affecting the reservoir model. A number of synthetic loading time series were created from the historical reservoir input data by taking 50% of the combined water and material loads from March and April and redistributing these into a different month. In all, five synthetic loading records were created which redistributed the March-April loads into January and February to simulate the expected future shift to earlier winter runoff, and also forward in time to May, June and July. This facilitated examination of the response to shifting the loads into stratified as opposed to isothermal conditions. Shifting 50% of the spring nutrient load to January or February (Figure 3.6A) resulted in virtually no change in the annual pattern of mixed layer chlorophyll or in the magnitude of the chlorophyll concentrations, which is consistent with the lack of relationship in Figure 3.5. On the other hand, the model predicts significant changes in the timing of peak biomass, as well as levels of biomass (Figure 3.6B) when the spring nutrient loading is shifted forward into thermally stratified period. During winter the average light exposure experienced by the phytoplankton is low as a consequence of deep isothermal mixing, and light exposure is also limited due to lower incident irradiance during the winter months and the presence of lake ice and snow cover. Under such conditions simulated rates of phytoplankton growth are strongly light limited, and the input of TDP is not utilized, and remains biologically available. Following the onset of thermal stratification the mixed layer becomes shallower and the phytoplankton circulating through this mixed layer are exposed to much higher average light intensity. Growth can then proceed until limited by nutrient availability. This is the classic explanation for the timing of the spring bloom (Riley, 1947;

Sommer et al., 1986), and its coincidence with the transition from light-limited to nutrient-limited growth. Our models correctly simulate this transition. What is less clear is whether the models are correctly simulating the conditions that occur during the winter that affect phytoplankton growth and TDP bioavailability. For the models to be completely insensitivity to the timing of TDP inputs during the winter period (Figure 3.6A), requires that virtually no phytoplankton growth occurs, and that no processes impact the bioavailability of TDP inputs during the winter. Both assumptions are not supported by lake studies under winter conditions. There are a number of studies that suggest microbial (Tulonen et al., 1994; Reitner et al., 1997) and phytoplankton (Phillips and Fawley, 2002; Kiili et al., 2009) growth under winter conditions which would reduce the store of bioavailable TDP prior to the onset of thermal stratification. Furthermore there are also numerous studies that have reported the phytoplankton blooms occurring under ice cover e.g. (Catalan, 1992; Pettersson et al., 2003; Twiss et al., 2012) or during deeply mixed ice free conditions prior to the onset of thermal stratification (Horn et al., 2011). Correctly simulating these effects would require accurately simulating the onset and loss of lake ice, stratification and mixing under ice, phytoplankton light adaptation to deeply mixed low light conditions and the effects of microbial activity on phosphorus bioavailability. The lack of sensitivity of our models to the changes in winter nutrient loading should not be seen as a failure of the models, since our models were developed to simulate peak phytoplankton concentrations during the period of thermal stratification when drinking water concerns and the effects of watershed management would be most evident. Emphasis was placed on simulating the processes that occur during this period, and model process studies and calibration (Auer and Forrer, 1998; Doerr *et al.*, 1998) were almost entirely focused on the stratified period. As a result, the models do respond as expected when spring nutrient loads are shifted into the summer period (Figure 3.6B).

Studies of climate change focused attention on the winter and the effects of processes whose importance is changing as the seasonality of model drivers changes with the climate. This study illustrates the importance of carefully examining model assumptions and testing the sensitivity of models to changes that would be expected as a consequence of future climate change. This study also illustrates the added advantage of testing models beyond the realm of typical concern. Considering the effects of climate change on snow, snowmelt hydrology and the seasonality of nutrient loading focused our attention on the winter period and illuminated model processes that need further investigation even under contemporary conditions. In the NYC water supply region, snow accumulation and melt are naturally variable, so that the proportion of winter nutrient loading is highly variable even today (Figure 3.3). As a result, the need for studies examining the relative importance of the timing of nutrient loading as well as the magnitude of nutrient loading on the NYC water supply reservoirs has become clear.

This study highlights the challenges and pitfalls associated with simulating the future impacts of climate change using complex ecosystem models. Such models are by necessity simplifications of the lake/reservoir system, and focus on the processes considered most important for the question/interest at hand. Phytoplankton models therefore, often focus on processes affecting growth and succession during the period of thermal stratification when biomass is greatest and blooms could become problematic. Climatic impacts affecting winter processes in these models may not be well represented. As model use shifts to simulating expected effects of climate

change, impacts need to be clearly articulated and the model structure and algorithms simulating these need to be systematically evaluated.

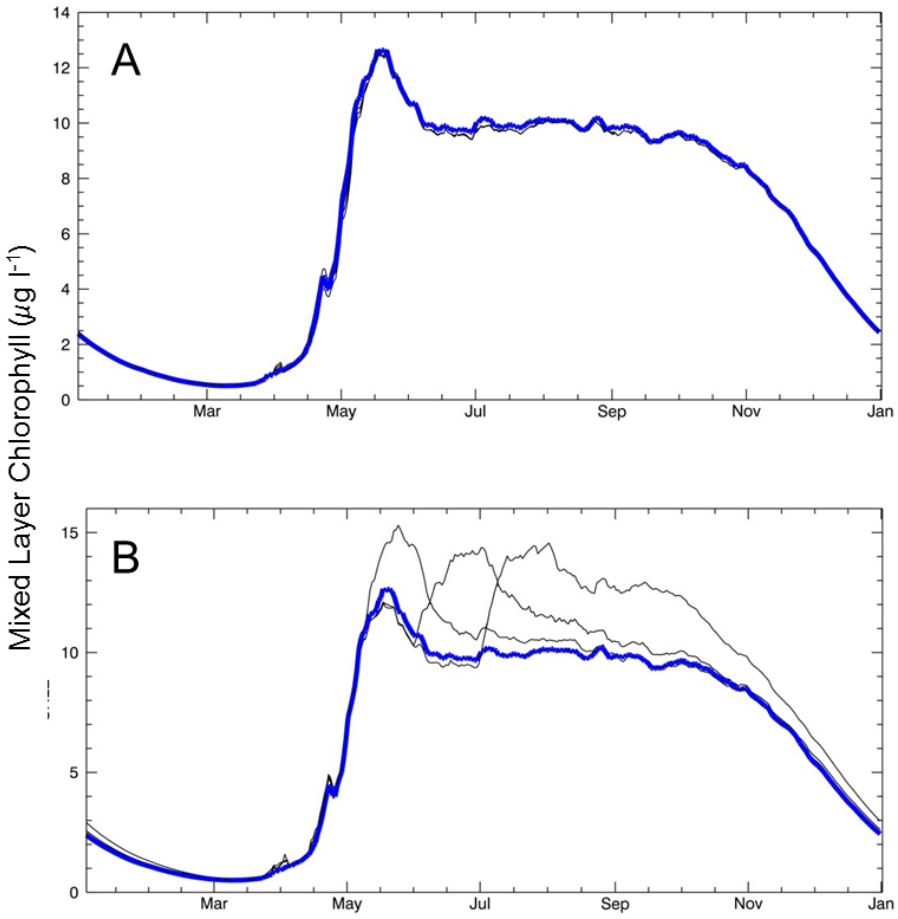

Figure 3.6. Sensitivity analysis which examined the effects of shifting 50% of the March + April nutrient load to winter conditions (A January and February) and summer conditions (B May, June, and July). Figures show mean daily patterns calculated from the full simulation time period. Thick line shows results under baseline conditions with no redistribution of the nutrient loads. Thin lines show traces associated with redistributed loads. These are results using the UFI V3.5 model. The PROTBAS model showed similar results.

3.3. Effect of Projected Changes in Winter Streamflow on Stream Turbidity in Esopus Creek

Introduction

High suspended sediment loads and the resulting turbidity can impact the sustained use of rivers for water supply and other designated uses. Changes in stream turbidity can also be an indication of changes in material fluxes, aquatic geochemistry, water quality, channel morphology and aquatic habitats (Walling, 2009). Therefore, understanding the processes and quantifying stream turbidity under present and future conditions will be valuable for watershed-scale management of stream turbidity and maintaining high water quality. The Catskill Mountain streams provide up to 90% of the municipal water supply for about 9 million residents of NYC through a network of six reservoirs draining approximately 3,885 km^2. The Upper Esopus Creek that drains into the Ashokan Reservoir along with water diverted from the nearby Schoharie Reservoir (via the Shandaken Tunnel) provide 40% of this unfiltered drinking water supply. The water quality is typically high in the Catskill streams. However high magnitude runoff events can cause significant increases in stream and reservoir turbidity, which at times limits the use of this unfiltered drinking water supply (Gelda et al., 2009).

An examination of historical data and results of model simulations for the Catskill region have shown an increasing trend in both mean annual precipitation (8-26 cm/50 years) and streamflow over the past fifty years (Burns et al., 2007; Zion et al., 2011). Major climate change impacts identified and predicted for this region include reduced snowfall and an earlier occurrence of snowmelt driven runoff due to increasing mean annual air temperature at the rate of 0.5-2.0 ^oC over a 50 year period (Burns et al., 2007). Ongoing research efforts to identify climate change impacts on water resources in NYC watersheds include selecting Global Climate Models (GCM) reasonable for the region, detecting changes in seasonal streamflow and, predicting future changes in water supply and water quality (Anandhi et al., 2011a; Matonse et al., 2011; Zion et al., 2011; Mukundan et al., 2012). The purpose of this study is to improve our understanding of the potential impact of climate change on stream turbidity in the NYC water supply. In this study we perform a sensitivity analysis of stream turbidity to ongoing and anticipated changes in the seasonality of streamflow, with a focus on the winter period, using data from the Esopus Creek watershed. Stream channel processes are a major contributor of stream turbidity in this watershed (DEP, 2008a). A long term (1931-2010) record of measured streamflow data from the U.S. Geological Survey gauge (#1362500) at Coldbrook, where the Esopus Creek enters the Ashokan reservoir shows that majority of bankfull discharge events with 1.5 year return interval occur during the period from beginning of November to end of April. Therefore, it is important to have a better understanding of potential changes in stream turbidity during this period where major changes in streamflows are observed and predicted to change due to changes in timing of snowmelt runoff

Methods

Turbidity monitoring in the Esopus Creek watershed

The Esopus Creek watershed drains an area of 493 km^2 and is dominated by forests which occupy more than 90% of the watershed area. The elevation of the watershed ranges from about 194 m near the watershed outlet at Coldbrook to 1275 m at the headwaters. An automated turbidity monitoring system was installed on the main tributary entering the Ashokan Reservoir near the confluence of the creek and the reservoir. Water is pumped into a riverside hut where measurements of turbidity, specific conductivity and water temperature were made using a water quality sonde. Water samples are also periodically collected and analyzed for turbidity (*Tn*, NTU) and total suspended solids (TSS, mg/L) in the laboratory. These data are then used to correct the automated data to account for any drift in the turbidity measurements. The United States Geological Survey (USGS) gauging station at Coldbrook provides streamflow data at a daily and 15 min interval. Since 2003, turbidity measurements have been made at intervals between 15 min and 1 hr. Sub-daily observations are flow-weighted to provide daily average values, which are comparable in frequency to the most widely available daily USGS streamflow data, and are at the time step used by DEP's reservoir water quality models.

Time series model of average daily turbidity

Although continuous turbidity measurements have been made for most periods between June 2003 and August 2011, there were periods where turbidity measurements could not be made due to storm related damage and fouling of turbidity sensors. Therefore, turbidity values for missing days are estimated using a time series model. Ordinary least square regression models on time series data often shows highly correlated residuals and this is particularly true for daily time series data (Richards et al., 2008; Walker et al., 2009). Since the ordinary regression residuals are not independent for time series data, they contain information that can be used to improve the prediction of future values (Reed et al., 2008). More importantly, addressing autocorrelation can avoid incorrect conclusions on significance of parameters, confidence limits for predicted values, and estimates of regression coefficients. The AUTOREG procedure in SAS (SAS Institute, 2003) was used to fit a linear regression with autoregressive errors. Three predictor variables were used for the linear regression; streamflow at the watershed outlet, point source turbidity, and a parameter representing the hysteresis effect in streamflow-turbidity relation. For point source effect a daily time series of measured instantaneous turbidity at the outlet of Schoharie Tunnel was used. Hysteresis effect on stream turbidity was derived using the method proposed by Hirsch (1988). Our previous analysis has shown that in general a given value of streamflow on the rising limb of streamflow hydrograph contributes higher turbidity compared to the falling limb (Mukundan et. al., 2010). The hysteresis term will account for such differences. A detailed description on the development of the time series turbidity model and its use as an operational predictive tool is outlined in Wang et al. (2012).

Future climate scenarios

The potential effect of climate change on in-stream turbidity was evaluated using baseline and future climate scenarios derived from a suite of five GCMs and three greenhouse gas emission

scenarios that represent a wide range of future climate conditions, during the 2046-2065 and 2081-2100 time slices and a baseline (20C3M) scenario representing historical (1960-2000) conditions. In this study, the A1B, A2 and B1 scenario from the Special Report on Emission Scenarios (SRES) in the IPCC Fourth Assessment Report (IPCC, 2007) were used. Projected values from the selected GCMs for the region surrounding the NYC water supply were extracted and interpolated to a common 2.5^{o} grid using bilinear interpolation for the baseline and future emission scenarios. Climate scenarios were downscaled using a 25-bin change factor methodology. This methodology divides the variable cumulative distribution function into 25 equally spaced percentiles and a monthly delta change factor (Anandhi et al., 2011a) is developed for each bin. Monthly change factors (CFs) were calculated from the difference between baseline and each future GCM/scenario simulation. These monthly CFs were used to adjust the local meteorological data from 1927-2009 and used to generate future climate conditions associated with a given GCM. The use of long-term observed data in generating future climate scenarios has an advantage of representing the observed regional climate patterns but has the disadvantage of relying only on the local historical variability of events (Matonse et al., 2012). We applied a calibrated GWLF model to simulate daily streamflow, when the model was driven using daily time series of baseline and simulated future precipitation and air temperature that were created as described above.

Developing future stream turbidity scenarios

A combination of measured and interpolated daily in-stream turbidity data and measured streamflow data were used to derive empirical relationships that relate a wide range of streamflow to stream turbidity (rating curves). To reduce the effect of Schoharie Reservoir inputs on Esopus Creek turbidity, particularly on low flow turbidity, only streamflow-turbidity pairs from days when the flow diversion from Schoharie Reservoir was less than 10% of the total Esopus Creek daily streamflow were used. Separate turbidity rating curves were developed for winter (November-April) and summer (May-October) periods to account for seasonal variability in turbidity inputs. The rating curves were then applied to baseline and future time series of streamflow simulated by the GWLF-VSA model to develop baseline and future stream turbidity scenarios. These scenarios were then used to calculate average daily turbidity, average daily turbidity loads, and annual cumulative turbidity loads. Previous studies support the concept of turbidity loading (i.e., units of NTU m^3 s^{-1}), as a water quality measure of concern since turbidity levels are of regulatory concern for water supply operation (Peng et al., 2009). Additional support for this approach is provided by the additive nature of turbidity i.e., the turbidity of a mixture of two volumes can be computed by volume averaging (Davies-Colley et al., 2003).

Results

Stream Turbidity Time Series

A continuous time series of average daily stream turbidity from June 13, 2003 to August 31, 2011 was used for this analysis. Missing turbidity data were estimated using the time series model described in the methods section. Residual analysis from the ordinary least square regression model using the three predictor variables showed a lag of 4 days in the autocorrelation

function. This information was used in selecting an autoregressive model capable of predicting log-transformed daily turbidity. The selected regression model with AR4 error is as follows:

$$Y(t) = \beta x(t) + v(t) \quad (3.1)$$

$$v(t) = \sum_{i=1}^{4} \phi_i v(t-i) + \varepsilon_t \quad (3.2)$$

where $x(t)$ is a vector of predictor variables at time t, β is a vector of regression parameters, ϕ_i represents the autoregressive parameters, $v(t)$ is the model error at time t and ε_t is "white noise" which is normally distributed with a mean of 0 and a variance of σ^2

The selected model was evaluated for its performance in predicting mean daily stream turbidity using coefficient of determination (R^2), Nash-Sutcliffe efficiency (NSE) (Nash and Sutcliffe, 1970), and percent bias (PBIAS). The autoregressive daily time series model performed reasonably well with R^2 of 0.71 and NSE of 0.46 and PBIAS less than 2%. Model performance was affected by predictions for two data points without which the R^2 and NSE improved to 0.82 and 0.62 respectively. The model predicted average daily turbidity for 04/16/2007 was 1205 NTU when the measured value was only 253 NTU and for 01/25/2010 the predicted value was 196 NTU when the measured value was 904 NTU. These outliers can be the result of certain watershed processes such as streambank collapse under baseflow conditions resulting in high stream turbidity, or from turbidity plumes from other sources that cannot be explicitly captured by a time series regression model.

Projected Changes in Stream Turbidity

Modeled long-term average daily in-stream turbidity for the baseline scenario showed a peak in April and this peak was maintained in future scenarios (Figures 3.7A and B). However, the height of the peak was reduced in the future time slices (2046-2065 and 2081-2100) due to the shift in timing of snowmelt runoff and the resulting increase in streamflow in earlier winter months. Moreover, a decrease in the amount of precipitation received as snow is predicted in the future as reported in other studies (Frei et al., 2002; Mukundan et al., 2012). The projected increase in ambient stream turbidity during January and February as a result of this shift in streamflow was up to 45% for the 2046-2065 period and up to 68% for the 2081-2100 period compared to baseline. Projected changes in average daily stream turbidity loads yielded similar results (Figures 3.7C and D). Maximum increase in winter turbidity loads is projected for the month of January and maximum decrease is projected in April. Figures 3.7E and F show the modeled long-term average annual cumulative turbidity load for baseline and future scenarios. The percent change in average annual cumulative turbidity load was only +3% and +5% for the 2046-2065 and 2081-2100 time slices and corresponds well with the projected average annual change in streamflow volumes (+4% and +6% respectively) for the same time period. This is interesting as analysis of climate change effects on turbidity loads at the annual time scale would yield no major effects even though there is a major seasonal effect in the winter due to a shift in the timing of snowmelt runoff. The modeling results presented here should be viewed as a general sensitivity analysis rather than absolute numerical predictions, considering the uncertainty in future climate projections, and in the streamflow versus turbidity relationship.

Potential changes in frequency of extreme events are not captured by GCMs and the downscaling method used in this study, and the frequency of extreme events can have a large effect on the loading during any given year. Our projected changes in winter stream turbidity are consistent with the projected changes in winter hydrology as discussed in Matonse et al. (2011) and Zion et al. (2011) for the same region.

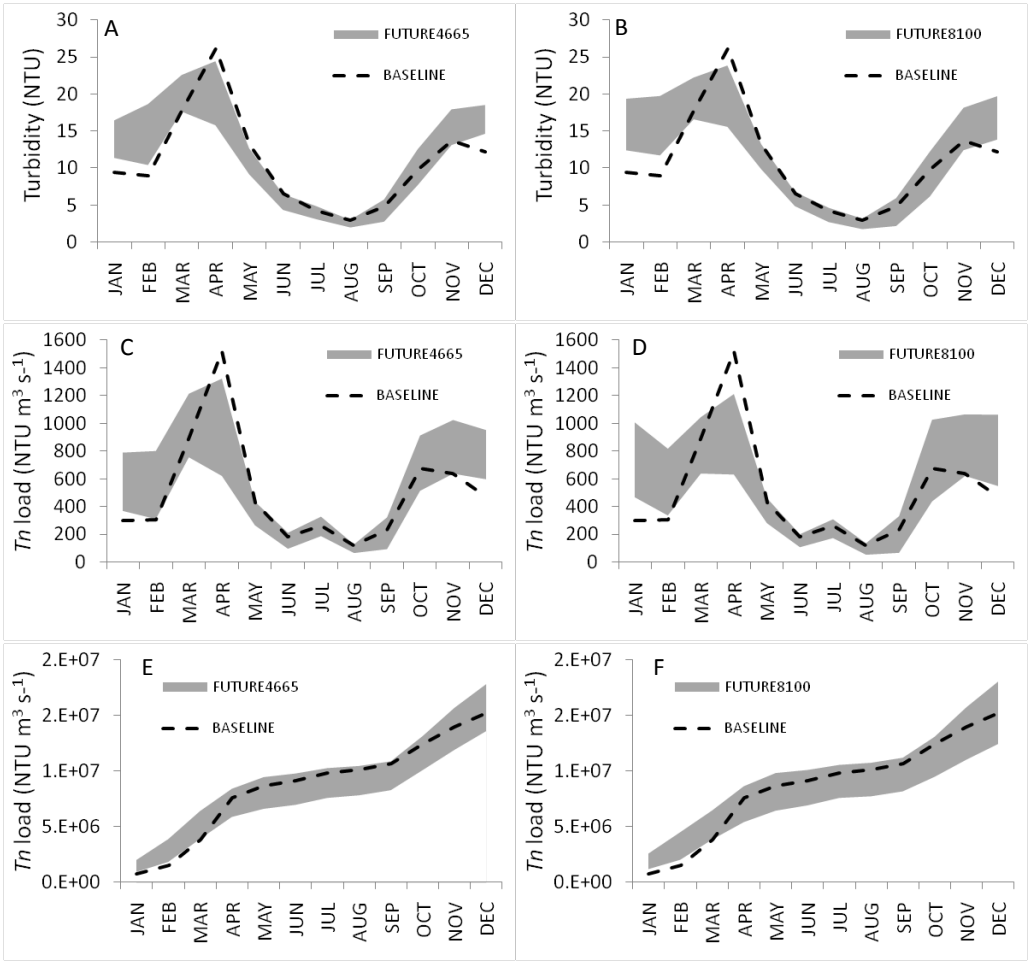

Figure 3.7. Comparison of baseline *vs.* future ambient stream turbidity for the 2046-2065 period (A) and 2081-2100 period (B); projected change in average ambient turbidity load by month for the 2046-2065 period (C) and 2081-2100 period (D); projected change in average annual cumulative turbidity loads (E and F).

Summary and Conclusions

Our study reports on the effects of projected changes in winter hydrology on winter stream turbidity in the Esopus Creek watershed. We use both measured historical data and simulated future scenarios to specifically compare differences in stream turbidity between present and future climate scenarios. Results of model simulations using a suite of five GCMs, three emission scenarios, and two time slices indicate a relative increase in ambient stream turbidity from November-March and a decrease during April for the future period. These changes are the result of increased winter rainfall, reduced snowfall and a backward shift in the timing of snowmelt runoff that is expected to occur in this region, as reported in previous studies. Changes in turbidity loading followed the same pattern as ambient stream turbidity for most months. Despite changes in the seasonality of turbidity loading, changes in average annual cumulative turbidity loads were minimal. This is largely due to the fact that the predicted future winter streamflow pattern leads to a significant redistribution but only a small increase in the total streamflow volume. Under future conditions we predict higher streamflows and turbidity loading from January-March and a reduction in the traditional April peak associated with snowmelt runoff.

3.4. Potential Effects of Climate Change on Winter Turbidity Levels in Ashokan Reservoir

Intermittent inflows of high concentrations of suspended particles to Catskill system reservoirs is one of the water quality concerns affecting the New York City water supply system (NYCWSS). Turbid water in a reservoir has negative aesthetic and recreational appeal. Mitigating the impacts of high turbidity may require changes in reservoir operations which may increase water delivery and treatment costs. Following high streamflow events when high loads of inorganic particles are transported, elevated turbidity (T_n, NTU) levels with complex spatial pattern in downstream lakes and reservoirs can occur (Effler et al., 2006a; Gelda and Effler, 2007a; Prestigiacomo et al., 2008; Gelda et al., 2012). Distribution and transport of these particles in lakes and reservoirs are time and space varying (Casamitjana and Schladow, 1993) and are further influenced by the hydro-meteorological forcings. Changes in meteorological forcings can lead to changes in reservoir thermal stratification resulting in changes in the distribution of turbidity. In the unstratified winter period, a reservoir is well mixed and high turbidity levels may be observed due to winter storm events (Lou and Schwab, 2000).

Various studies have been undertaken on particle size, particle distribution and transport processes (Casamitjana and Schladow, 1993; MacIntyre et al., 1999; Brach-Papa et al., 2006; Bilotta and Brazier, 2008; Chakraborti et al., 2009; Chung et al. 2009; Gelda et al., 2009, 2012), but specific mechanisms concerning temperature effects on particle transport following large and small events in a large reservoir system have not been thoroughly addressed, especially effects that would occur during low temperatures and isothermal conditions. The seasonality of streamflow and particle transport may vary under future climate due to changes in winter snowmelt and shifts in seasonality of streamflow in the northeastern region of the U.S (Mukundan et al., 2012; Matonse et al., 2011, 2012). In context of the seasonal variability in streamflow and associated changes in stream turbidity, this investigation is made to document the effects of summer and winter turbidity inputs to the Ashokan reservoir and to assess the turbidity and temperature distributions in the reservoir prior to and after several summer and winter turbidity inputs. The effects of temperature on settling rate in the reservoir following summer and winter events and the potential impact of climate change on future turbidity level in reservoir are examined.

Historical simulations

The fate and transport of turbidity loads entering the Ashokan Reservoir is determined using W2 model (Cole and Buchak, 1995; Cole and Wells, 2002), which has been adapted, calibrated and rigorously tested for the Ashokan Reservoir (Gelda et al., 1998 and 2009). The simulations presented here are for the West Basin of Ashokan Reservoir which is represented in the model by a grid of cells with 28 longitudinal segments and vertical layers of 1 meter thickness (Figure 3.8). The driving data for the model under historical conditions (1948-2011) include measured time series of daily reservoir inflows with associated stream temperature (T) and turbidity Tn; meteorological data (hourly air temperature, dew point, solar radiation, wind speed and wind direction); and daily records of operational information (withdrawal, spill and release volumes, and reservoir water surface elevation).

Model results for in-reservoir water temperature and turbidity for more recent years (2006-2011) were compared with data collected at automated profile buoys located within the reservoir. The two buoys were located at sites about midway longitudinally from the Esopus Creek inflow to the dam (site 1.4) and near the dam (site 3.1). We presented the buoy measurements near the dam (buoy 3.1) for calibration. Data are collected four times a day (6 hour increments) and includes water temperature and turbidity measured from the surface to the bottom of the reservoir at 1 meter depth increments (Gelda et al., 2009). Event-based sampling is also conducted in order to support our modeling study.

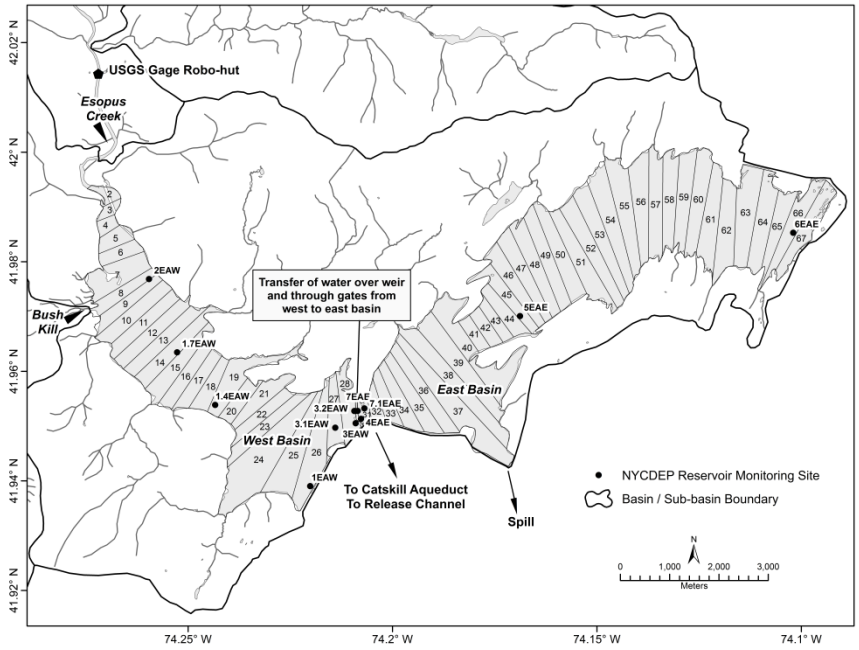

Figure 3.8. Ashokan Reservoir (West and East Basin): mouth of Esopus Creek and Bush Kill with model segment identification number

Table 3.2. General Circulation Models, emission scenarios and time slices applied in this study.

GCM	Emission scenarios	Time Slices
GCMs: CGCM3.1 (Canada)	A1B, A2, B1	2081-2100
	B1	2046-2065
CNRM-CM3 (France)	B1	2046-2065, 2081-2100
MRI-CGCM2.3.2 (Japan)	B1	2081-2100

Future Climate Scenarios

Climate scenarios were developed from the output of three GCMs: CGCM3.1, CNRM-CM3 and MRI-CGCM2.3.2. Table 3.2 summarizes the climate scenarios and time periods used in this study. Scenarios of daily air temperature and precipitation were created by downscaling the different GCMs (Anandhi et al. 2011a) and scenarios for the region of study using a 25-bin change factor methodology. Change factors created by this method were applied to historical records of daily meteorological data to develop local future climate scenarios.

For reservoir model application hourly meteorological future climate scenarios were created from the daily climate scenarios. Hourly air temperature was estimated using future simulated daily minimum (*Tmin*) and maximum (*Tmax*) air temperatures and the WAVE model as described in Reicosky et al., (1989). The WAVE model uses today's *Tmin* and *Tmax* together with next day *Tmin* to compute hourly air temperature from today's sunrise (*Rise*) to 1400h and from 1400h to sunrise of the next day. Hourly temperature (*T(H)*) is estimated as:

$$T(H) = Tave + Amp(\cos(\pi H' / Rise))) \text{ for } 0 \le H < Rise \text{ and } 1400\text{h} < H \le 2400\text{h} \quad (3.3)$$

$$T(H) = Tave - Amp(\cos(\pi(H - Rise)/(14 - Rise))) \text{ for } Rise \le H \le 1400\text{h} \quad (3.4)$$

where *H* is the time in hours, *H'=H+10* if *H< Rise, H'=H-14* if *H*>1400h, *Tave = (Tmin +Tmax)/2* and *Amp=(Tmax-Tmin)/2*. In the absence of future sunrise data we used historical regional daily sunrise times. The dew point temperature for W2 climate change simulations is set equal to simulated hourly *Tmin,* and future wind and solar radiation are set equal to local historical hourly values.

Climate change inflows to the West Basin Ashokan Reservoir are simulated on a daily time step using the Generalized Watershed Loading Functions-Variable Source Area (GWLF-VSA) model (Schneiderman et al., 2007; Schneiderman et al., 2002; Haith and Shoemaker 1987). The GWLF-VSA model was calibrated using historical inputs to simulate streamflow from Esopus Creek at Coldbrook and Bush Kill which contribute to West Basin Ashokan Reservoir inflow. In addition, inflow from ungaged areas draining to the reservoir is estimated using Bush Kill estimates and a ratio between Bush Kill and ungaged drainage areas. A rating curve (Gannett Fleming & Hazen and Sawyer, 2008) developed empirically using historical data is used to estimate turbidity concentration *Tn* based on simulated Esopus Creek flow Q_{Esp} and has the form

$$\log Tn = 1.033 - 0.986 \log Q_{Esp} + 0.691(\log Q_{Esp})^2 \quad (3.5)$$

A lower bound $Tn = 4.8$ is used for $Q_{Esp} < 5.17$ cms. Total daily turbidity is then partitioned into three particle sizes using the following criteria

$T_{n1} = 0.10 * Tn$ (3.6a)
If $Q_{Esp} > 40$ cms, $T_{n2} = 0.45 * Tn$, and $T_{n3} = 0.45 * Tn$; (3.6b)
IF $Q_{Esp} <= 40$ cms $T_{n2} = 0.65 * Tn$ and $T_{n3} = 0.25 * Tn$. (3.6c)

Future values of Esopus Creek water temperature at hour i (T_i) is calculated in ^oC using the following regression equation developed by the Upstate Freshwater Institute (UFI) and published in DEP (2007)

$$T_i = a_0 + a_1 * T_{air,i-2} + a_2 * \log Q_{Esp} + a_3 * a_5 * T_{STP,i}^{a_4} \quad (3.7)$$

where T_{air-2} is the simulated local air temperature of two hours back (in ^oC), $a_0 - a_5$ are the model coefficients calibrated on a monthly basis using historical data, Q_{Esp} is the simulated Esopus Creek daily average streamflow in cubic meters per second (cms), and $T_{STP,i}$ is the Shandaken Tunnel Portal temperature at the i^{th} hour. Coefficient a_5 is 0 when the Shandaken Tunnel is off and 1 when the tunnel is on.

When running future climate scenarios operational flows are obtained from OASIS model (HydroLogics, Inc., 2007) simulations using similar climate change inflows. For the West Basin Ashokan Reservoir these include the Shandaken Tunnel flows, the gate flows in the dividing weir between the West and East Basins of the Ashokan Reservoir and release channel withdrawals from West Basin Ashokan. The time series for these flows are obtained from OASIS on a daily time step.

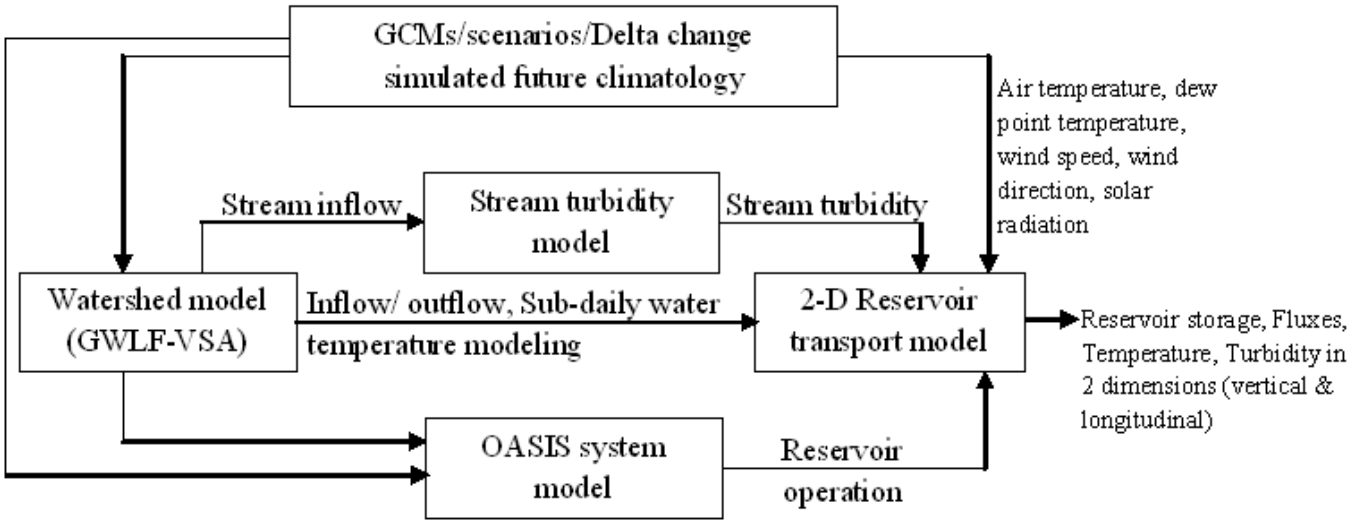

Figure 3.9. Modeling frame work: model connections and data flow

Figure 3.9 illustrates the modeling framework applied for this study. Inputs to the W2 model include downscaled GCM/Scenarios climate data, simulated hourly climate developed using various methods based on simulated daily hydrology and climatology, watershed model simulated daily streamflow, daily stream turbidity simulated using a turbidity model that uses simulated streamflow, daily reservoir operations simulated by the OASIS (Hydrologics, Inc., 2007) reservoir system model.

Results and Discussion

Evaluation of W2 model performance using historical data

The W2 model was previously calibrated and validated for the Ashokan reservoir using volume weighted epilimnetic and hypolimnetic temperature as described in Gelda et al., 2009. For further testing the model was driven with the actual observed streamflow and stream turbidity for the period 2003 to 2011, and evaluated by comparing model versus observed data of: (1) reservoir water surface elevations (June 2003 to September 2011) (Figure 3.10); (2) reservoir turbidity measured at robotic monitoring site 3.1 for 2006 to 2011 (Figure 3.11).

The model simulates well the fluctuations in water surface elevations both during low and high flow event period except for 11 May 2006 (Figure 3.10). The three drops in water surface elevations below 174 m are observed on 23 September 2007, 19 October 2008 and 04 September 2010 and are well represented by the model simulation. Sharp rises in water surface elevations correspond to large storm event inputs of water to the reservoir.

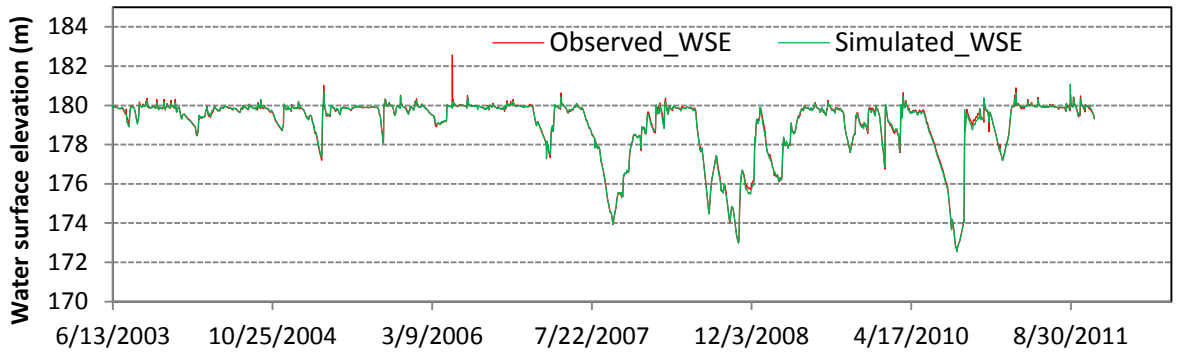

Figure 3.10. Model simulated and observed water surface elevations in Ashokan Reservoir for the period 2003-2011

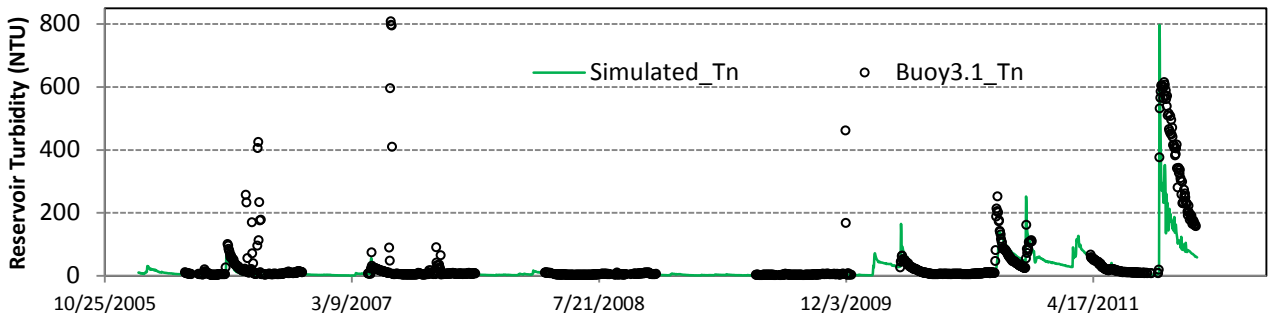

Figure 3.11. Model versus observed turbidity (Tn, NTU) in Ashokan Reservoir, 2006-2011, where the green line represent the model turbidity at segment 28 (Withdrawal point)

Table 3.3. Same size paired events during summer and winter. *represent turbidity at segment 28

Summer				Winter			
Date of peak streamflow	Streamflow (m^3/s)	Peak stream turbidity (NTU)	Peak reservoir turbidity* (NTU)	Date of peak streamflow	Streamflow (m^3/s)	Peak stream turbidity (NTU)	Peak reservoir turbidity* (NTU)
09-07-1999	191	228	12	11-28-1993	233	283	83
09-18-2004	250	15	12	12-08-1974	240	306	58
10-21-1995	254	351	28	12-2-1996	271	413	92
06-28-2006	322	468	68	11-08-1977	304	557	95
06-28-2006	322	468	68	03-23-2010	350	595	165
10-01-2010	500	1440	138	04-03-2005	500	315	69

*Turbidity at segment 28

Figure 3.11 illustrates how the model simulated reservoir turbidity compares to observed data at buoys 3.1 of the West Basin available for the period 2006-2011. The model simulated turbidity levels are similar to the buoy measured data in all cases except in case of a few high outlying measurements late October and early November. While it is impossible to state the source of these errors, the intermittently high measured data suggests the problem is more likely with the buoy measurements

Event sampling from simulated time series

In order to evaluate and better understand the seasonal pattern between streamflow, stream turbidity and reservoir turbidity, we sampled the historical model results for two seasons; summer (May-October) and winter (November-April) during more than six decades of historical record (1948-2011). A total of 12 events considering a wide range of streamflows were examined (Table 3.3). when choosing these events, an average daily streamflow of 146 m^3/ was selected as minimum streamflow that caused the average reservoir turbidity to rise above 10 NTU Figure 3.11 Illustrates summer and winter turbidity response using data from two different storm events

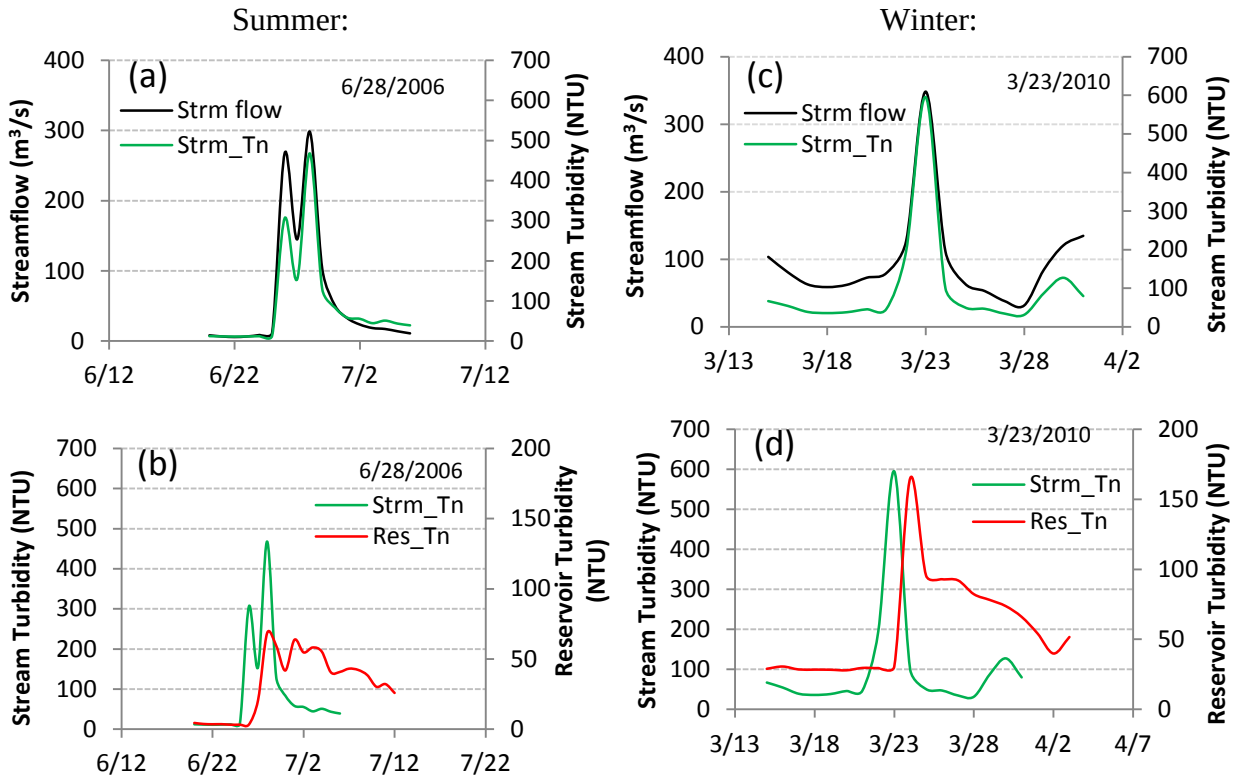

Figure 3.12. Similar size paired summer and winter event; the reservoir turbidity is at segment 28 (withdrawal point)

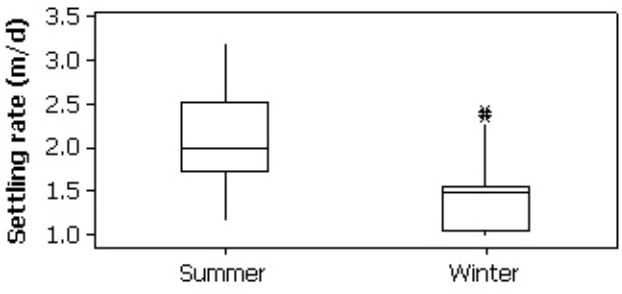

Figure 3.13. Summer and winter settling velocities based on Stokes' Law

For similar streamflow size events the reservoir turbidity was found to be higher in the winter compared to summer, as illustrated by the examples in Figure 3.12. These results can be explained given the fact that higher temperatures in summer lead to faster settling rates and resulted in lower turbidity (Figure 3.13). High turbidity events tend to be more frequent during winter. Because of the winter isothermal condition, the turbidity plumes have a longer travel time in the reservoir resulting in overlapping effects between consecutive turbidity events.

Event specific temperature-turbidity profiles in Ashokan reservoir

Longitudinal variations in simulated reservoir water temperature and turbidity are represented as color isopleths during summer and winter events and are shown in Figures 3.14-3.17. The reservoir temperature is stratified before the occurrence of an event during summer (Figure 3.14) and near isothermal during winter (Figure 3.16). During the summer event warmer epilimnetic temperature forms an upper mixed layer and the wind induced turbulence energy is not sufficient to establish an isothermal water column (Figure 3.14). The warmer epilimnetic temperatures in part reflect higher ambient air temperature during the summer event period. For these two events the summer and winter streamflow events are of similar size (Figure 3.12a), but summer event turbidity is found to be higher in upper few meters (5-10 m) and lower (< 5 NTU) below the upper mixed layer (Figure 3.15). This behavior is related to temperature (density) of input stream water matching temperature of epilimnion and turbidity being concentrated above thermocline and being transported as a plume due to slow settling of clay particles.

Before the winter event (Figures 3.16 and 3.17), the turbidity appears evenly distributed at about 30-40 NTU throughout the reservoir due to a preceding event. A turbidity plume is initially simulated to moves in the upper reservoir layer, but is soon dispersed throughout the largely isothermal water column.

The contrasting location of the plume during summer and winter conditions is dependent on the ambient stratification regime and the density of the inflow waters, whereas the magnitude of the impact is a function of the loading. In the case of the summer event (Figures 3.14 and 3.15) the reservoir is stratified and turbidity moves as a plume above the thermocline. For the winter event (Figures 3.16 and 3.17), the reservoir is near isothermal and turbidity is eventually mixed throughout the water column and moves as a plug from upstream to downstream.

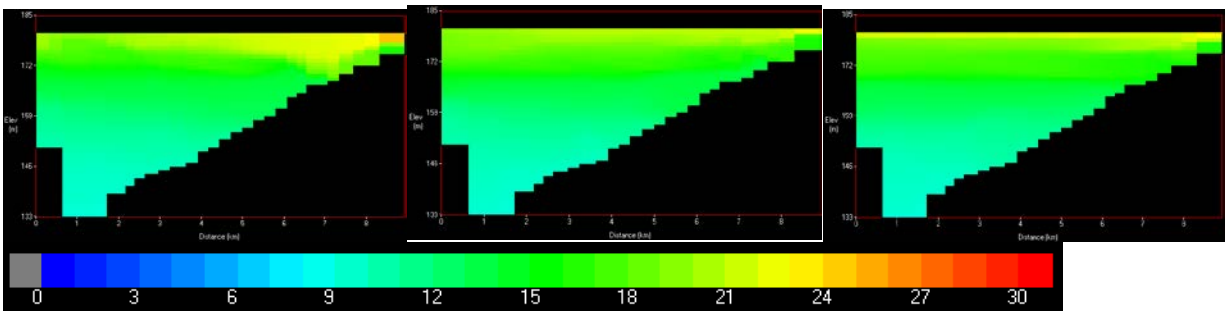

Figure 3.14. Temperature distribution before, during and after a summer event (06/28/2006)

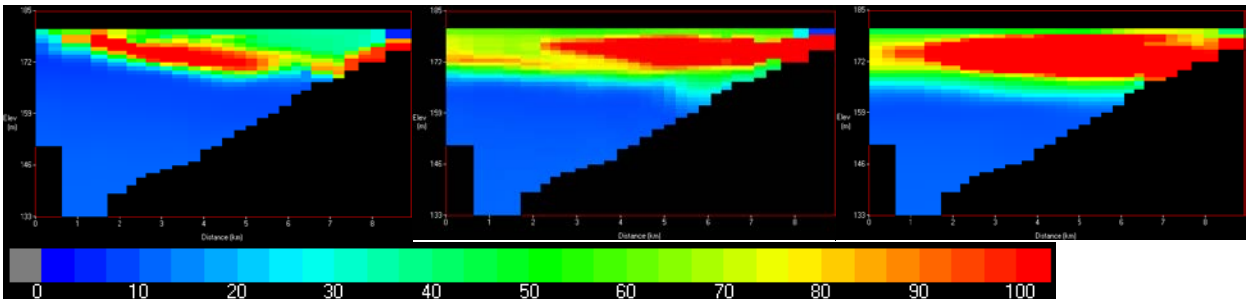

Figure 3.15. Turbidity distribution before, during and after a summer event (06/28/2006) (X-axis: Distance (km) from model segment 28 (0 km) to segment 1 (9 km); Y-axis: Elevation (m) from bottom (133 m) with scale factor 13 meter)

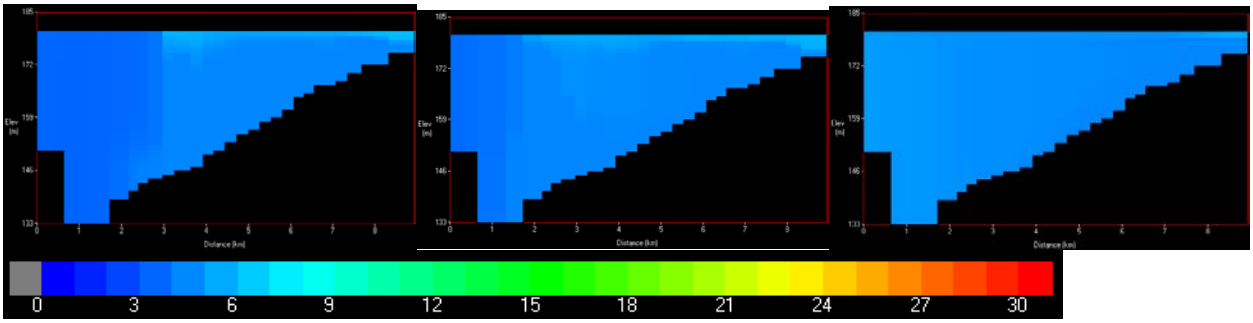

Figure 3.16. Temperature distribution before, during and after a winter event (03/23/2010)

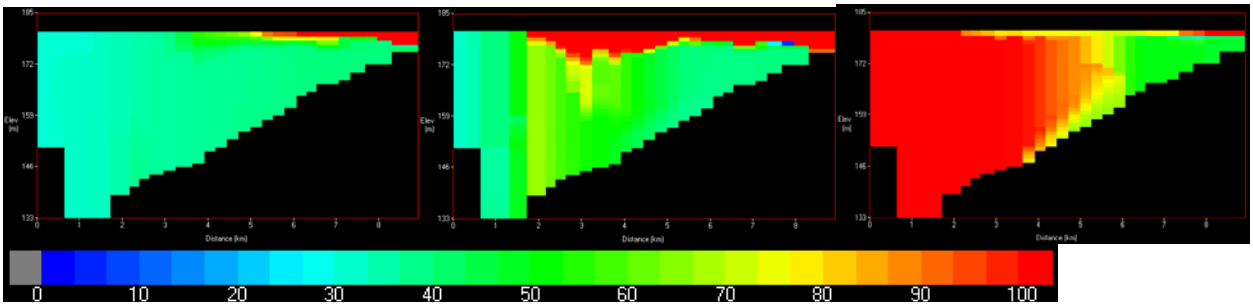

Figure 3.17. Turbidity distribution before, during and after a winter event (03/23/2010) (X-axis: Distance (km) from model segment 28 (0 km) to segment 1 (9 km); Y-axis: Elevation (m) from bottom (133 m) with scale factor 13 meter)

Driving parameters and reservoir turbidity under future climate

We have shown how Ashokan Reservoir experiences elevated turbidity levels following summer and winter events. In figure 3.18 through 3.21, we compared boxplots representing simulated average monthly future conditions for 2046-2065 (future_4665) and 2081-2100 (future_8100) time periods against baseline conditions for air temperature, streamflow, stream turbidity, reservoir water surface elevation, water temperature, reservoir turbidity and settling velocity. The boxplots represent the 25th (Q1) and 75th (Q3) quartiles (or the interquartile range) from all six climate change scenarios; for both time slices and baseline, the whiskers represent the lowest and highest data values within the lower (Q-1.5×(Q3-Q1)) and upper (Q3+1.5×(Q3-Q1)) limits; the dark horizontal lines in the box plots represent the median and the asterisks represent outliers.

The air temperature as shown in Figure 3.18 is projected to increase under future climate conditions with the difference from the baseline being slightly higher for the future_8100 period. The projected average increase in air temperature is +2.0 and +3.5 by future_4665 and future_8100, respectively. The summer and winter season average annual air temperatures is projected to increase by +2.1 and +1.8 by future_4665, whereas it is +3.3 and +3.7 by future_8100 periods. These values are consistent with seasonal trends in historical temperature where average increases in winter temperature are slightly higher than during summer (Hayhoe et al., 2007; Matonse et al., 2011). The higher winter temperature will lead to a reduction in snowpack and may cause more precipitation to fall as rain (Matonse et al. 2012). As a result of changes in snow and precipitation early winter streamflow is projected to increase (Figure 3.19a) under future climate scenarios. The streamflow is projected to decrease during March and April and show minor changes in the following months till October. A similar seasonal pattern is projected for stream turbidity (Figure 3.19b).

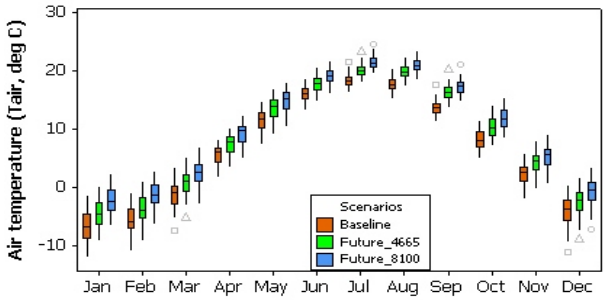

Figure 3.18. Average monthly air temperature (^{0}C) for the baseline and simulated future period (2046-2065) and 2081-2100.

Ashokan Reservoir seasonal water surface elevation (Figure 3.20a) is simulated to increase during the winter period. The reservoir water temperature (Figure 3.20b), which is a function of atmospheric forcings and inflows, shows a similar seasonal variation as air temperature (Figure 3.18). On average, the reservoir water temperature is increased by +1.0 (+1.8), +1.4 (+2.4) during summer and +0.6 (+1.3) during winter by future_4665 (and future_8100) periods. This is an indication of stronger stratification during summer but little change in the largely isothermal conditions during winter. The high winter turbidity and low summer turbidity (Figure 3.21a) under future climate scenarios are results of increased winter turbidity loading associated with increased future winter stream discharge and also to the variation in winter and summer settling rates (Figure 3.21b) of turbidity causing particles in the reservoir. The increase in future water temperature influences the mobility of suspended particles and consequently the settling rate.

Under future scenarios, the average annual streamflow is increased by 5% and 7%, which results in an annual increase in reservoir turbidity by 3% and 5% for the future_4665 and future_8100, respectively. However, the average winter reservoir turbidity is increased by 11% and 17% as result of increased in winter stream flow by 12% and 20% for the future_4665 and future_8100, respectively. The climate change scenarios clearly show a shift in timing of streamflow and turbidity loading to the reservoir from a peak in April to earlier in the winter (December-March). This shift in snowmelt driven events causes increased in-reservoir turbidity during December-March, and decreased turbidity in April-May as the peak events of April move to earlier in the year.

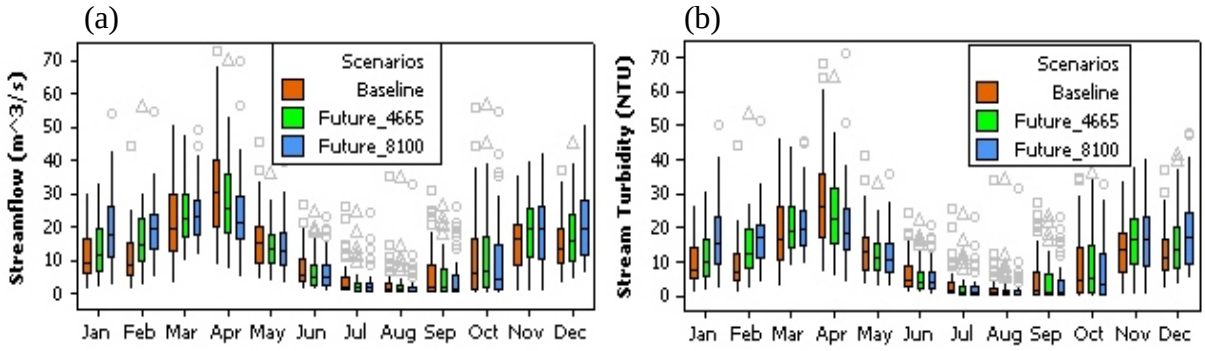

Figure 3.19. (a) Average monthly inflow (m^3/s); (b) Average monthly Stream Turbidity (Tn, NTU) for the baseline and simulated future period (2046-2065) and 2081-2100.

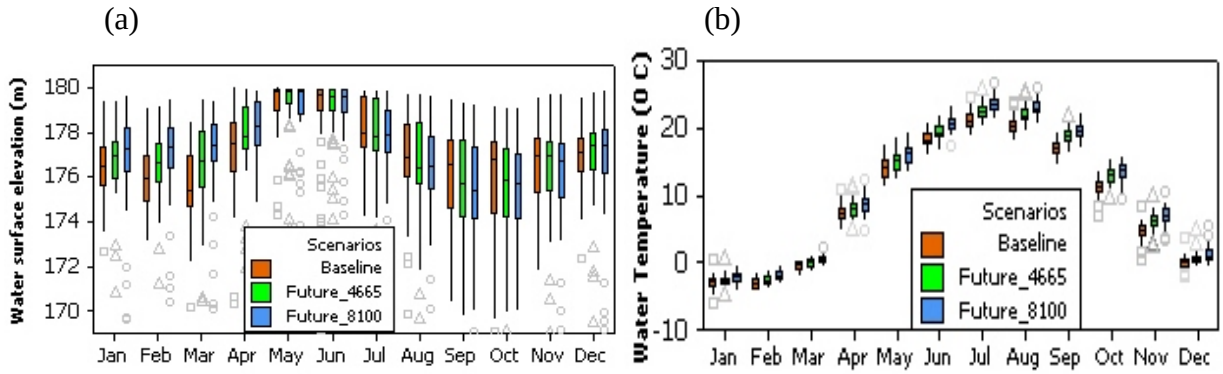

Figure 3.20. (a) Average monthly water surface elevation (m); (b) Average monthly in-reservoir water temperature (^{o}C) for the baseline and simulated future period 2046-2065 and 2081-2100.

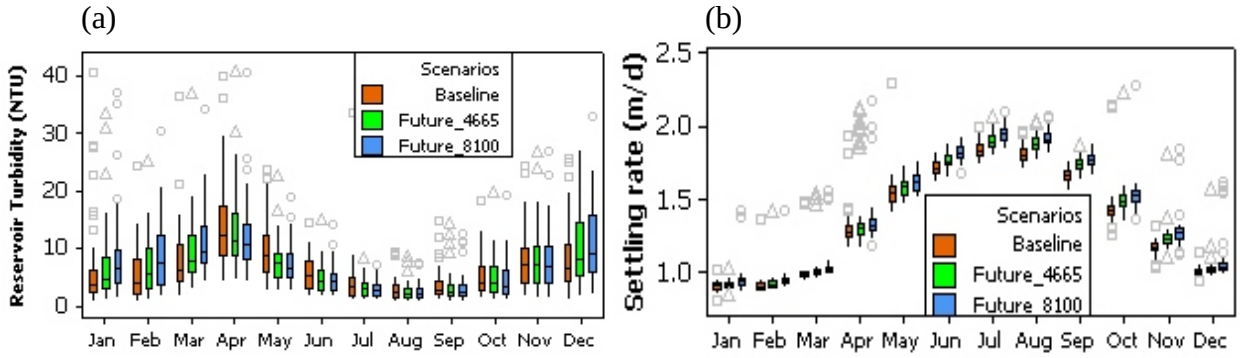

Figure 3.21. (a) Average monthly reservoir turbidity (Tn, NTU); (b) Average monthly settling velocity (m/day) for the baseline and simulated future period 2046-2065 and 2081-2100.

Conclusions

Our results show that the W2 model accurately simulates reservoir water surface elevation and event specific reservoir turbidity over a long term historical record. Based on seasonal and event based comparison, the model simulates higher reservoir turbidity during winter compared to summer. As a result of seasonal differences in thermal stratification the reservoir turbidity generally moves as a plume above the thermocline in summer following a storm event, while in winter turbidity is generally mixed throughout the water column.

Simulated future, reservoir turbidity levels are expected to change due to earlier snowmelt and resulting shifts in streamflow and turbidity load. Winter isothermal conditions are expected to continue in the future and as a result of relatively low water temperature turbidity settling velocity will remain low. This combined with higher projected future turbidity loads in the winter is expected to increase reservoir turbidity under winter conditions.

4. Model Development

4.1. Comparison of Snowpack Models for New York City Watersheds

Introduction

The ability to simulate snow, snowpack development, and snowmelt on both basin and finer scales is important for reservoir operational support, watershed management, and long-term planning of the NYC water supply. Snow is a substantial component of annual precipitation in mountainous regions around the world including NYC water supply watersheds in the Catskill Mountains. The pattern of snow accumulation and snowmelt has important implications for streamflow dynamics and for the management of water resources (Lundquist et al., 2005; Vicuna and Dracup, 2007; Matonse et al., 2011). On a broad scale the snowpack may vary considerably from one major reservoir basin to the next, as well as temporally, and operational responses to variability in basin snow water storage in winter are routinely made to optimize reservoir storage for spring melt. On a finer scale the spatial distribution within a basin of snowmelt as a pollutant diluting and transport agent has important consequences for water quality (Johannessen and Henriksen, 1978; Watson and Putz, 2012).

Snowmelt is a major contributor to spring refill of the NYC water supply reservoir system (Matonse et al., 2012). Spring refill has traditionally been of primary concern and a guideline for the operation of the reservoir system; a target of 100% system refill by June 1 drives operational decisions throughout the year via probability of refill analyses, which accounts for the current day's storage deficit, expected future water diversions and releases, and system-wide inflow forecasts (Matonse et al., 2011). This target and related operating rules have been incorporated in NYC Operational Analysis and Simulation of Integrated Systems (OASIS) model (HydroLogics Inc., 2007) that is part of an Operations Support Tool (OST) which simulates the outcome of alternative operational decisions based on short-term weather forecasts and historical patterns (DEP, 2011). Short-term near real time projections of basin inflows and storages, including snowpack, are used in OST to provide guidance for reservoir system operations. Basin-scale snowpack estimates are used in long-term hydrologic model simulations to estimate the potential effects of changing land use, climate on water quantity and quality (e.g. Johannessen and Henriksen, 1978; Stottlemyer and Toczydlowski, 1999; Suzuki, 2003; Matonse et al., 2012; Pradhanang et al., 2012; Pierson et al., 2012; Samal et al., 2012a).

The quality of water entering the reservoirs is increasingly a major driver of operational decision and watershed management. While nutrients, carbon, and sediment loads to reservoirs directly impact reservoir eutrophication, trihalomethane (THM) precursors and turbidity which are also regulated water supply constituents. Watershed loads depend on the spatial distribution of runoff in relation to landscape sources. The spatial distribution of snowpack and snowmelt within a basin has important consequences for water quality, and the ability to simulate these distributions is important for watershed water quality simulation modeling.

The potential effects of climate change on snowpack and the subsequent effect on water supply quantity and quality are actively being investigated in many regions around the world including NYC (Stewart, 2009; DEP, 2008b; Zion et al., 2011; Matonse et al., 2011 and 2012). An

increasing trend in air temperature has been observed for the Catskill region (Burns et al., 2007) and simulated climate change climatology and hydrology for the region has suggested a measurable impact on snowpack and streamflow in the NYC watersheds (Matonse et al., 2011; Zion et al., 2011). An observed shift in streamflow to earlier in the winter and spring associated with warmer winters, lower snowpacks, and shift from snow to rain events in winter/spring is expected to intensify under climate change (Matonse et al., 2011). These changes may have significant implications for reservoir system planning and management, as the basis for the traditional operational focus on spring refill and the snowpack contribution becomes less reliable (Matonse et al., 2012). Climate change studies rely on simulating watershed hydrology under varying future climate scenarios. Snowpack modeling is an important component of these modeling studies.

NYC currently estimates snowpack for the six major reservoirs in the Catskill and Delaware systems of the NYC water supply from bi-weekly snow survey data (Figure 4.1). Recently the Water Quality Modeling Section has begun to complement snow survey data with data from the NOAA National Operational Hydrologic Remote Sensing Center (NOHRSC) Snow Data Assimilation System (SNODAS), which combines the NYC snow survey data with observer station and remote sensing data and with simulation modeling to produce 1-km gridded near real time and historical sub-daily snow, snowpack, and snowmelt estimates (see Section 6.4). However, neither the snow survey data nor the SNODAS product satisfies the need to readily simulate snowpack under alternative meteorological scenarios.

Snowpack models vary in complexity and resolution. The simplest is the daily lumped-parameter temperature index approach, where the snowpack for a basin is a single storage of snow water equivalent (SWE) to which precipitation as snow is added and from which water as snowmelt is removed daily. A melt parameter that linearly relates snowmelt to air temperature is empirically determined (e.g. Fontaine et al., 2002). This approach has minimal data requirements and has been incorporated into widely used watershed water quality simulation models like GWLF (Haith and Shoemaker, 1987; Schneiderman et al.,, 2002, 2007) and SWAT (Neitsch et al., 2005; Arnold and Allen, 1996; Arnold et al., 1998). More complex snow models explicitly simulate an energy balance of snowpack and upper soil layers, at sub-daily time-steps, and as a spatially-distributed process such as in RHESSys model (Band et al., 2000; Tague and Band, 2004), and a newly developed distributed simplified process-based approach for SWAT (Fuka et al., 2012). With the added complexity comes increasing data requirements and depending on the objectives of the model application sometimes the end effect does not justify the additional effort (e.g. Watson and Putz, 2012).

We tested three snowpack modeling approaches of varying complexity and spatial resolution for their ability to simulate basin-average SWE for the major NYC reservoir watersheds and to simulate the spatial variability of snowpack within a basin. The three modeling approaches are a) the lumped-parameter temperature-index approach from the GWLF watershed model, b) a spatially-distributed temperature index (SDTI) approach, and c) the 1km gridded NOAA SNODAS product. Model testing included: comparison of simulated basin-average SWE to estimates based on snow survey data for each of the major reservoir watersheds of the NYC West of Hudson water supply; comparison of the spatial distribution of SWE as simulated by the spatially-distributed approaches (SDTI and SNODAS) to the collection of snow survey data

locations across the West of Hudson watershed area; and comparison of the statistical distributions of SWE within selected reservoir watershed basins for the two spatially-distributed approaches.

Study Site

For this study we used six watersheds that are major tributaries to water supply reservoirs for NYC within the Catskill Mountain region of New York State (Figure 4.1). These mountainous watersheds range in size from 100-859 km^2 and span an elevation range of 188-1276 m (Table 4.1). The watersheds are mostly forested with some agricultural land use (corn, hay, and pasture lands) within the Cannonsville watershed and, to a lesser extent, also within the Schoharie and Pepacton basins. A number of small hamlets are also scattered throughout the area. Except for a slight decline in agricultural activity in Cannonsville, there has been little change in land development over the past decade.

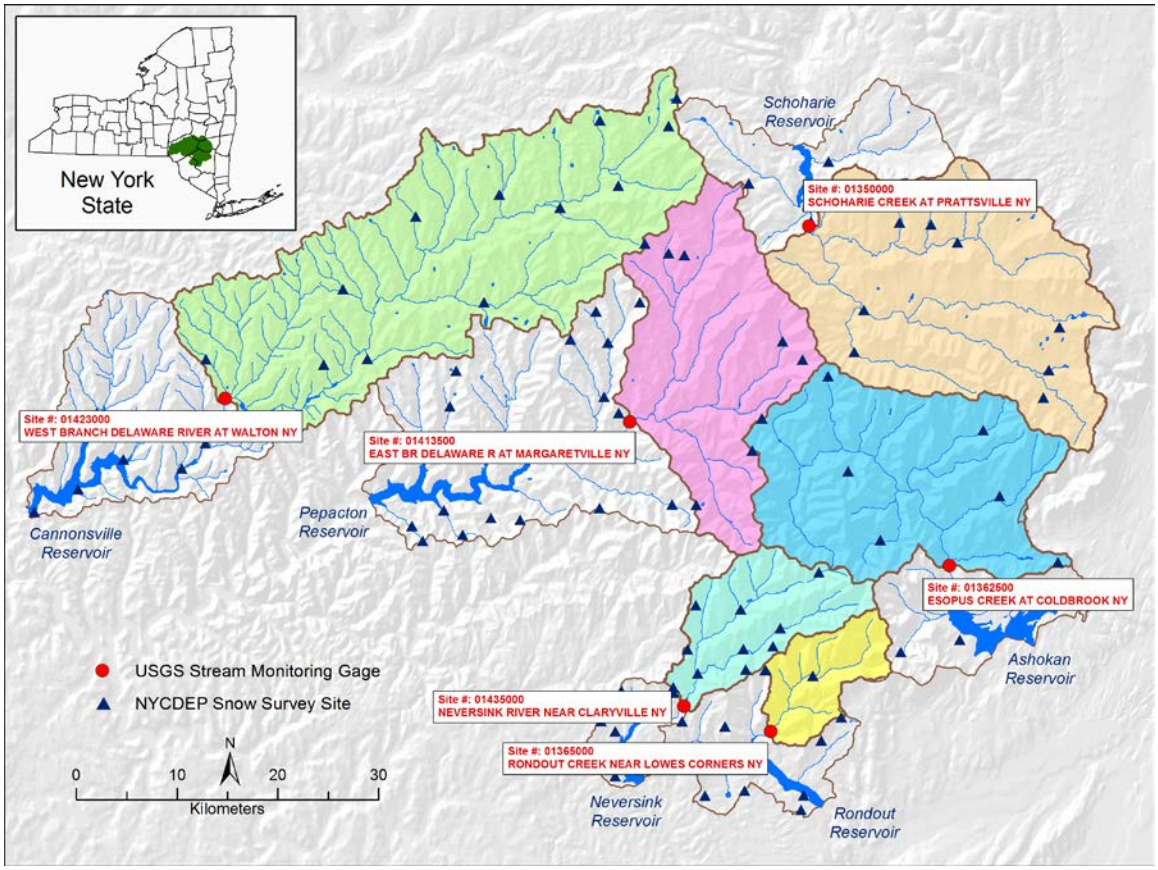

Figure 4.1. Snow Survey Sites and major gaged reservoir watersheds in NYC West of Hudson Water Supply

Table 4.1: List of study watershed characteristics.

Reservoir Watershed Name	USGS Gauge No.	Watershed Description	Watershed Area (km^2)	Mean Elevation (m)	Min. Elevation (m)	Max. Elevation (m)
Ashokan	01362500	Esopus Creek at Coldbrook	493.2	600	188	1276
Cannonsville	01423000	West Branch Delaware River at Walton	859.3	592	360	1020
Neversink	01435000	Neversink River near Claryville	172.5	770	463	1275
Pepacton	01413500	East Branch Delaware River at Margaretville	421.7	668	396	1181
Rondout	01365000	Rondout Creek near Lowes Corners	99.5	629	263	1175
Schoharie	01350000	Schoharie Creek at Prattsville	612.5	653	344	1234

Data and Methods

Meteorological Data

Gridded 4-km resolution daily precipitation, which could include both rain and snow, and air temperature data were obtained from the Northeast Regional Climate Center (NRCC) at Cornell University, Ithaca, NY. The product is available in near-real-time for the entire Northeast US starting in 2005 (http://compag.tc.cornell.edu/sciencegateway/) (See also Section 6.4). This product represents a high-spatial-resolution precipitation developed using radar-guided interpolation in which radar-based precipitation is adjusted on a daily time step using rain-gauge observations to reduce spatially varying errors in the radar estimates and assuming that rain-gauge values represent true values (DeGaetano and Wilks, 2009). Radar-based interpolation helps reduce model uncertainty by reducing interpolation errors independently from season or precipitation magnitude. Spatially-distributed air temperatures are estimated at grid points by interpolation from observation stations and application of an environmental lapse rate that adjusts for elevation effects on temperature. The precipitation data, obtained in a polar coordinate system, were re-gridded to match the air temperature 4-km grid by nearest neighbor analysis, and the final grid was clipped to produce a consistent spatial distribution of 324 4-km grid cells for the NYC west of Hudson watershed area (Figure 4.2.).

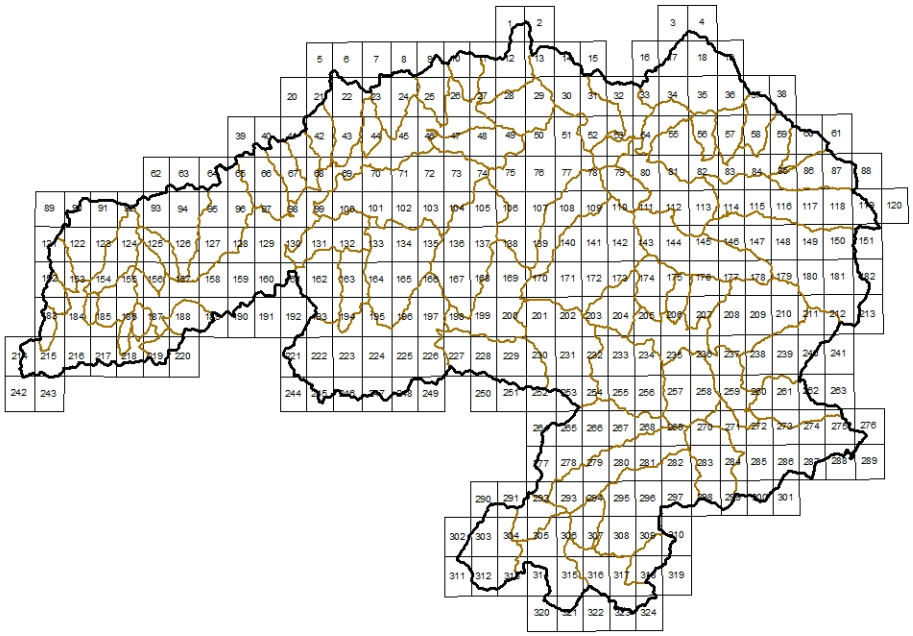

Figure 4.2. Spatially-distributed 4 km meteorological data grid for NYC West of Hudson watersheds.

DEP Snow Survey Data

The DEP snow survey at established sites (Figure 4.1) is conducted biweekly during the winter months. Snow cores are taken at each site and measured for SWE, starting around Jan.1 and continuing through April. Sixty seven sites with contiguous records from 2005-2011 were used in this study. The sample sites are located throughout the west of Hudson watersheds at varying elevations from 257 to 826 m above sea level. For each of the major NYC reservoir watersheds (Table 4.1) the basin-average SWE was estimated by simple arithmetic average of the survey site measurements within the basin. For purposes of analyzing model performance in simulating snow survey site to site variability, the snow survey sites were characterized by elevation band (low: 250-450m, medium: 451-650m, and high: 651-850m); land use (forest (evergreen, deciduous, and mixed); agriculture (row crop, pasture and hay); and commercial (high intensity commercial/industrial); and aspect (8 compass directions).

SNODAS Product

Gridded SNOw Data Assimilation System (SNODAS) snow water equivalent (SWE) and snowmelt were downloaded for this study from the National Operational Hydrologic Remote Sensing Center (NOHRSC) web site (www.nohrsc.noaa.gov). SNODAS is a modeling and data

assimilation system developed by the NOAA National Weather Service's (NWS) NOHRSC to provide to the research and management community the best possible estimates of snow cover and associated parameters. SNODAS aims to achieve a physically consistent framework that integrates snow data from satellite, airborne platforms, and ground stations with model estimates of snow cover from the numerical weather prediction (NWP) model for the conterminous U.S. (CONUS) (Carroll et al., 2001; Carroll, 2005). To implement this process first the original 13 km^2 resolution NWP forcings are downscaled to a 1 km^2 resolution; downscaled NWP estimates of air temperature, relative humidity, wind speed, precipitation, incident solar radiation, and incident long wave radiation forcings are then used as inputs to the NOHRSC Snow Model (NSM). The NSM is an energy-and-mass-balance, spatially-uncoupled, vertically-distributed, multi-layer snow model that runs operationally at 1 km^2 spatial resolution and hourly temporal resolution of the CONUS input data. Driven by gridded NWP climate data, NSM has run continuously at hourly time steps since the 2004-2005 snow season in an operational mode (see also Section 6.4).

Temperature Index Snowpack Models

The lumped-parameter temperature index snowpack algorithm in the GWLF model (Haith and Shoemaker, 1987; Schneiderman et al., 2007) is as follows. Daily precipitation is snow that is added to the snowpack if mean daily air temperature (T) <= 0 ^oC, otherwise it is rain. Daily snowmelt occurs when T exceeds 0 ^oC at the rate of the product of the melt coefficient and air temperature ($cm \cdot day^{-1}$) but not to exceed the available water in SNOWPACK. SNOWPACK is a storage which is updated daily by snow additions and snowmelt withdrawals as SWE.

$$SNOW(t) = P(t) \text{ if } T(t) <= 0\ ^oC, \text{ else } 0 \quad (4.1)$$

$$RAIN(t) = P(t) \text{ if } T(t) > 0\ ^oC, \text{ else } 0 \quad (4.2)$$

$$SNOWPACK(t) = SNOWPACK(t-1) + SNOW - SNOWMELT(t) \quad (4.3)$$

$$SNOWMELT(t) = \min(SNOWPACK(t-1), \text{Melt Coeff} * T(t)) \text{ if } T(t) > 0\ ^oC, \text{ else } 0 \quad (4.4)$$

where (t) denotes current time step (day) and (t-1) denotes previous day, and P denotes daily precipitation.

A spatially-distributed temperature index (SDTI) model based on the GWLF algorithm (equations. 4.1-4.4) was developed and applied by first dividing up the watershed into 4km meteorologic zone cells (Figure 4.2) that correspond to the grid of available spatially-distributed meteorological (precipitation and air temperature) data from the Northeast Regional Climate Center (NRCC). Each 4-km grid cell is further sub-divided by elevation band. Air temperature for each meteorologic zone/elevation band is calculated from the cell air temperature modified by the product of a lapse rate and elevation difference between the meteorologic zone grid point and the mean elevation of the elevation band. The model calculates air temperature, snow vs. rain, snowpack and snowmelt for each meteorologic zone /elevation band in the watershed.

Model Calibration and Testing

The two temperature index models were calibrated by adjusting the melt coefficient to maximize the Nash-Sutcliffe coefficient (NS) of model efficiency (Nash and Sutcliffe, 1970) for observed (snow survey) basin-average SWE vs. modeled SWE for the calibration period. The six year period of available snow survey data was split into a three year calibration period (2005-2008) and three year validation period (2008-2011). The NS model efficiency and differences in mean results were used to evaluate model fit to measured data during the calibration and validation periods.

Results

Daily Basin Averaged SWE

The basin average of DEP snow survey data from 2006 to 2011 are compared with the results of the lumped parameter GWLF-VSA watershed model, the SDTI model, and SNODAS product. For each date with available data, all of the snow survey measurements of SWE within each watershed were averaged to obtain a basin average SWE value.

The scatterplots of the daily results of the two models and the SNODAS product versus the basin averages snow survey SWE are shown in Figure 4.3 and the NS efficiency and mean values for each basin and model are shown in Figure 4.4. Overall, the scatterplots show that both the two models and the SNODAS product reasonably capture the temporal variability found in the average snow survey data (Figure 4.3). The NS efficiency coefficients (Figure 4.4) for the lumped GWLF model appears to perform similarly to SDTI for most watersheds except in Schoharie watershed where the NS efficiency for the GWLF model during the validation period is quite weak (0.05). Much of this low value is due to an individual point at Schoharie in March of 2010 when the survey recorded 15.3 cm of SWE and the model has melted the snowpack completely. The NS efficiency for the SNODAS data is also fairly consistent across each of the basins, except for Schoharie, where the SNODAS tends to give a considerably higher estimate of SWE than the survey average.

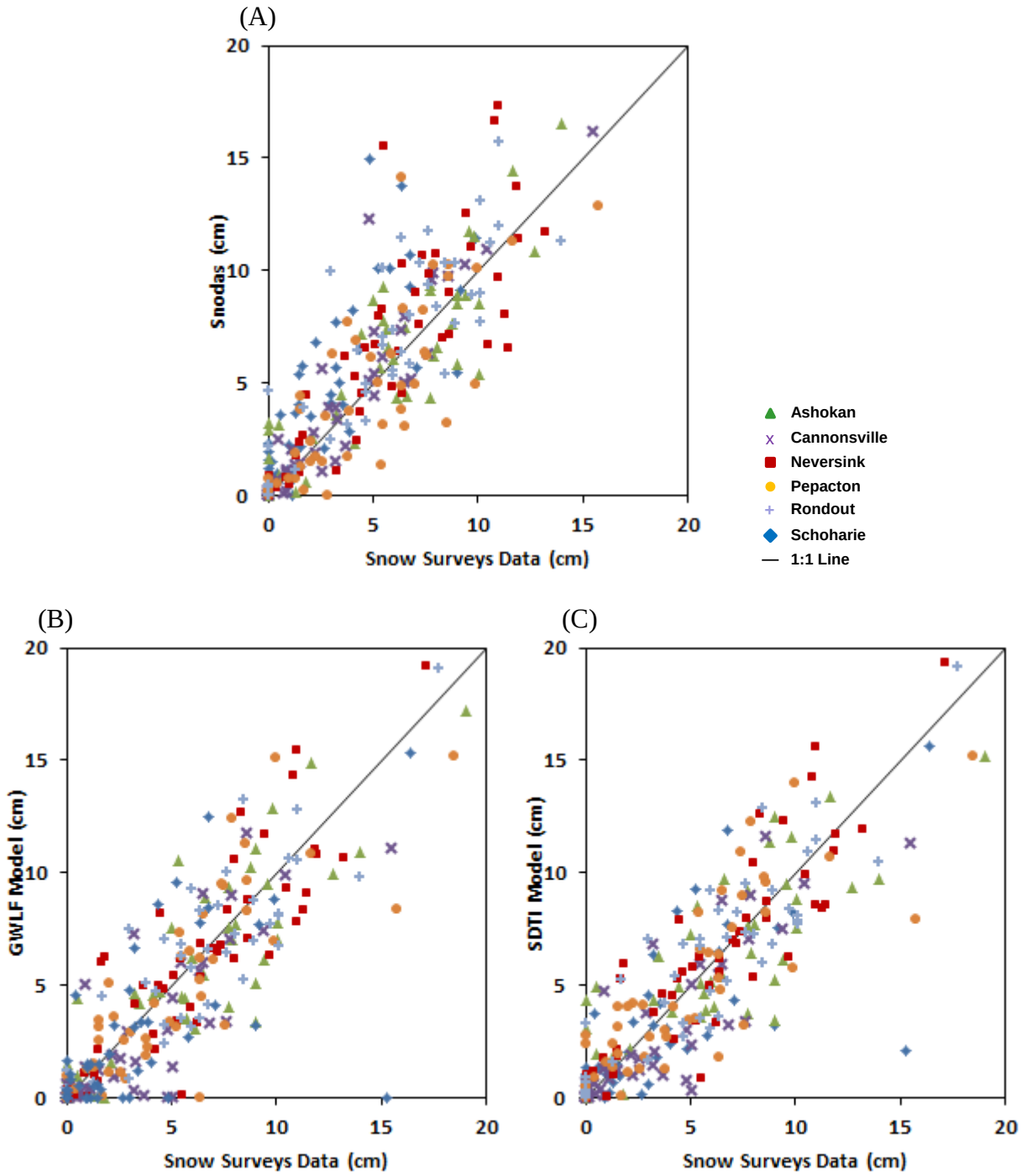

Figure 4.3. Scatterplots of daily basin average SWE as estimated by (A) SNODAS, (B) the GWLF model and (C) the SDTI model versus daily average SWE as measured at DEP snow survey sites.

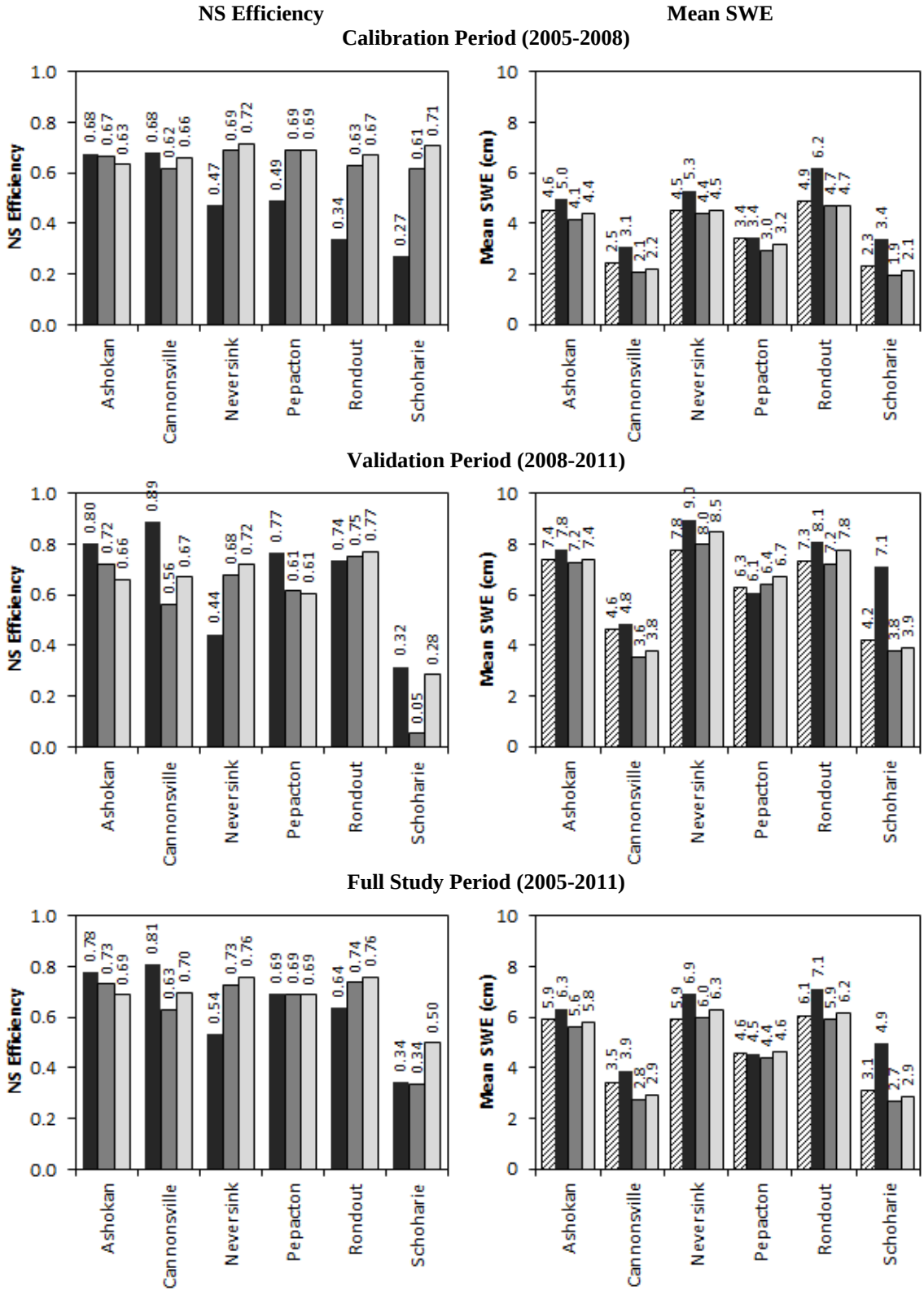

Figure 4.4. NS efficiency and mean values for each basin for SNODAS product (black), GWLF model (medium grey) and SDTI model (light grey) compared to DEP snow survey basin average values (striped).

Looking at the basin mean SWE for the full period (Figure 4.4 – lower right panel), the average basin SWE derived from the SNODAS product tends to be greater than both the snow survey average and the average of the two model results. This higher estimation is also evident in the scatterplot (Figure 4.3A). Since the GWLF and SDTI models were calibrated to the basin-average snow survey data, it makes some sense that these calibrated models would estimate the basin average of the snow survey data well. It is important to note, however, that the snow survey sample sites may not adequately represent high elevations and thus the basin-average estimates of SWE based on simple averaging of the snow survey data may underestimate the "true" basin-average SWE. Therefore, the differences between the SNODAS and snow survey average could be due to the potential low bias in the survey average or, it could be that the SNODAS product is reporting a value that is higher than the "true" snowpack value.

A closer inspection of example winter time series of model, SNODAS and survey results illustrates some issues with each of the SWE estimations. Figure 4.5 shows the winter time series of average basin SWE for Schoharie and Neversink watersheds for the winters of 2008-2009 and 2009-2010. As noted previously, the high estimate of the SNODAS product as compared to the survey data is quite apparent for the Schoharie watershed for the 2009-2010 period, however, in Neversink the SNODAS product tracks well with the average survey data for both winters.

In each of these cases illustrated in Figure 4.5, the two models, GWLF and SDTI, seem to track fairly closely. This makes sense as the model use similar temperature index algorithms and the input meteorological forcings are based on the same underlying data. The only difference between these two models is the spatial resolution of the snowpack algorithm. This difference is most apparent at the end of the season when the SDTI model tends to continue to show SWE values for a few extra weeks in the spring. This is due to the SDTI model having areas of snowpack at higher elevations that take longer to melt, while the lumped GWLF model, with its average snowpack and average temperature forcings does not explicitly account for the colder portion of the watershed. In the Neversink examples, it is interesting to note that the timing of the spring melt for the SDTI model and the SNODAS match quite well, suggesting that the spatial distributed component of the SDTI model is helpful in accounting for this elevation related process.

Since the GWLF and SDTI models are not adjusted to match the measured snow course data, differences in model results and survey data can persist for long periods into the winter. For example, in the Neversink watershed, the GWLF model estimated about 1.5 cm less SWE than the survey data indicated by mid-January 2010. This difference then persisted and remained about the same through late-February.

(a) Schoharie Watershed, Winter 2008-2009

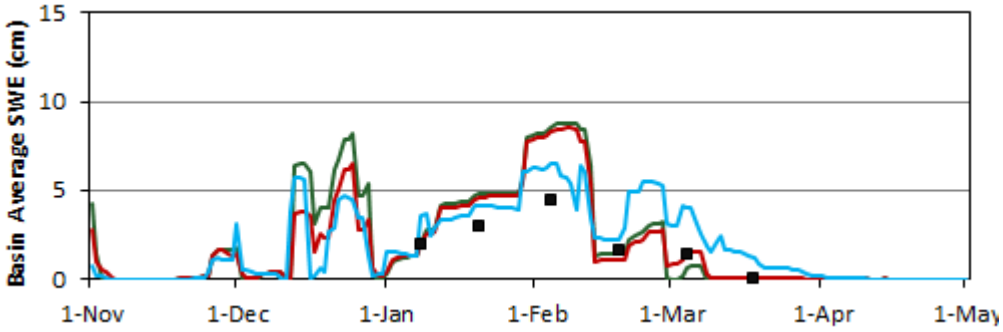

(b) Neversink Watershed, Winter 2008-2009

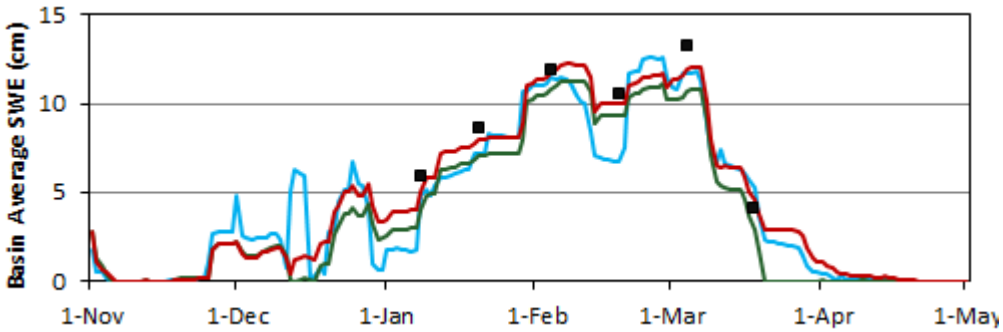

(c) Schoharie Watershed, Winter 2009-2010

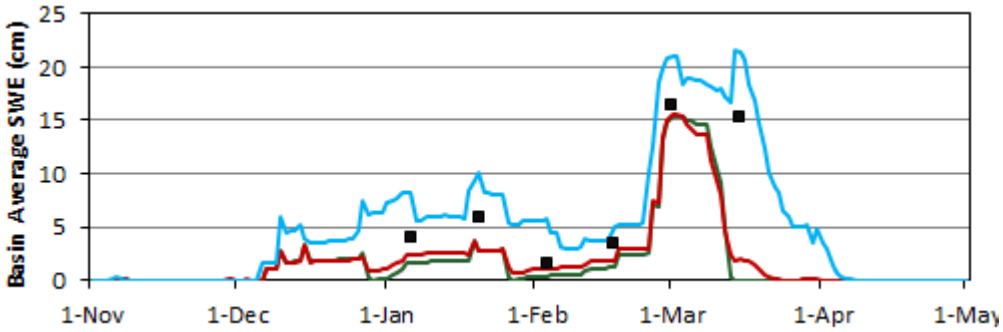

(d) Neversink Watershed, Winter 2009-2010

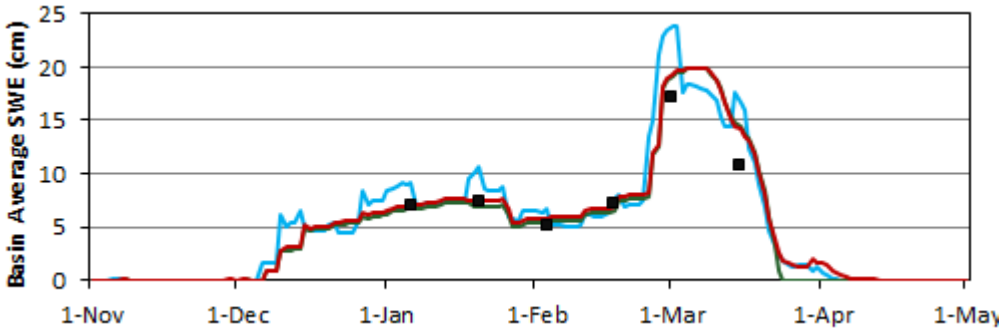

Figure 4.5. Example time series of basin average SWE with average of DEP snow survey measurements (black squares), SNODAS product (light blue), GWLF model results (green) and SDTI model results (red) for Schoharie and Neversink watershed for winters of 2008-2009 and 2009-2010.

Spatially-Distributed SWE

The SDTI and SNODAS simulate SWE on a gridded format across the six watersheds. The scatter plot in Figure 4.6 is based on all grid cells in our study area that overlap with a snow survey location on the ground. Each dot in the scatter represents a pair of model versus survey data. In general the SNODAS plot appear closer to the 1:1 line and show a lower spread at all ranges of SWE compared to SDTI, which, as was the case with the lumped GWLF estimates, tends to under predict large SWE values. Figure 4.6 clearly shows that SNODAS simulates site to site variability in SWE quite well, while SDTI tends to underestimate snow survey site SWE and does not simulate site to site variability well.

Figure 4.7 scatterplots depict how elevation, land use and aspect impact SDTI and SNODAS performance to simulate measured SWE. With respect to elevation SNODAS appears to slightly and systematically overestimate SWE at all elevation ranges (lower Figure 4.7A). SDTI appears to perform well at the lower elevations while underestimating SWE at medium and high elevations (upper Figure 4.7A). Figure 4.7B reveals no direct relationship between performance and land use for both models. Clow et al. (2012) compared SNODAS SWE to point measurements in the Colorado Rocky Mountains and found the model did well in forested areas but showed poor agreement with measurements in Alpine areas, seemingly due to wind redistribution of snow in open areas. Therefore, fine-scale wind-induced spatial variability of SWE at the snow course locations may hinder the use of individual point measurements to represent aerial representations of SWE for model calibration and testing. As most of the snow accumulates during winter, when deciduous trees have no foliage, the wind effect appears less significant in our study area. With regard to aspect (Figure 4.7C) there are differences between the two models: SDTI show no pattern for S, E, SE, and SW facing sites (though with SWE of most locations below the 1:1 line, except for S facing sites where values are more evenly distributed above and below the 1:1 line) while SNODAS systematically overestimates SWE on these sites; SDTI underestimate NE while SNODAS overestimate NE; SDTI underestimates NW while SNODAS shows no pattern; Both models show no pattern for N and W facing sites.

In Figure 4.8 we compare SNODAS and SDTI statistical distributions of SWE for selected daily events across three basins during the 2007-2008 winter period. Of interest are patterns indicating accumulation and melting processes, starting December 15th and ending March 30th. The two models appear to simulate the sequence of the two processes similarly though the magnitude of SWE associated with individual cumulative frequencies by each model may be different and reflect the results in Figure 4.6. The difference in pattern among basins can originate from different basin location, topography and timing of snowfall as well as other basin characteristics.

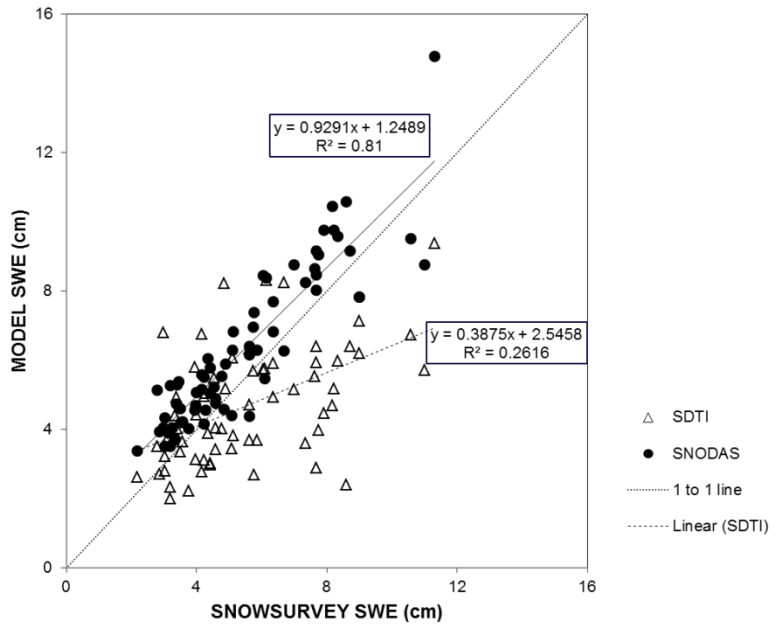

Figure 4.6. Scatter plot of model versus snow survey SWE in centimeters.

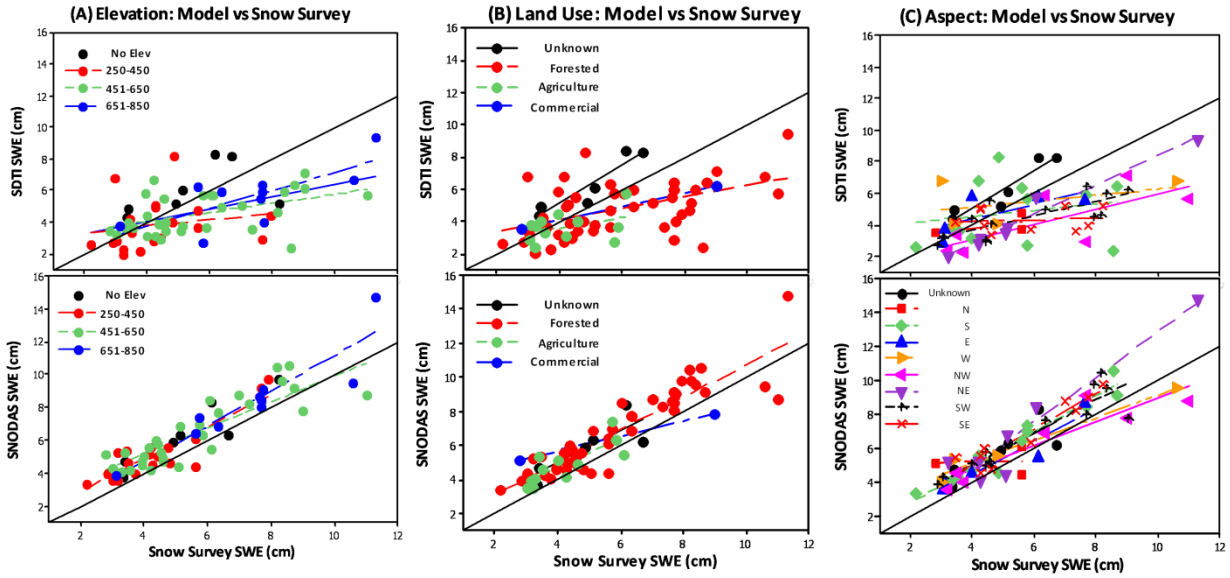

Figure 4.7. Scatter plots of model versus snow survey SWE in centimeters. The plots illustrate the model performance as a function of (A) elevation, (B) land use, and (C) aspect. The upper row shows the SDTI results; the bottom row shows the SNODAS results. The black diagonals represent a 1:1 line.

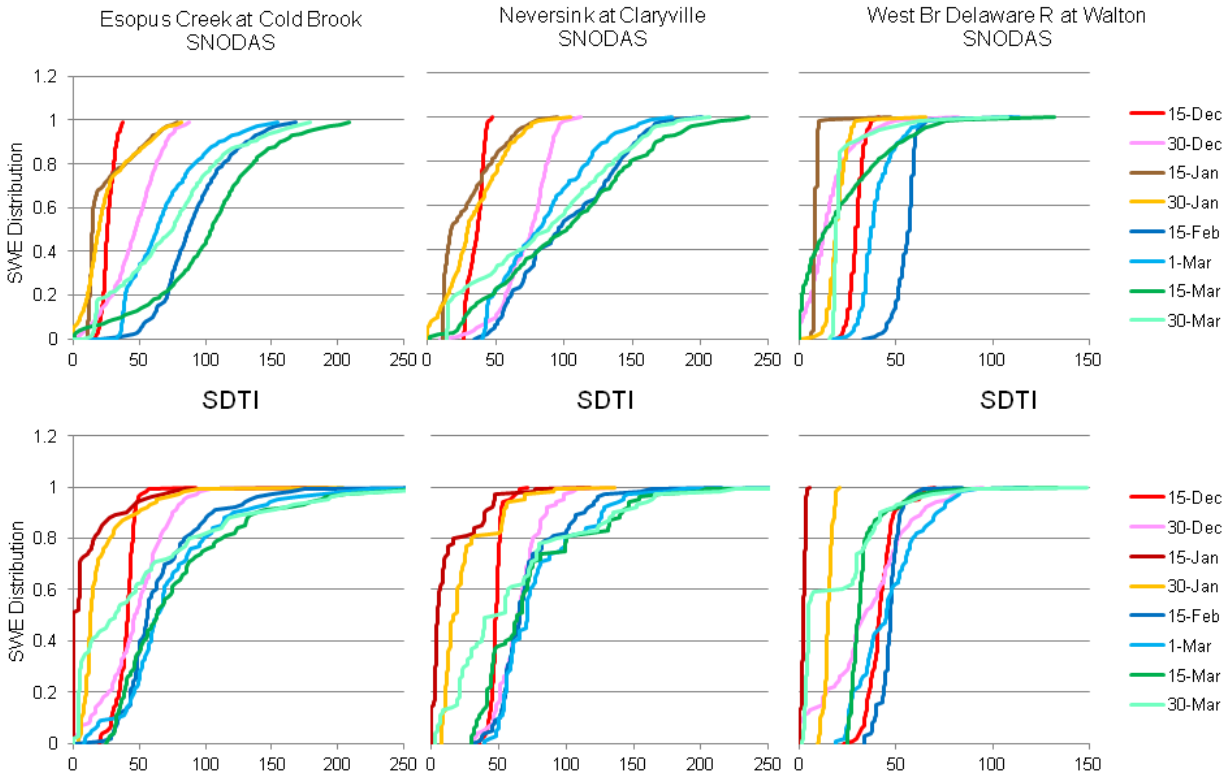

Figure 4.8. Comparison of SDTI and SNODAS SWE distributions for selected days during the winter of 2007-2008. Top row is based on the SNODAS simulated SWE Bottom row is based on simulated data from the SDTI model.

Summary and Conclusions

In this study we compared 3 different snowpack modeling approaches – the NOAA SNODAS product, a basin-scale temperature index model (GWLF), and a spatially-distributed temperature index model (SDTI) – against snow survey data. The models were tested based on the simulation of basin-scale average snowpack SWE, the spatial distribution of SWE within each watershed and SWE measured at point locations within a basin. The SNODAS product is fundamentally different from the two other model approaches in that SNODAS combines simulation model results with both remotely sensed and observer station snowpack data to produce historical and near real time estimates of the snowpack and other snow variables (Houser et al., 1998; Mandapaka and Germann, 2010; Clow et al., 2012). In this hybrid model-data approach the model effectively extends the data beyond the spatial location(s) of data sampling points while the data is used to nudge the model results to as closely match the measured data as possible (Simanton and Osborn, 1980; Paniconi et al., 2003). It is challenging for even the hybrid approach to estimate the spatial distribution of SWE particularly in areas with high spatial variability of SWE. Nevertheless this approach should provide the best available SWE estimates, based on both data and modeling. The disadvantage of the hybrid approach is that it is by nature retrospective and not useful for forecasting and simulating future scenarios, though NOAA is experimenting with short-term snowpack forecasts, presumably

using the underlying snowpack simulation model results stripped of the data assimilation components of SNODAS.

All three modeling approaches performed well in estimating basin-scale SWE for most of the basins studied. Comparison of modeled SWE vs. snow survey data (Figure 4.4) showed better NS fit by SNODAS for some but not all basins. SNODAS tended to estimate a higher basin SWE when compared to a snow course average in 5 of the 6 basins. Both TI models yielded similar basin-average estimates. It must be noted that basin average snow survey SWE data estimation assumes that the snow survey sites are an unbiased representation of the entire basin area, which is an unverified assumption. Results were somewhat equivocal regarding a "best model" for basin-scale estimation. Basin-scale SWE estimation is important for modeling basin-outlet streamflow. Several widely-used continuous simulation watershed models utilize a TI approach for snowpack modeling. Our results suggest that for NYC reservoir watersheds that the SDTI and the lumped GWLF approach yield comparable snowpack, except late in the snow season when the SDTI approach simulates a longer lasting snowpack due to simulation of a high-elevation snowpack. That said, the simpler basin-scale TI approach with the least data requirements may be sufficient for the purposes of basin-average SWE estimation.

In estimating the spatial distribution of SWE in the NYC watersheds the SNODAS product performed well, and clearly showed better agreement to snow survey data than the SDTI approach (Figure 4.6). The performance of SNODAS may reflect the retrospective assimilation of SWE data from the Catskill Mt. region in the gridded SWE estimates, and/or better performance of the process-based SNODAS simulation model relative to the TI approach. Fuka et al. (2012) suggest process-based snowpack models may simulate the spatial distribution of SWE better than TI models. We did not find systematic errors in the SDTI model results related to aspect or vegetative cover (Figure 4.7) that might suggest that incorporation of these variables into the SDTI model could improve its performance. While the ability to simulate site to site SWE variability with the SDTI approach may be wanting, SDTI did simulate the statistical distribution of SWE within a basin similarly to SNODAS (Figure 4.8).

4.2. A Planning Level Tool to Identify Stream Channel Erosion Sites

Introduction

Sediment is one of the top pollutants impacting water quality in over 100,000 miles of streams and rivers in the United States (USEPA, 2006). Studies have shown that as much as 85-90 % of watershed sediment yield could be from streambank erosion (Wynn and Mostaghimi, 2006; Simon and Klimetz, 2008). Identifying stream reaches based on the potential for channel erosion is important for prioritizing stream restoration projects, and for improving our understanding of the effects of channel erosion on stream water quality. As a screening tool, predictions of spatial variations in the susceptibility of stream banks to erosion within a watershed can be used to quickly identify potential sites of stream restoration projects for improving channel stability and water quality.

Accurate prediction of stream channel erosion at the watershed scale is challenging due to the complexity of the erosional process as well as variation in erosion rates in both space and time (Bartley et al., 2008). Current hydrologic models capable of predicting stream channel erosion vary in level of complexity and applicability. Simple models such as the ArcView Generalized Watershed Loading Function (AVGWLF) (Evans et al., 2003) use an empirical function that accounts for watershed characteristics when predicting channel degradation. More complex models such as Conservational Channel Evolution and Pollutant Transport System (CONCEPTS) (Langendoen, 2000) can simulate fluvial erosion and bank failures, but require detailed input data requirements that may limit its applicability. An intermediate approach to assessment of stream channel erosion at the watershed scale is taken in the Soil and Water Assessment Tool (SWAT) (Neitsch et al., 2005). The SWAT model uses a modified stream power equation for simulating fluvial erosion within a channel. Stream power has been widely used to explain channel processes such as sediment transport (Bagnold, 1966, 1977) and streambank erosion (Lawler et al., 1999). Several authors have observed a non-linear trend in downstream variation in stream power (Lane et al., 1994; Lawler, 1992, 1995; Knighton, 1999). Barker et al. (2009) reported that this non-linear trend may be useful in identifying reaches where fluvial adjustment processes including bank erosion are most apparent. According to Thorne et al. (1997), medium and long term streambank retreats are fluvially controlled irrespective of the precise failure mechanism, nature of the bank material, erosion and weathering processes.

In this study we compare stream power based estimates of channel erosion susceptibility to channel erosion sites identified using the bank erosion hazard index (BEHI) and rapid geomorphic assessment (RGA) indices at the reach scale. The two different indices were used because they represent the best available field verification data for the study sites. The test is done on three catchments: the Stony Clove Creek in the Catskill Mountains north of New York City (NYC) that drains into the Ashokan Reservoir, one of the drinking water reservoirs of the NYC water supply system; the North Fork Broad River in the Georgia Piedmont, USA; and the Choteau Creek in the glaciated plains of South Dakota, USA. These catchments were chosen because rapid channel erosion assessment methods had been applied along with the substantial field data collection needed to calculate these indices. The objective of this study is to test a simple stream power based approach for ranking the relative susceptibility of channel reaches to degradation caused by fluvial erosion at the watershed scale. To do so we evaluate whether the

relative contributions to sediment yield from different stream reaches calculated according to our stream power model are consistent with those given by rapid assessment methods.

Methods

Stream power estimation

Reach -scale variation in fluvial adjustments such as bank retreat is influenced by the stream power that can be defined as the energy available within the channel for overcoming channel resistance and sediment transport. Stream power per unit channel length can be expressed as (Bagnold, 1966):

$$\Omega = \rho g Q S \qquad (4.5)$$

where Ω is the total stream power per unit length of channel (W m^{-1}), ρ is fluid density (kg m^{-3}), g is acceleration due to gravity (m s^{-2}), $\underline{Q}$ is discharge (m^3 s^{-1}) and S is the longitudinal channel slope. Another expression of stream power is specific stream power which is a measure of the rate of energy expenditure per unit area of channel bed and is expressed as:

$$\omega = \frac{\Omega}{W} \qquad (4.6)$$

where ω is specific stream power (W m^{-2}) and W is the average width (m) of the channel over the length of the reach.

Stream power calculation by reach

Total and specific stream powers were calculated for each stream reach in the three watersheds at bankfull discharge. Bankfull discharge is the maximum discharge that can be contained within the channel without overtopping the banks (Leopold et al., 1964). Bankfull discharge for each reach of Stony Clove Creek was calculated using the regional curve equation for the Catskill region (Miller and Davis, 2003). Bankfull discharges for the stream reaches in the NFBR and for Choteau Creek were calculated using the regional curve equations for the Piedmont and the Northwestern Glaciated Plains respectively (Simon et al., 2004). Watershed delineation and determination of channel slope and geometry for the three watersheds was done using the watershed delineation interface for the ArcSWAT model. A Digital Elevation Model (DEM) of 10-m resolution obtained from the DEP was used for the Stony Clove basin and a 30-m resolution DEM developed by the USGS was used for the other two basins. The ArcSWAT model uses ArcGIS Spatial Analyst tools including the flow direction, flow accumulation and stream link algorithms for watershed and stream network delineation from DEMs. For calculating stream width and depth the ArcSWAT interface uses a two-step approach. In the first step a neural network (Muttiah et al., 1997) is used to predict the two-year peak stream discharge This network is trained using discharge, drainage area and elevation data from regional basins throughout the United States. In the second step width and depth are derived from a regional regression analysis relating channel geometry to stream discharge (Allen et al., 1994). For each reach, slope is calculated based on the difference in elevation between the upper and lower end of the reach and the length of the reach.

Stream power mapping for channel assessment

While the above analyses were used to establish relationships between reach scale variation in stream power and channel erosion indices, they do not identify specific locations within a reach that may be susceptible to channel erosion due to excess shear stress from high stream power. To estimate fine scale variations in stream power which could be used for inter-reach analyses, we developed a geographic information system (GIS) tool for mapping the longitudinal distribution of stream power along a stream network following the method used by Vocal-Ferencevic and Ashmore (2011), and we tested this method using differing resolution DEM data available at the Stony Clove site. In this approach streamflow is routed from one upstream cell (pixel) to one downstream cell thus creating a channel network that is one cell wide. Figure 4.9 describe the steps involved in calculating stream power for each cell in the network.

Most steps in the process were straightforward except for calculation of channel slope. When calculating the slope for an individual DEM cell in a GIS framework, algorithms typically consider the eight adjoining cells and identify the rate of maximum change in z-value for each individual cell. However, in our analysis the "horizontal slice slope" approach (Knighton, 1999; Jain et al., 2006) was used for slope calculation, and we calculated slope in the direction of the stream channel to estimate channel slope for use in the total stream power equation. Measuring channel slope over short distances may provide extreme local values that are not representative to the scale of study. However, slope calculation over too long a distance may smooth out local variations in features along the longitudinal channel profile (Vocal-Ferencevic and Ashmore, 2011). We used a moving window of 100-m radius on either direction of the cell of interest (that is part of a channel) for estimating and mapping channel slope along the stream network.

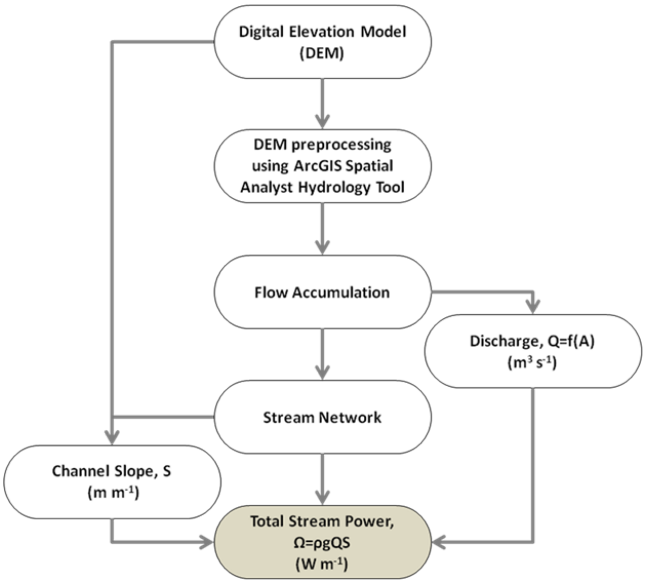

Figure 4.9. Flow chart of GIS processes involved in estimating stream power

The stream channel slope tool was tested for the Stony Clove Creek using two DEMs; a 1:24 k USGS quad contour derived DEM at 10-m spatial resolution and a LiDAR derived DEM of 3-m spatial resolution. Stream discharge estimates were based on the bankfull discharge calculated using the regional curve equation for the Catskill region that relates drainage area to bankfull discharge (Miller and Davis, 2003). Peaks in total stream power along the longitudinal channel profile were compared to real channel features using high resolution (30cm) aerial photography.

Results and Discussion

Comparison of reach scale stream power and rapid channel assessment indices

A summary of the relationship between specific stream power and the rapid channel assessment indices within the same reaches is shown in Figure 4.10. Results in Stony Clove Creek showed good correlation ($R= 0.70$, $P<0.05$) with BEHI scores. Comparison of specific stream power to channel stability index based on RGA was carried out in nine reaches of the main stem in the NFBR watershed. This analysis showed that channel stability index was highly correlated ($R= 0.77$, $P<0.01$) to specific stream power. Like the other two watersheds, stream reaches in the Choteau Creek also showed good correlation ($R= 0.89$, $P<0.001$) when specific stream power was compared to channel stability index from RGAs. In this watershed the highest specific stream power values were estimated in the major tributary reaches that also had the highest channel stability index scores, which indicate a greater potential for erosion and bank failure. This was a result of channel slope being an order of magnitude greater in the tributary reaches compared to the main stem of this watershed.

These analyses show that changes in stream power can be used to identify potential sites of channel instability. Variations in stream power were comparable with the results of field observations of stream channel stability. The BEHI and RGA data used in this study were from sites where bank erosion was apparent and hence the scores may be considered as an index of relative susceptibility to bank erosion. These geomorphic assessment indexes are qualitative metrics of channel stability considering both erosional as well as depositional processes. This includes consideration of dominant erosional processes such as mass wasting and fluvial erosion. Whereas, specific stream power represents relative changes in transport capacity among stream reaches. One could therefore, argue that higher transport capacities are a major factor causing higher rates of stream channel erosion in these watersheds. The results suggest that although channel vegetation and nature of bank and bed material can influence the resistance of these channels to erosion, the major factor controlling channel erosion in these natural stream channels is the stream power generated within a stream reach.

Longitudinal trends in reach scale stream power

The changes in stream power from upstream to downstream in each of the study watersheds are illustrated in Figure 4.11. The three study watersheds showed contrasting behavior in terms of the general downstream trend in stream power. Lecce (1997) reported that stream power may increase, decrease or remain constant downstream along a stream network. Downstream change

in stream power is determined by the confounding influence of channel slope and channel cross-section.

For Stony Clove, the longitudinal variation in stream power did not show a monotonic trend from upper to lower reaches. While the highest values were observed in the downstream reaches, there were also large variations between adjacent reaches. These results are consistent with the observations made by Barker et al. (2009) who observed a non-monotonic downstream change in stream power in several rivers in western Britain. Unlike the Catskill watershed, there was a general non-linear downstream decrease in specific stream power in the Piedmont watershed (Figure 4.11). Decrease in stream power in the downstream direction may be an indication of a depositional environment whereas, an increase in stream power in the downstream direction suggests an erosional environment (Graf, 1983). For the Choteau Creek, high values for both specific stream power and channel stability index were observed in lower reaches, the mid-section of the main stem showed the lowest values.

Longitudinal mapping of stream power using GIS

Figures 4.12a shows the longitudinal variation in total stream power estimated along the main stem of Stony Clove Creek based on high resolution estimates of stream slope developed using the 3m DEM that was available for this watershed. Although an increasing trend in stream power was observed in the downstream direction, peaks were also observed between regions of low values.

The most significant peak was observed near the 4000 mark on the horizontal axis (Figure 4.12a) where the total stream power increased from near 2,000 W m^{-1} to over 10,000 W m^{-1}. This increase was due to a combination of increased stream discharge as well as relative increase in channel slope at this location (Figure 4.12b and Figure 4.12c). Such non-linear increase in stream power may be used to identify potential areas of channel disturbances due to excess shear stress. By overlaying the generated stream power map with the high resolution aerial photographs we were able to compare the predicted "hotspots" of channel instability with real channel features. These results are consistent with Vocal-Ferencevic and Ashmore (2011) who used a similar approach to map potential sites of geomorphic changes after a 2005 flood in an urban watershed in Canada.

Our study addresses the concern by others on the suitability of commonly available DEMs such as the 10-m DEM used in this study for use in stream geomorphic assessments (Reinfelds et al., 2004; Flores et al., 2006). The use of high resolution LiDAR derived 3-m DEMs improved the identification of potential problem sites within the stream network. This type of stream power mapping has implications for stream management strategies such as identification and selection of best possible stream restoration practices at different sections along the stream network. For example, erosional sites identified in regions of relatively low stream power may be restored using vegetation that protects the stream bank whereas erosional sites identified in regions of high stream power may require more robust protection such as engineering structures.

With extreme streamflow events being observed and predicted to increase in the future, stream power mapping provides an opportunity to predict stream locations that may be more sensitive to

changes in storm discharge. These potential locations may be undisturbed under current hydroclimatic conditions, but may be more susceptible to erosion under future conditions. Another potential use of stream power mapping is for distinguishing streams that are degrading where stream power shows an increasing trend downstream *versus* aggrading streams where stream power may show a decreasing trend in the downstream direction.

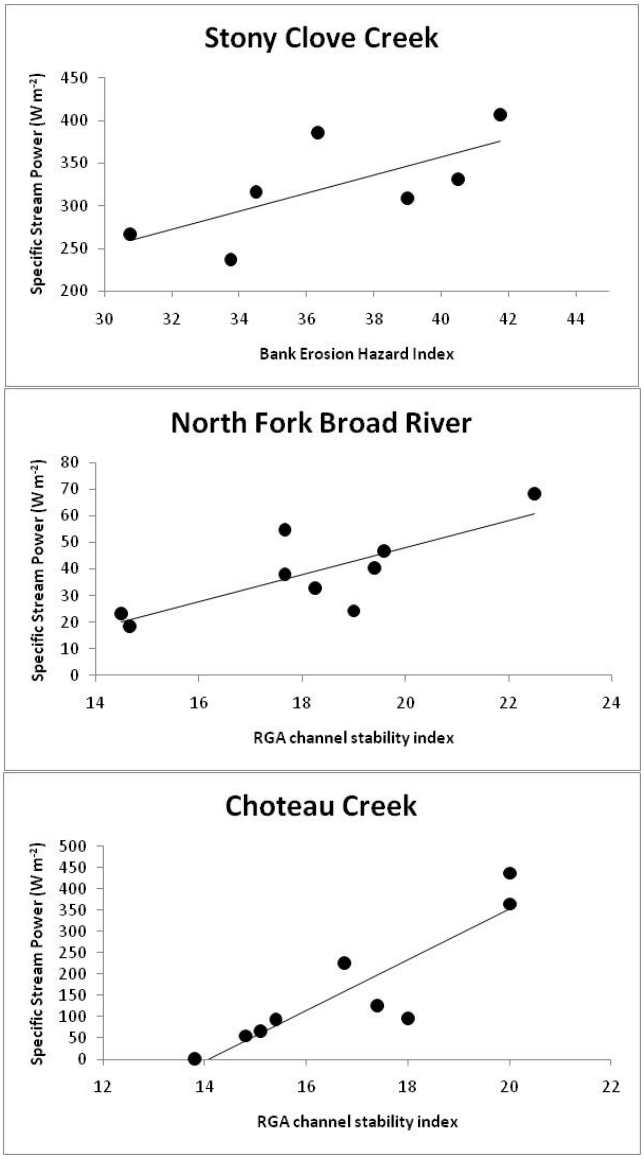

Figure 4.10. Relationship between specific stream power and channel stability indices calculated for reaches within the three study watersheds. Increased values of the BEHI or RGA Indices indicate an increased potential for erosion and bank failure

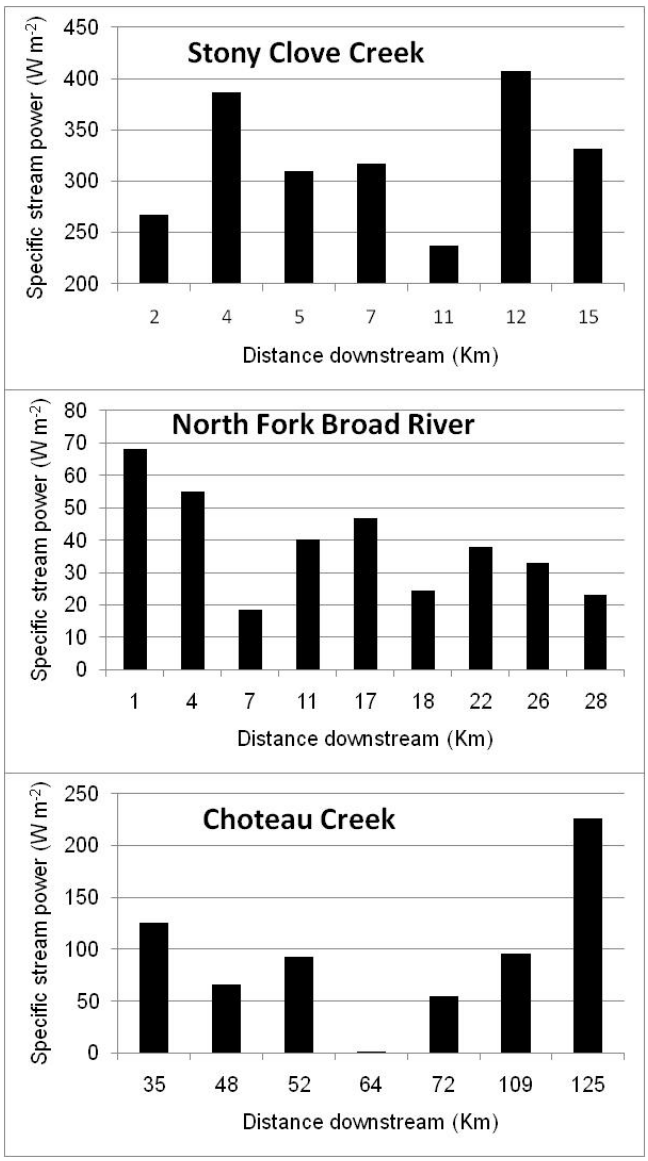

Figure 4.11. Longitudinal trends in specific stream power along the main stem of the three study watersheds

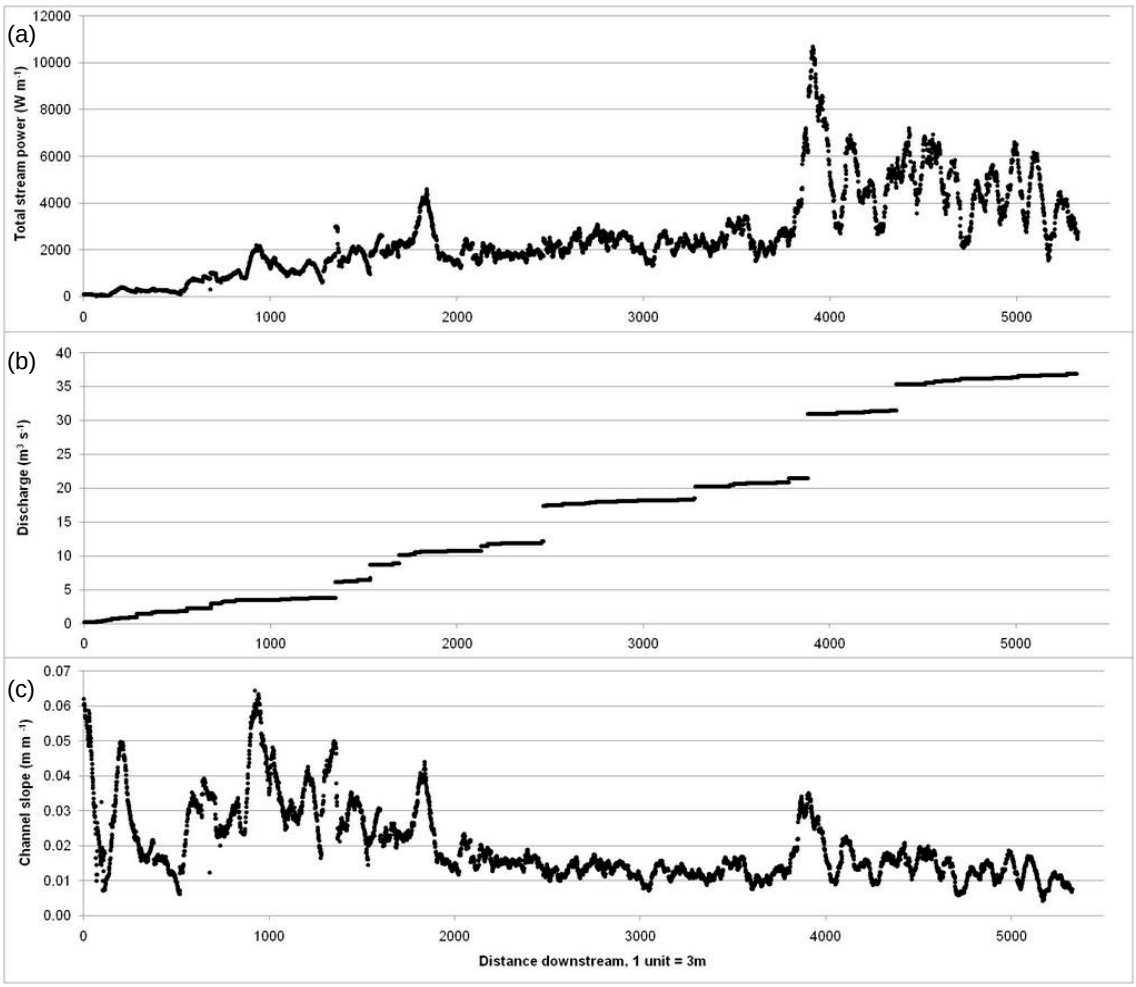

Figure 4.12. Stony Clove Creek: longitudinal variation in (a) total stream power; (b) bankfull discharge and (c) channel slope along the main stem using a 3-m DEM.

Conclusions

This study shows that estimation of reach scale variation in stream power may be a simple, quick and effective tool for identifying sites of potentially higher erosion that may be candidates for stream restoration projects that improve water quality. High resolution LiDAR derived DEMs along with high resolution aerial photographs were used to identify and confirm the location of problem sites within a stream network. Initial identification of potential erosion sites could be especially valuable in large watersheds with complex terrain and inaccessible reaches, where a watershed wide field campaign might be costly and impractical. The initial application of the proposed stream channel assessment method to three watersheds of different geomorphology was successful, however, more testing and validation of the proposed methodology at various geographical locations using qualitative and quantitative field measurements would be valuable. The interplay of stream power and channel resistance drives fluvial processes and hence we believe that more accurate channel assessments could be made by incorporating additional information, such as geology, bed and bank material and vegetation, into a GIS analysis. Once erosion sites are identified, field studies should be undertaken to determine specific rates of erosion. The cost of stream restoration is high and increasing. Therefore, identification and comprehensive evaluation of sensitive stream reaches is needed to allow stream managers to invest available resources as effectively as possible to provide both maximum sediment load reduction and improvement in water quality.

4.3. Use of Gridded Meteorological Data from the Northeast Regional Climate Center in GWLF Watershed Model Applications

Spatially-distributed meteorological (met) data for the NYC watersheds is becoming available from the National Weather Service. Work has begun to access, evaluate, and use these data in simulation model applications. Spatially-distributed data explicitly accounts for the considerable spatial variability in meteorology in the NYC watersheds due to orographic effects and variable storm types and paths, particularly in the mountainous terrain of the Catskills. Improved meteorological estimates on the broad reservoir watershed scale as well as fine-spatial-scale meteorological time series are possible.

Simulation model applications presently utilize meteorological estimates based on National Weather Service observer stations. Through the 1990's there were 18 observer precipitation stations in the NYC West of Hudson (WOH) region with long-term consistent coverage that were used to estimate precipitation inputs to the NYC watersheds. However, the number of active stations has declined since 2000 and now there are only 8 active stations (Figure 4.13). Deriving unbiased estimates of precipitation from this sparse network of data is increasingly problematic.

Gridded 4-km resolution daily precipitation and air temperature data are available from the Northeast Regional Climate Center (NRCC) at Cornell University, Ithaca, NY. These data products are available in near-real-time for the entire Northeast US starting 1/1/2005 and continuing through the present. The precipitation data represents a high-spatial-resolution developed using radar-guided interpolation in which radar-based precipitation is adjusted on a daily time step using rain-gauge observations to reduce spatially varying errors in the radar estimates and assuming that rain-gauge values represent true values (DeGaetano and Wilks, 2009). Radar-based interpolation helps reduce model uncertainty by reducing interpolation errors independently from season or precipitation magnitude. Spatially-distributed air temperatures are estimated by NRCC at grid points by interpolation from observation stations and application of an environmental lapse rate that adjusts for elevation effects on temperature. The precipitation data obtained from NRCC in a polar coordinate system is re-gridded to match the air temperature 4-km grid by nearest neighbor analysis, and the final grid is clipped to produce a consistent spatial distribution of 324 4-km grid cells for the NYC west of Hudson watershed area (Figure 4.13).

Initial testing of the NRCC Gridded Met Data was done by using the gridded data to drive GWLF (Generalized Watershed Loading Function) watershed models of major gaged inflows to the WOH reservoirs, and comparing model performance with the GWLF models driven by met data derived from observer station data. GWLF is a lumped-parameter model that takes single time series of daily watershed-average precipitation, minimum air temperature and maximum air temperature as input. For each of 10 gaged watersheds (Table 4.2, Figure 4.14), time series of daily precipitation, minimum air temperature and maximum air temperature were derived for period 1/1/2005 – 9/30/2009 by averaging the NRCC Gridded Met data grid-points within the watershed (with areal weighting at the watershed boundaries);by inverse distance squared interpolation of observer met stations relative to the centroid of the basin for air temperature; and by Thiessen polygon based interpolation of observer based precipitation data . For each

basin and each case (Gridded data driven vs. Observer Station data driven) the model was calibrated for period 1/1/2005 – 9/30/2009 and GWLF model performance compared.

Figure 4.15 compares the Nash-Sutcliffe (NS) goodness of fit model statistics for GWLF models driven by observer station met data vs. NRCC gridded met data. The NS statistic measures how closely the simulated variable tracks observed data, where NS=1 is a perfect score. NS statistics are compared for streamflow, surface runoff, and baseflow at daily and event time steps. The models driven by the NRCC gridded data substantially outperformed the observer station driven models in almost all cases at both daily and event time steps. These results support the use of the NRCC gridded met data for 2005 onwards in NYC West of Hudson watershed model applications.

Table 4.2: Gaged watersheds that provide major inflows to NYC West of Hudson Reservoirs

Reservoir	USGS Gauge No.	Watershed Description	Watershed Area (km^2)	Mean Elevation (m)	Min. Elevation (m)	Max. Elevation (m)
Ashokan	01362500	Esopus Creek at Coldbrook	493.2	600	188	1276
Ashokan	01362200	Esopus Creek at Allaben	164.8	672	305	1138
Cannonsville	01423000	West Branch Delaware River at Walton	859.3	592	360	1020
Neversink	01435000	Neversink River near Claryville	172.5	770	463	1275
Pepacton	01413500	East Branch Delaware River at Margaretville	421.7	668	396	1181
Pepacton	01415000	Tremper Kill near Andes	85.5	611	392	1137
Pepacton	01414500	Mill Brook near Dunraven	63.8	715	395	1045
Rondout	01365000	Rondout Creek near Lowes Corners	99.5	629	263	1175
Schoharie	01350000	Schoharie Creek at Prattsville	612.5	653	344	1234
Schoharie	01350080	Manor Kill near Gilboa	84.0	592	387	1045

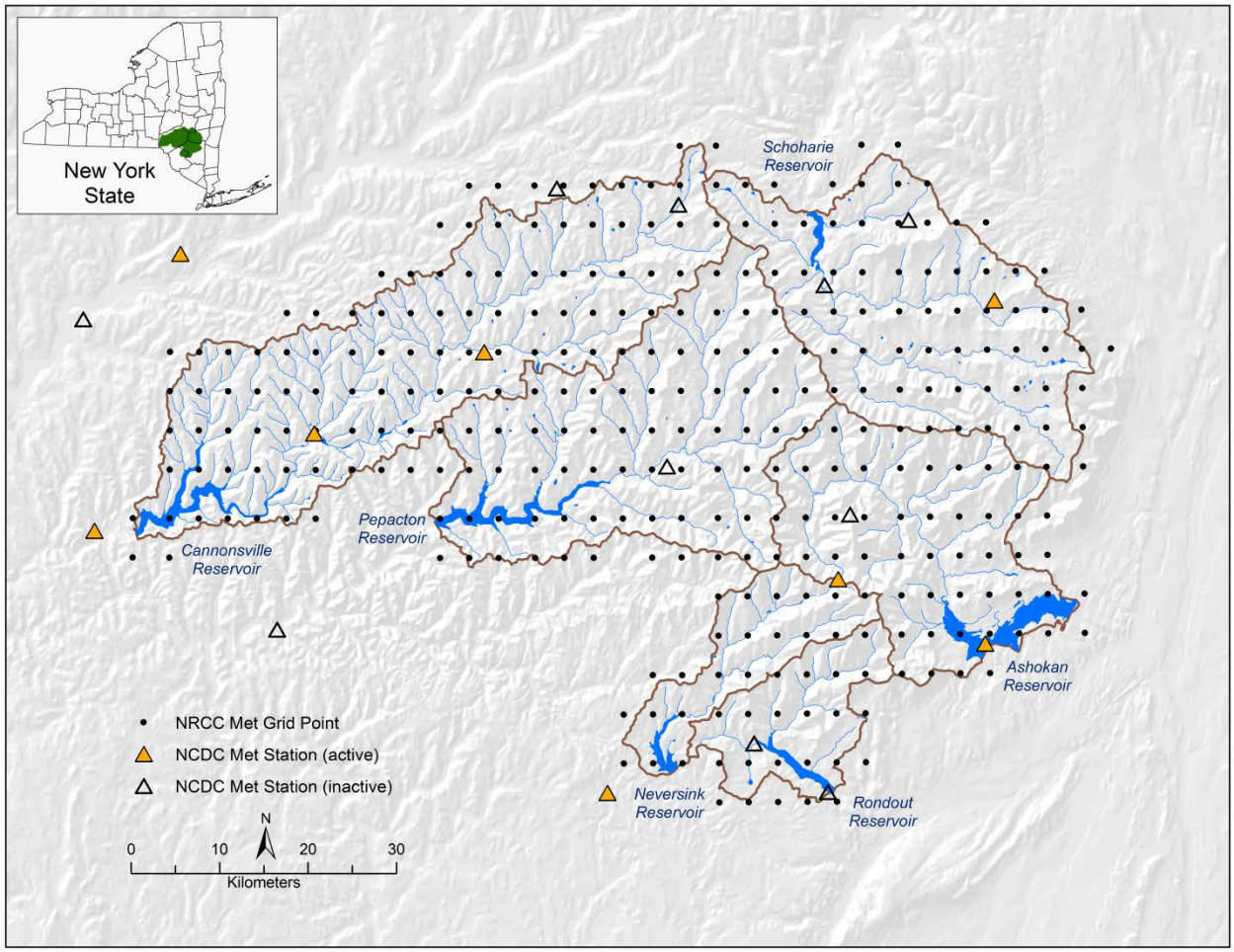

Figure 4.13: NCDC met stations and NRCC 4km. gridded met data grid-points in or near NYC West of Hudson watersheds

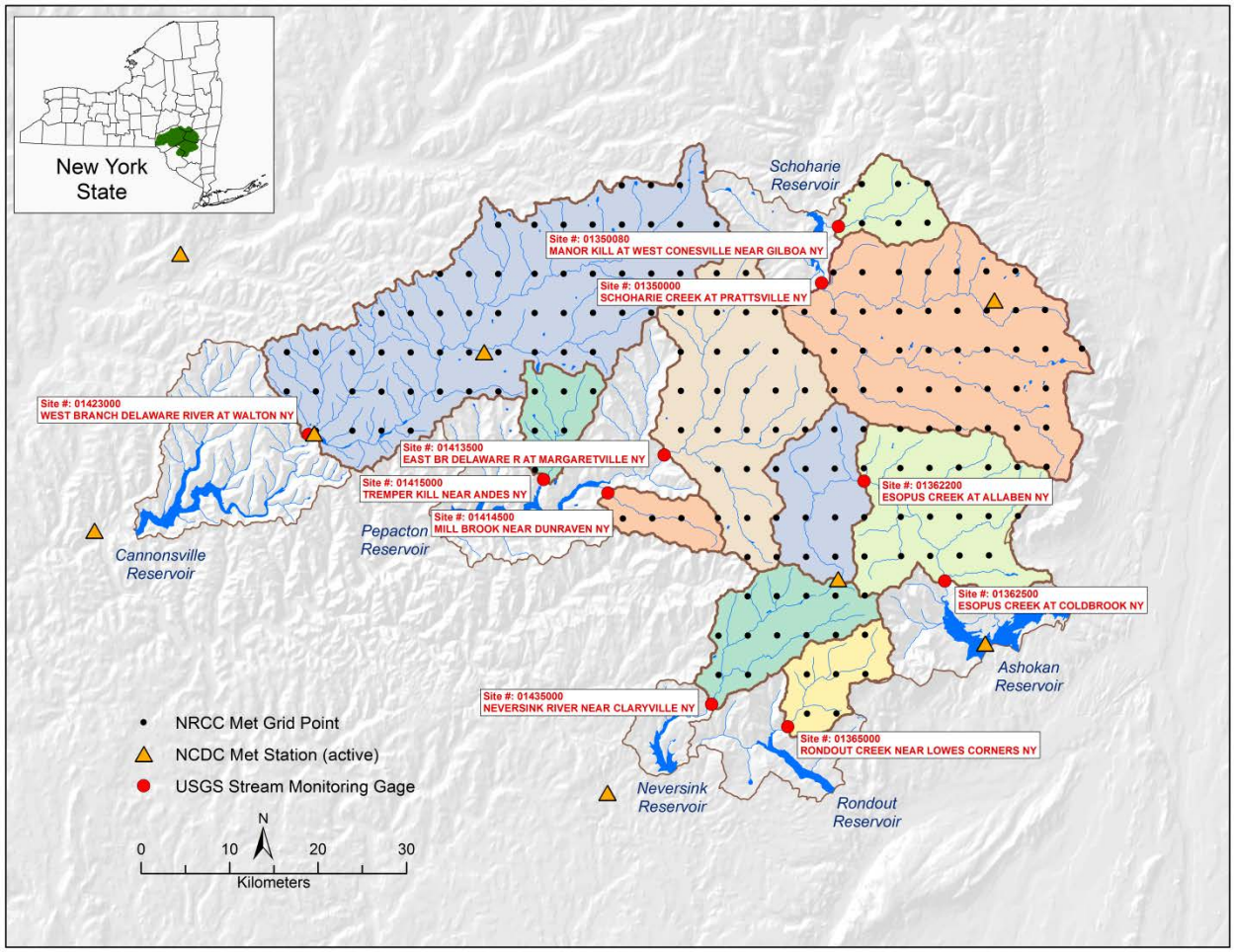

Figure 4.14: Gaged watersheds that provide major inflows to NYC West of Hudson Reservoirs, and met data sources.

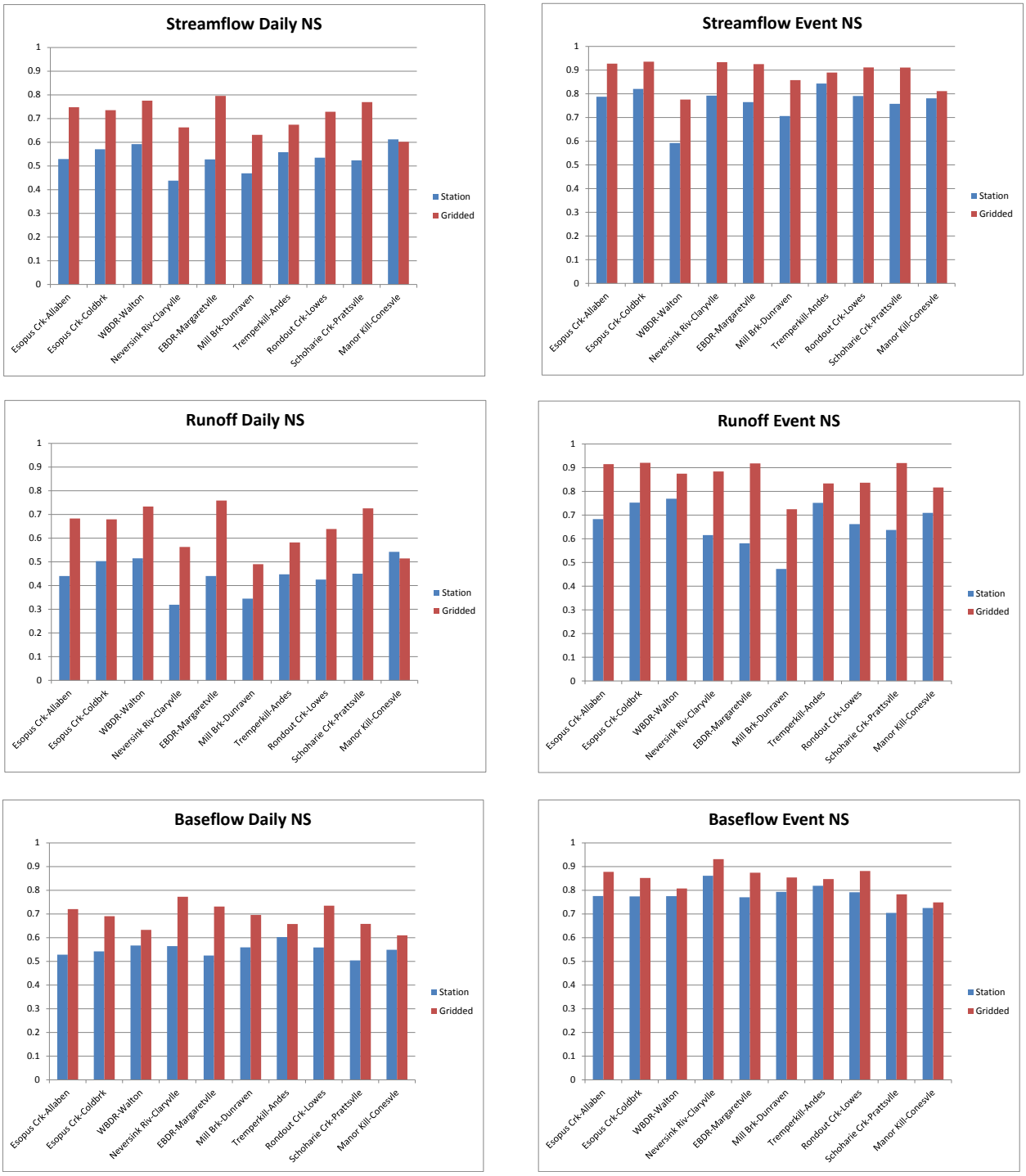

Figure 4.15: Nash-Sutcliffe (NS) goodness of fit model statistics for GWLF models driven by observer station met data vs. gridded met data.

4.4. Time Series Models for In-stream Turbidity Prediction in the Esopus Creek

Streamflow based turbidity rating curves are widely used for in-stream turbidity prediction. Turbidity rating curves have been developed from flow and turbidity data collected at the two USGS gauges in the Esopus Creek watershed (Figure 4.16). One area to improve the use of a deterministic turbidity rating curve is to include hysteresis, a phenomenon where the rate of sediment transport for a given discharge during the rising limb of the hydrograph will be different from that of the falling limb. Our previous analysis has shown that for a given value of streamflow the rising limb of streamflow hydrograph contributed higher turbidity compared to the falling limb (Mukundan et. al., 2010). Another area for improvement is to include serial correlation. Like streamflow, turbidity is serially correlated at the daily time step. This is explained in a plot of the sample autocorrelation function (ACF) of log-transformed turbidity in the Esopus Creek at Allaben (Figure 4.17). The plot shows the correlation of the turbidity observations at different time steps. Statistically significant values show up above the blue dotted line in Figure 4.17.

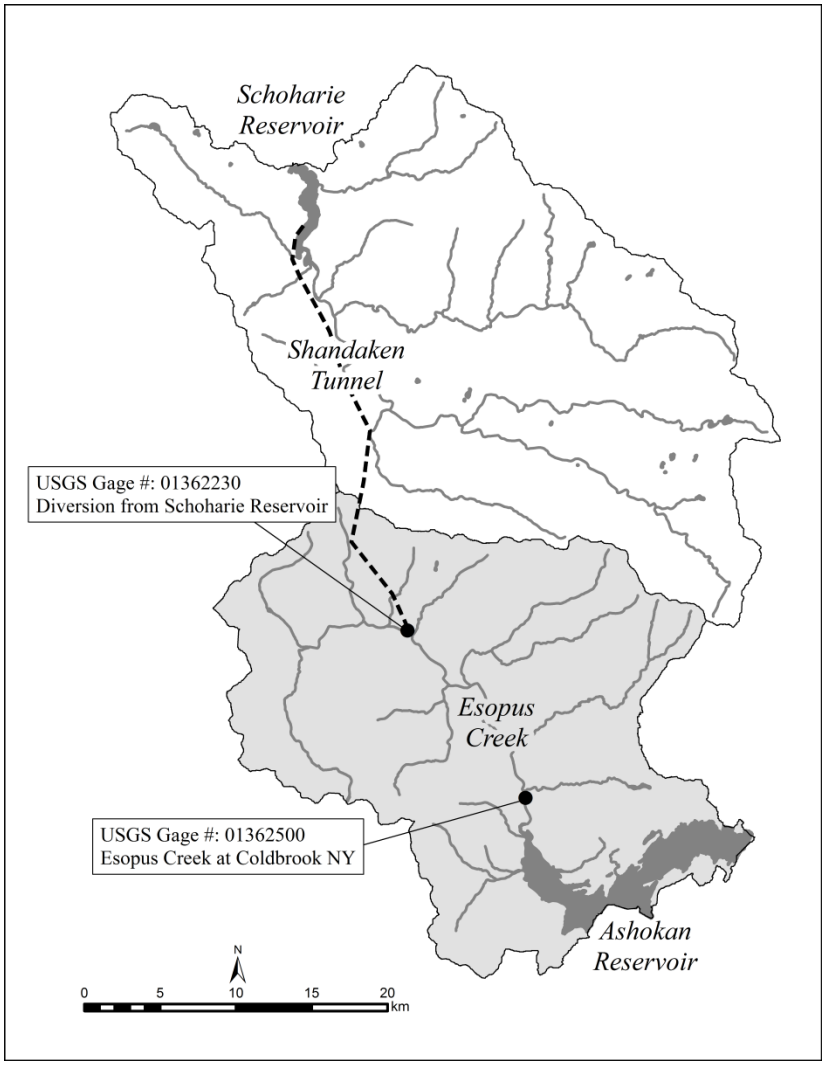

Figure 4.16. The Esopus Creek watershed, NY showing location of Coldbrook sampling location and diversion tunnel from the adjacent Schoharie reservoir

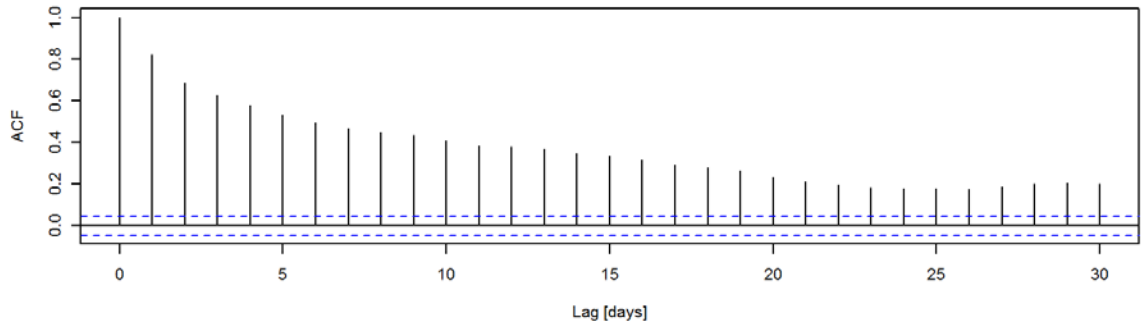

Figure 4.17: ACF of log-transformed turbidity at Allaben

Hysteresis

Hysteresis effects on stream turbidity can be derived using the method proposed by Hirsch (1988) which is briefly outlined below. The hysteresis effect (HE) is defined by the following equation:

$$HE = c^r \qquad (4.7)$$

where c is the coefficient that maximizes the correlation between HE and the dependent variable (turbidity in this case) and has a value between 0 and 1. For the Allaben gauge, c was computed to be 0.5. r is the "recession variable", computed by scanning the streamflow time series and setting $r = 0$ each day when flow is rising. A day is considered to be rising if flow on the current day is greater than 1.1 times flow from the previous day. On any day that is not rising, r is set to the number of days since the last rising day. A detailed description on the development of the time series turbidity model and its use as an operational predictive tool is outlined in Wang et al. (2012).

Serial Correlation

Ordinary least square regression models on time series data often shows highly correlated residuals and this is particularly true for daily time series data (Richards et al., 2008; Walker et al., 2009). Since the ordinary regression residuals are not independent for time series data, they contain information that can be used to improve the prediction of future values (Reed et al., 2008). The ACF of the model residuals (Figure 4.18, top) may show a strong serial correlation, violating the linear regression assumption that errors are uncorrelated. In this case, the partial ACF (Figure 4.18, bottom) is more useful in identifying a suitable time series model to describe the residual behavior. More importantly, addressing autocorrelation can avoid incorrect conclusions on significance of parameters, confidence limits for predicted values, and estimates of regression coefficients.

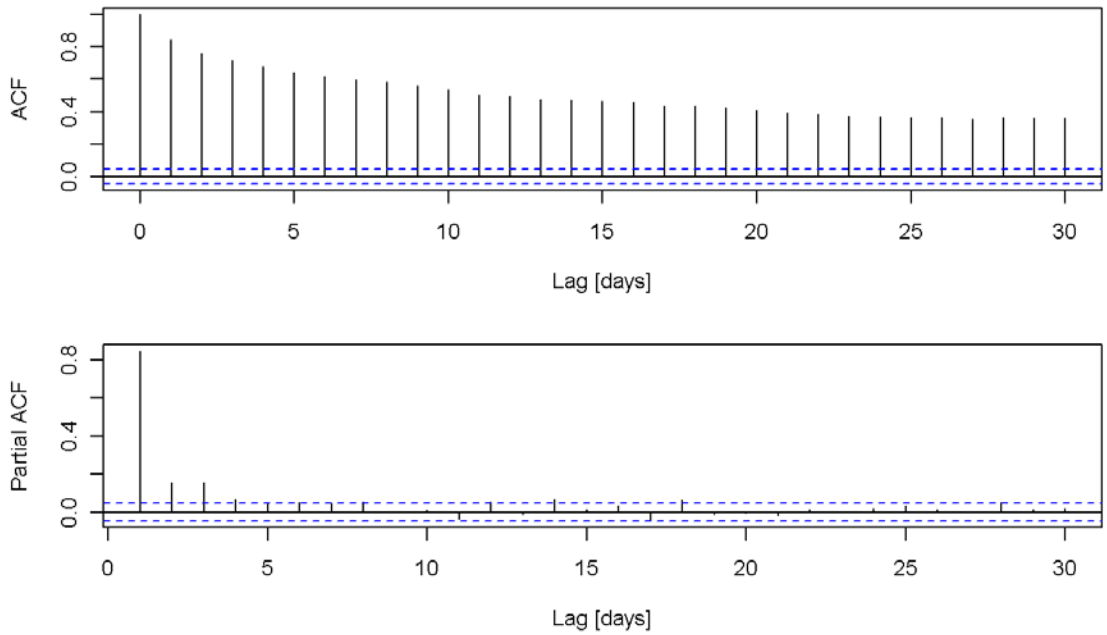

Figure 4.18. ACF (top) and partial ACF (bottom) of the multiple linear regression model residuals.

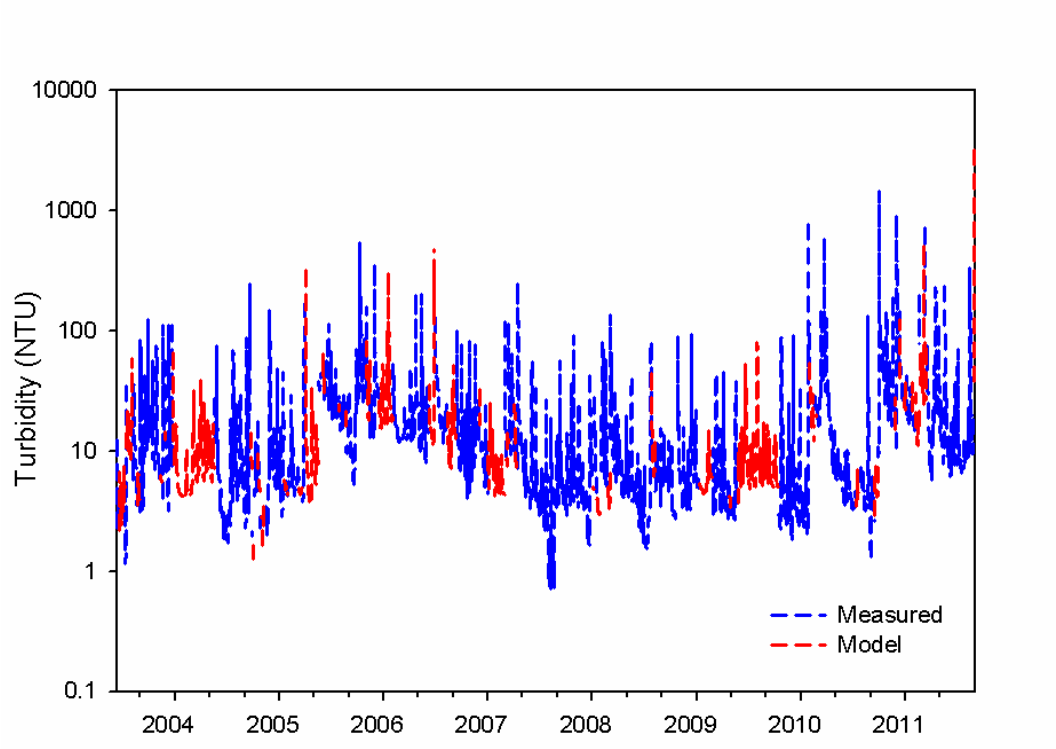

Figure 4.19. Continuous time series of average daily turbidity at Coldbrook showing the range in observed turbidity, and the data filled in using the autoregressive model.

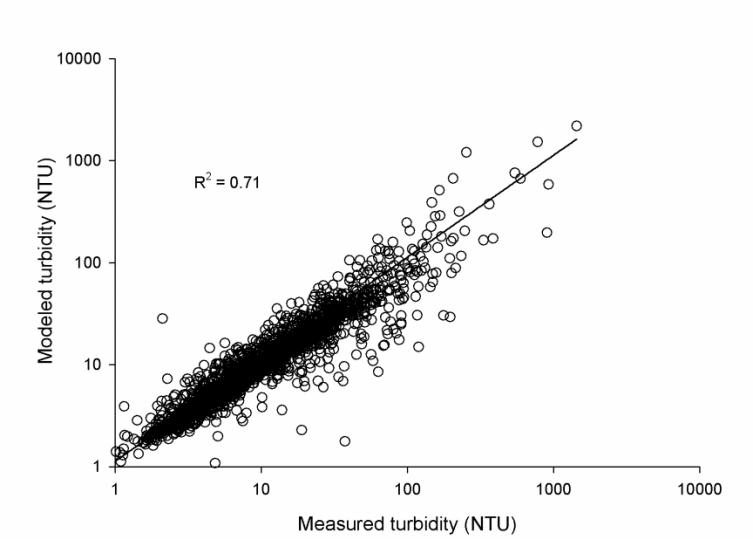

Figure 4.20 Scatter plot of measured and modeled turbidity pairs relative to the 1:1 line.

Model application

A continuous time series of average daily stream turbidity from June 13, 2003 to August 31, 2011 in the Esopus Creek at Coldbrook was used for this analysis. The objective was to estimate missing turbidity data using a time series model. A daily time series of measured instantaneous turbidity at the outlet of Schoharie Tunnel was used to account for the effects of point source inputs to the Esopus Creek (Figure 4.16). Residual analysis from the ordinary least square regression model using the three predictor variables (streamflow at the watershed outlet, point source turbidity, and hysteresis effect in streamflow-turbidity relation) showed a lag of 4 days in the autocorrelation function. This information was used in selecting an autoregressive model capable of predicting log-transformed daily turbidity. The AUTOREG procedure in SAS (SAS Institute, 2003) was used to fit a linear regression with autoregressive errors. The selected regression model with AR4 error is as follows:

$$Y(t) = \beta x(t) + v(t) \tag{4.8}$$

$$v(t) = \sum_{i=1}^{4} \phi_i v(t-i) + \varepsilon_t \tag{4.9}$$

where $x(t)$ is a vector of predictor variables at time t, β is a vector of regression parameters, ϕ_i represents the autoregressive parameters, $v(t)$ is the model error at time t and ε_t is "white noise" which is normally distributed with a mean of 0 and a variance of σ^2.

Figures 4.19 and 4.20 show the results of applying this type of turbidity loadin model. Potential applications for the time series water quality modeling approach includes

- Short-term water quality forecasting for operational decision support
- Interpolating missing values in a time series
- Determining optimal sampling (baseflow) frequency for water quality parameters

4.5. A Preliminary Test of the CONCEPTS Channel Evolution Model

High magnitude runoff events with flood frequency recurrence intervals greater than 10 years cause significant suspended sediment turbidity conditions, which can at times limit the use of the Catskill water supply. The Catskill Mountains were glaciated in the Pleistocene and the stream network is variably incised into the glacial "legacy" sediments which are enriched in fine sediment. When streams intersect clay-rich glacial till and/or glaciolacustrine silt and clay, fine sediment is entrained during high runoff giving the streams a characteristic red-brown turbidity.

A research project has been initiated to investigate the processes that control erosion, entrainment and transport of fine sediment in Catskill Mountain streams as well as developing conceptual and quantitative modeling tools capable of simulating the evolution of stream channels under a range of hydro-climatic and watershed physical conditions. A preliminary analysis using the CONservational Channel Evolution and Pollutant Transport System (CONCEPTS) model for Stony Clove Creek, a tributary of the Esopus Creek watershed that drains to the Ashokan Reservoir is presented here. This deterministic, numerical model is unique in that it accounts for the hydraulic and geotechnical processes that control streambank erosion, in addition to bed processes and the routing of flow and sediment. . In addition to predicting changes in channel geometry, CONCEPTS is also capable of predicting sediment transport at each section of a reach based on size classes. The preliminary test using data from Stony Clove was expected to provide insight into the potential limitations and modifications needed to the current version of CONCEPTS if it is to be applied in a glaciated mountain fluvial system.

A 4.2 km reach of the Stony Clove Creek upstream of the main stem of the Esopus Creek was selected for the preliminary test. The reach was divided into 10 sections based on measured channel cross-sections (acquired 01/19/2012) at intervals ranging from 231 m to 592 m. The cross-sections provided the boundary conditions for channel dimensions required by the model. In the absence of measured data of stream channel geotechnical properties, most parameter values including particle size distribution and bulk density for the bank and bed material were based on literature values. A test scenario was run to simulate channel changes and sediment transport under flood events of different recurrence intervals. Peak discharges for recurrence intervals of 2-year, 5-year, 10-year, 25-year and 50-year were estimated using regional curves based on drainage area (USGS, 2006). Output from the model was evaluated for relative change in channel geometry and bed elevation change relative to the initial condition.

Model output showed that the model is predicted both deposition and degradation of the stream channel based on the simulated bed elevation changes at different cross-sections (Figure 4.21). Two representative sites; one showing deposition and the other showing degradation are presented in Figures 4.22a and b. The CONCEPTS based predictions of deposition and degradation seems to be too high, when using the limited input data that were available. The current version of the model is capable of simulating transport of sediments with 14 predefined particle size classes ranging from clay to small cobbles. Necessary modifications in the model algorithm to accommodate larger particle sizes found in the Catskill stream beds may help improve model prediction of stream channel processes
A more realistic simulation of CONCEPTS in the Catskill Mountains would require better model characterization of the bed material representative of the Catskills and collection of site specific

data on resistance to erosion properties, and representative channel geometry. This would allow comparison of model simulations with monitoring data on channel geometry and water quality (fine sediment) as well as to develop scenarios of management and climate change impacts. DEP Water Quality Modeling and Stream Management Sections are supporting a research application that would fund the developers of CONCEPTS at the USDA National Sediment Lab and collaborators at Cornell University to undertake detailed study and model development in the Stony Clove watershed (see Section 7.3).

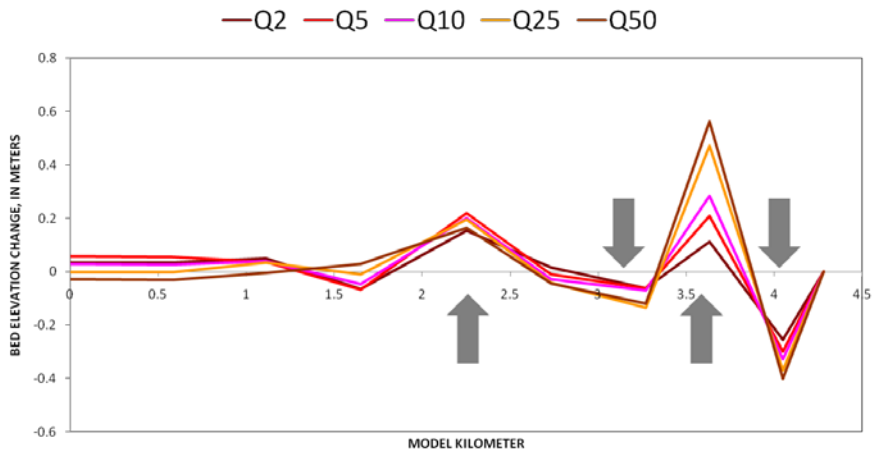

Figure 4.21. Bed elevation change under different discharge events

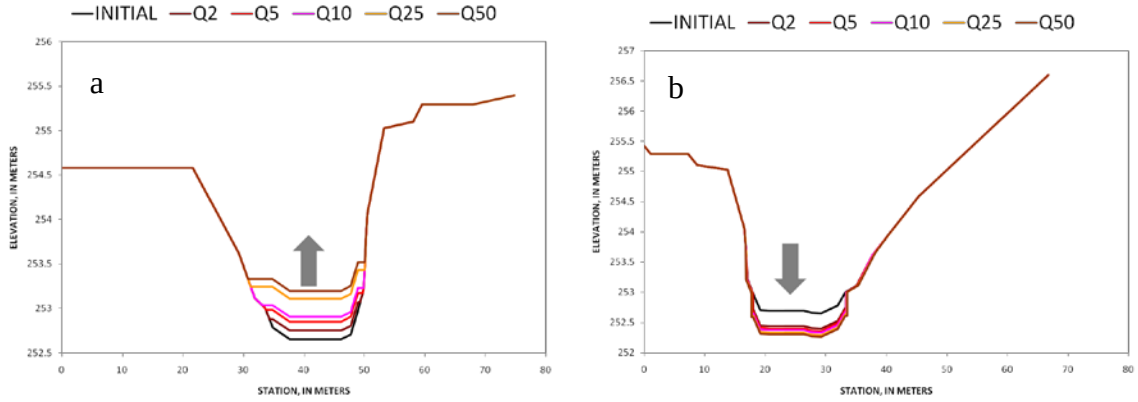

Figure 4.22. Channel deposition (a) of sediment and degradation (b) predicted by CONCEPTS

4.6. Calibration of the one-dimensional hydrothermal and water quality model for Pepacton Reservoir

Introduction

A one-dimensional hydrothermal and water quality model has been set up to simulate the thermal structure, nutrients and phytoplankton for Pepacton Reservoir (UFI, 2001). The model has been calibrated using four years of observed data. This study attempts to improve the performance (accuracy) of the reservoir model through automated calibration with long-term measurement data.

Study area

Pepacton Reservoir is 24 km long and about 1.12 km across at its widest point (see Figure 4.23). The surface area of the reservoir is 19.9×10^6 m^2. Its volume is 538.8×10^6 m^3 with the maximum depth of 53 m and mean depth of 27.1 m. The average hydraulic retention time (HRT) of the reservoir is 234 days. Six sampling sites have been set up in the reservoir and water quality samples are taken regularly at two week to one month intervals at the depths of 3, 15 and 30 meters at each sampling sites.

The reservoir has a catchment area of 939.4 km^2. The catchment is mainly rural with forest being the predominant land-use. Roughly 94% of the total watershed area is undeveloped with about 3% of the watershed classified as agricultural landuse. In addition, there are several towns in the catchment which discharge treated wastewater into the main river that flows into the reservoir. Nutrient inputs to the reservoir have decreased as a result of FAD watershed management programs to reduce non-point source inputs and upgrades to the sewage treatment facilities.

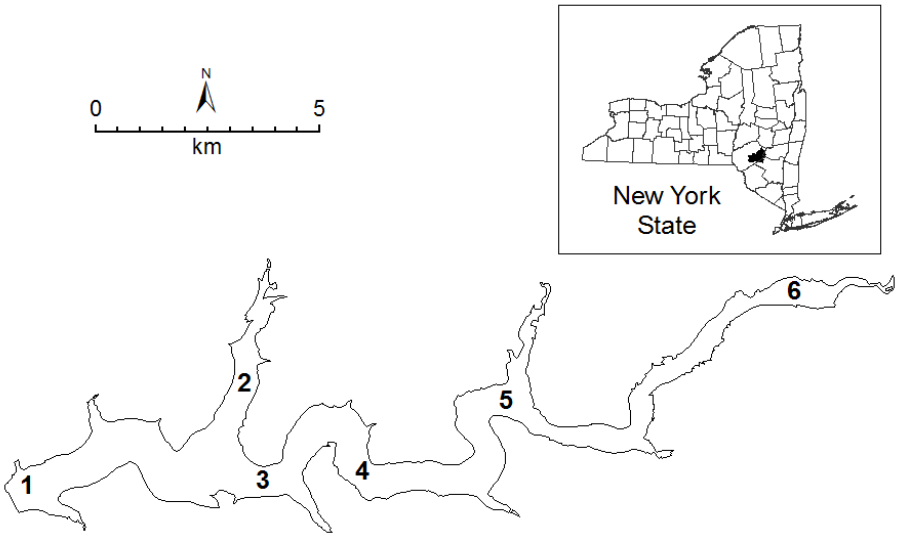

Figure 4.23. Pepacton Reservoir and sampling sites #1-6.

Reservoir Model

A one dimensional reservoir model was developed by the Upstate Freshwater Institute (Owens, 1998; Doerr et al., 1998; UFI, 2001) to simulate the hydrothermal and water quality conditions in the Pepacton Reservoir. The model consists of three components: a hydrothermal sub-model, a nutrient sub-model, and a phytoplankton sub-model.

The *hydrothermal sub-model* simulates the vertical dynamics of reservoir thermal structure based on changes in such critical (state) variables as meteorological, hydrological and operational conditions. The *nutrient sub model* describes the transformation and fate of the nutrient loads in the reservoir. Nutrients enter the water column at a depth corresponding to the temperature of the inflowing water. The reservoir model further distributes nutrients vertically through the water column based on vertical mixing coefficients derived from the hydrothermal sub-model, and the nutrient inputs are partitioned into different forms based on model coefficients. Nutrient transformations occur within the model, which affects the form and bioavailability of the nutrients. Ultimately nutrients remain within the water are taken up by the phytoplankton, or are lost from the reservoir in outflows or by sedimentation.

The *nutrient-phytoplankton sub-model* simulates the kinetic processes of five components: phosphorus, nitrogen, carbon, phytoplankton and dissolved oxygen. Phytoplankton biomass is predicted in terms of algal carbon and is a balance between growth (photosynthesis), and losses due to respiration, grazing, sedimentation and outflow. Growth is a function of light, temperature and nutrients. Phosphorus is the nutrient that predominately limits growth in Pepacton Reservoir. Thus, the most important and manageable input condition or factor affecting primary production and phytoplankton biomass addressed with these models is the external phosphorus loads. Chlorophyll *a*, the most widely used measure of phytoplankton biomass, is calculated from the algal carbon based on reservoir-specific stoichiometric relationships.

Reservoir Model Setup and Parameters

To set up the one-dimensional reservoir model to simulate the hydrothermal and water quality conditions of Pepacton Reservoir, the reservoir is discretized into 53 layers vertically with the depth of 1 meter for each layer. The model is fed with daily meteorological data (air temperature, dew point temperature, cloud cover, wind speed and solar radiation) and other data related to the water balance (including water elevation, inflow discharge, dam spill and release, and aqueduct outflow). Daily time series which are generated by a watershed model (i.e. GWLF model) are used as the input of the reservoir model. These time series include streamflow, dissolved phosphorus and nitrogen, particulate phosphorus, dissolved organic carbon, and total suspended solids. The reservoir model can output daily simulated values for more than 40 variables such as temperature and dissolved oxygen and chlorophyll *a* for epilimnion and hypolimnion layers, and for the reservoir as a whole.

In total, about 100 hydrothermal and kinetic parameters (also called coefficients) are used in the model and about half of them can be adjusted during model calibration. The value of many of the model parameters were based on published values, specific process studies that were carried out as part of the model development process and as a result of calibration using four years of

measured data (UFI, 2001). These values are indicated as pre-calibrated values in this study. The Morris method (Morris, 1991; Saltelli et al., 2004) is employed to identify the sensitive parameters in the model. It is found that 16 parameters are sensitive in simulating the variables including dissolved oxygen (DO), total phosphorus (TP) and chlorophyll *a* (Chla). See Huang and Liu (2008) for a detailed description of the application of the method to the identification of the sensitive parameters in a water quality model. These parameters as well as their pre-calibrated values, and their lower and upper bounds are presented in Table 4.3. These parameters, once identified as most strongly affecting outputs become the focus in model calibration, and only their values are varied in model calibration. The bounds in Table 4.3 are those suggested according to the recommendations provided by the model developer (UFI, 2001) and were refined to ensure the numerical stability of the model.

Table 4.3. Sensitive reservoir model parameters

	Name	Calibrated value	Pre-calibrated value	Lower bound	Upper bound	Definition
1	aC2CHL	82.571	48	40	100	Ratio of carbon to Chl (µgC/µgChl)
2	aC2P	140.49	150	80	150	Ratio of carbon (C) to phosphorus (P) (ugC/µgP)
3	betaw	0.4876	0.4	0.3	0.7	Surface adsorption fraction
4	emisi	0.913	0.95	0.9	0.99	Ice emissivity
5	eta	1.4186	1.3	1	1.5	Wind mixing
6	fardl	0.6284	1	0.5	1	Fraction algal respiration as dissolved labile
7	htcwi	0.0331	0.05	0.01	0.1	Ice transfer
8	kc	0.0336	0	0	0.05	Chlorophyll (Chl) multiplier (L/µgChl/m)
9	kldoc	0.0127	0.008	0.01	0.015	Oxidation of labile dissolved organic carbon (DOC) (1/d)
10	kldop	0.0829	0.06	0.01	0.1	Decay of labile dissolved organic phosphorus (DOP) (1/d)
11	phir	0.1248	0.1	0.01	0.15	Respiration multiplier - growth
12	PPvel	1.4463	0.88	0.264	1.496	Settling organic particulate phosphorus (m/d)
13	rz	0.2802	0.4	0.2	0.6	Exponent
14	sod	0.4378	0.4	0.32	0.48	Sediment oxygen demand ($g/m^2/d$)
15	trncon	0.0032	0.0028	0.001	0.005	Evaporation multiplier
16	turb	2.6608	2.2	2	3	Atmospheric turbidity

Reservoir model calibration and validation

In this study, a hybrid genetic algorithm (HGA) consisting of a real-encoded genetic algorithm (a global search method) (Haupt and Haupt, 2004) and the Nelder-Mead simplex (NMS) algorithm (a local search method) (Nelder and Mead, 1965) is used as an optimization algorithm to vary the values of the 16 sensitive parameters. An overall objective function is designed to measure the degree of fitness between the measurements and the predicted values of the selected variables including water temperature (Temp), DO, TP and Chla. More detailed descriptions of the HGA and the overall objective function are given by Huang and Liu (2010).

The model was calibrated against the measured data over the time period of 1986-1999, while model validation was performed using 2000-2004 data. The calibrated parameter values are presented in Table 4.3.

Figures 4.24 and 4.25 depict the time series of simulated daily Temp and DO (with the pre-calibrated and calibrated parameter values) for both epilimnion and hypolimnion layers, respectively. The simulated curves with the pre-calibrated parameter values and calibrated parameter values almost overlap each other, meaning that model calibration resulted in little change to the simulated curves of Temp and DO. It can also be seen that the simulated curves show similar patterns of variability so that most measurements fall on the simulated curves, suggesting that the parameter values produce reasonable agreements between the measured and simulated values for temp and DO.

Figure 4.26 presents the time series of simulated daily TP for both epilimnion and hypolimnion layers, respectively. In general, the simulated curves with the calibrated parameter values are closer to the measured data and thus match the measured data better than the curves with the pre-calibrated parameter values. In addition, although not all the measurements are on the simulated curves, the simulated curves suggest realistic patterns of variation and the ranges of the simulated values are almost the same as the ranges of measured values. It can be said that the model is improved slightly through calibration.

Figure 4.27 presents the time series of simulated daily Chla. In general, the simulated curves with the calibrated parameter values are much closer to the measured data than the curves with the pre-calibrated parameter values. It can be observed that the model is improved significantly through calibration on simulating Chla. Like TP, although not all the measurements are on the simulated curves, the simulated curves show reasonable patterns of variation and the ranges of the simulated values are almost the same as the ranges of measured values. Considering the great variations of the measurements, the simulated results match the measured data reasonably well.

Figure 4.28 shows the simulated and measured Temp, DO, TP and Chla for the epilimnion and hypolimnion layers over the validation time period of 2000-2004 when the model is run using the calibrated parameters in Table 4.3. The model validation shows that, the simulated curves of Temp and DO are similar using either pre-calibrated parameter values or calibrated parameter values. The independent validation data also confirms that, the model is improved slightly through calibration when simulating TP. The model validation results for Chla improved

significantly with the calibration. These findings indicate that the validation results are consistent with the calibration results.

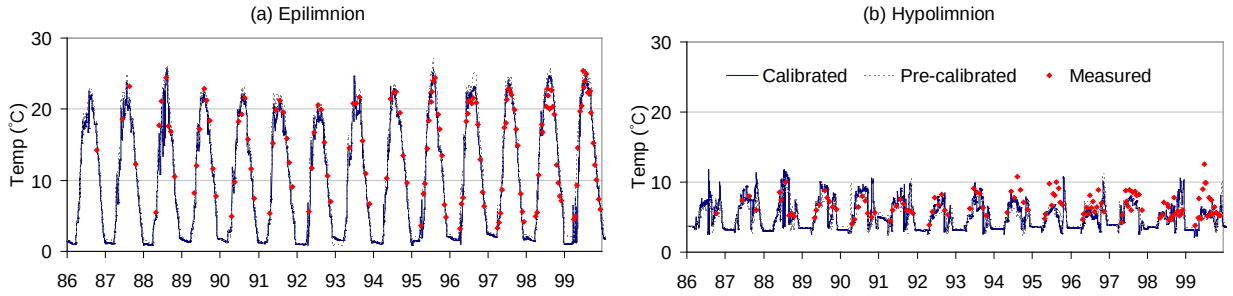

Figure 4.24. Simulated and measured daily Temp in epilimnion and hypolimnion layers for the calibration period of 1986-1999.

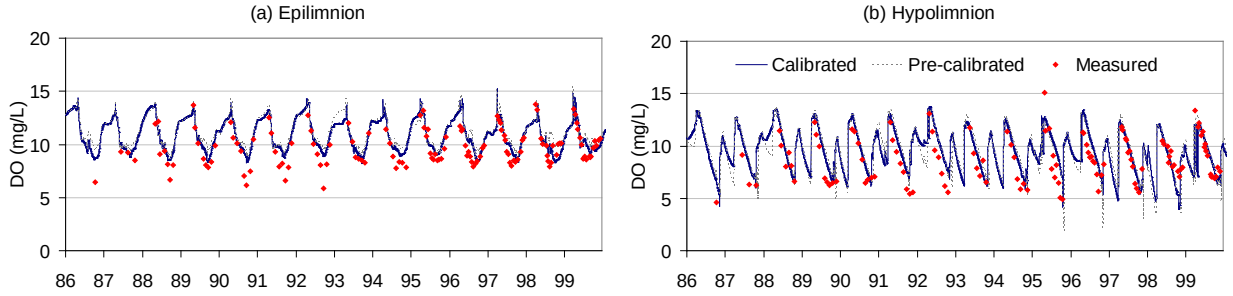

Figure 4.25. Simulated and measured daily DO in epilimnion and hypolimnion layers for the calibration period of 1986-1999.

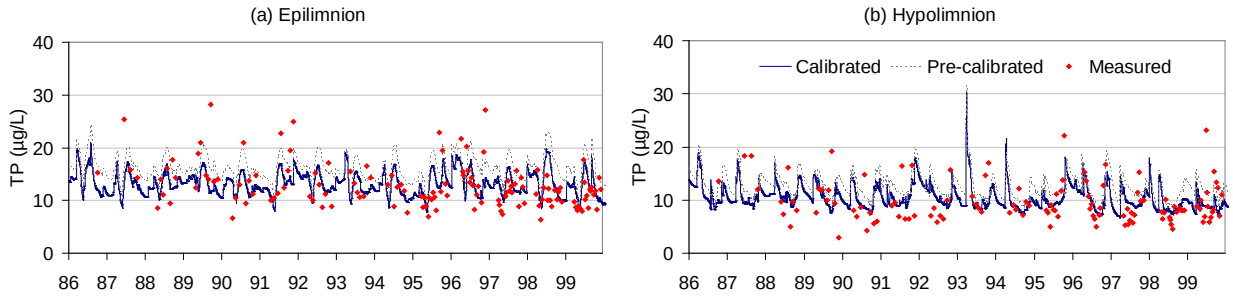

Figure 4.26. Simulated and measured daily TP in epilimnion and hypolimnion layers for the calibration period of 1986-1999.

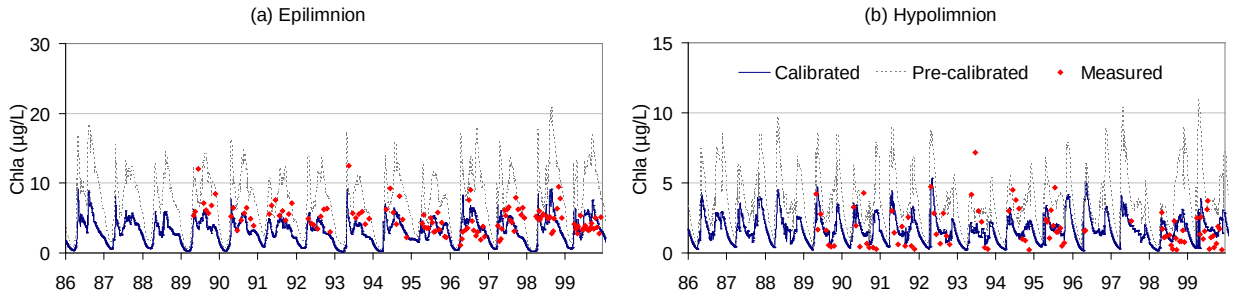

Figure 4.27. Simulated and measured daily Chla in the epilimnion and hypolimnion layers for the calibration period of 1986-1999.

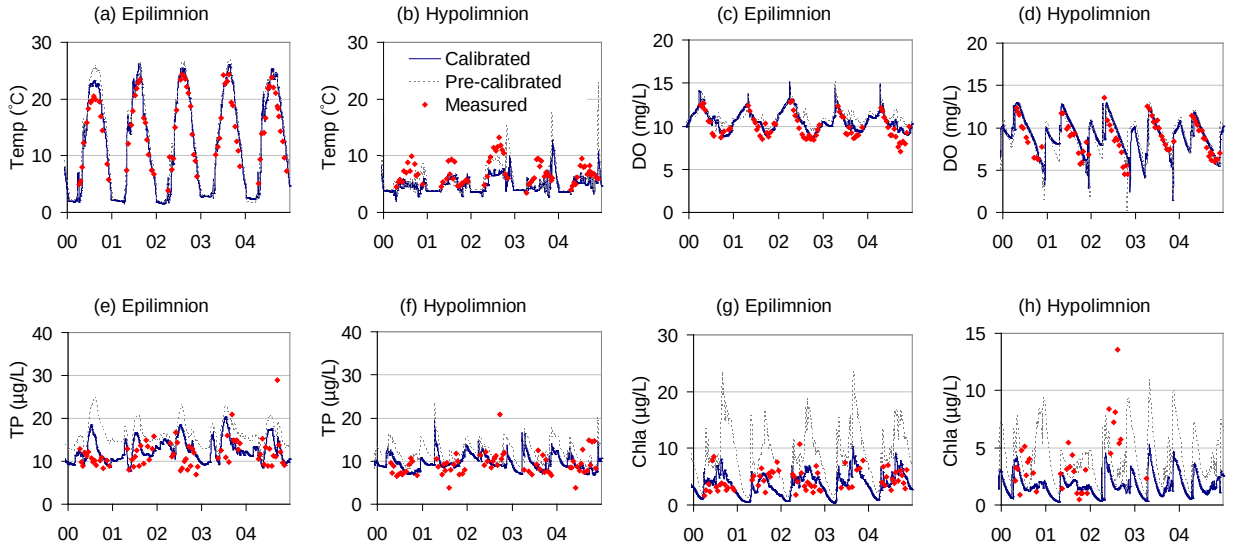

Figure 4.28. Simulated and measured daily Temp, DO, TP and Chla in the epilimnion and hypolimnion layers for the validation period of 2000-2004.

Summary and conclusions

This study demonstrates the improvement of a reservoir model through automated calibration using long-term measurement data. A hybrid genetic algorithm consisting of a real-coded genetic algorithm and a local search method was developed as an optimization algorithm and an overall objective function was designed to measure the degree of fitness between the measurements and the simulated values for all variables included in model calibration. They were used in the calibration of a reservoir model which was set up to simulate the hydrothermal and water quality of Pepacton Reservoir. After calibration, the model produced simulated values that better matched the observed data, suggesting that the performance of water quality models was improved through this calibration.

5. Data Analysis to Support Modeling

5.1. Analysis of Tropical Events Irene and Lee in Historical Context and Frequency of Extreme Hydrological Events

In August and September of 2011 Hurricane Irene (Irene) (Aug 26 – Aug 29, 2011) was followed less than two weeks later by Tropical Storm Lee (Lee) (Sep 5 – Sep 8, 2011), both of which precipitated large amounts of rain across various parts of the eastern US. Based on the damage caused by Irene and Lee, which occurred in close spatial and temporal proximity to each other, a number of communities, including some in New Jersey, New York State, and Vermont, have perceived this episode to be among the historically largest precipitation events, and unprecedented flooding events, on record.

Historically, the occurrence of extreme weather and climate events such as these storms have been associated with loss of human life, waterborne disease outbreaks, water quality issues, and high costs for recovery (Easterling et al., 2000; Karl and Easterling, 1999; Curriero et al., 2001; Weniger et al., 1983; Towler et al., 2010). Recently, the Intergovernmental Panel on Climate Change (IPCC) has emphasized the importance of new approaches to address the management of risks associated with extreme events and disasters as these may be directly affected by climate change and as a necessity to improve climate change adaptation (IPCC 2012). Ashley and Ashley (2008) reported that at least 815 fatalities between 1996 and 2005 are connected to flooding events in the United States. Studies of recent events around the world, including tsunamis, flooding, storm damage, and extreme heat or cold weathers, have revealed exponentially increasing costs on the order of billions of dollars (Easterling et al., 2000; Karl and Easterling, 1999; Pielke and Landsea, 1998; Towler et al., 2010).

A number of studies have shed light on trends in extreme events across the globe and regionally. In most studies observed changes in precipitation are occurring concurrently with changing air temperature; for example Burns et al. (2007) studied the Catskill Mountain region in NY and found a 0.6 degree Celsius increase in mean annual temperature associated with 136 mm increase in yearly cumulative precipitation in the past 50-year period. Two recent studies of precipitation and drought over NYC Water Supply region demonstrate that the period since the 1970s has been particularly wet when viewed in the context of station observations since the early 20th century (Seager et al. 2012), as well as in the context of longer term hydrological variations based on tree ring reconstructions (Pederson et al. 2012). These studies show that both the drought of the 1960s and the subsequent wet period (which continues until today) were caused by internal atmospheric variability (Seager et al. 2012) and that periods of more extensive drought have occurred in earlier centuries (Pederson et al. 2012). Thus, based solely on climatology, the implication is that water supplies in this region are vulnerable to significant climatic variations beyond what has been experienced during the last 100 years. In any case, the relationship between extreme weather and climate events and climate change and how it directly affects society and sustainable development remains uncertain. Reducing uncertainty will require (among other aspects) more data on extreme events covering longer periods of record; as well as a better understanding of the physical processes and evidence linking extreme events to climate change (IPCC 2012).

In light of Irene and Lee, and the public perceptions of these events, this report section focuses on two questions. (1) How extreme, in the context of available station records, were Irene and Lee in the Mid-Hudson Valley and Catskill Mountain regions in southern New York State? and, (2) Has there been a change in the frequency of extreme events in this region? To achieve these objectives both parametric and non-parametric statistics are applied to precipitation and stream gage records, some of which extend back over a century.

Study Area and Data

The study area encompasses the Mid-Hudson Valley and Catskill Mountain regions in southern New York State. The Catskill Mountain region is part of the Allegheny Plateau consisting mainly of sedimentary bedrock (Burns et al., 2007), and contains rugged topography through which numerous tributaries drain naturally into the Hudson and Delaware Rivers. The study area, located between 80km and 250km north of New York City, extends through Delaware, Greene, Orange, Ulster, Schoharie, and Sullivan counties of New York State. The climate of the region is humid continental with mean daily air temperatures ranging between -5 to 0 ^{o}C during winter and 15 to 20 ^{o}C during summer. The temperature of the Catskill Mountain region is strongly impacted by elevation which rises to approximately 1200 m from the Hudson River. Regional hydrology is influenced by snow and snowmelt during winter and early spring particularly at higher elevations (Matonse et al., 2012). Average annual precipitation from the stations included in this study ranges from 1005 to 1580 mm. Average daily streamflow for the selected gauges ranges from 1.6 to 31 m^3/s.

Our analyses include three data sets:

(i) Gridded daily precipitation was obtained from the Northeast Regional Climate Center (NRCC) at Cornell University, Ithaca, NY. This product, at 4-km spatial resolution precipitation, is produced using original hourly radar Multisensor Precipitation Estimates (MPE) that are aggregated and adjusted on a daily time step using rain-gauge observations and an optimized inverse distance weighting (IDW) to reduce spatially varying errors in the radar estimates and assuming that rain-gauge values represent true values (DeGaetano and Wilks, 2009). We refer to DeGaetano and Wilks (2009), Simanton and Osborn (1980) and Mandapaka and Germann (2010) for a detailed description about IDW parameters calibration and model application;

(ii) Historical precipitation records from rain-gauge stations across our region were obtained from both the National Climatic Data Center as well as the Northeast Regional Climate Center. A total of 12 rain-gauge stations with historical precipitation records met our criteria for inclusion in this study (Table 5.1): stations must have at least 30 years of continuous data, and must include data for Irene and Lee in fall, 2011. Three stations have >100 years of data. Stations with extended periods of missing data were removed. All trace precipitation was set to zero as these have no effect on maximum time series. Table 5.1 also includes 4-day total precipitation during Irene (Aug 26 – Aug 29, 2011)

and during Lee (Sep 5 – Sep 8, 2011). The geographic locations of precipitation gauges are shown in Figures 5.1 and 5.2.

(iii) Historical daily average and annual peak streamflow records are obtained from USGS stream gage stations. Ten USGS gauges (Table 5.2) are selected in the Greater Catskill and Mid-Hudson valley watersheds for use in flood frequency analysis (Table 5.2). The selection is based on following two criteria: (1) the gauge is presently active and has 30 or more years of annual maximum streamflow records; (2) the site is unregulated or has very low impact of regulation. No processing was performed to replace missing values. The geographic locations of stream gauges are shown in figures 5.1 and 5.2.

Table 5.1. Precipitation stations used in this analysis. Also shown are 1-day and 4-day precipitation totals during Irene and Lee events, and the difference between Irene and Lee.

Station ID Number	Station Name	County	Record Period Available	Station Elevation (m)	Irene Max Daily Rain (cm)	Lee Max daily rain (cm)	Irene 4-day precip (cm)	Lee 4-day precip (cm)	Difference 4-day Precip Irene minus Lee (cm)
300254	Arkville	Delaware	1948 - 2011	399.3	0.5	5.9	n/a	16.5	n/a
302036	Delhi	Delaware	1926 - 2011	432.8	7.7	6.4	11.1	13.3	-2.2
302060	Deposit	Delaware	1962 - 2011	304.8	5.3	8.0	9.5	14.3	-4.8
302582	Ellenville	Ulster	1948 - 2011	106.7	6.0	6.7	n/a	19.2	n/a
304731	Liberty	Sullivan	1950 - 2011	472.1	10.4	5.5	13.8	14.4	-0.6
305310	Middletown	Orange	1951 - 2011	213.4	n/a	8.6	n/a	20.1	n/a
305426	Mohonk Lake	Ulster	1896 - 2011	379.5	20.9	6.3	23.6	17.9	5.7
306774	Port Jervis	Orange	1893 - 2011	143.3	11.1	6.0	16.9	11.6	5.4
307274	Rosendale	Ulster	1956 - 2011	12.2	21.6	5.5	22.7	10.5	12.1
307799	Slide Mtn	Ulster	1948 - 2011	807.7	21.9	7.2	30.2	18.5	11.7
308932	Walton 2	Delaware	1956 - 2011	451.1	5.5	7.9	12.0	17.5	-5.5
309292	West Point	Orange	1890 - 2011	97.5	11.2	5.1	20.9	14.6	6.3

Table 5.2. USGS gauges used in this study. Also shown are drainage area, gauge elevation, basin average slope, and streamflow peak discharge during Irene and Lee

USGS ID Number	Gauge Name	County	Record Period Available	Drainage Area (sq.km)	Gauge Elevation (m)	Basin Average Slope (%)	Irene Peak Flow (cms)	Lee Peak Flow (cms)
1350000	Schoharie Creek at Prattsville	Greene	1936 - 2011	613.8	344.9	21.1	3398.0	345.5
1362200	Esopus Creek at Allaben	Ulster	1964 - 2011	165.0	304.2	32.0	1118.5	113.3
1362500	Esopus Creek at Coldbrook	Ulster	1936 - 2011	497.3	189.4	31.5	2146.4	580.5
1371500	Wallkill River at Gardiner	Ulster	1936 - 2011	1800.0	56.6	4.6	858.0	778.7
1421900	West Branch Delaware Tiver Upstream from Delhi	Delaware	1937 - 2011	347.1	411.9	17.4	250.9	199.9
1423000	West Branch Delaware River at Walton	Delaware	1937 - 2011	859.9	362.8	18.4	453.1	523.9
1413500	East Branch Delaware River at Margaretville	Delaware	1937 - 2011	422.2	397.0	23.5	945.8	300.2
1414500	Mill Brook Near Dunraven	Delaware	1958 - 2011	65.3	395.8	25.8	107.9	54.9
1415000	Tremper Kill Near Andes	Delaware	1951 - 2011	86.0	391.9	21.6	49.0	45.6
1435000	Neversink River Near Claryville	Sullivan	1939 - 2011	172.5	464.0	23.3	603.1	158.6

Methods

Both parametric and non-parametric statistics are applied to precipitation and streamflow records in order to evaluate extreme events. All analyses are performed for annual, warm season, and cold season separately. Warm season analyses include data from June 1st through October 31st, and cold season analyses include data from November 1st through May 31st. These seasonal definitions effectively separate events associated with snow (i.e. melt and rain-on-snow events) from those associated with heavy precipitation. For much of non-parametric analysis, our definition of "extreme event" includes all events with magnitudes greater than or equal to the 95th percentile. This definition is applied to each station individually; then, for some parts of the analysis, results from all stations are summarized.

Parametric statistics include hydrologic frequency analysis (HFA) using annual-maximum series (AMS) (El Adlouni and Ouarda, 2010). In addition, HFA is also employed using seasonal-maximum time series from warm season and cold season separately. HFA provides the magnitude of events as a function of average return period (also known as recurrence interval).

A return period "percent difference" is used to compare annual versus warm season return periods for Irene and Lee. The percent difference is calculated as

$$Warm\%\,Return = \frac{(Warm\,Return - Annual\,Return)}{Annual\,Return} * 100 \qquad (5.1)$$

where *AnnualReturn* and *WarmReturn* represent annual- and warm period-based HFA return period estimates.

In contrast to the statistics described above that were based on maximum peak streamflows, we also calculated percent differences using average daily streamflow and total daily precipitation in order to be consistent with the daily mean values used in other portions of this analysis.

Annual streamflow HFA

For annual streamflow HFA, at each gauge location annual peak discharges are fitted to a log Pearson type III distribution (LP3) (Stedinger et al., 1993; Interagency Advisory Committee on Water Data, 1982). This distribution is chosen because it has been recommended and extensively used in the United States for developing flood frequency analysis. Instantaneous peak streamflows are used in this study for developing annual streamflow frequency analysis while daily average streamflows are applied to estimate a percent difference using equation 5.1. Our application of the LP3 model followed the description in Stedinger et al. (1993). A similar LP3 distribution assumption was applied for the warm season maximum streamflows.

Annual and warm season precipitation HFA

For precipitation frequency analysis of 24-hour rainfall AMS are assumed to follow a Gumbel distribution (Stedinger et al, 1993). The Gumbel distribution has been most often used with precipitation AMS and was applied for developing a Rainfall Frequency Atlas in the US

including for our region of study (Hershfield, 1961; El Adlouni and Ouarda, 2010; Frederick et al., 1977; Smith, 1993). The same Gumbel distribution that is used for annual maximum precipitation is also applied to warm and cold season analyses.

Non-parametric data analysis

Prior to applying non-parametric statistics, we use daily total precipitation data to calculate 4-day, 30-day antecedent, and 60-day events. 4-day events represent individual storms. We choose the 4-day averaging period because Irene and Lee both resulted in precipitation over 4 days at some stations. An event is defined as any series of consecutive days (including only one day) with precipitation. All events included in this analysis are non-overlapping. The procedure is described here using the 4-day averaging period as an example, but other averaging periods are calculated in an equivalent fashion. Also, time series for individual seasons are calculated in an equivalent fashion by including only days during the season in question. The procedure used to calculated 4-day events is as follows:

First, calculate the total precipitation over all 4-day intervals, including overlapping intervals, which is equivalent to the 4-day running sum of the daily precipitation time series. Second, identify all 4-day events in the resultant time series by eliminating all zero running sum values. Thus, an "event" is any group of four consecutive days with non-zero total precipitation. By this definition, events that last less than four days are still included as part of a 4-day event, and are not excluded from the analysis.

Second, we include only non-overlapping events. Two overlapping events might include, for example, a 4-day event ending on January 20 (which is the total precipitation for January 17-20) and a 4-day event ending on January 21 (which is the total precipitation for January 18-21). For all such overlapping events, only the one with the largest precipitation amount is retained for analysis; others are set to zero, and are therefore no longer considered in the analysis. This procedure results in a time series for each station, and for each period of analysis. Extreme events are defined from these time series as any event greater than or equal to the 95th percentile of the distribution of all 4 day cumulative precipitation values, which is calculated for each station, and each season. While this explanation uses 4-day events as an example, we perform the identical procedure for 30-day and 60-day events.

We also examine antecedent conditions. Ideally, antecedent conditions for warm season events would be determined by observations of soil moisture. However, in the absence of sufficient soil moisture observations, we used the cumulative 30-day precipitation occurring just prior to an extreme event as an indicator of antecedent wetness. These are calculating by identifying all extreme 4-day precipitation events, and calculating the total precipitation during the 30-days immediately prior to (and not overlapping with) the 4-day event. This results in a time series of 30-day antecedent precipitation totals for extreme 4-day events. This way, we can evaluate whether hydrologic conditions immediately prior to Irene and Lee were unusual compared to conditions immediately prior to other extreme events (i.e. not in comparison to all 30-day periods on record).

Overview of precipitation during Irene and Lee

Figures 5.1 and 5.2 show the location of the rain-gauges and stream gauges used in this study and contours of 4-day total precipitation during Irene and Lee. During Irene (Figure 5.1), 4-day total precipitation varied spatially over the study area between 8 and 38 centimeters with highest rainfall volumes occurring in northeastern and southeastern parts of our study area. During Lee (Figure 5.2) 4-day total precipitation varied between 12 and 22 cm, with higher values along the eastern and southeastern portions of the region, similarly to Irene.

However, in contrast to Irene, precipitation during Lee was less variable across the study area. As a result, over the eastern and southeastern portions of the study more precipitation fell during Irene, while over the western portion of the study area more precipitation fell during Lee. The region of greatest difference is found over the northeastern corner of the region, which contain a series of peaks known to locals as the Blackhead Range.

Irene and Lee in context of long term historical events

In this section we examine precipitation and streamflow magnitudes during Irene and Lee. Results are presented using the standard method, for which a parametric return period analysis is performed using data from all months of the year; as well as using data from the warm season only. Precipitation and streamflow frequency analyses are performed at various cumulative probability levels corresponding to various return periods from 2 to 1000 years. Return periods for Irene and Lee are estimated by comparing the size of the maximum daily rainfall or instantaneous peak streamflow during Irene and Lee with results from annual or seasonal frequency analyses.

Precipitation frequency analysis

Return period estimates for Irene and Lee are presented in tabular form in Tables 5.3 and 5.4, and graphically in Figures 5.1 and 5.2. Precipitation return periods for Irene calculated using AMS (annual return period) are greater than twenty years at only three stations, which have return periods of 88, 407, and 472 years (Table 5.3). This of course is in good part an artifact of the sparsity and non-homogeneous spatial pattern of the precipitation stations relative to the actual spatial pattern of precipitation for the storms, and thus cannot be used as an indicator of how extreme these storms were. All annual return periods for Lee are under ten years.

The same analysis applied to warm season events are presented in Table 5.3. Precipitation return periods using only warm season values indicate that Irene had return periods more than 100 percent greater than return periods based on annual statistics at seven stations. At three stations Irene was so extreme that estimated return periods were in the thousands of years. The four stations for which Irene warm season return periods were equal to, or lower than the annual based return periods are all located in the western portion of the study area. In contrast, precipitation return periods during Lee were all under ten years. Thus, with regards to the maximum daily precipitation during the warm season, Irene was an extremely unusual event in the eastern portion of the study area, while Lee was of a more common magnitude and spatially less variable throughout the region.

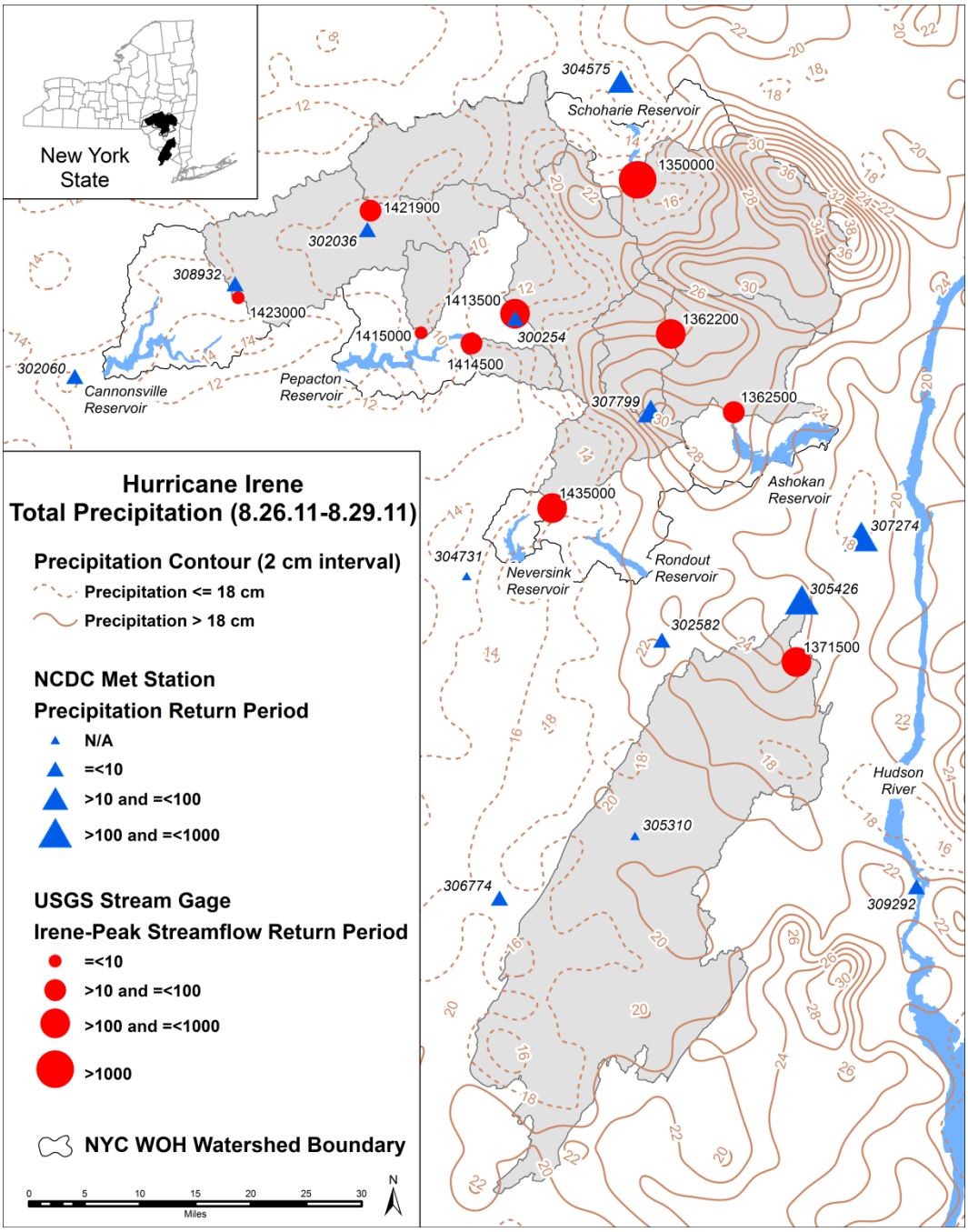

Figure 5.1. 2 cm contour lines for 4-day precipitation amount during Irene (Aug 26 – Aug 29, 2011). Circles at each USGS stream gauges represent the magnitude of Irene return period from the gauge Streamflow annual frequency analysis. Triangles at each rain gauge give the magnitude of Irene return period based on the rain gauge precipitation annual frequency analysis.

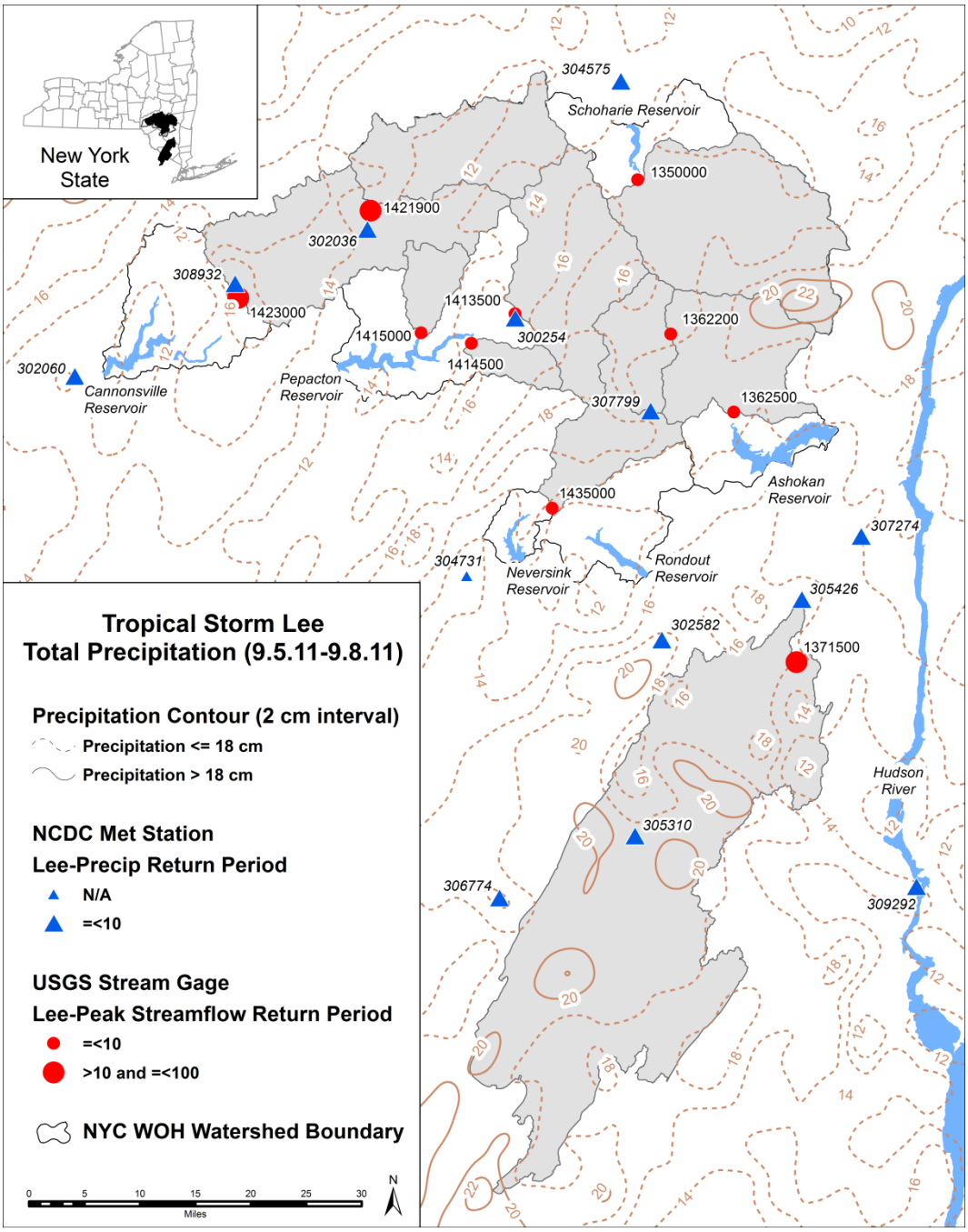

Figure 5.2. 2 cm contour lines for 4-day precipitation amount during Lee (Sep 5 – Sep 8, 2011). Circles at each USGS stream gauges represent the magnitude of Lee return period from the gauge Streamflow annual frequency analysis. Triangles at each rain gauge give the magnitude of Lee return period based on the rain gauge precipitation annual frequency analysis

Table 5.3. Irene and Lee estimated precipitation return periods. Percent difference is calculated as [((warm-annual)/annual)*100], where "annual" and "warm" are the return periods based on annual maximum and warm season maximum 24-hour precipitation, respectively. A similar record period (instead of full available period in Table 5.1) was used for all precipitation stations so that that the results for the frequency analysis are comparable.

Station ID Number	Station Name (County)	Record Period for Frequency Analysis	Irene Annual Return Period (yrs)	Irene Warm Period Return (%)	Lee Annual Return Period (yrs)	Lee Warm Period Return (%)
300254	Arkville (Delaware)	1952 - 2011	<2	0	2	106
302036	Delhi (Delaware)	1952 - 2011	7	9	4	23
302060	Deposit (Delaware)	1962 - 2011	2	-10	7	8
302582	Ellenville (Ulster)	1952 - 2011	2	0	2	25
304731	Liberty (Sullivan)	1952 - 2011	16	23	2	0
305310	Middletown (Orange)	1952 - 2011	n/a	n/a	7	8
305426	Mohonk Lake (Ulster)	1952 - 2011	407	-5	<2	0
306774	Port Jervis (Orange)	1952 - 2011	9	19	2	0
307274	Rosendale (Ulster)	1958 - 2011	472	-5	<2	0
307799	Slide Mtn (Ulster)	1952 - 2011	88	93	<2	0
308932	Walton 2 (Delaware)	1956 - 2011	2	0	6	15
309292	West Point (Orange)	1952 - 2011	7	18	<2	0

Table 5.4. Irene and Lee estimated streamflow return periods. Warm percent return difference is calculated as [((warm-annual)/annual)*100], where "annual" and "warm" are the return periods based on annual maximum and warm season maximum daily average streamflow, respectively.

USGS ID Number	Gauge Name (County)	Drainage Area (sq.km)	Record Period for Frequency analysis	Irene Annual Return Period (yrs)	Irene Warm %Return (%)	Lee Annual Return Period (yrs)	Lee Warm %Return (%)	Rank of 2011 60-day mean stream flow
1350000	Schoharie Creek at Prattsville (Greene)	613.8	1936 - 2011	> 1000	n/a	4	119	3
1362200	Esopus Creek at Allaben (Ulster)	165.0	1964 - 2011	981	43	2	128	1
1362500	Esopus Creek at Coldbrook (Ulster)	497.3	1936 - 2011	77	123	4	246	1
1371500	Wallkill River at Gardiner (Ulster)	1800.0	1936 - 2011	116	116	64	100	1
1413500	East Branch Delaware River at Margaretville (Delaware)	347.1	1937 - 2011	385	-16	6	10	1
1414500	Mill Brook Near Dunraven (Delaware)	859.9	1937 - 2011	22	n/a	4	215	4
1415000	Tremper Kill Near Andes (Delaware)	422.2	1937 - 2011	3	293	3	262	n/a
1421900	West Branch Delaware River Upstream from Delhi (Delaware)	65.3	1958 - 2011	31	206	11	153	n/a
1423000	West Branch Delaware River at Walton (Delaware)	86.0	1951 - 2011	7	290	12	120	1
1435000	Neversink River Near Claryville (Sullivan)	172.5	1939 - 2011	109	-55	< 2	174	2

Streamflow frequency analysis

Both Irene and Lee were more unusual streamflow than precipitation events (Table 5.4, Figures 5.1 and 5.2). As mentioned before generalizing about the spatial distribution of hydrologic frequency based on the precipitation analysis is difficult due to the sparsity of precipitation stations. The streamflow frequency analysis, which provides a better indicator of spatial distribution of hydrologic frequency since streamflow integrates precipitation over large catchment areas, Irene annual streamflow return periods were greater than 20 years at eight of ten stations, and greater than 100 years at five of ten stations. Streamflow return periods for Lee

were less extreme than for Irene, with only one station greater than 20 years. When considering warm season events only, return periods for Irene increase in comparison to annual results in about half of the stations (> 100% increase). For Lee, warm season results increase in comparison to annual results at nine of ten stations. A higher return period for the warm season (positive percent difference) indicates that the magnitude of the event being analyzed is less common in the season than when considering the annual time series.

These results partially explain the perception among communities across the region that these events were higher than the corresponding return periods obtained from conventional annual frequency analysis suggests: in fact, the events were more extreme when considering only the warm season. However, a more complete explanation of the discrepancy between the traditional return period analysis and common perceptions of these events is discussed in the next section.

Has the frequency of extreme events changed during the period of record?

Finally, we examine variations in the frequency of extreme events during the periods of record for stations in this region. For each precipitation and streamflow gauge station we calculate the magnitude of the 95th percentile event (4-day total precipitation or cumulative streamflow) using all events from the entire period of record, and then make a yearly count of how many such events occur, resulting in an annual time series.

An example of such an analysis for one station (Middletown in Orange County) is shown in Figure 5.3. Figures 5.3a and b show scatter plots of 4-day precipitation for each season (with one cross for each event); 95th percentile values are indicated by the horizontal line. Warm season extreme (95th percentile) events are greater than cold season extreme events at this station (and, in fact, at all stations). The resulting annual time series of the number of extreme events per year (figures 5.3c and d) indicate significant interannual variations. Superimposed on the annual time series is the smoothed (11-year centered mean), which we use to represent decadal scale fluctuations in the frequency of extreme events. The maximum smoothed value (or values, if two or more years had the same maximum value) is indicated with a circle. For this station, one can see that the number of extreme events per year during the cold season peaked near 1980, while the number of extreme events during the warm season has peaked in the most recent decade.

To provide a time series that represents regional scale variations in the frequency of extreme events, results from individual stations are combined for precipitation (Figure 5.4) and streamflow (Figure 5.5). These are produced by calculating the mean, for each year, of the number of extreme events at all available stations. The dry 1960s and the wet 1970s are apparent during the cold season, but not during the warm season or in the annual mean precipitation results (Figure 5.4). A dramatic increase in extreme precipitation frequency since the 1980s is apparent during the warm season (and in the annual mean records) but not during the cold season. The mean number of extreme precipitation events per year has increased from approximately 0.6 during the early 1980s to approximately 1.8 during the most recent decade. Also shown is the time series of number of stations per year included in the regional mean (Figure 5.4d).

The regional mean frequency of extreme streamflow events was relatively high during the 1970s and low during the 1960s in both the cold and warm seasons (Figure 5.5). During the warm season only (Figure 5.5c) the occurrence of extreme streamflow has increased dramatically since the mid-1990s, and has peaked in the most recent decade. The regional mean frequency of extreme events has increased from approximately six per year in the mid-1990s to approximately sixteen per year during the most recent decade. This recent increase in warm (but not cold) season streamflow is related to the increased frequency of extreme precipitation events, and also to an increase in the frequency of extreme 30-day antecedent totals prior to extreme precipitation events (not shown here).

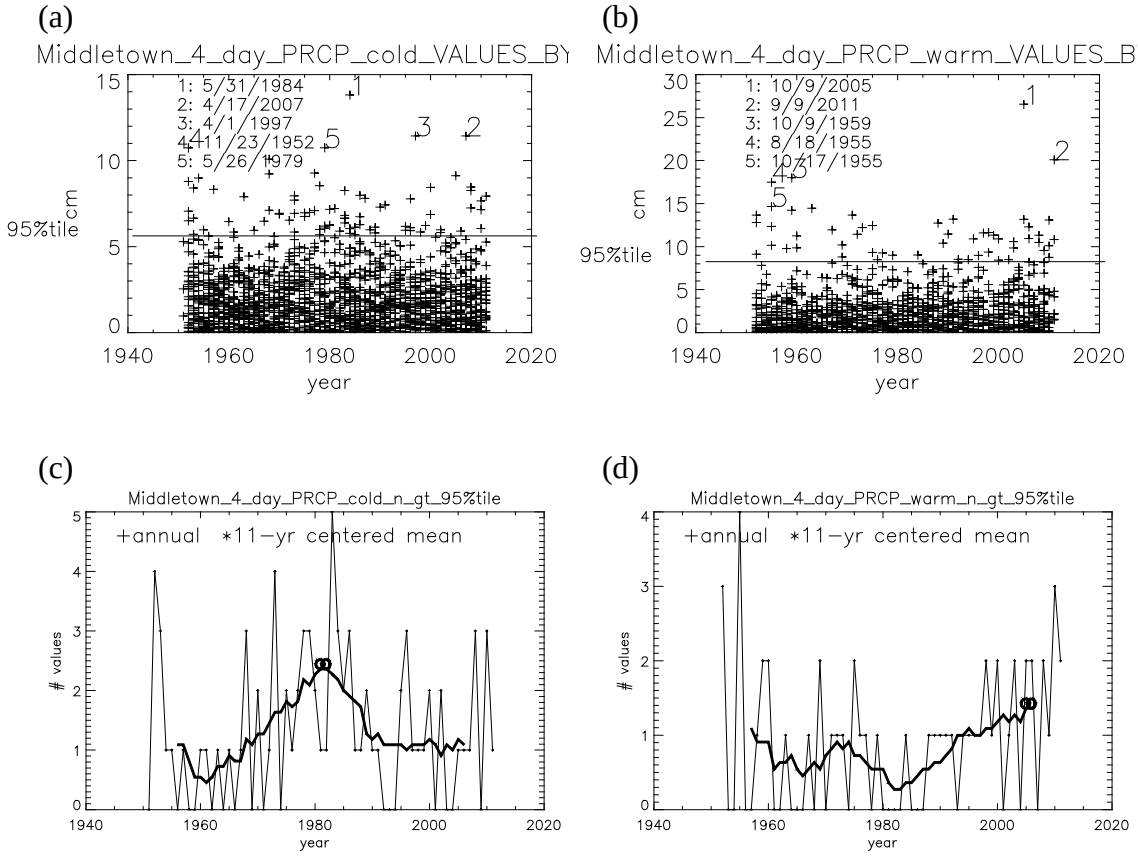

Figure 5.3. Example of nonparametric analysis for the Middletown precipitation record. (a) and (b) show the magnitudes of every 4-day precipitation event on record during (a) cold and (b) warm seasons. Also shown are the 95th percentile value and the top 5 historical extreme events (numbers and dates). (c) and (d) show the number of extreme (i.e. >=95th percentile) events per year, as well as a smooth (11-year centered mean) line and circle indicating the year(s) with the highest smoothed value.

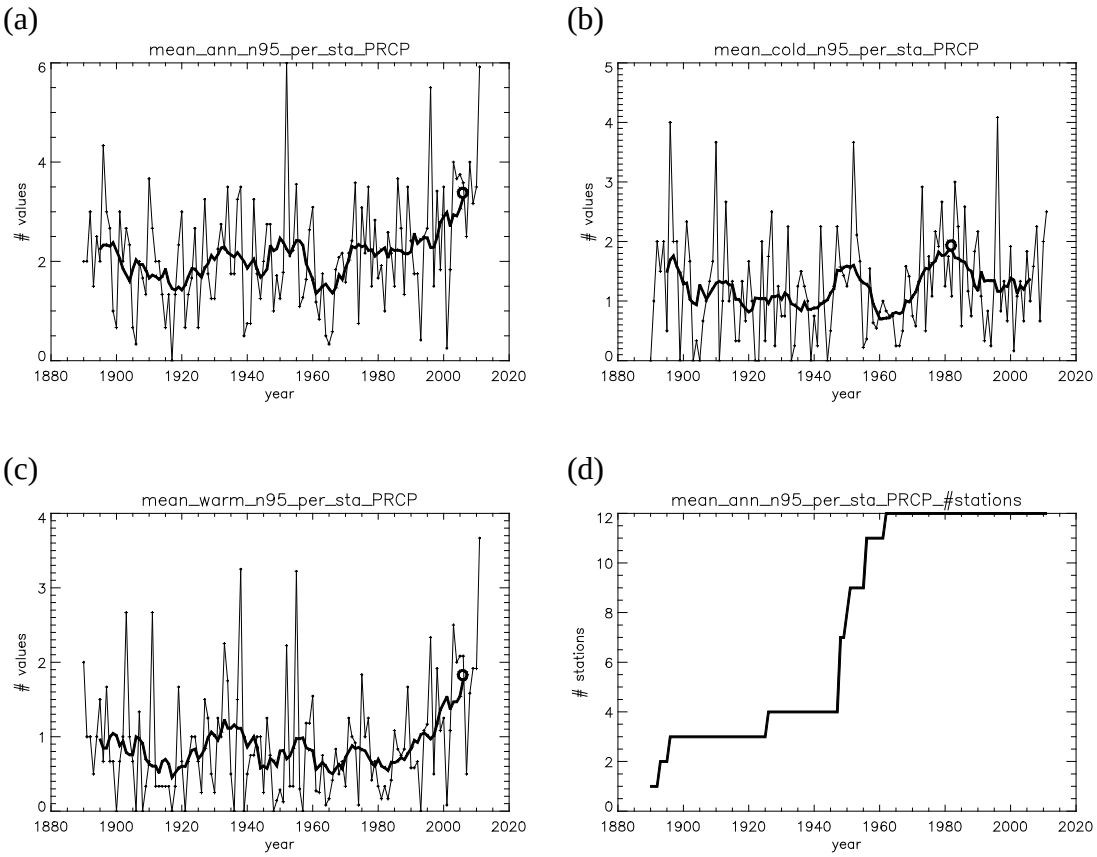

Figure 5.4. Regional mean number of 95%tile 4-day precipitation values per year. For each year, the number of 95%tile values per year, averaged over all stations available, is shown (solid line) along with the 11-year running mean (bold line) and a circle indicating the year with the highest smoothed value. Panel a) includes values from all months; b) includes cold season values only; c) includes warm season values only; d) shows the number of stations available for each year of calculations.

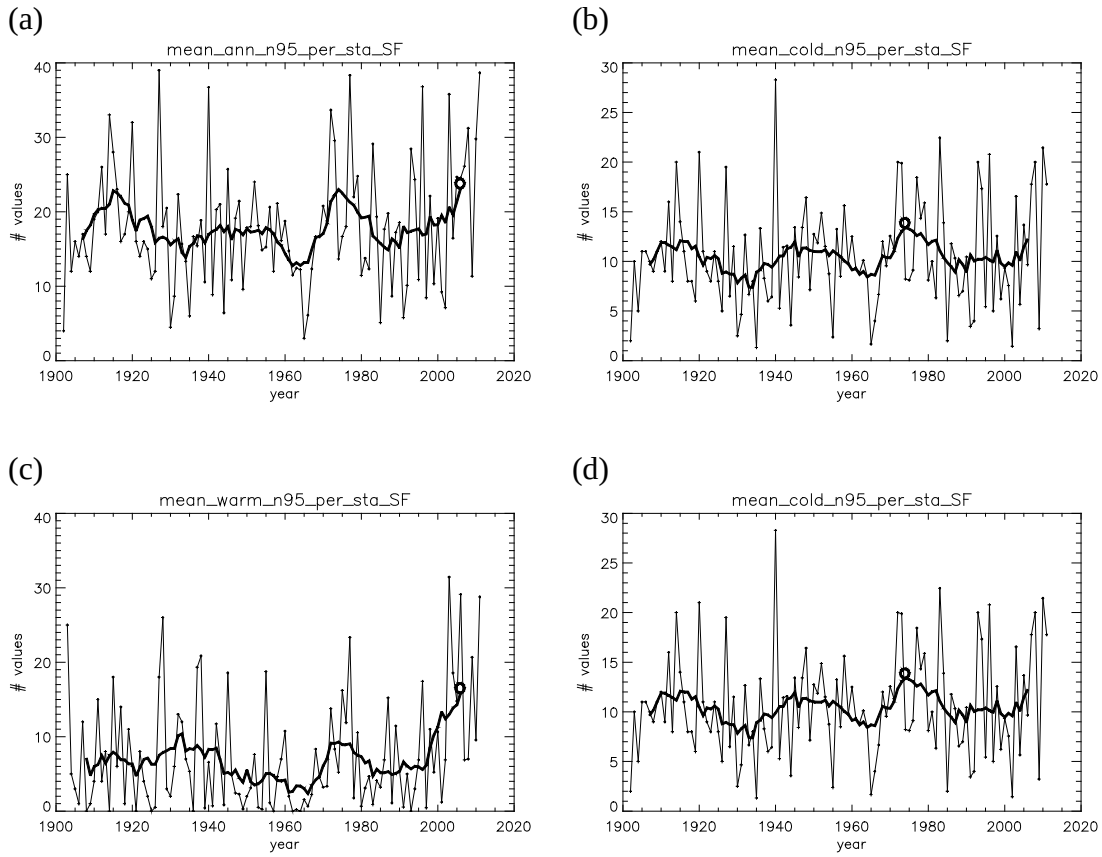

Figure 5.5. Regional mean number of 95%tile daily streamflow values per year. For each year, the number of 95%tile values per year, averaged over all stations available, is shown (solid line) along with the 11-year running mean (bold line) and a circle indicating the year with the highest smoothed value. Panel a) includes values from all months; b) includes cold season values only; c) includes warm season values only; d) shows the number of stations available for each year of calculations

Summary and Conclusions

During Fall, 2011, Irene and Lee precipitated 8cm to 38cm and 12cm to 22cm, respectively, during 4-day periods over the Hudson Valley and Catskill regions of Southern New York State. Parametric and non-parametric statistics for precipitation and streamflow are analyzed to evaluate the relative magnitude of these two storms, to determine how unique the series of events during fall 2011, were when considered in historical context, and to detect possible changes in the frequency of extreme hydrological events during the period of historical records available.

Our main conclusions are:

(i) Irene and Lee were both devastating, but the impacts were spatially variable across the region, and between the two events. The maximum precipitation rates for the entire

region were higher for Irene than for Lee. However, Irene was more unusual in the eastern portion of the study region while Lee was more unusual in the western section.

(ii) Results of standard (parametric) hydrological frequency analyses indicate that Irene and Lee were quite uncommon for some sites, but not uncommon nor unprecedented for others. Return periods for Irene and Lee are larger at most sites when using warm season only rather than either annual or cold season statistics are considered. Seasonal analysis is important for understanding the nature of the events in a climatological framework, and for purposes of public perception, the seasonal nature of these variations, and the hydrological context in which they occurred.

(iii) Taken together, the events of fall 2011, including Irene and Lee, were unprecedented in this region as evidenced by highest ranking of 60-day mean streamflow over period of record for >50% of the streamflow drainage area analyzed (Table 5.4).

(iv) Extreme warm season events in this region have been more frequent during the last two decades than at any time on record. Increasing trends in 11-year running mean warm season precipitation and streamflow statistics are observed from the mid-1980s to present. The frequency of extreme warm period precipitation and streamflow events during the first decade of the twenty first century has risen to levels 40-70% higher than at any earlier time on record. It remains unclear whether this recent pattern in extreme events is part of a trend that will continue, or just a short-term fluctuation.

5.2. Ecosystem Effects of a Tropical Storm Irene on New York City Reservoirs

In late August 2011, Tropical Storm Irene (hereafter Irene) moved through the Caribbean and up the east coast of North America. This significant storm made its third landfall near New York City, New York; heavy rain and tropical storm force winds persisted as the storm moved northward (Figure 5.6). Most of the damage in North America was due to wind, heavy rainfall, and flooding (Avila et al., 2011) and the effects were visible across terrestrial landscapes and in stream and river flooding.

The wind and rain associated with tropical cyclones can also lead to significant changes in the physical structure and biological functioning of aquatic ecosystems. Lake and estuarine studies from the southeastern US, where tropical cyclones are relatively common, show that the storms affect vertical thermal structure (Jennings et al., 2012), primary production (Havens et al., 2012; Paerl et al., 2006), and fish production (Paerl et al., 2001; Rogers and Allen, 2008). In the northeastern US, major tropical cyclones are infrequent (hurricane landfall recurrence intervals ~15-30 years (Blake et al., 2011), and although tropical cyclone frequency may or may not increase with climate change, future storms are nonetheless likely to be more intense with higher rainfall rates (Knutson et al., 2010). Due to their size and potential longevity, these storms can affect large geographic areas. However, there has been no evaluation of the immediate regional impacts of tropical cyclones on aquatic systems in northeastern North America.

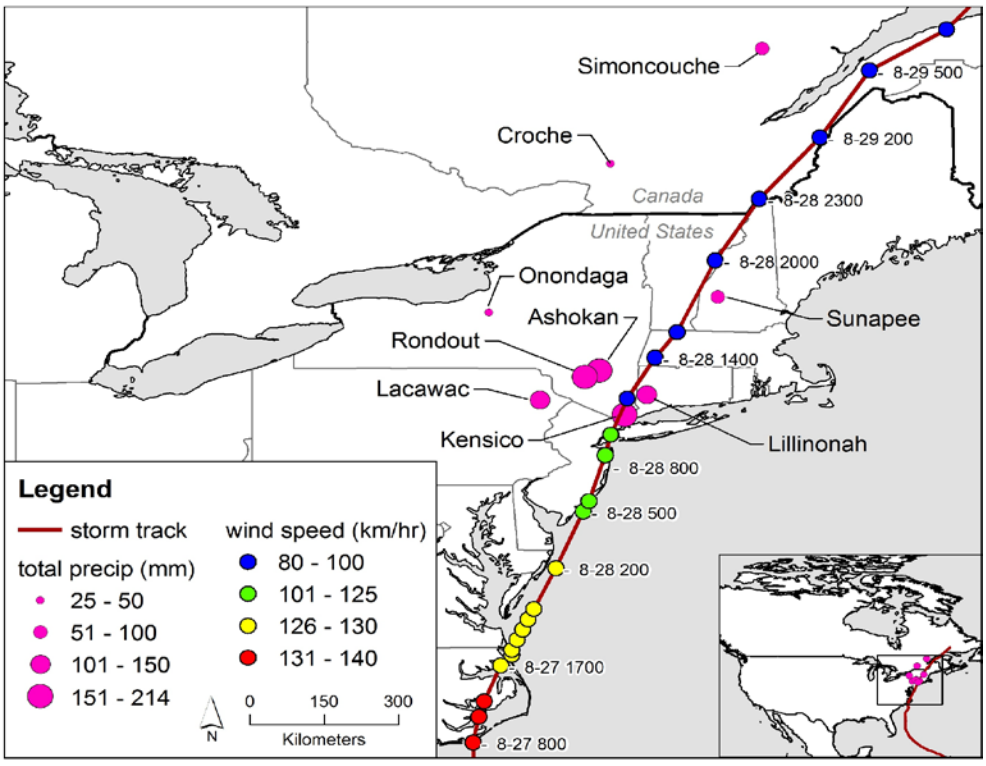

Figure 5.6. Map of study region and Irene storm track. Map of northeastern United States and southeastern Canada with study sites shown as pink circles. Size of the circle indicates the total precipitation from Tropical Cyclone Irene recorded at or near each lake or reservoir.

The research described here is part of a regional study undertaken jointly with participants in the Global Lake Ecological Observatory Network (GLEON), which examined the effects of Irene on thermal stability and ecosystem metabolism in the New York City reservoirs and 6 other lakes in the vicinity of the Irene storm track (Figure 5.6) We used a set of *in situ,* automated, monitoring systems that record data at high frequency (3-6 hours) to document the timing, magnitude, and duration of changes in the condition of lakes with previously unavailable precision. We focused on the derivation and application of metrics that allowed for physical and biological comparison across systems that vary widely in their characteristics, including, catchment size and land cover, water residence time, bathymetry, and the initial state of systems at the time of the event. We then used these metrics to evaluate the temporal sequence of disturbance and recovery of biotic and abiotic characteristics that occurred as the storm passed through the region.

Methods

Automated sensors located on floating buoys measured water temperature and dissolved oxygen and had been previously deployed in Ashokan, Rondout and Kensico reservoirs and the other sites across northeastern North America. Meteorological data were collected from the buoys or from other nearby sources, and barometric pressure measurements were normalized to sea level using the hypsometric equation (Table 5.5). To assess the whole-lake energetic impact of this major physical disturbance, we quantified lake thermal stability as Schmidt stability (J m^{-2}), a measure of the amount of work required to overcome density stratification and completely mix a lake (Idso, 1973; Read, et al. 2011). Daily Schmidt stability was calculated as in Idso, 1973 using the software program Lake Analyzer (Read, et al. 2011). Schmidt stability is calculated using the equation

$$Stability = \frac{g}{A_s}\int_0^{Zd}(z - z_v)\rho_z A_z \, \partial z \qquad (5.2)$$

where g is acceleration due to gravity, A_s is the surface area of the lake, z_d is the maximum depth of the lake, z is the depth of the lake at any given interval, z_v is the depth to the center volume of the lake, ρ_z is density of water at depth z, and A_z is the area of the lake at depth z. The calculation did not take into account the effect of changing lake depth; such changes would have negligible effects on our results because Schmidt stability is calculated using temperature and bathymetry profiles at 1 meter resolution and storm inputs resulted in <1 m change in depth in lakes for which we have information. We have complete lake depth information for Ashokan. For that system, including lake depth in the calculations decreased daily Schmidt stability by 0-4% and overall change in stability by only 0.03% (see below).

Table 5.5. Lake and catchment characteristics, storm intensity metrics, and potential volume replacement for the nine study lakes and reservoirs, northeastern North America. Potential volume replacement (PVR) is the ratio of the volume of water that fell on the catchment plus the lake during Irene relative to lake volume.

Reservoir	Latitude	Longitude	Elevation (m)	Area (ha)	Catchment Area (ha)	Catchment Area / Lake Area (ha/ha)	Mean Depth (m)	Lake Volume (10^9 m^3)	Residence Time (days)	Irene Rainfall (mm)	Max Wind Gust[*] (m/s)	Min Baro-metric Pressure (mbar)	Potential Volume Replacement (%)
Ashokan	41.952	-74.208	180	1218	60416	50.6	13.9	0.174	77	213[†]	18.01	974.5[†]	75.5[#]
Rondout	41.826	-74.472	256	825	23877	30.0	22.5	0.205	51	213[†]	18.01	974.5[†]	25.7[#]
Kensico	41.089	-73.745	108	837	2593	4.1	12.9	0.161	58	168[†]	21.10	971.1[†]	5.6[#]

[†]Data from airport or other nearby weather station; [‡]Data from buoy or onsite weather station

[*]Data from best-fit airport for Irene storm (see Methods)

[#]Includes water from outside catchment delivered via aqueducts; Aqueduct water increases PVR values by up to 2%.

Stability is influenced by lake morphometry, so for each lake we quantified daily Schmidt stability and used it to calculate two metrics of relative change: overall change in stability and the post-storm derivative of stability. The overall change in stability was calculated as the percent change from pre-storm stability (the value on August 26, 2011) to minimum Schmidt stability in the three- day period (August 29-31, 2011) following Irene. We chose August 26 as our pre-storm value because it was the last full day before storm influence. To calculate the post-storm derivative of stability, we first scaled Schmidt stability as a percentage of the initial seven day average (August 1-7, 2011) for each lake. The post-storm derivative of stability is the minimum derivative (maximum absolute rate of change) observed during the three days following the storm.

We examined catchment characteristics, lake morphometry, lake thermal structure, and local storm intensity as potential drivers of change in stability. Because the overall change in lake stability appeared to indicate a threshold change as a function of the potential volume replacement (PVR: the ratio of the volume of water falling on the catchment and lake relative to lake volume, expressed as a percentage; Figure 5.7a), we separated lakes into those above and below the PVR threshold for further analysis. We then analyzed the natural-log-transformed minimum derivative of the scaled stability using ANCOVA analysis with minimum barometric pressure (representing the magnitude of storm effect) as a covariate and PVR (> or <50%) as a categorical explanatory variable. We used the full ANCOVA model including the interaction term to test the assumption of homogeneity of regression slopes. There was a significant interaction effect ($F_{1,5}$=80.11, $p<0.001$) indicating heterogeneity of slopes. Therefore, we used the Johnson-Neyman procedure (D'Alonzo, 2004) on back-transformed data to identify regions of storm intensity where there was a difference between PVR groups.

Storm effects on biological processes

To assess storm effects on biological processes, we used high-frequency dissolved oxygen, water temperature, and meteorological measurements to calculate net ecosystem production (NEP), respiration (R), and gross primary production (GPP) (Van de Bogert, et al. 2007). Seven lakes were included in the metabolism calculations. Kensico and Lacawac were not included due to lack of appropriate oxygen data. We modeled dissolved oxygen dynamics for each 24-hour period using a simple model (Van de Bogert, et al. 2007)

$$\frac{dO_2}{dt} = GPP - R + D \qquad (5.3)$$

where dO_2/dt is the rate of change in dissolved oxygen concentration, GPP is the average daily rate of photosynthesis (mg O_2 L^{-1} d^{-1}), R is the average rate of respiration (mg O_2 L^{-1} d^{-1}), and D is the flux of oxygen between the lake water and the atmosphere.

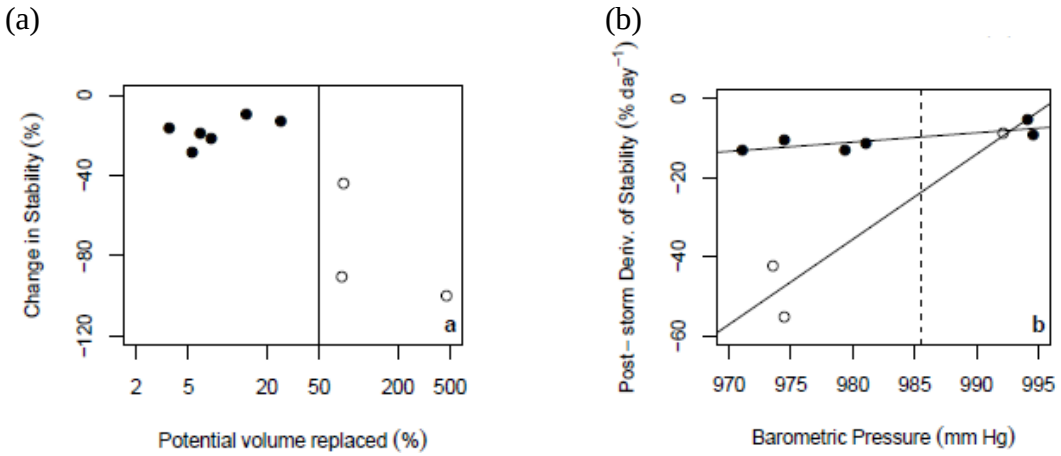

Figure 5.7. Lake stability response to storm and catchment drivers. a) Relationship between percent change in stability (% change from 26 August 2011 to minimum value in the week following the storm) compared to potential volume replacement for each lake. Solid line indicates 50% PVR, the mid-point between lakes in our study with low PVR (closed circles, all ≤26%) and high PVR (open circles, all ≥75%). (b) The relationship between minimum barometric pressure during Irene and the post-storm derivative of stability (minimum derivative in the week following the storm). Open circles represent systems with >50% PVR and closed circles represent systems with <50% PVR. The dotted line identifies the pressure (987.3 mm Hg) below which the high PVR lakes (Post-storm Deriv. of Stability = 1.9*BP – 1904) are significantly different from the low PVR lakes (Post-storm Deriv. of Stability = 0.21*BP – 213) identified using the Johnson-Neyman procedure. Each point represents one lake.

Results and Discussion

Irene's effect was dramatic across the focal region of our study. Thermal stratification, which characterizes most north-temperate lakes during the summer and early autumn and controls fundamental aspects of biogeochemistry and the distribution of organisms, was disrupted in all the reservoirs (Figure 5.7). The thermal stratification was much more clearly defined in all three reservoirs before the Irene and the Schmidt Stability declined abruptly in all three reservoirs following Irene. Deep reservoirs were more stable before the storm, but pre-storm stability did not predict the magnitude of change following the storm. However, the effect of storm has less influence on Kensico Reservoir as compared to other two reservoirs, whereas Rondout Reservoir exhibits weak stratification with deepened upper mixed layer following the storm (Figure 5.8). It is a combination of storm intensity and catchment and lake characteristics that were the best predictor of overall change in reservoir thermal stability.

We used barometric pressure as a surrogate for storm intensity, as barometric pressure was negatively correlated with both maximum wind gust (r=-0.78, p=0.013) and precipitation (r=-0.86, p=0.003). PVR clearly mediated the post-storm derivative responses to storm intensity; at low barometric pressure (i.e., higher storm intensity) lakes with >50% PVR had greater rates of

changes in stability than those with PVR <50% (Figure 5.7b; Johnson-Neyman procedure (D'Alonzo, et al. 2004) $p<0.05$). Thus, while water loading was clearly important to changes in stability, neither storm intensity nor catchment and lake characteristics alone predicted the energetic disturbance of stability. Furthermore, although the greatest disruption of stability occurred in lakes with high PVR as observed in Ashokan Reservoir, even lakes with low PVR had rapid and dramatic changes in stability related to storm intensity, as well as large inputs of water, leading to pronounced effects on water retention time.

The loading of water that drove, in part, changes in physical structure also can affect ecosystem-wide biological processes such as gross primary production (GPP), respiration (R), and net ecosystem production (NEP = GPP-R) via changes in temperature or delivery of terrestrially derived organic matter, nutrients, or inorganic sediment (Paerl, et al. 2001; Pierson, et al. 2003; Tsai, et al. 2011).

NEP changed following Irene but the degree of change was not related to storm magnitude, changes in stability, the depth of the mixed layer, or characteristics of catchments or lakes. Across lakes, the change in GPP was predicted well by the change in temperature ($p=0.02$, $r^2=0.67$), and the temperature changes were greatest in high PVR lakes (Ashokan and Rondout) (Figure 5.9).

Reductions in water temperature could have impacted GPP via a direct physiological pathway or could be indirectly related to the increased terrestrial inputs in the high PVR lakes; in these highly affected systems, increased light limitation was likely due to absorption of light by inputs of particulate and dissolved organic matter (Figure 5.10) (Pierson, et al. 2003). In addition, existing primary producers may have been flushed as a result of lowered residence times due to water influxes (Tsai, et al. 2011).

In some lakes, R increased following the storm (e.g., Ashokan, Rondout, and Sunapee), whereas R decreased in others (e.g., Lillinonah). However, across the region, the change in NEP in lakes was strongly negatively correlated with change in R ($p=0.002$, $r^2=0.87$) (Figure 5.11) and was not correlated with change in GPP ($p>0.05$). In many of our study lakes, increases in carbon loading from flooding and erosion were likely the cause of increased R which created or magnified net heterotrophic conditions. Across lakes, GPP and R were tightly coupled before Irene ($p<0.001$, $r^2=0.98$) (Figure 5.11a), indicating a balance between internal production and respiration. After the storm, autochthonous production appeared to decrease in importance as a carbon source for respiration as GPP and R were decoupled ($p=0.21$) (Figure 5.11b). Despite the importance of temperature change to the change in GPP, it does not appear to be responsible for the decoupling of GPP and R as GPP_{20} was strongly coupled to R_{20} prior to Irene ($p=0.001$, $r^2=0.97$) and decoupled following Irene ($p>0.05$).

The changes in R and NEP observed in our study are likely a consequence of event-based loading of dissolved (DOC) and particulate (POC) organic carbon. In fact, up to 86% of annual DOC export from forested catchments, including sites from the Rondout and Ashokan catchments, has been shown to occur during these types of runoff events (Raymond and Saiers, 2010). Hyrdologic flows following Irene were the largest on record for some of our catchments,

and terrestrial carbon transported to lakes during this period was likely a substantial portion of the annual carbon input.

As observed here across a large region, the effects of disturbance of lake stability generally may be shorter-lived than those of material inputs. Post-Irene recovery of Schmidt stability was rapid in most lakes and was related to the magnitude of initial effect (r^2=0.5, p=0.033). All but one system (Ashokan) recovered to within 80% of pre-storm stability within one week, supporting the observation that event-driven changes in stability tend to recover quickly (Jennings, et al. 2012; Valiela, et al. 1998) given favorable post-storm conditions. In contrast, recovery from effects associated with increased terrestrial organic matter and nutrient loading will depend on how long the material is retained within the system (Paerl, et al. 2006) and the degree to which its composition differs from background composition (Buffam, et al. 2001; Inamdar, et al. 2011). For example, DOC often leaves at a rate that depends on the residence time of the lake (~1 month to 3 years for the systems in this study) and the rate at which DOC is assimilated or degraded. In contrast, POC associated with high turbidity storm water settles in lakes and, if not stored permanently, can increase respiration for years (Cole, et al. 2007) (Figure 5.10).

Managing material flux from land to water is particularly important in systems where maintenance of trophic status or water clarity is critical to management of water quality. Another of the heavily affected sites, Ashokan Reservoir is frequently subject to turbid inputs as a result of stream channel erosion of catchment clay deposits (Peng, et al. 2009). Turbidity in the reservior following Irene was some of the highest recorded, and remained elevated for more than eight months following the storm (Figure 5.10). In-lake high-frequency sensor data directly influenced active management of the water delivery system; by understanding which systems had been impacted by turbidity and at what depths, reservoir operations were managed such that high quality drinking water continued to be delivered to consumers in New York City without interuption. This regional event illustrates the importance of anticipating and mitigating storm-related water quality impacts and the use of high-frequency data to underpin adaptive management scenarios during extreme events.

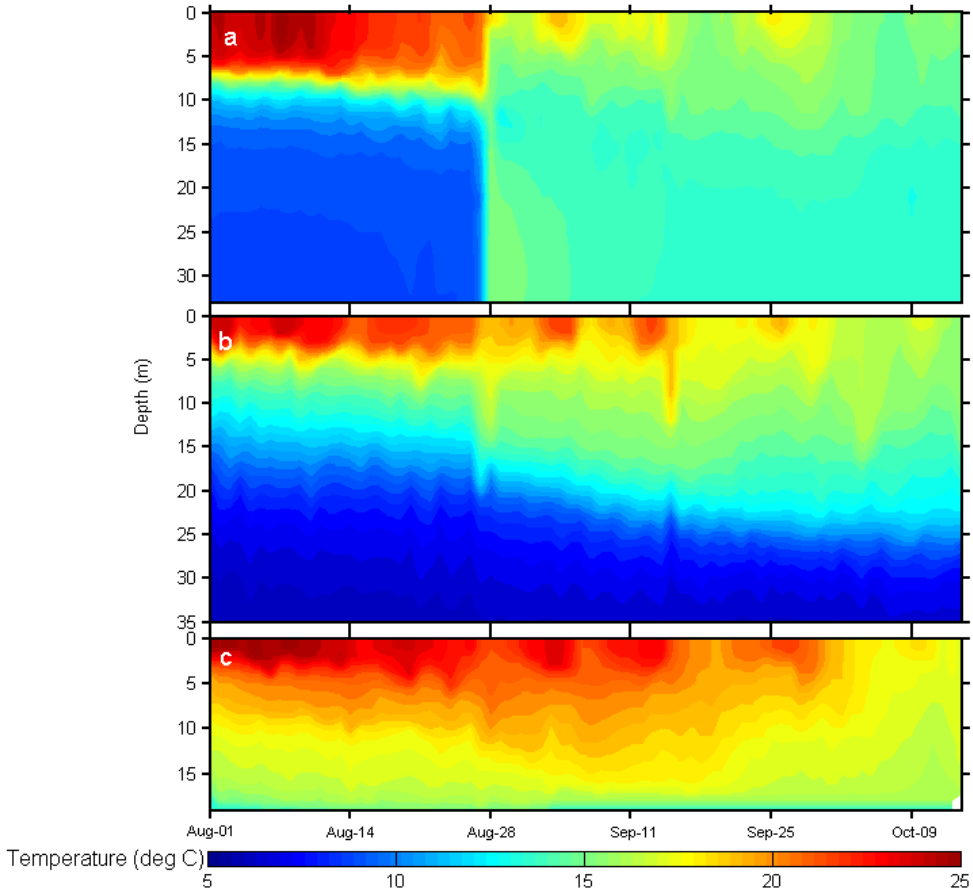

Figure 5.8. Temporal variation in water temperature across reservoirs (a: Ashokan Reservoir, b: Rondout Reservoir and c: Kensico Reservoir)

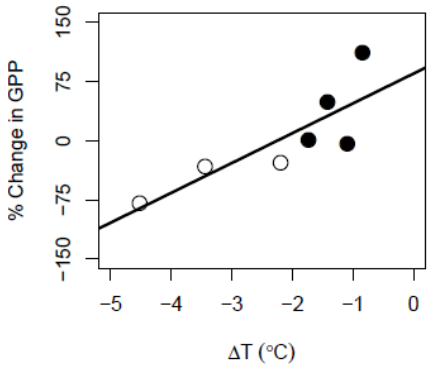

Figure 5.9. Relationship between storm responses of water temperature and gross primary production. Each point represents one lake, where open circles denote lakes with high potential volume replacement and closed circles are those with low potential volume replacement (see Figure 5.7).

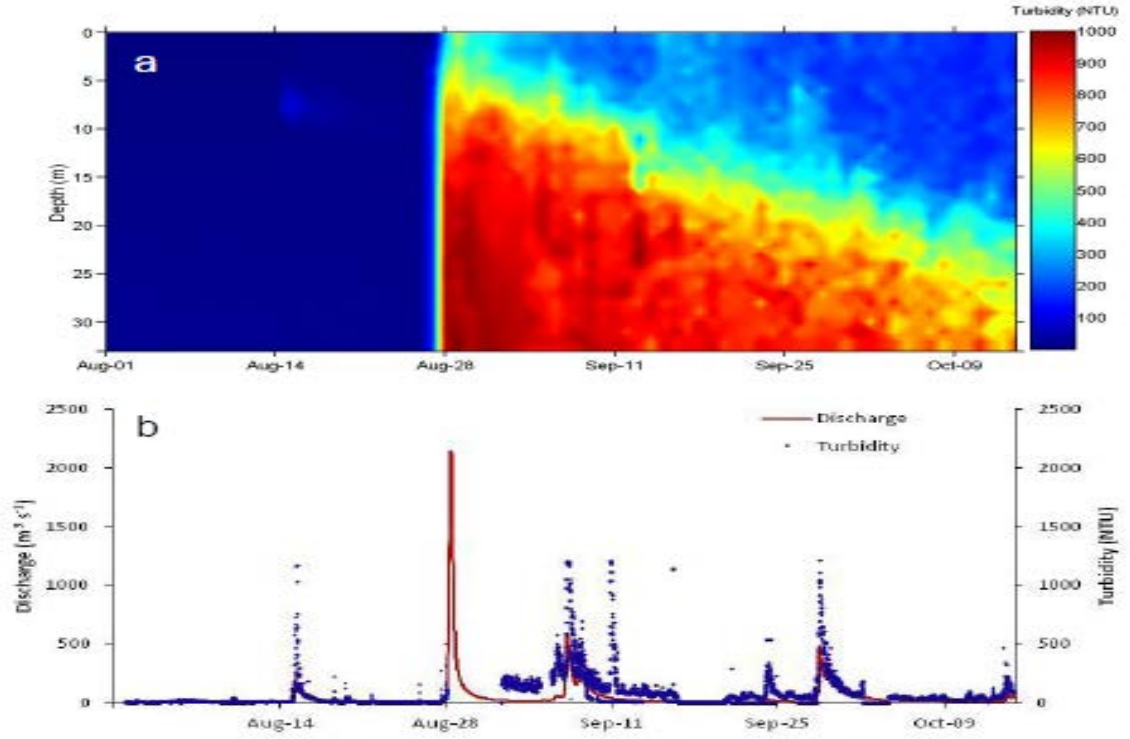

Figure 5.10. Turbidity in a stream and reservoir associated with Tropical Storm Irene. (a) Turbidity isopleths calculated from automated profile measurements made in Ashokan Reservoir, New York, from 01 August 2011 to 15 October 2011. Profiles were measured at 3-6 hour intervals at 1 meter vertical resolution. (b) Stream discharge and streamwater turbidity measured in the main inflow to the reservoir. Storm damage during peak discharge on 28 August prevented stream turbidity measurements, but turbidity in the stream likely exceeded 1000 – 1500 NTU.

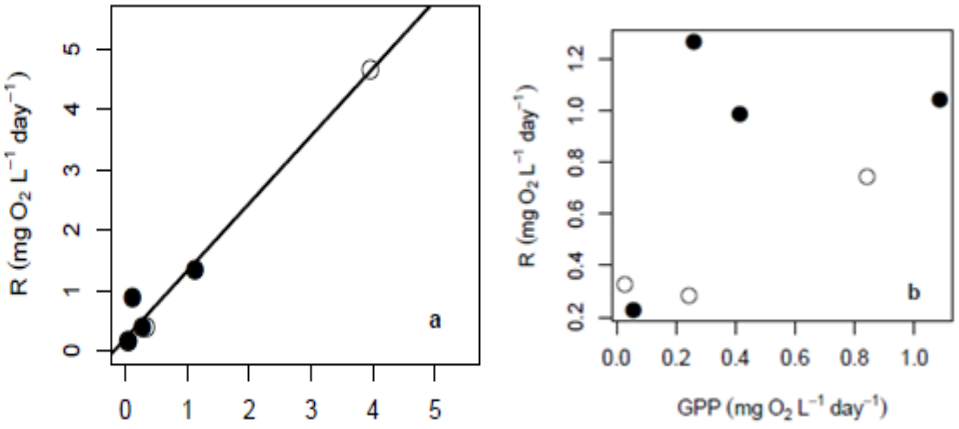

Figure 5.11. Decoupling of respiration and gross primary production following Irene. The relationship between average gross primary production (GPP) and average respiration (R) (a) pre-Irene (R=1.1*GPP + 0.2, p<0.001,r^2=0.98, DF=5; slope ± SE (1.1 ± 0.08) not statistically different from 1, t_4=1.48, p=0.2) and (b) post-Irene (p=0.22, DF=5). Pre-Irene is defined as 10 days before and post-Irene as 10 days after the storm. Each point represents one lake, where open circles denote lakes with high potential volume replacement and closed circles are those with low potential volume replacement (see Figure 5.7).

5.3. Rain-on-Snow Runoff Events in New York

Introduction

Rain-on-snow (ROS) is an important winter and spring phenomenon that plays a significant role in generating high streamflow and has greater potential for generating serious floods than does radiation-induced snowmelt (Kattelmann 1985). The term "rain-on-snow" is interpreted in many different ways. While the literal meaning of the term "rain-on-snow" would be snow melted by warm rain, many researchers have recognized that this is not entirely the case. Introduction of liquid water into snow weakens the bond between grains and alters the snow texture which results in reduced mechanical strength of the snowpack. Rain-on-snow is an important process for flooding in the eastern United States as well (Graybeal and Leathers 2006). For example, in January 1996, a combination of thaw with three days of very mild temperatures and intense rainfall increased the levels of streams and lakes causing massive flooding in many parts if Northeastern US (Leathers et al. 1998). In that case, the runoff from the snowmelt and the heavy rainfall, which may have been enhanced by orographic effects, combined to create the severe flooding.

In order to improve streamflow prediction for reservoir operation, flood control and design of major structures, models are needed to estimate the timing, amount and rate of outflow from the snowpack under rain-on-snow events (McCabe et al., 2007). Such knowledge is enhanced by a thorough understanding of processes associated with liquid water storage, natural and rain-induced melting, and transmission through the snowpack. Wankiewicz (1978) emphasized the quantitative effect of snow cover on the various runoff mechanisms and Kattelmann (1985) discussed the necessity of accurate forecasting snowmelt particularly during rainy conditions. Peak flow that result from low values of precipitation are small and of little consequence in terms of erosional damage in upland areas or downstream flooding. But if rapid snowmelt occurs during rainfall, the erosional potential of storm runoff may increase. Because high daily rainfall rates cause high streamflow levels, even a small addition of snowmelt water during high daily rainfall most likely would increase storm runoff volume and the size of instantaneous peak flows, thereby increasing the chance of not only channel erosion and landslides in upland watersheds but also downstream flooding (Harr 1981).

Limited documentation of rain-on-snow events makes anticipation and mitigation of potential hazards difficult. To help overcome the lack of useful information, this investigation provides basic information on the spatial and temporal patterns and temporal trends of rain-on-snow events in New York. This study, one of its first kind in the Northeastern U.S will therefore, provide important information on rain-on-snow events including, their frequency of occurrence, seasonal patterns, magnitude of snow water equivalent and snowmelt generation; data necessary for water managers to improve their management plans.

Methods

Streamflow and climate records for 31 watersheds in New York State (Figure 5.12; Table 5.6) were used to determine frequency of runoff events resulting from rainfall on snowpack or snowmelt. The area of these watersheds ranged from as small as 29 sq. km to 1574 sq. km and the mean elevation ranged from 105 m to 788 m.

Streamflow data were downloaded from USGS National Water Information System for each of 31 watersheds. The first step in hydrograph analysis entails separation of stream flow into surface runoff and base flow components. Baseflow separation is done using filter method outlined in (Arnold et al. 1995). Event runoff is defined as the direct surface runoff component of the baseflow-separated daily hydrograph summed over a period that lasts from the first day of streamflow hydrograph rise (t_1) until the beginning of the next event (t_2) (Hewlett and Hibbert 1967).The length of the runoff event is defined as the period between the first day of streamflow rise (t_1) until beginning of the next event (t_2).

Snow accumulations prior to runoff events were determined from snow depth from Snow Data Assimilation System (SNODAS) ((NOHRSC) 2010). The SNODAS is a modeling and data assimilation system has been developed by the National Weather Service's National Operational Hydrologic Remote Sensing Center (NOHRSC) to provide estimates of snow cover, snow water equivalent, snowmelt, and associated snowpack variables at a 1-km spatial resolution to support hydrologic modeling and analysis. SNODAS includes procedures to ingest and downscale output from Numerical Weather Prediction (NWP) models; a physically based, spatially-distributed energy-and-mass-balance snow model; and procedures to assimilate satellite-derived, airborne and ground-based observations of snow covered area (SCA) and snow water equivalent. For this study, we analyzed liquid precipitation, snowpack depth, snowmelt, and snow water equivalent from October to April (2003-2012). To obtain averages or totals for desired parameters representative of the USGS basins, the gridded (~1km) SNODAS data was extracted based on the areal extent of the watersheds. Since air temperature is not one of the output variables of SNODAS, we used spatially distributed air temperature data from the Northeast Regional Climate Center (NRCC) at Cornell University, Ithaca, NY ((DeGaetano and Belcher 2007). The 4 km resolution air temperature data was spatially averaged for 31 watersheds.

Rain-on-snow runoff events were characterized based on snowmelt, snow depth, liquid precipitation (rain) and solid precipitation (snow) information obtained from SNODAS. Two ROS variables are calculated for each watershed:

- a ROS day for a site was defined as a day when precipitation occurred as rain and snowpack was present
- a ROS runoff event was defined as a runoff event, as previously defined, with at least 1 ROS day occurring within the event.

The Spearman rank correlation test was used for exploratory data analysis. Correlation analysis was done to understand relationships between elevation, temperature, rain-on-snow, and precipitation characteristics. Spearman rank correlation is often used as a statistical tool to detect monotonic relationship. It is a non-parametric technique and therefore not affected by the statistical distribution of the population. Because the technique operates on ranks of the data, it is relatively insensitive to the outliers and there is no requirement that the data be collected over

regularly spaced temporal intervals (Helsel and Hirsch 1992) . The Spearman rank correlation coefficient (r) is calculated using:

$$r = 1 - \frac{6\sum_{i=1}^{n} d_i^2}{n^3 - n} \qquad (5.4)$$

where d_i is the difference between rank for each x_i, y_i data pair and n is the number of data pairs. The strength of the relation is indicated by r, which ranges from -1 (strong negative correlation) to +1 (strong positive correlation) with a value of 0 denoting no correlation. A two-tailed significance test (α=0.05) was done to assess significance of correlation between variables.

Annual peak flow for 31 basins was analyzed for the period of record when data were available. Peak flows were ranked by size for periods of records, and SNODAS were used where possible to separate peak flows caused by rainfall from peak flows caused by rain-on-snow. Peak flow sources were identified for 2003-2012 period using SNODAS model information by identifying the date of peak flow occurrence and the occurrence of runoff due rain-on-snow. Peak flow return period was calculated using Log Pearson Type III analysis (Graybeal and Leathers 2006).

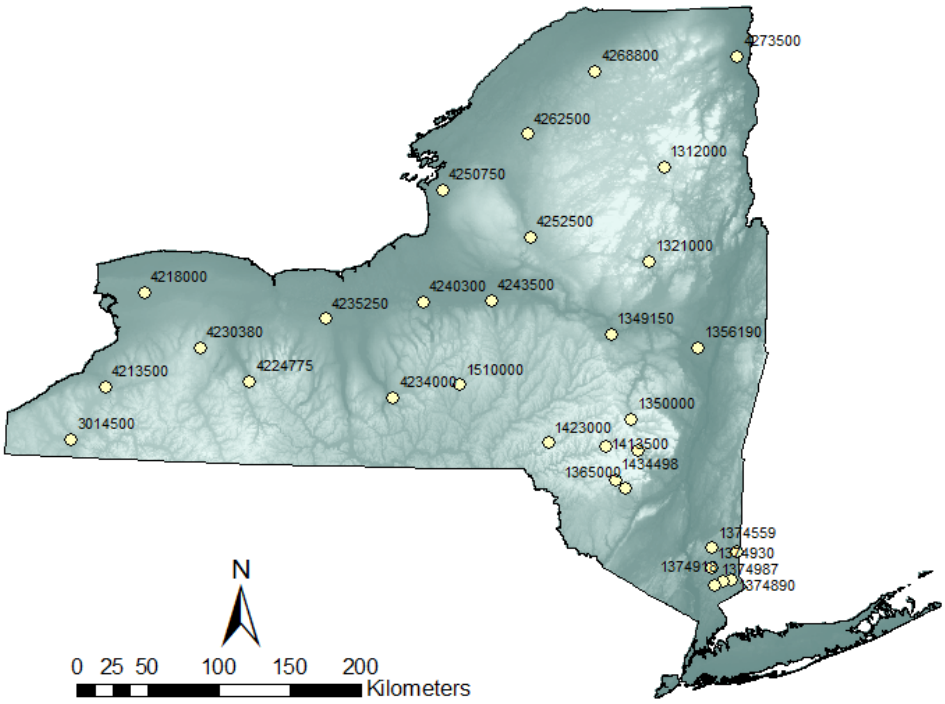

Figure 5.12. Map of New York State and USGS gage stations for rain-on-snow events study

Table 5.6. Watershed area and average elevation of 31 USGS gages. The watersheds are arranged by regions and in ascending order of elevation (

USGS Gage No.	Gage Description	Area (sq. km)	Basin Mean Elevation (m)	Elevation Range (m)	Region
4262500	West Branch Oswegatchie River	668.2	399.9	181-538	Adirondack
4268800	West Branch Regis	442.9	474.9	89-838	Adirondack
4273500	Saranac at Plattsburgh	1574.7	499.5	29-501	Adirondack
4252500	Black River near Boonville	787.4	499.9	220-645	Adirondack
1321000	Sacandaga River near Hope	1271.7	581.4	235-668	Adirondack
1312000	Hudson River near Newcomb	497.3	660.0	456-1095	Adirondack
1423000	West Br Delaware River at Walton	859.9	592.1	350-777	Catskill
1365000	Rondout Creek near Lowes Corners	99.2	628.6	256-1173	Catskill
1350000	Schoharie Creek at Prattsville	613.8	652.6	344-956	Catskill
1413500	East Br Delaware R. at Margaretteville	422.2	667.3	390-1057	Catskill
1362200	Esopus Creek at Allaben	165	671.5	180-1042	Catskill
1434498	West Br. Neversink at Claryville	87.5	788.2	439-903	Catskill
1356190	Lishakill NW of Niskayuna	40.4	104.9	55-154	East
1349150	Canajoharie Creek at Canajoharie	154.6	310.5	86-703	East
4235250	Flint Creek at Phelps	264.2	338.1	139-654	Finger Lake
4240300	Ninemile Creek at Lakeland	297.9	272.2	110-582	Finger Lake
4243500	Oneida Creek at Oneida	292.7	312.3	112-162	Finger Lake
4234000	Fall Creek at Ithaca	326.3	414.7	116-575	Finger Lake
1510000	Ostellic River at Cincinnatus	380.7	483.2	286-636	Finger Lake
1374987	Kisco River below Mt. Kisco	45.6	137.8	63-245	Southeast
1374918	Stonehill River South of Katonah	48.4	146.2	66-265	Southeast
1374890	Cross River near Cross River	44.3	169.3	103-304	Southeast
1374930	Muscoot River near Baldwin Place	35.0	204.7	155-344	Southeast
13744980	East Br. Croton River near Putnam Lake	160.8	213.6	117-406	Southeast
1374559	West Br. Croton River at Richardsville	28.5	257.1	155-357	Southeast
4218000	Tonawanda Creek at Rapids	903.9	236.7	173-244	West
4250750	Sandy Creek near Adams	354.8	331.4	74-521	West
3014500	Chadokoin River at Falconer	502.5	454.6	377-568	West
4230380	Oatka Creek at Warsaw	101.3	468.7	156-588	West
4213500	Cattaraugus Creek at Gowanda	1129.2	492.1	174-709	West
4224775	Canaseraga Creek above Dansville	230.3	498.6	160-690	West

Results and Discussion

Rain-on-Snow Runoff Events and Elevation Relations

Daily precipitation as rain and snowfall, snow water equivalent and snowmelt of 31 USGS gage watersheds in New York were used to examine the spatial and temporal patterns of rain-on-snow runoff events for water year 2003 through 2012. Figure 5.13 shows the spatial and temporal pattern of runoff events with rain-on-snow on a monthly basis that occurred during the period of study. ROS runoff events are found to be most frequent in the Catskill and western region New York during December and varied spatially. The total number of ROS runoff events was the largest in the Adirondack, western and Catskill regions of NY. In general, ROS runoff events are less frequent in southeast New York and Finger Lakes regions. The ROS runoff events generally occur in most watersheds as early as October and as late as April Although it is quite possible that some watersheds in the far north and west of New York may experience snowfall and subsequent runoff as early as September and as late as May, these earlier and later months were not investigated as these events generally represented a small fraction of ROS events.

During March and April when rain-on-snow frequencies are the highest, decrease in snow water equivalent is greatest. In March and April, the largest snowmelt per ROS runoff event occurred in the Central and Northern New York. The magnitude of snow depth is largest in the northern NY during spring, thus, April ROS runoff events in these locations can still melt a significant amount of snow. The number of rain days at a site is an important precipitation characteristic related to the frequency of ROS runoff events. For the study period, the percentage of rain-on-snow days is about 19-24% of total rain days at the lowest elevation basins (located in the southeast region), and this percentage increases with increased elevation and locations of the watersheds (greater than 60% in the Adirondack Region) (Table 5.7). The proportion of ROS runoff events to the total number of runoff events was highest in the Adirondack region followed by the Catskills region. Another important condition for ROS runoff events is an accumulation of snow on the ground. Temperatures at the lower elevation sites are warmer, reducing the number of days with snowpack on the ground, and thus reducing the number of potential rain-on-snow days.

During the late fall and winter, the frequencies of both ROS runoff events and ROS days increased with elevation. At the lowest elevation the percentage of cool season precipitation days that are ROS days is close to zero for most of the sites. This elevation relationship with ROS runoff events and ROS days during the late March and April is primarily related to the number of days that snow is on the ground. The Spearman correlation analysis between elevation and rain days, ROS days, and ROS runoff events are presented in Table 5.7. The analysis was done for two seasons i.e., OND (October-November-December), JFMA (January-February-March-April), and for all months (October-April). All variables are positively correlated with elevations. ROS DAYS showed the highest positive correlation (0.72 for JFMA, 0.55 for OND, and 0.65 for October -April) with elevation and were significant at the 0.05 level. Similar significant positive correlations with elevation were observed for ROS runoff events for seasons. Snow on the ground days were positively correlated to elevation. Average snow water equivalent (SWE) increased with increasing elevation. The frequency of occurrence of ROS days, and rain days also showed locational pattern. The number of ROS runoff events tended to increase in the

Table 5.7. Precipitation characteristics and rain-on-snow events in 31 USGS gage watersheds. The watersheds are arranged by regions and in ascending order of elevation. (2003-2012).

USGS Gage	Total Rain Days	ROS Days	Percent of Rain Days that are ROS days	Total number of runoff events (Oct-April)	ROS Runoff Events	Percent of runoff events that are ROS Runoff Events	Annual Peak Flow caused by rain-on-snow (2003-2012)
04262500	712	434	61	112	66	59	9
04268800	674	410	61	127	74	58	9
04273500	750	554	74	168	78	46	8
04252500	708	481	68	154	90	58	5
01321000	692	470	68	143	80	56	8
01312000	659	482	73	110	63	57	8
01423000	670	379	57	157	98	62	6
01365000	632	361	57	170	71	42	7
01350000	661	398	60	163	79	48	7
01413500	656	388	59	149	70	47	7
01362200	645	392	61	141	69	49	7
01434498	589	326	55	182	78	43	7
01356190	552	181	33	217	46	21	8
01349150	650	302	46	197	78	40	6
04235250	715	322	45	159	64	40	8
04240300	752	378	50	170	74	44	8
04243500	715	330	46	208	75	36	7
04234000	687	327	48	207	76	37	9
01510000	724	392	54	183	85	46	8
01374987	602	136	23	144	44	31	3
01374918	600	135	23	127	43	34	3
01374890	577	139	24	154	36	23	6
01374930	569	135	24	170	38	22	5
013744980	582	110	19	134	42	31	6
01374559	577	136	24	140	44	31	6
04218000	776	356	46	146	68	47	9
04250750	725	408	56	156	86	55	9
03014500	868	457	53	95	57	60	5
04230380	679	259	38	207	68	33	7
04213500	799	436	55	200	103	51	7
04224775	702	338	48	138	58	42	8

Adirondack, Catskill and western regions while there were less ROS runoff events in the southeast region. The relatively small differences in basin elevation may also mean that the observed differences in ROS days and ROS runoff events are better indexed by the location of these watersheds. There is little low elevation snow at these times and occasional precipitation causes a lower number of runoff events.

Rain-on-Snow Runoff Events and Temperature Relations

Many studies that have shown increasing temperature in Northeastern United States during the past several decades with subsequent effects on hydrological conditions including decreasing snowpack and shifts to earlier snowmelt runoff (Burns et al. 2007, Hayhoe et al. 2008). Modeling studies in watersheds in New York have also indicated that climate change may result in decrease in snowpack and shift timing of annual peak and annual low flows (Pradhanang et al. 2011, Zion et al. 2011). The intensity and occurrence of runoff events are dependent on the development of snowpack and subsequent melt runoff event, we performed correlation analysis between *ROS runoff events* and average annual minimum and maximum temperature of each watershed under study.

The Spearman correlation analysis between the average maximum and minimum temperatures calculated over different seasonal time periods and rain days, ROS days, and ROS runoff events are presented in Table 5.8. The analysis was done for two seasons similar to the analysis of elevation i.e., JFMA (January-February-March-April) and OND (October-November-December). ROS days and ROS runoff events were negatively correlated with average maximum temperature during JFMA and were found to be significant at the 0.05 level. Average annual minimum temperature showed significant negative correlation with ROS days for JFMA. The results were not significant for OND except for ROS days. The correlation analysis of rain-on-snow variables with average maximum and minimum temperature for, October-December, January-April and October-April showed significant negative correlation (Table 5.8). The negative correlations between average temperature and ROS runoff event frequencies indicate that as temperature increases ROS runoff events become less frequent. The negative correlations are most common for low elevation sites that are located in the southern part of NY.

Table 5.8. Spearman rank correlation coefficients for elevation, maximum and minimum temperature and rain-on-snow variables

Variables	Elevation			Average Maximum Temperature			Average Minimum Temperature		
	OND	JFMA	Oct-Apr	OND	JFMA	Oct-Apr	OND	JFMA	Oct-Apr
Rain Days	0.24	0.22	0.19	-0.47*	-0.25	-0.40*	-0.16	-0.34	-0.28
ROS Days	0.55*	0.72*	0.65*	-0.73*	-0.75*	-0.80*	-0.78*	-0.79*	-0.78*
ROS Runoff Events	0.68*	0.46*	0.57*	-0.78*	-0.49*	-0.67*	-0.54*	-0.71*	-0.64*
Snow on the ground days	0.79*	0.79*	0.79*	-0.91*	-0.79*	-0.90*	-0.89*	-0.91*	-0.92*
Average SWE	0.67*	0.54*	0.75*	-0.90*	-0.85*	-0.94*	-0.63*	-0.74*	-0.71*

* Correlation is significant at the 0.05 level - 2-tailed test of significance is used

October:

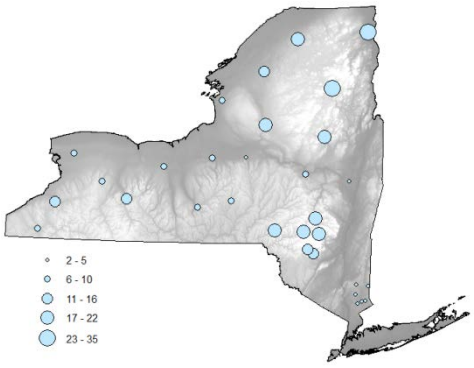

November:

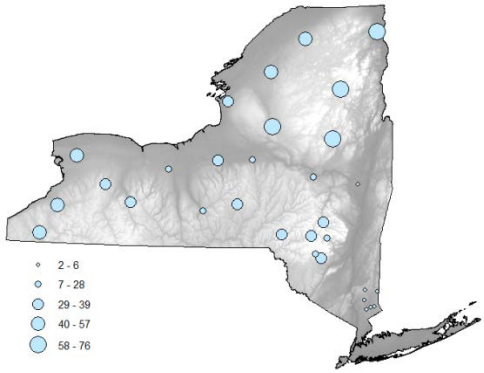

December:

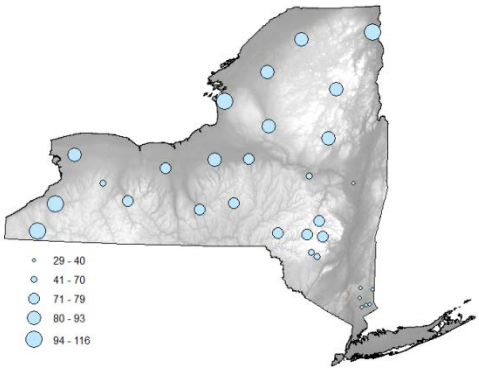

January:

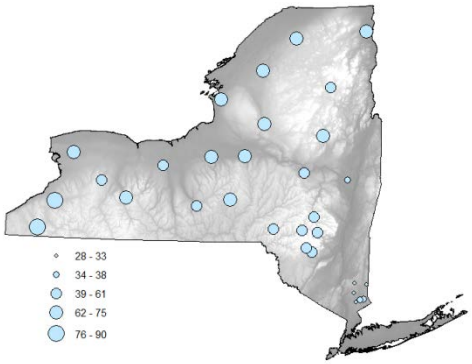

February:

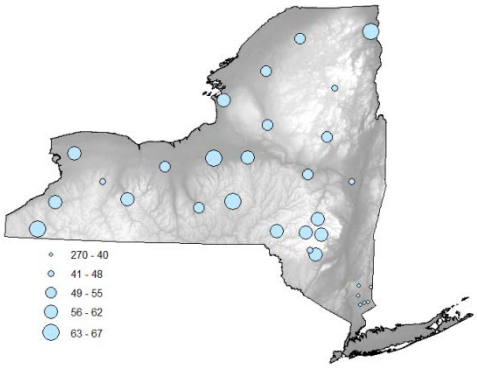

March:

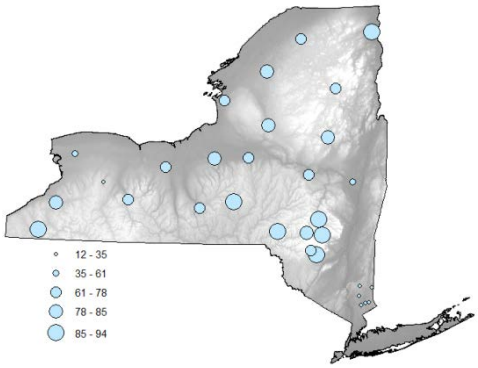

April:

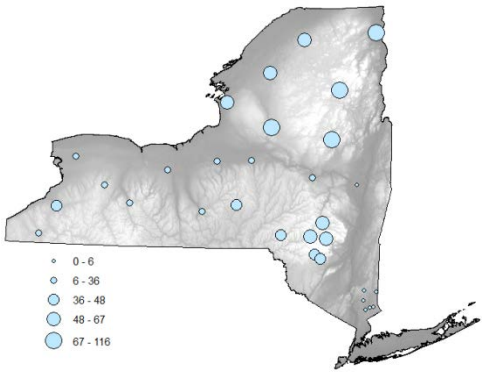

October-April:

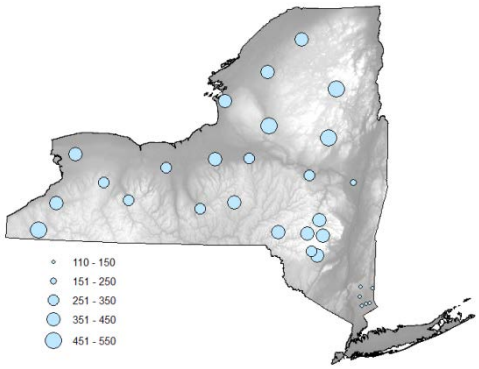

Figure 5.13. ROS runoff events, October to April during 2003-2012**.**

(a)

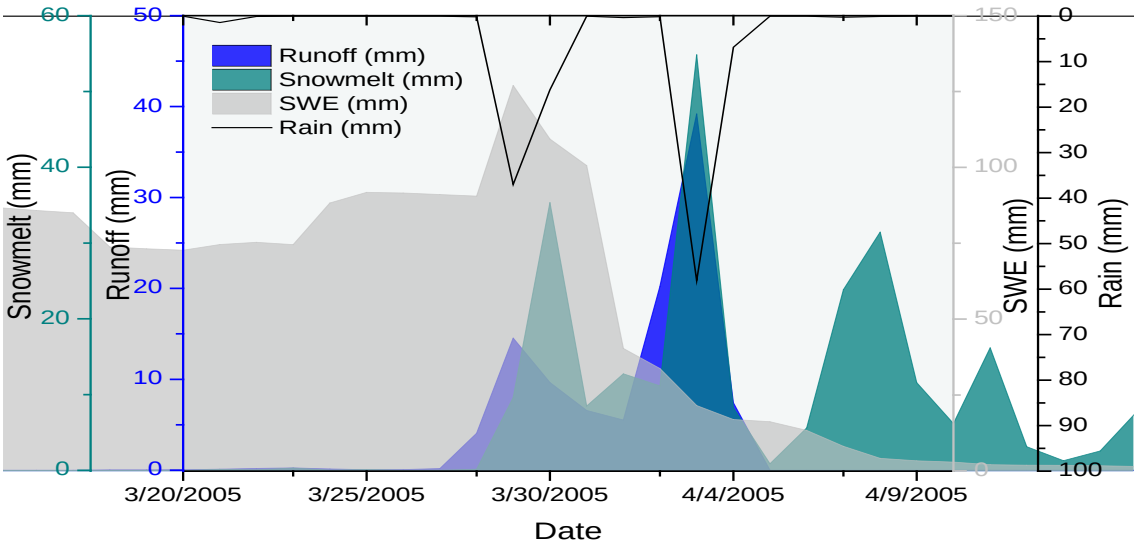

(b)

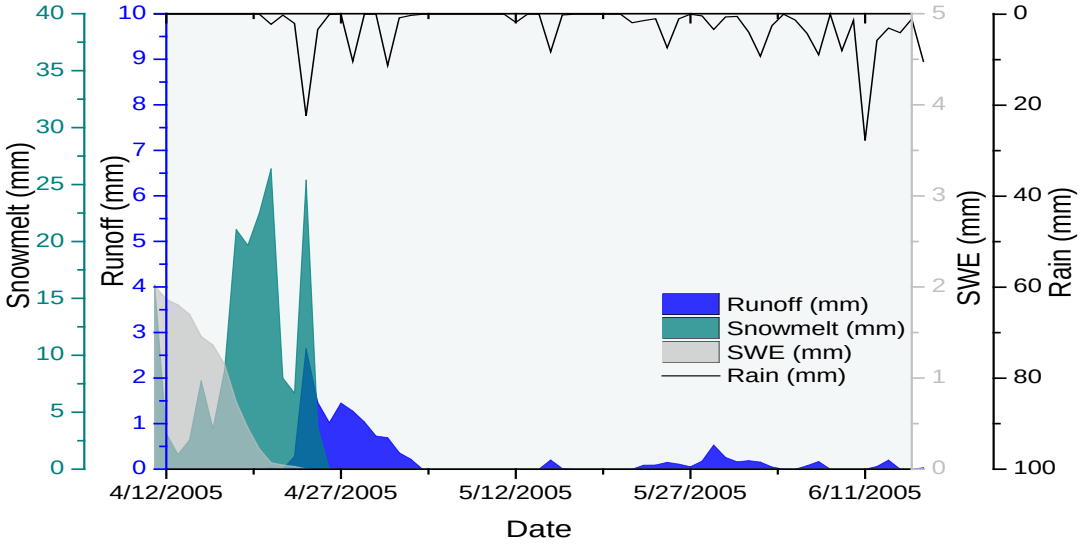

Figure 5.14. Hydrograph characteristics of a) rain-on-snow, and b) snowmelt and rain induced streamflow

Streamflow Characteristics

Rain-on-snow conditions produce streamflow hydrographs that generally differ from hydrographs caused by rain alone. Figure 5.14 shows example of a typical hydrograph resulting from rain-on-snow, snowmelt and rain only runoff events. Rising limbs of rain-on-snow hydrographs are generally steeper than those associated with rain-only hydrographs. Differences in size of peak flows and rates of hydrograph rise might be expected due to differences in the amount and rate of water input. The combination of a ripened snowpack, snowmelt and rain-on-snow generate large runoff compared to the runoff from snowmelt or rain alone. Peak flow sources were identified for 2003-2012 period using SNODAS model information. Ranking peak flow, as to whether or not snowmelt contributed substantially to the peaks was done. The causes of peak flow were then identified based on rain and snow information from SNODAS. The results suggest that snowmelt during rainfall added to many annual peaks from 2003 to 2011. On average, 7 of 10 annual peaks were associated with *ROS* runoff events across all of the study sites. The sites that had less rain-on-snow related annual peaks were located in the southeast NY (Table 5.7). Most of rain-on-snow related peaks ranked highest in the record of study. Peak flow and return interval analysis showed that most of the highest annual peak flows occurred during mid to late March. The comparison of the boxplots of event cumulative runoff identified as rain-on-snow generated and runoff generated by rain only is shown in Figure 5.15. The intensity of ROS runoff events compared to rain only runoff events tended to be greater in the Adirondack and Catskill regions of NY and increased with elevation. The southeast region showed greater cumulative runoff for rain only events. Other regions showed mixed results.

Conclusions

In conclusion, a first attempt has been made in documenting frequency of rain-on-snow events and their spatial and temporal distribution in New York. The period of 2003-2012 was selected to establish spatial and temporal patterns of ROS days and ROS runoff events, their correlation with elevation and temperature and to compare hydrograph characteristics of ROS runoff events and rain only events. Seasonal snowfall amounts, rain on snowpack, or snowmelt were found to possibly play an important role in flooding in most of the areas in NY during 2005, 2007 and 2010. Flooding events caused by rain-on-snow can be devastating from human and economic perspectives, and also presents fascinating hydrologic phenomena in which climatological preconditioning and the occurrence of an unusual weather condition combine to create disastrous results. Our analyses on ROS days and ROS runoff events appear to follow logical climate relations, and provide one of the first inventories of the magnitude of these relations, as well as description of elevation and regional differences in the relations. This information is useful as a base for additional research into rain-on-snow events, which should improve both flood forecast and assessments of flood risks.

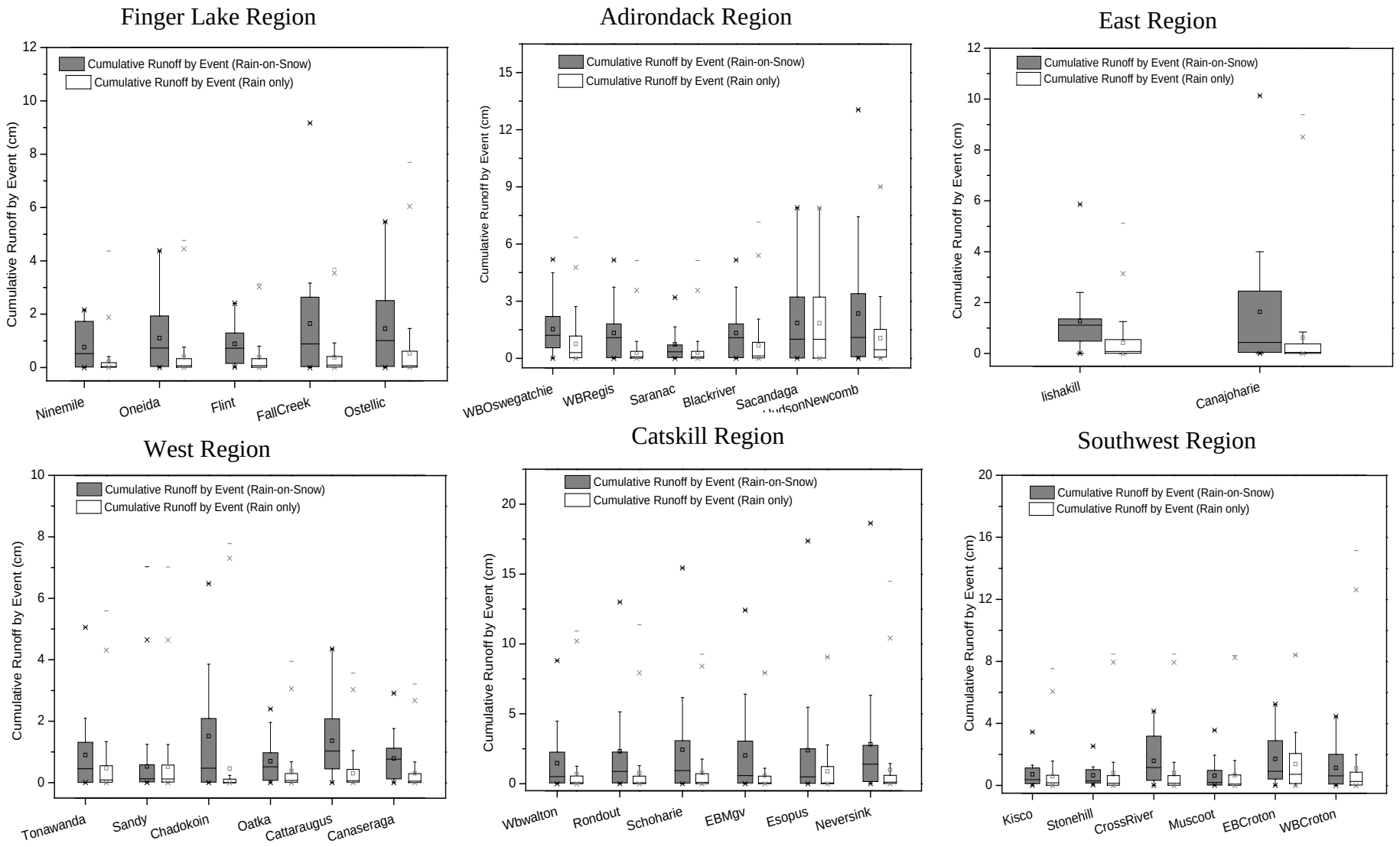

Figure 5.15. Boxplots of cumulative runoff by event for events due to rain-on-snow (grey shaded box) versus events due to rain-only. The boxes indicate the range of values between the 25th and 75th percentiles, the dark horizontal lines indicates the median, the ends of the dashed lines indicate the 1st and the 99th percentiles of the distribution and the small squares show the average.

5.4. Reservoir Stratification and Mixing Event Analysis from High-Resolution Monitoring Data

In this study, we analyze automated monitoring data collected from a buoy placed in West Basin of Ashokan Reservoir. Here we present a brief overview of the type of information that can be obtained from automated monitoring data, and the insights that can be gained regarding the processes regulating the mixing and distribution of materials in the reservoir. Based on the in situ measurements of depth-water temperature, conductivity, turbidity and dissolved oxygen and the meteorological data, statistics of stratification and mixing events are estimated in terms of non-dimensional numbers such as lake number, Schmidt stability and Wedderburn number and other measures including the thermocline depth and buoyancy frequency. The analysis of these high-resolution monitoring data leads to a better understanding of changes in thermal structure over a range of both spatial and temporal scales. The response of these indices to the short-term changes in the weather and their relationship to variations in dissolved oxygen and turbidity are examined. The results show that the seasonal changes in stratification and mixing have significant effect on the vertical profile of turbidity as well as dissolved oxygen in reservoir. This study investigates to what extent the movement of thermocline can affect the transport of the suspended particles in the reservoir.

Background

Thermal stratification in lakes and reservoirs is important in controlling the vertical transport of dissolved and particulate constituents. Vertical transport affects the distribution of heat and momentum and influences the nutrient and oxygen budget in deep layers. The mechanisms driving this exchange and the diffusion process into deep water layers in lakes and reservoir systems are not fully understood. The energy transfer at air-water interface is modulated by surface waves, currents and internal waves and dissipated along a progressive gradient of scales. Previous work by a number of authors, based on numerical and experimental studies has explored the behavior of hydrodynamic events (stratification and mixing) on a long-term time series of ecological and hydrothermal data (Peeters et al. 2002, Markensten and Pierson, 2007 Maclntyre et al. 2009, Samal et al. 2009). Studies have also used high resolution buoy data to better understand changes in thermal structure and mixing over a wide range of temporal scales (Read et al. 2011, Yeates et al. 2008 and Tsai, J.-W. et al. 2008). In the work described here we used high frequency data collected by a water quality monitoring buoy to examine the effects and persistence of extreme events on reservoir mixing and thermal structure, and on variations in dissolved oxygen and turbidity in Ashokan Reservoir.

Data and Methods

To estimate various hydrodynamical indices during the period of 2009-2011, a YSI monitoring buoy collected in situ measurements of depth-water temperature, dissolved oxygen and turbidity and the above surface measurement of meteorological data (wind speed). These data were then processed using the program Lake Analyzer (Read et al 2011) developed by Global Lake Ecological Observatory Network (GLEON) which was used to estimate hydrodynamic indices, such as, Schmidt stability (St, J m^{-2}), Lake number (Ln), Wedderburn number (W), Buoyancy frequency (N^2, s^{-2}), Thermocline depth (thermD, m).

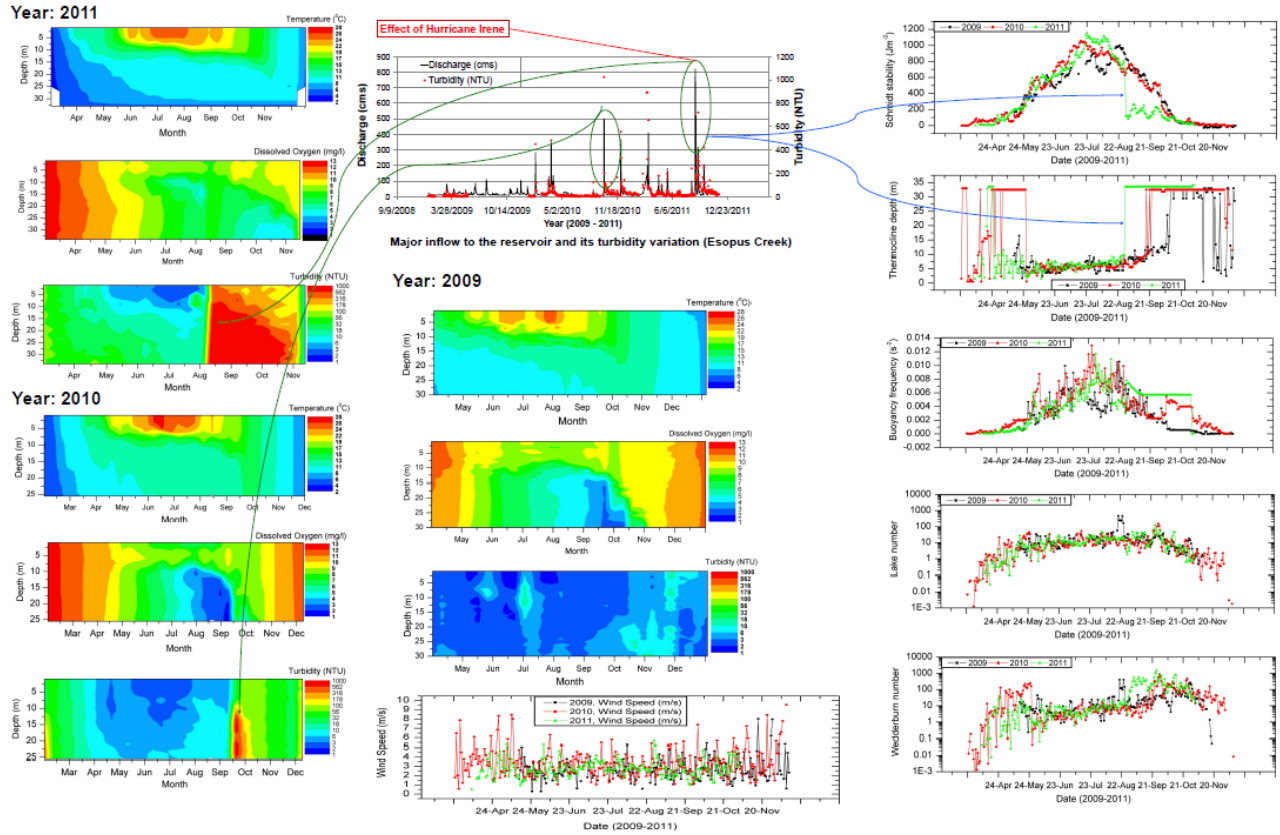

Figure 5.16. Year-wise isopleths for temperature, dissolved oxygen and turbidity and the hydrodynamic indices over the study period (2009-2011)

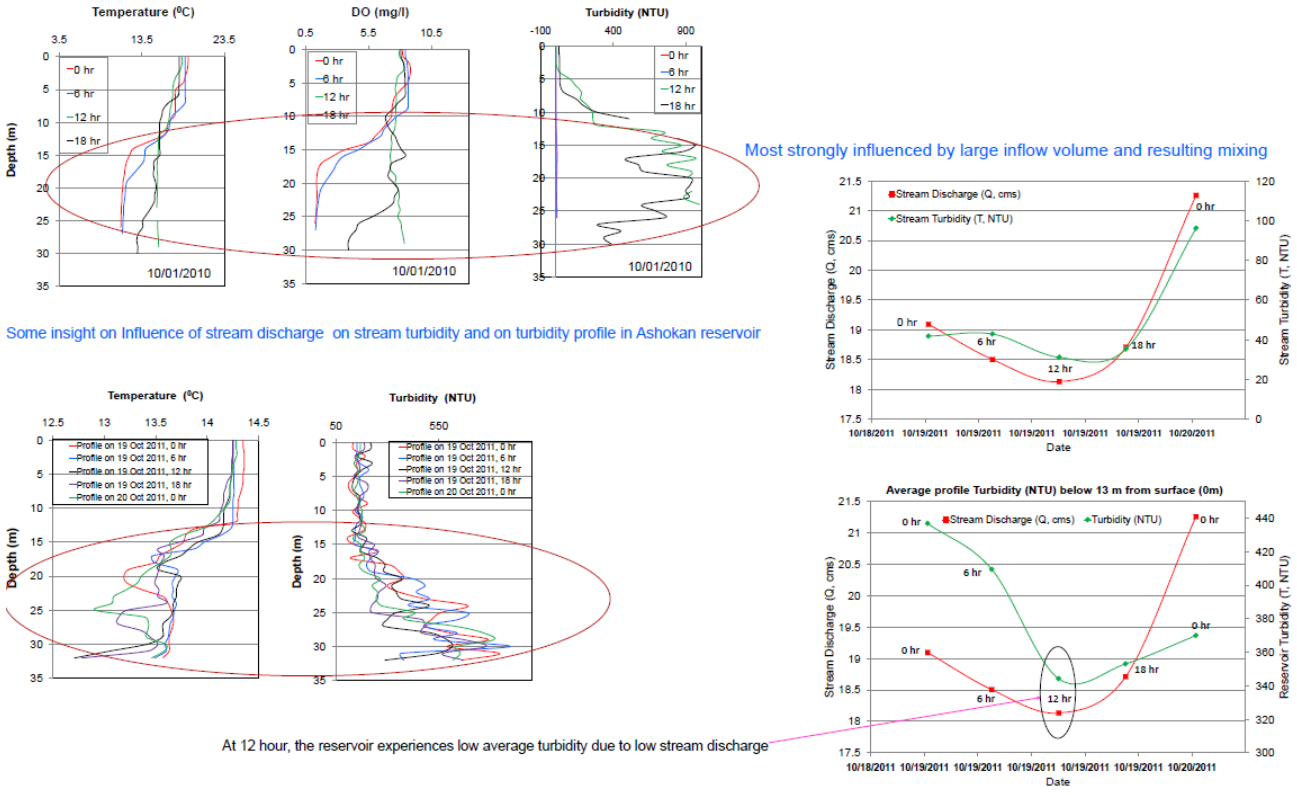

Figure 5.17. Vertical profiles of temperature, dissolved oxygen and turbidity before, during and after 2010 storm.

Results and Discussion

The isopleths for temperature, dissolved oxygen and turbidity in the reservoir in the years 2009, 2010 and 2011 indicate the inter-annual vertical variation in temperature, available dissolved oxygen and turbidity. The effect of Tropical Storm Irene in 2011 and a lesser storm in 2010 was to replenish oxygen levels in the reservoir while at the same time increasing turbidity levels (Figure 5.16)

The nature of vertical profiles of temperature, dissolved oxygen and turbidity before, during and after 2010 storm is analyzed in Figure 5.17. It is observed that storm discharge and turbidity loading strongly influences the turbidity profile in Ashokan reservoir. During 2010, the hypolimnion turbidity is increased by the large inflow volume and resulting mixing.

Other conclusions that can be obtained from the data in Figures 5.16 and 5.17 include:

- During this study extreme hydrological events strongly influenced mixing material transport and water quality

- Vertical profiles of dissolved oxygen (DO) show late summer declines in hypolimnetic O_2 levels in 2 of the 3 years studied. In 2011, Hurricane Irene completely destratified and reaerated the system before low oxygen levels occurred.
- Rapid change both in dissolved oxygen and turbidity were observed and were related to storm event inflow. At 12 hour, the reservoir experiences low average turbidity due to low stream discharge
- The Schmidt stability, which represents the strength of stratification, shows a consistent seasonally increasing trend; however, there was a sharp drop in stability as a consequence of Hurricane Irene. The change in buoyancy frequency due to the strong upwelling and turbulence shows the breakdown of thermal stratification and the possible wave propagation
- The thermocline depth located at the maximum temperature gradient is observed to be similar during early summer during all three years except following Hurricane Irene where complete destratification occurred.

6. Model Data Acquisition and Organization

6.1. GIS Data Development for Modeling

Water Quality Monitoring Sites

Additional locations were added throughout the reporting period to the ArcSDE feature class of DEP water quality monitoring sites ("aqua.ARCLIB.wq_monitor_site"). The dataset is comprised of stream, reservoir, keypoint, and other DEP water quality monitoring sites included in the Laboratory Information Management System (LIMS). A spatial view in the geodatabase joins each record of the feature class to attribute data found in LIMS and in the Site Assessment and Management Inventory (SAMI) database. These non-spatial attribute databases are stored in SQL Server.

DEP Snow Pillow Sites

A feature class of the locations of the seven snow pillows DEP has installed in the West of Hudson watershed was created and placed in the "Project\WWQSR" directory of the SDE spatial data library.

SSURGO2 Soil Data

New versions of SSURGO2 soil data for the eight NYS watershed counties and Connecticut were downloaded and merged to create an updated polygon dataset (shapefile) and ACCESS database of soil attributes. These data were used in conjunction with the Soil Data Viewer (SDV) extension for ArcGIS to derive approximately two dozen soil property layers. The attribute layers were joined to the shapefile and imported to the SDE spatial data library. Soil data remain available in shapefile format for use with SDV and in the geodatabase for mapping and analysis applications.

Stream Power

Work continued on using ArcGIS ModelBuilder to derive values of stream power, a function of stream gradient and stream discharge, for each cell of raster representations of several tributaries to Esopus Creek in the Ashokan basin (see also Section 4.2). Results from a 10-meter DEM derived from USGS elevation contours and a 3-meter DEM derived from LiDAR data were compared. Generally, the 3-meter results more accurately define stream channels while indicating reaches of potentially increased stream power that merit field investigation.

Miscellaneous

Data development and mapping support were provided throughout the reporting period to various members of the DEP modeling unit, the Watershed Water Quality Science and Research group, and the Water Quality Directorate. A majority of this support was related to preparation of DEP reports, peer-reviewed publications, conference posters, and conference presentations.

Such events included the annual Watershed Science Technical Conference, the Eastern Snow Conference, and the annual meeting of the American Geophysical Union, among others.

6.2. Ongoing Modeling/GIS Projects

Bathymetric Survey of NYC Water Supply Reservoirs

Substantial progress was made on establishing an Intergovernmental Agreement with USGS to provide bathymetric surveys of the six West of Hudson reservoirs, last surveyed in the mid- to late-1990s. Final products that will be delivered to DEP include a TIN surface model of reservoir bottom, 2-foot elevation (depth) contours, and an updated elevation-area-capacity table for each reservoir. Undertaking the work as an Investigative Study, USGS will prepare a final report, available online, in which a map sheet for each water body describes the survey methodology, includes at least a portion of the updated capacity tables, and graphically presents reservoir bottom surface and contour data. It is anticipated that work will begin spring 2013, with three reservoirs surveyed that year and three during 2014. The possibility of unusually low water levels could delay a portion of the work until 2015.

Watershed Atlas

Work continued towards completion of the New York City Watershed Atlas by improving various maps and informational pages. Each reservoir basin overview map was redesigned using an ESRI online basemap product displaying streets and topography. Land cover/land use pie charts were developed for the East of Hudson reservoir basins. Existing system overview maps were downloaded and incorporated into the Atlas introduction. A reservoir information page was created for each water body, one that includes a brief narrative describing a reservoir's history, its place in the system, and land cover/land use areas, along with photographs taken at the reservoir or within its watershed.

6.3. Time Series Data Development

An inventory of the necessary raw time series data for watershed and reservoir model input and calibration is presented in Tables 6.1 and 6.2, respectively. The time series data includes meteorology, streamflow, water quality, and point source loads for watershed models. For reservoir models the data includes meteorology, streamflow, stream, reservoir and key point water quality and reservoir operations. Data sets are updated as new data become available. Lag times between the current date and the dataset end dates are the result of QA/QC processes at the data source and/or procurement timelines driving the acquisition of any purchased data.

For this reporting period, the Northeast Regional Climate Center (NRCC) Meteorology, DEP Stream and Limnology Water Quality, and DEP Key Point through calendar year have either become available via online sources and/or have been added to the inventory.

The NYSDEC Water Quality data has provided the Modeling Group with a robust dataset from baseline and storm event sampling of the West Branch of the Delaware River at Beerston from 1992 to the 2010. Historically the NYSDEC has collected the samples and calculated the

nutrient loads. DEP now calculates the nutrient loads and has done so through WY 2010. DEP has now begun the collection and analysis of samples from this site and, as such, the data from this site is now included in the DEP Water Quality dataset.

The NRCC Meteorological Data is now also available via the NRCC's Applied Climate Information System (ACIS). ACIS is a data access system developed by the NRCC to assist in the dissemination of data. In addition to access to updated data from the NRCC cooperative stations the ACIS will provide access to gridded meteorological data sets. Staff members have attended an ACIS training session and expect to begin utilizing ACIS in the upcoming year.

Table 6.1. Inventory of data used for watershed modeling.

Data Type	Data Source	Data Description	Dates*	Modeling Needs
Meteorology	Northeast Regional Climate Center	Daily Precipitation and Max/Min Temperature	Pre 1960-2011	Model Input
Wastewater Treatment Plants	DEP	Monthly WWTP Nutrient Loads	1990-2009	Model Input
Streamflow	USGS	Daily and Instantaneous Streamflow	Pre 1960-2010**	Hydrology Module Calibration / Nutrient and Sediment Loads
Water Quality	DEP	Routine and Storm Stream Monitoring	1987-2011	Nutrient and Sediment Loads for Water Quality Calibration
	NYSDEC***	Stream Monitoring at West Branch Delaware River	1992-2010	Nutrient and Sediment Loads for Water Quality Calibration

*Dates represent total span for all data sets combined. Individual station records vary.
**Calendar year 2010 stream flow data is provisional from November to December and will be replaced once the USGS has finalized their water year 2011 dataset. Also available on line.
***Now part of the DEP Water Quality dataset.

Table 6.2. Inventory of data used for reservoir modeling.

Data Type	Data Source	Data Description	Dates*	Modeling Needs
Meteorology	DEP	Air Temp., Relative Humidity, Solar Radiation., PAR, Wind Speed, Wind Direction, and Precipitation	1994-June, 2010	Model Input
Key Point and Reservoir Operations	DEP	Tunnel Water Quality, Flow and Temp.; Reservoir Storage, Spill, Withdrawal, and Elevation	1987-2011	Model Input
Streamflow	USGS	Daily and Instantaneous Streamflow	Pre 1960-2010**	Model Input
Stream Hydrology	DEP	Stream Water Quality, Flow and Temperature	1987-2011	Model Input
Limnology	DEP	Reservoir Water Quality, and Temperature Profiles	1992-2011	Model Input

*Dates represent total span for all data sets combined. Individual station records vary.
**Calendar year 2010 stream flow data is provisional from November to December and will be replaced once the USGS has finalized their water year 2011 dataset. Also available on line.

6.4. Gridded Meteorologic and Snow Data

Gridded Meteorological Data from Northeast Regional Climate Center

Gridded 4-km resolution daily precipitation and air temperature data were obtained from the Northeast Regional Climate Center (NRCC) at Cornell University, Ithaca, NY. The product is available in near-real-time for the entire Northeast US starting in 2005 (http://compag.tc.cornell.edu/sciencegateway/). This product represents a high-spatial-resolution precipitation developed using radar-guided interpolation in which radar-based precipitation is adjusted on a daily time step using rain-gauge observations to reduce spatially varying errors in the radar estimates and assuming that rain-gauge values represent true values (DeGaetano and Wilks, 2009). Radar-based interpolation helps reduce model uncertainty by reducing interpolation errors independently from season or precipitation magnitude. Spatially-distributed air temperatures are estimated at grid points by interpolation from observation stations and application of an environmental lapse rate that adjusts for elevation effects on temperature. The precipitation data, obtained in a polar coordinate system from NRCC, are re-gridded to match the air temperature 4-km grid by nearest neighbor analysis, and the final grid was clipped to produce a consistent spatial distribution of 324 4-km grid cells for the NYC west of Hudson watershed area (Figure 6.1). Use of these data in model applications is being tested and evaluated (see Section 4.3 on use of gridded met data in GWLF).

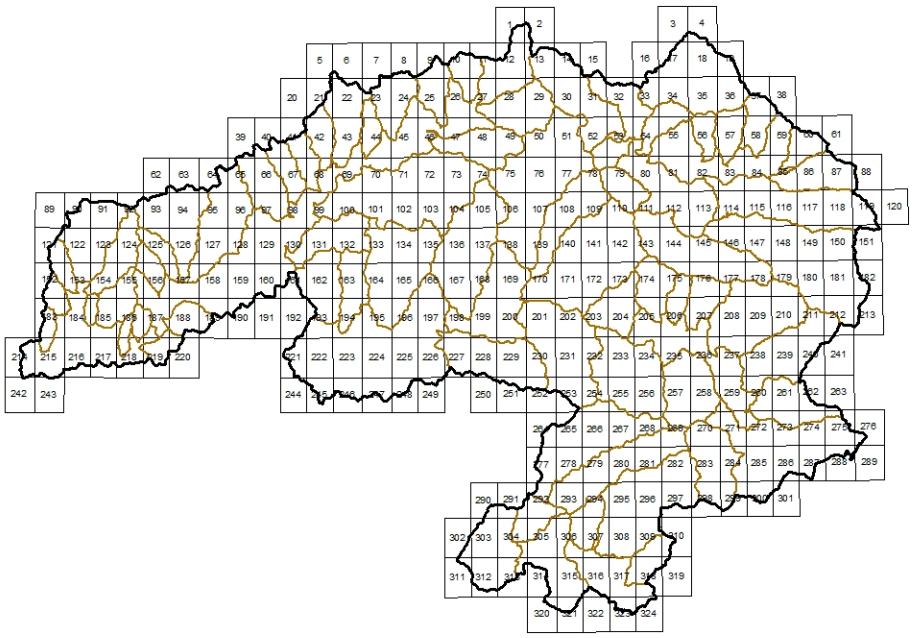

Figure 6.1. Spatially-distributed meteorological data grid for NYC West of Hudson watersheds.

Gridded Snow Data from NOAA

Gridded SNOw Data Assimilation System (SNODAS) snow water equivalent (SWE) and snowmelt were downloaded from the National Operational Hydrologic Remote Sensing Center (NOHRSC) web site (www.nohrsc.noaa.gov). SNODAS is a modeling and data assimilation system developed by the NOAA National Weather Service's (NWS) NOHRSC to provide to the research and users community the best possible estimates of snow cover and associated parameters. SNODAS aims to achieve a physically consistent framework that integrates snow data from satellite, airborne platforms, and ground stations with model estimates of snow cover from the numerical weather prediction (NWP) model for the conterminous U.S. (CONUS) (Carroll *et al*., 2001; Carroll, 2005). To implement this process first the original 13 km^2 resolution NWP forcings are downscaled to a 1 km^2 resolution; downscaled NWP estimates of air temperature, relative humidity, wind speed, precipitation, incident solar radiation, and incident long wave radiation forcings are then used as inputs to the NOHRSC Snow Model (NSM).

The NSM is an energy-and-mass-balance, spatially-uncoupled, vertically-distributed, multi-layer snow model that runs operationally at 1 km^2 spatial resolution and at the hourly temporal resolution for the CONUS data. Driven by gridded NWP climate data, NSM has run continuously at hourly time steps since the 2004-2005 snow season in an operational mode. The NSM simulated state variables are nudged towards ground-based and remotely-sensed snow observations daily to constitute the NOHRSC National Snow Analysis (NSA) (Clow *et al*., 2012). The NSA output products include (1) daily National and regional maps for nine snowpack characteristics, (2) seasonal, two-week, and 24-hour movie-loop animations for nine snowpack characteristics, (3) text summaries, (4) a suite of interactive maps, text, and time series products, (5) selected hourly and daily gridded snow products for the CONUS, and (6) 3-D visualization products suitable for viewing with KML interpreters such as Google Earth. The NSA provide information about snow water equivalent (SWE), snow depth, surface and profile snowpack temperatures, snowmelt, surface and blowing snow sublimation, snow-surface energy exchanges, precipitation, and weather forcings all in multiple formats (Barrett, 2003). Use of these data in model applications are being tested and evaluated (see Sections 4.1 and 4.3).

GIS Analysis and Visualization of Gridded Data

The tools of ArcGIS 10 and ModelBuilder were used to develop and evaluate various ways of importing, formatting, sub-setting, and visualizing the SNODAS and NRCC spatially-distributed climate data products. Daily time-series data in TIF, NETCDF, GRIB, and binary formats were utilized with varying degrees of success. Animation procedures were implemented using ArcGIS Time Slider functionality. Issues regarding data management, screen refresh rates, and automated legend creation were overcome more easily using the NRCC data, subset of the West of Hudson watershed, but remained problematic with the SNODAS products. Best results were obtained by using the GIS to develop a binary mask for each watershed of interest, and then identifying the subset of data points falling within that watershed. The masks were used outside of the GIS to extract daily data for these points of interest. ArcGIS animation tools allowed for informative visualization of daily precipitation data over the watershed for the extreme events of Hurricane Irene and Tropical Storm Lee that occurred in late-August/early-September 2011.

7. Modeling Program Collaboration

7.1. Participation in Ongoing External Research Projects

In the last year the Water Quality Modeling Section has participated in several projects related to the Section's ongoing work on testing and improving models simulating watershed hydrology and water quality, reservoir water quality and reservoir system operations. A number of projects also supported Water Quality Modeling Section evaluation of climate change as outlined in DEP's Climate Change Integrated Monitoring Project (CCIMP).

Water Research Foundation Project 4262 - Vulnerability Assessment and Risk Management Tools for Climate Change: Assessing Potential Impacts and Identifying Adaptation Options
Collaborators: Hazen and Sawyer, National Center for Atmospheric Research, Hydrologics, Stockholm Institute, Rand Corporation.

The main focus of the CCIMP is to identify potential climate change impacts on the water supply using the structured quantitative framework of water quality models. Project 4262 compliments the CCIMP by going one step further. Once climate change impacts have been identified this project seeks to develop risk management approaches that will help managers prioritize risks and decide on a course of action. To date a variety of scenarios have been developed and analyzed. These evaluated the combined risks associated with future climate change, changing water demands, and future changes in water quality (turbidity). DEP watershed models were used to simulate future inputs and reservoir water quality and system operation models were used to simulate impacts. To judge impacts and risk a variety of performance metrics were evaluated under current system conditions and taking in to account possible changes in reservoir system operation and infrastructure. This project is entering its final year and will end in April 2013. During the past year DEP has contributed significantly to project 4262 and a more detailed description of our contribution is given in Section 3.1 of this report.

Water Research Foundation Project 4306 – Analysis of Reservoir operations under Climate Change

Collaborators: Hazen and Sawyer, National Center for Atmospheric Research, Hydrologics.

WRF project 4306 will evaluate the possibilities of adapting and modifying reservoir operation policy to mitigate the impacts of climate change on water supply quantity and quality. The project will develop the tools and methodologies needed to systematically evaluate and update operational policies in response to a changing climate. Analyzing future reservoir operations and how they differ from those used under current conditions will clearly benefit the CCIMP and allow us to better tailor OASIS model simulations to future conditions. The OASIS model, as well as the coupled OASIS – CE Qual W2 models contained within DEP's Operation Support Tool (OST) are being used by the Water Quality Modeling Section to investigate the effects of climate change on water supply storage, reservoir water quality and reservoir operations. We will be well positioned to support the goals of project 4306 due to our past experience in simulating reservoir turbidity to support operational decisions (e.g. Section 2), our support of OST development, and our work with climate change. Hydrologics, the developer of the OASIS model and Hazen and Sawyer the contractor responsible for development of the OST will also be participants in project 4306. This insures that DEP will obtain assistance with modeling issues related to CCIMP use of OASIS and the OST, and that project deliverables have direct relevance to DEP's modeling efforts. Work on project 4306 is underway at the time of this report. Since this project is closely related to WRF project 4262, there is considerable cooperation between the two projects and the Water Quality Modeling Section. This project will also end in April 2013.

Water Utility Climate Alliance (WUCA) Piloting Utility Modeling Applications (PUMA)

WUCA is a group of ten of the nation's largest water utilities, whose mission is to improve research on the effects of climate change on drinking water supplies, and to help water supplies to develop strategies to cope with the potential impact of climate change (http://www.wucaonline.org). The purpose of the PUMA project is: 1) to identify climate modeling tools and techniques that are appropriate for analysis of climate change impacts on water supplies; 2)develop guidelines for the use of climate data and model simulation data including methodologies for describing uncertainty; 3) to suggest how these data can be used to support water planning and decision making; 4) to build and enhance collaboration between water utilities and NOAA Regional Integrated Sciences and Assessment (RISA) centers; and 5) to identify future research investments that would serve the water utility community. The Water Quality Modeling Section has participated in the WUCA/PUMA project by attending the project kickoff meeting in December 2010, and by participating in regular phone conferences and planning meetings since then. The NYC water supply and the work undertaken as part of the CCIMP will be highlighted as a case study in a white paper that will be product of the PUMA project. The NYC water supply provides an unique case study since climate change impacts expected for the Northeastern United States are more water quality related as opposed to the water quantity concerns that are more prevalent in the Western United States. Furthermore, financial support for the CCIMP (as part of FAD funding) is unusually generous allowing DEP to have one of the most extensive climate change research programs of any of the WUCA utilities. DEP is the only utility using post-doctoral support scientists to carry out much of its climate change research in house, whereas other utilities have instead rely more extensively on contracts with outside consultants to evaluate climate change impacts. Information for the case study is being collected through a series of interviews and surveys developed by Status Consulting for WUCA. DEP was one of the first Utilities to participate in the survey and during the coming year we will re-surveyed to follow our progress in the CCIMP.

NASA Earth Science Division, Applied Sciences Program. Application of evapotranspiration and soil moisture remote sensing products to enhance hydrological modeling for decision support in the New York City water supply.
Collaborator: CUNY CREST

This project is being led by the City University of New York (CUNY) Remote Sensing of the Earth Science and Technology (CREST) center. The DEP Water Quality Modeling Section supported a research proposal developed by CUNY CREST that has been funded by NASA. The purpose of the project is to evaluate shortwave, thermal, and microwave remote sensing products that could provide DEP with independent and spatially variable estimates of soil moisture and evapotranspiration. These remote sensing products will be used to test, calibrate and verify watershed hydrology models in the WOH region under present climate conditions.

Presently watershed model calibration and testing must be based on comparison to measured discharge and nutrient loads at the outlets of large watersheds in the WOH region, since these are the only data available for calibration purposes. While models can successfully simulate watershed scale outputs there are multiple models processes that influence the watershed output. The accuracy of model representations of such processes such as evapotranspiration or soil water storage cannot at present be independently verified. Consequently even though watershed outputs are simulated with good accuracy, the simulated watershed processes can be in error since differing contributions from differing processes result in similar outputs. Correctly representing soil moisture and evapotranspiration in our watersheds models will be critical for simulating future changes in watershed hydrology, especially during summer periods when low flows and drought conditions could occur. This project will allow us obtain independent estimates of soil moisture and evapotranspiration that will in turn allow us to gain a better understanding of how well these processes are simulated in our watershed models and if necessary provide data to support improved model representations of these processes

The project has been underway for approximately four months. The DEP Water Quality Modeling Section has supplied a version of the GWLF-VSA watershed hydrology a water quality model used by DEP to CUNY CREST, and provided support in setting up and running the model. Initial comparisons between model output and the remote sensing products are encouraging. In general model simulation of soil moisture and evapotranspiration show seasonal patterns that are similar in timing and magnitude; however, there are interesting and important differences between the measured and simulated results. This project will continue into the next year. Following a first year feasibility study an additional three years of NASA support is possible if the remote sensing data is found to provide valuable information to DEP.

NASA SMAP Early Adopter Project
Collaborator: CUNY CREST

The Soil Moisture Active Passive (SMAP) satellite (is being developed by NASA and is scheduled for launch during November of 2014. The SMAP satellite mission focuses on measurements valuable water resources using a combination of passive and active microwave sensors. Products include estimates of soil moisture and soil freezing which will be made at greater accuracy and at higher spatial and temporal resolution than with the current generation earth observing satellites. SMAP soil moisture data will therefore be of use to DEP for the reasons described in the project above, but will be of greater accuracy and improved resolution. Changes in the timing and extent of soil freezing in an expected effect of climate change in the WOH water supply watersheds, and changes in soil freezing have documented effects on watershed hydrology and biogeochemistry. Monitoring soil freezing will therefore be of importance for monitoring the impacts of climate change, and for providing data to develop and test simulation models that include processes affecting soil freezing. During 2012 CUNY CREST and DEP have been chosen to be early adaptors of SMAP data products. This status allows us to test pre-launch simulated data products and provides us with early access to actual data once the satellite is operational. This work is clearly complimentary to the project above and ensures that DEP will be able to rapidly make use of the SMAP data products as soon as they become available.

7.2. Modeling Program Contract Management

Presently the Water Quality Modeling Section is managing four external contracts that support our work. These contracts provide data that are used for testing, calibrating and verifying models, provide support for the development and testing of models. In the case of the contract with the Research Foundation of the City University of New York (CUNY-RF), support for model and data development is provided by post-doctoral scientists who work with the Water Quality Modeling Section on a day to day basis. These contacts are listed below.

Contractor: Upstate Freshwater Institute.
Contract Title: Integrated Program of Measurement, Process Studies and Modeling for the Turbidity Problem at Schoharie Creek and Esopus Creek.

This long running contract involves data collection, process studies and the development and testing of turbidity models in Schoharie, Ashokan and Kensico Reservoirs. Models developed by this project are routinely used by the Water Quality Modeling Section to predict turbidity levels in the above reservoirs, and these models have also been incorporated in to the DEP Operation Support Tool (OST). This contract is scheduled to end in December of 2012. A number of peer reviewed publications have been produced from the work accomplished in this project (Effler and Matthews, 2004; Effler et al., 2006a; Effler et al., 2007; Gelda and Effler, 2007a, 2007b, 2007c, 2008; Peng and Effler, 2007, 2012; Perkins et al., 2007; Gelda et al., 2009, 2012; Owens, 2009; Peng et al., 2009; O'Donnell et al., 2011; Owens et al., 2011). In addition UFI is in the process of producing a final project report and ensuring that all the models and data sets developed by the project have been transferred to DEP.

Contractor: Upstate Freshwater Institute.
Contract Title: Robotic Monitoring of Selected New York City Reservoirs and Major Tributaries

This contract involves setting up a network of automated reservoir monitoring buoys and stream water quality monitoring stations through the Catskill reservoir system (Schoharie and Ashokan Reservoirs), Kensico Reservoir and Rondout Reservoir. The emphasis is on turbidity measurements. Near real time turbidity data is collected from three stream monitoring sites and eight reservoir monitoring buoys. Data from this system is used by DEP to monitor reservoir turbidity levels as an aid to operational decisions (particularly at times of elevated turbidity), and to provide data to initialize and verify DEP reservoir turbidity transport models. It is planned that data from the monitoring network will be input to the OST. During the past year UFI has supported the transfer of the monitoring network to DEP operation and control, so that DEP is now responsible for all aspects of monitoring site maintenance and operations, as well as data collection and archiving. Following hurricane Irene and tropical storm Lee in 2011 this contact was extended by one year and is now scheduled to end in Dec 2012. The one year change order allowed UFI to repair storm related damage to the monitoring network, to collected storm related samples of reservoir sediment characteristics, and to address issues of reservoir model performance that became evident as a result of the extreme conditions associated with these storms. A number of peer reviewed publications have been produced from the work accomplished in this project (Effler et al., 2006b, 2008; O'Donnell and Effler, 2006; Prestigiacomo et al., 2008). In addition UFI is in producing a final report on the model improvements developed in the change order period as well as ensuring that all the models and data sets produced by the project have been transferred to DEP.

Contractor: United States Geological Survey.
Contract Title: Turbidity and Suspended Sediment Monitoring in the Upper Esopus Creek Watershed, Ulster County, NY

This contract involved involves retrofitting the five existing USGS flow gauges in the Esopus Creek watershed to automatically monitor turbidity at high (15 min) frequency. These five stations will provide a high frequency record of flow and turbidity that will allow the water quality modeling group to evaluate temporal and spatial variations in turbidity sources and transport within the Esopus creek watershed; develop improved turbidity vs. discharge rating relationships; and collect high quality data that can be used to develop and test watershed sediment erosion and transport models. Approximately two years of data have been collected so far, and these data are presently being analyzed, and used for model testing. This project is scheduled to end in 2013. Channel best management practices (BMP) are being implemented in tributaries of the Esopus Creek during 2012 and several are planned for 2013. These are intended to reduce suspended sediment entrainment with consequent reductions in turbidity. Turbidity monitoring at these tributaries will allows quantification of BMP effects. These high frequency monitoring data can also aid in integrating point measurements of suspended sediment and turbidity to stream habitat, macroinvertebrate, periphyton, and fish population sampling temporally and spatially throughout the watershed.

Contractor: Research Foundation City University of New York.
Contract Title: Scientific Modeling Support
This contract provides CUNY with the funding needed to hire seven post-doctoral research associates (post-docs) who are jointly advised by CUNY faculty, external faculty advisors, and DEP scientists. The post docs are stationed in Kingston, New York working with the Water Quality Modeling Section on a day-to-day basis. The positions are for an initial two year period, with the possibility of an additional two year extension. This project was originally scheduled to end in 2013, but has been extended in time to ensure that all of the hired post docs have a chance to use their full four year term of employment.

The present post-doc positions are for

- Climate Data Analysis
- Reservoir system modeling
- Reservoir turbidity modeling
- Reservoir eutrophication modeling
- Watershed nutrient modeling
- Watershed sediment erosion and transport modeling
- Forest ecosystem modeling

This contract has been very successful leading to improved model applications, new and improved data sets including future climate scenarios used by the CCIMP and the development and test of new applications. To date 8 peer reviewed publications (Anandhi et al., 2011a, 2011b; Matonse et al., 2011, 2012; Pradhanang et al., 2011; Zion et al., 2011; Mukundan et al., 2012; Samal et al., 2012b) have resulted from this project. The sections of this report describing model applications, model development and data analysis benefited from the work of our post-doctoral scientists. Furthermore, many of the conference presentations made in the last year (Section 8.2) were the result of work by the post-doctoral scientists.

7.3. Support of Applications for External Research Funding

All of the collaborative projects described above result from the Water Quality Modeling Section collaborating with universities and research institutes to prepare and submit grant applications to different research funding organizations. During the past year the Water Quality Modeling Section has supported two grant applications.

USDA - Taking Upland, Channel and Future Climate Into Account For Effectively Managing Erosion And Sediment: The Stony Clove Watershed.
Collaborators: Cornell University, USDA ARS National Sediment Laboratory DEP Stream Management Program, Cornell Cooperative Extension, Ulster County Soil and Water Conservation District.

This project will develop and test the CONservational Channel Evolution and Pollutant Transport System (CONCEPTS) modeling framework for estimating sediment erosion and transport, and for evaluating stream management practices for reducing suspended sediments in the NYC watersheds. CONCEPTS was developed by Eddy J. Langendoen of the USDA ARS National Sediment Laboratory who is a principal investigator on this project. Presently DEP relies on different sediment rating curve techniques to make predictive estimates of stream suspended sediment concentration and turbidity as a function of stream discharge. CONCEPTS take a more mechanistic approach of attempting to simulate long-term stream channel and streambed changes, and sediment transport. To do so the model application involves collecting a large amount of data describing stream channel morphometry and bed and bank material properties. If successful the model will provide several advances over the sediment rating based estimates of stream sediment transport. CONCEPTS can be applied at the scale of stream management projects and offers the potential as a tool for evaluating the effects of stream management projects. On the watershed scale simulation of turbidity loads by CONCEPTS should account for changes in stream channel properties over time. This should allow for more realistic long term simulation of stream sediment transport, particularly in relation to ongoing climate change work in the CCIMP. Also, as part of model testing and calibration, a large amount of valuable information on stream bank and bed sediment characteristics related to erosion and sediment sources will be collected. This will potentially be of great value to DEP.

It should be stressed that if funded this project will attempt a unique application of the CONCEPTS model in mountain streams with a geomorphology that to date has not been simulated by the model. An important aspect of the project will be adapting and testing CONCEPTS to the Esopus Creek watershed and for this reason collaboration with the model developers and experts in regional hydrologic processes will be especially beneficial.

National Science Foundation. Collaborative Research: Macrosystem controls on nitrogen cycling and export through terrestrial and aquatic ecosystems in the eastern forest biome
Lead Principal Investigator: Lawrence E. Band, University of North Carolina – Chapel Hill

Other collaborators: Cary Institute for Ecosystem Studies, Penn State University, UC Santa Barbara, University of New Hampshire, Plymouth State University (NH), Virginia Tech University, United States Geological Survey, United States Forest Service, University of Western Ontario, (Canada)

The principle investigator on this grant proposal Dr. Lawrence Band, has also been serving as an advisor to the Water Quality Modeling Section, helping us develop an application of the RHESSys forest model in the WOH watersheds. The proposed project will combine monitoring and modeling to evaluate how hydrologic and biogeochemical cycles regulated by forest processes vary along a latitudinal gradient ranging from North Carolina to Northern Ontario. Specific processes that are known to vary along this gradient include snow accumulation and melt, vegetative cycles and their effect on nutrient uptake, seasonal cycles in the air temperature and growing season, and variations in forest species composition. If funded this project will provide additional support for DEP's efforts to develop forest models for the WOH watershed area, and will lead to valuable scientific review and feedback on this effort from the many other project participants. By comparing our results with a large number of sites covering a broad latitudinal gradient DEP will gain additional insight into the role of forests regulating hydrological and biogeochemical processes in the WOH reservoir watersheds. In relation to our work in the CCIMP understanding how regulatory processes vary along a latitudinal gradient will also provide valuable insight into how these processes might also be expected vary under a warming climate.

8. Modeling Program Scientific Papers and Presentations

8.1. Published Work

Below is a listing of journal articles in which Water Quality Modeling Section members have been authors during the previous year. Copies of the articles are included in Appendix A of this report.

Matonse, A.H., D.C. Pierson, A. Frei, M.S. Zion, A. Anandhi, B. Wright, and E. Schneiderman, 2012. Investigating the impact of Climate Change Impact on New York City's Primary Water Supply. *Climatic Change*, **113.** doi: 10.1007/s10584-012-0515-4.

Mukundan, R., S. Pradhanang, E. Schneiderman, D.C. Pierson, A. Anandhi, M. Zion, A. Matonse, D. Lounsbury, and T. Steenhuis, 2012. Suspended Sediment Source Areas and Future Climate Impact on Soil Erosion and Sediment Yield in a New York City Water Supply Watershed, USA. *Geomorphology*, (2012). doi: 10.1016/j.geomorph.2012.06.021.

8.2. Conference Presentations

During this reporting period members of the Water Quality Modeling Section have made presentations regarding our modeling activities at a number of scientific meetings. Below the presentations and associated abstracts are listed for each of the meetings

Association of American Geographers Meeting February 2012 New York City, NY

Mukundan, R[1]., E. Schneiderman[2], D. Lounsbury[2], D. Pierson[2], M. Zion[2], S. Pradhanang[1] and A. Matonse[1]. 2012. ***Stream-Power Map as a Stream Channel Assessment Tool***

[1] CUNY Institute of Sustainable Cities/DEP
[2] DEP Bureau Water Supply

Abstract:

Stream channel erosion is one of the leading causes of high stream sediment loads. While watershed models have a demonstrated ability to simulate total sediment at the watershed outlet, the ability to reasonably identify the individual reach sources of the total watershed sediment load is still a modeling challenge. This study presents a simple method for predicting potential stream channel erosion sites based on variations in stream power. The method was tested in three headwater stream watersheds in three geographic regions. Channel erosion sites predicted were comparable with qualitative field measurements of stream channel stability in the same watersheds. We also mapped reach scale variation in stream power for one of the major drinking water reservoir watersheds in the NYC water supply system using LiDAR derived Digital Elevation Model (DEM) at 3m spatial resolution, and 1:24k USGS quad contours derived DEM at 10m spatial resolution. The derived maps can be easily overlaid with other available field measured information. The methods outlined in this study can serve as a simple and effective planning level tool to identify potential channel erosion sites and stream restoration projects at the watershed scale. Identification of sensitive stream reaches provides stream managers with an opportunity to make decisions on where to invest available resources in order to achieve maximum sediment load reduction and improvement in water quality.

AGU Fall Meeting, 5-9 December 2011. San Francisco, California

McHale, M1., B. Baldigo[1], A. Smith[1], R. Mukundan[2], J. Siemion[1], and C. Mulvihill[1]. 2011. ***An integrated approach to monitoring the effect of sediment and turbidity on aquatic biota and water quality in the New York City water supply.***

[1] USGS, Troy N.Y., USA
[2] CUNY Institute of Sustainable Cities/DEP

Abstract:

The New York City water supply system provides drinking water to more than 9 million people. About 90 percent of New York City's water is supplied by six surface-water reservoirs in the Catskill Mountains in southeastern New York State. The Ashokan Reservoir is a focus of concern because high turbidity and suspended sediment concentration can affect the drinking water supply and the integrity of aquatic biota in the reservoir and its tributaries. The U.S. Geological Survey, New York State Department of Environmental Conservation, and New York City Department of Environmental Protection are collaborating to identify suspended sediment and turbidity source areas and evaluate the effectiveness of stream stabilization projects to improve water quality in the 497 square kilometer Upper Esopus Creek watershed, the primary source of water to the Ashokan Reservoir. This research combines point measurements of stream habitat, macroinvertebrate, periphyton, and fish population sampling, and water quality sampling with continuous turbidity measurements and watershed modeling to integrate point measurements temporally and spatially throughout the watershed. Preliminary results suggest that although stream stabilization projects appear to have reduced sediment and turbidity concentrations and improved aquatic habitat, interpreting results has been confounded by a series of large storms during the last several years. Indeed, storms large enough to reshape channel morphology can have long-lasting effects on sediment and turbidity concentrations and aquatic biota. This framework for integrating temporal and spatial point measurements using high frequency monitoring and watershed modeling appears to hold great promise to inform policy concerning the water supply of one of the world's largest cities.

Mukundan, R[1]., S. Pradhanang[1], E. Schneiderman[2], M. Zion[2], A. Anandhi[3], D. Pierson[1] and T. Steenhuis[4] 2011. ***A modeling study on soil moisture effect on soil erosion under future climate in a humid continental watershed.***

[1] CUNY Institute of Sustainable Cities/DEP
[2] DEP Bureau Water Supply
[3]Kansas State Univ., Manhattan, Kansas
[4]Cornell Univ. Ithaca, N.Y., USA

Abstract:

Quantifying spatial and temporal patterns of soil erosion under present and future climate is important both for understanding sediment transport processes as well as watershed-scale management of sediment and associated pollutants. A case study from one of the major watersheds in the New York City Water Supply System is presented. The objective of this study is to apply SWAT-WB, a physically based semi-distributed model to simulate the impact of antecedent soil moisture on soil erosion and suspended sediment yield in the study watershed for a set of future climate scenarios representative of the period 2081-2100. Scenarios developed using nine global climate model (GCM) simulations indicate that future climate related changes in soil erosion appeared more pronounced in the winter due to a shift in the timing of snowmelt and also due to a decrease in the proportion of precipitation received as snow. However, preliminary results indicate that in the future, impact of changes in antecedent soil moisture on soil erosion was less important in the winter. Although an increase in future summer precipitation is predicted, soil erosion and sediment yield appeared to decrease owing to an increase in soil moisture deficit and a decrease in water yield due to increased evapotranspiration.

Pradhanang , Soni M.[1], Rajith Mukundan[1], Elliot M. Schneiderman[2], Mark Zion[2], Aavudai Anandhi[3], Donald C. Pierson[2], Allan Frei[1], Zachary M. Easton[4], Daniel Fuka[4] and Tammo S. Steenhuis[4]. 2011. ***Streamflow responses to climate change in New York City water supply watershed.***

[1] CUNY Institute of Sustainable Cities/DEP
[2] DEP Bureau Water Supply
[3]Kansas State Univ., Manhattan, Kansas
[4]Cornell Univ. Ithaca, NY

Abstract:

The impact of climate change in the North Eastern US is already observed in the form of shorter winter, higher annual average temperature, and more frequent extreme heat and precipitation events. Further changes could have profound effects on the New York City (NYC) Water Supply and ecological integrity of the watersheds. The implications of climate change are not well understood in the north eastern US where soils are generally shallow. The objective of this study is to examine how expected changes in precipitation and air temperature may translate into changes in streamflow in the NYC Water Supply watershed. Streamflow was simulated using the Soil and Water Assessment Tool-Water Balance (SWAT-WB) that represents the variable source hydrology prevailing in the NYC watersheds. A comparative analysis between simulated streamflow for baseline period (1964-2008) and future scenarios (2081-2100) was carried out for streamflow indicators that are important for understanding how river flow dynamics will impact the water supply, aquatic health, and physical structures in the stream corridor. We analyze the impacts of changes in the magnitude, timing, duration, frequency, and rate of hydrologic events using the Indicators of Hydrologic Alteration (IHA) tool. Our results indicate that warming during the winter and the early spring diminishes snowpack and influence timing of snowmelt. The winter and spring streamflow are projected to increase but summer will be drier in future. Decreased flow during April and summer months will influence timing of fish spawning and their habitats. Low flows, hydrograph pulses, rise and fall rates are expected to increase due to climate change, potentially creating unfavorable conditions for native species and aquatic invertebrates inhabiting along river's edge, and affecting streambank stability and physical structures and also affects the water supply of NYC.

Samal, N.R[1]., Pierson[2], D.C., Frei, A[1]., Haung, Y[1]., Pradhanang, S.M[1]., Mukundan, R[1]., Matonse, A.H[1]., Lounsbury, D[2], Schneiderman, E.M[2]., Zion, M.S.[2] and Owens, E.M.[3]
2011. ***Stratification and mixing event analysis from high-resolution monitoring data for New York City Water Supply reservoir.***

[1] CUNY Institute of Sustainable Cities/DEP
[2] DEP Bureau Water Supply, USA
[3]Upstate Freshwater Inst., Syracuse, NY

Abstract:

In this study, we analyze the field observations from a buoy placed in west basin of Ashokan reservoir, which is located 73 miles north of New York City. The reservoir consists of two basins separated by a concrete dividing weir and roadway holds 122.9 billion gallons at full capacity. On an average over past few years, Ashokan reservoir supply 500 million gallons per day, or roughly 42% of the total average daily consumption, to New York City and additional one million Upstate consumers. Based on the in situ measurements of buoy data (depth-water temperature, conductivity, turbidity and dissolved oxygen) and the meteorological data, statistics of stratification and mixing events are estimated in terms of non-dimensional numbers (lake number, Schmidt number and Wedderburn number) and other reservoir indices (metalimnion extent, thermocline depth, mode-1 vertical seiche period, Brunt-Vaisala buoyancy frequency). The analysis of these high-resolution monitoring data leads to a better understanding of changes in thermal structure over a range of both spatial and temporal scales. The responses of these indices to the short-term changes in the weather and the effect of wind induced-turbulent mixing on variation of dissolved oxygen in deep waters are established. The results show that the diurnal changes in stratification and mixing has significant effect on the vertical profile of turbidity as well as dissolved oxygen in reservoir. This study investigates to what extent the movement of thermocline can affect the transport of the suspended

American Water Works Association Meeting September 2012 Manalapan, N.J.

Matonse, A.[1], A. Frei[1], D. Pierson[2] and M Zion[2] 2012. ***Modeling in water supply management under changing weather and climate.***

[1] CUNY Institute of Sustainable Cities/DEP
[2] DEP Bureau Water Supply

Abstract:

During the fall of 2011, Hurricane Irene and Tropical storm Lee resulted in devastating effects across the eastern U.S. Precipitation and streamflow during these events were historically among the largest in the Catskill Mountains and Hudson River Valley in New York. Some locations in this region experienced the highest 60-day total precipitation ever recorded. Historical records also indicate that there has been a marked increase in the frequency of hydrologic extreme events during the last decade. Globally, the 2012 IPCC special report on extreme events indicates that there has been an overall decrease in the frequency of extreme cold temperatures, an overall increase in the frequency of extreme warm temperatures, and an increasing trend on hydrologic extreme events, although with regional variations.

Recent studies of possible effects of climate change on New York City water supply indicate that projected future changes in air temperature and precipitation are likely to have an impact on regional streamflow patterns and on NYC reservoir system operations. Simulated streamflow suggest that in the future, greater runoff will occur earlier in winter, and with more precipitation falling as rain and less accumulation as snow. These results from climate change predictions and historical patterns in extreme events have renewed concerns about common approaches in accounting for and managing extreme hydrologic events.

In today's environment, with growing water demands from a variety of users, in addition to evolving water quality requirements and environmental regulations, managing water supply systems is becoming more complex and challenging. Models are increasingly used as tools to support operations and long term planning. However, evidence of a changing climate raises questions about the concept of stationarity, one of the fundamental concepts in water-resource engineering. This presentation will discuss non-stationarity and the role of models in managing complex water supply systems under a changing environment.

Eastern Snow Conference, June 2012 Frost Valley, New York

Anandhi, A[1], 2012. ***Past and future changes in frost day indices in Catskill Mountain, NY, USA.***

[1]Kansas State Univ., Manhattan KS, USA

Abstract:

The objective of this study is to investigate the current and future changes in minimum temperatures (Tmin) and six frost indices in six reservoir watersheds in Catskill Mountains. These changes have potentially important implications for the water supply of New York City. Frost day is defined as a day with Tmin < 0°C. The frost indices studied are number of frost-free days (nFFDs), number of months with frost (nFMs), last spring freeze (LSF), first fall freeze (FFF), growing season length (GSL) and frost season length (FSL). The changes in the past were studied using a single time series of Tmin for a watershed obtained from observed values for the period 1960–2008. Future scenarios of daily Tmin were derived by downscaling of simulations from Global Climate Model (GCM) simulations using 25 bin change factor methodology. GCM simulations at daily timescale are obtained from the World Climate Research Programme's (WCRP's) Coupled Model Intercomparison Project Phase 3 (CMIP3) multi-model dataset. The simulations used in the study are for baseline scenario (20C3M), future scenarios (A1B, A2, B1) and two twenty-first century time periods (2045-2065, 2080-2100). Our results indicated a general increase in average Tmin, and GSL, decrease in number of nFFDs, nFMs and FSL, LSF and FFF in the year during the historical and future time periods. Our results add local precision to the earlier findings in which encompassed larger areas.

Infante, José [1], Tarendra Lakhankar[1], Soni Pradhanang[2], Peter Romanov[3], Reza Khanbilvardi[1]
2012. ***Toward assimilation of merged satellite and model based snowpack properties for Flood Forecasting using Hydrological Models.***

[1] NOAA-CREST, City University of New York
[2] CUNY Institute of Sustainable Cities/DEP
[3] NOAA/NESDIS/STAR, Silver Spring, Maryland

Abstract:

Flood prediction has been the objective of several studies for the past couple of decades because of their destruction potential, money losses and demises. It has been observed that rapid snowmelt and rain on snow events are contributing to the problem considerably. Therefore, accurate estimates of snowpack properties on ground are necessary. The SWAT is a hydrological model to predict runoff quantity and quality of a watershed given its land cover and land use properties. The SNTHERM is a one-dimensional model to analyze the snowpack properties given the climatological conditions of the area. This project proposed a methodology to objectively merge in-situ stationed observation with satellite based microwave data to estimate gridded snowpack properties using SNTHERM and Microwave Snow Emission Model. Krigging method is used to produce gridded data from in-situ meteorological observations, which are not available in gridded format. These two sources of estimated snowpack data will be merged to incorporate in land surface model (SWAT). This project will improve the river discharge estimation considering both: Excess rainfall runoff and the snow melting process. Further, it is expected to eliminate the temporal and spatial limitations of the current models in analyzing in-situ data, giving new capabilities and boosting their potential on forecasting in the short and long term. In this presentation, we will present the preliminary results from this study.

Mukundan R[1]., N. Samal[1], D. Pierson[2], M. Zion[2], and E. Schneiderman[2] 2012. ***Turbidity in a New York City Water Supply Stream: Sensitivity to Projected Changes in Winter Streamflow.***

[1] CUNY Institute of Sustainable Cities/DEP
[2] DEP Bureau Water Supply

Abstract:

The winter period has been identified as important in the Catskill region of New York in terms of climate change impact on watershed hydrology, water quality and drinking water supply. Major climate change impacts identified and predicted for this region include reduced snowfall and a backward shift in the timing of snowmelt runoff due to increasing air temperature. In this study we examine the sensitivity of stream turbidity to ongoing and anticipated changes in the seasonality of streamflow, with a focus on the winter period, using data from the Esopus Creek watershed that is part of the New York City water supply system. We use both measured data and modeling to specifically compare differences in stream turbidity between selected winter and summer events and between present and future climate scenarios. Results from this analysis are expected to have potential implications for reservoir and watershed management under future conditions.

Pierson, D.C.[1] N Samal[2], Y. Huang[2], E. M. Schneiderman[1], M.S. Zion[1], and S.M. Pradhanang[2] 2012. ***Changes in the Timing of Snowmelt, and the Seasonality of Nutrient Loading: Can Models Simulate the Impacts on Freshwater Trophic Status?***

[1] DEP Bureau Water Supply
[2] CUNY Institute of Sustainable Cities/DEP

Abstract:

The winter period has been identified as important in the Catskill region of New York in terms of climate change impact on watershed hydrology, water quality and drinking water supply. Major climate change impacts identified and predicted for this region include reduced snowfall and a backward shift in the timing of snowmelt runoff due to increasing air temperature. In this study we examine the sensitivity of stream turbidity to ongoing and anticipated changes in the seasonality of streamflow, with a focus on the winter period, using data from the Esopus Creek watershed that is part of the New York City water supply system. We use both measured data and modeling to specifically compare differences in stream turbidity between selected winter and summer events and between present and future climate scenarios. Results from this analysis are expected to have potential implications for reservoir and watershed management under future conditions.

Pradhanang, Soni M.[1], Elliot M. Schneiderman[2], Allan Frei[1], Mark Zion[2], Tammo S. Steenhuis[3], Donald Pierson[2] 2012. ***Rain-On-Snow Runoff Events in New York.***

[1] CUNY Institute of Sustainable Cities/DEP
[2] DEP Bureau Water Supply
[3]Cornell Univ. Ithaca, NY

Abstract:

Rain-on-snow (ROS) events are usually associated with flooding, and are important hydro-meteorological phenomenon. The severity of ROS events depends on the magnitude of the precipitation, elevation, snow water equivalent and areal extent of the antecedent snowpack. Examining the consequences of all of these factors acting together creates challenges for both flood prediction and flood risk assessments. The purpose of this study is to provide information on the spatial patterns, seasonality and interannual variability of rain-on-snow events in New York. We examine the spatial and temporal variability of rain-on-snow events for water years 2004 to 2012 from SNOw Data Assimilation System (SNODAS) products for New York. Parameters such as, liquid and solid precipitation, snow depth, snow melt, snow water equivalent, snowpack average temperature and sublimation are examined.

Samal, N.R[1]., Mukundan, R.[1], Pierson, D.C.[2], Gelda, R.K.[3], Schneiderman, E.M.[2], Zion, M.S.[2], and Matonse, A.H.[1] 2012. ***Turbidity in a New York City Water Supply Reservoir: Sensitivity to Anticipated Future Changes in Winter Turbidity Loading.***

[1] CUNY Institute of Sustainable Cities/DEP
[2] DEP Bureau Water Supply
[3]Upstate Freshwater Inst., Syracuse, NY

Abstract:

Ongoing and expected changes in the seasonality of stream flow could potentially lead to increased flows and turbidity levels under winter conditions and a reduction in turbidity loads at the time of traditional spring runoff. In this study we examine the sensitivity of reservoir turbidity levels to anticipated changes in the seasonality of turbidity loading. The focus of this study is the Ashokan Reservoir that is part of the New York City water supply system, and which can at times receive significant watershed turbidity inputs resulting from stream channel erosion of glacial clays (see presentation by Mukundan et al). Both measured data and simulated turbidity loads are input to a reservoir turbidity transport model (CE Qual W2) to specifically look at the differences in settling rates between selected winter and summer events, and changes in turbidity transport as a result of differences in reservoir thermal structure. This analysis is expected to have potential implications for reservoir operations under winter conditions.

Schneiderman, Elliot M.[1], Adao H. Matonse[2], Mark S. Zion[1], David G. Lounsbury[1], Rajith Mukundan[2], Soni M. Pradhanang[2] and Donald C. Pierson[1]
Comparison of Snowpack Models for New York City Watersheds.

[1] DEP Bureau Water Supply
[2] CUNY Institute of Sustainable Cities/DEP

Abstract:

Snow is a substantial component of historical annual precipitation in New York City (NYC) water supply watersheds in the Catskill Mountains, and the pattern of snow accumulation and snowmelt has important implications for the management of the reservoirs and watersheds that are part of NYC water supply. NYC currently estimates reservoir basin scale snow throughout the snow season and retrospectively by extrapolation from bi-weekly snow survey data. Snowpack models are useful for both short-term projections to support reservoir operations and long-term simulations to evaluate the potential effects of climate change and land use on the water supply. We tested three snowpack modeling approaches of varying complexity and spatial resolution by comparison with snow survey data: the lumped-parameter temperature-index approach from the Generalized Watershed Loading Function (GWLF) watershed model; a spatially-distributed temperature index (SDTI) approach; and the 1-km gridded NOAA SNOw Data Assimilation System (SNODAS) product. All three approaches all provided reasonable basin-scale estimates of snow water equivalent (SWE). SNODAS simulated the spatial variability of snowpack among snow survey sites within a basin better than the SDTI model but both spatially-distributed approaches were comparable in simulating the statistical distribution of snowpack within a basin similarly.

Zion, Mark S.[1], Eliot M. Schneiderman[1], David G. Lounsbury[1], Donald C. Pierson[1], Adao H. Matonse[2], Soni M. Pradhanang[2] 2012. ***Influence of Winter Snowpack on Seasonal Streamflow for the Catskill Mountain Region.***

[1] DEP Bureau Water Supply
[2] CUNY Institute of Sustainable Cities/DEP

Abstract:

Snowfall is an important part of the yearly water balance, accounting for approximately 20% of yearly precipitation for the Catskill Mountains in New York State, the location of the West-of-Hudson water supply for New York City. Although it is possible to estimate the impact of an individual snowmelt event on the magnitude of a specific storm event, the influence of the annual variation in winter snowpack ablation on the timing and magnitude of streamflow through the entire winter and spring is not well understood. This timing of streamflow is critical in determining the seasonal patterns of reservoir water storage. In addition the streamflow is critical to the delivery of constituents to the reservoirs, and thereby, also influences reservoir water quality.

This study investigates how the snowpack during the winter affects the seasonal timing of streamflow and constituent loads critical to the understanding of the water supply reservoir system. Various sources of snowpack SWE information such as manually collected snow surveys and Snow Data Assimilation System (SNODAS) products are used to estimate watershed snowpack. These estimates are then used with simple hydrologic modeling analyses to better understand the influence of watershed snowpack development and ablation on the timing and magnitude of winter and spring streamflow and constituent loads to the reservoir system.

Global Lake Ecological Observatory Network Meeting, Oct 2011 Lake Sunapee, New Hampshire

Samal, N.R[1]., Pierson, D.C[2]. and Anandhi, A[3]. 2011. ***Analysis of future scenarios of simulated water temperature data using Lake Analyzer.***

[1] CUNY Institute of Sustainable Cities/DEP
[2] DEP Bureau Water Supply, USA
[3]Kansas State Univ., Manhattan KS, USA

Abstract:

Future climate scenarios were derived by examining the differences between simulations of baseline (1980-2000) and future (2045-2065 and 2080-2100) time periods associated with three GCM models available from the World Climate Research Programme's Coupled Model Intercomparison Project phase 3 (CMIP3) dataset. Based on these differences, change factors were developed and applied to local records of meteorological data to produce future scenarios of air temperature, precipitation, humidity, solar radiation and wind speed. These data are used to drive the Generalized Watershed Loading Functions-Variable Source Area (GWLF-VSA) watershed model to simulate the future inflows. A one dimensional hydrothermal model is applied to simulate the vertical water temperature over historical data sets and future scenarios for a reservoir. Stratification and mixing indices are derived from the simulated water temperature and the wind speed under the different climate scenarios using the lake analyzer program developed by GLEON network. Our results suggest that under future conditions water temperature will be warmer, stratification will be of longer duration and that the resulting vertical temperature gradients will be stronger. On average we predict that the length of stratification will increase by 10 and 21 days in the case of the A1B and A2 emission scenarios. Water temperature under these different climate scenarios will increase; with the mean surface water temperature increasing by 4.5% and 9.8% while the mean bottom water temperature increasing by 3.1% and 6.5%. The Schmidt stability calculated over the multiple years of baseline and future scenarios was found to increase by 15.27 % (A1B Scenario) and 29.4% (A2 Scenario) and buoyancy frequency showed a similar increase of 14.54% (A1B Scenario) and 25.83% (A2 Scenario) in the future scenarios. The Wedderburn number and Lake number both displays a high amount of variability and both of these dimensionless indices explain the potential for diapycnal mixing events. Despite the high levels of variability both indices increase in value under the future climate scenarios suggesting that the reservoir will experience stronger and longer period of stratification with weak likelihood of substantial diapycnal mixing during the stable stratification period.

Impacts of Tropical Storms Irene and Lee on the Hudson River, September 2012
Cary Institute of Ecosystem Studies, Millbrook, NY

Matonse, Adao[1], Allan Frei[1], David Lounsbury[2], Donald Pierson[2] 2012. ***Hydrological Impacts of Hurricane Irene and Tropical Storm Lee in historical context: is the frequency of extreme hydrological events changing in southern New York State?***

[1] CUNY Institute of Sustainable Cities/DEP
[2] DEP Bureau Water Supply

Abstract:

In August and September of 2011 Hurricane Irene and Tropical Storm Lee precipitated large amounts of rain, which resulted in unusual flooding and significant material damage across various parts of the eastern US, including our study area which includes the Catskill Mountains and Hudson River Valley in southern New York State. In this study we analyze precipitation and stream gage records in order to determine (1) how large these events were in comparison to earlier extreme events; and (2) whether this region has experienced a change in the frequency of extreme events in recent years. Statistical analyses are applied to streamflow records from ten USGS gauges and to precipitation records from twelve meteorological stations across the region. We find that taken together, Irene and Lee were unprecedented events in this region due to a combination of: the magnitude of precipitation in each event, the proximity in space and time of these two events, and antecedent and subsequent precipitation. For most areas in our study region return periods for Irene and Lee estimated using warm period statistics are larger compared to conventional annual maximum based statistics; this is consistent with the public perception that these events were much larger when considered in seasonal context. Furthermore, there has been a marked increase in the frequency of extreme hydrologic events during the last one to two decades. This increasing trend is more evident during the late summer and early fall, the season of the most extreme precipitation events.

Soil Science Society of America- Annual Meeting. October 2011. San Antonio, Texas.

Mukundan, R.[1], S. Pradhanang[1], E. Schneiderman[2], M. Zion[2], A. Anandhi[3], D. Pierson[2], A. Matonse[1] and T. Steenhuis[4] 2011. *Potential Impact of Climate Change on Soil Erosion and Sediment Yield in a New York City Water Supply Watershed.*

[1] CUNY Institute of Sustainable Cities/DEP
[2] DEP Bureau Water Supply
[3] Kansas State Univ., Manhattan, Kansas
[4] Cornell Univ. Ithaca, NY

Abstract:

High suspended sediment loads and the resulting turbidity exert an important control on the use of surface waters for water supply and other designated uses. Changes in fluvial sediment loads influence material fluxes, aquatic geochemistry, water quality, channel morphology, and aquatic habitats. Therefore, quantifying spatial and temporal patterns in sediment loads is important both for understanding and predicting soil erosion and sediment transport processes as well as watershed-scale management of sediment and associated pollutants. A case study from the 891 km^2 Cannonsville watershed, one of the major watersheds in the New York City water supply system is presented. The objective of this study was to apply SWAT-WB, a physically based semi-distributed model to identify suspended sediment generating source areas under current conditions and to simulate potential climate change impacts on soil erosion and suspended sediment yield in the study watershed for a set of future climate scenarios representative of the period 2081-2100. Future scenarios developed using nine global climate model (GCM) simulations indicate a sharp increase in the annual rates of soil erosion although a similar result in sediment yield at the watershed outlet was not evident. Future climate related changes in soil erosion and sediment yield appeared more significant in the winter due to a shift in the timing of snowmelt and also due to a decrease in the proportion of precipitation received as snow. Although an increase in future summer precipitation was predicted, soil erosion and sediment yield appeared to decrease owing to an increase in soil moisture deficit and a decrease in water yield due to increased evapotranspiration.

Pradhanang, Soni M.[1], Rajith Mukundan[1], Elliot M. Schneiderman[2], Mark Zion[2], Donald C. Pierson[2] 2011. ***Influences of Channel Processes on Phosphorus Export from the New York City Water Supply, Cannonsville Watershed***.

[1] CUNY Institute of Sustainable Cities/DEP
[2] DEP Bureau Water Supply

Abstract:

Watershed water quality models are useful to evaluate and support nutrient management planning in agricultural watersheds. Model applications for nutrient management typically focus on controlling nutrient sources and transport to the stream channel. However, stream processes that involve nutrient release and retention may control the timing and quantity of export at the watershed outlet. The importance of these processes has received increased attention in scientific community. In this study we investigate the significance of stream channel processes in regulating phosphorus (P) loading to the NYC Water Supply Cannonsville Reservoir. Watershed P processes can include mobilization and transport of non-point watershed P sources from land to the channel, and remobilization of transient stores of P from stream beds. A mass balance based comparison of estimated P inputs to the stream channel with observed P export at the watershed outlet was done to quantify P delivery and explore the non-conservative behavior of P. Stream channel transport of both dissolved and particulate P is found to be non-conservative, with dissolved P tending to be retained during low flows and particulate P released during high flows. The results suggest that differences in the magnitude and relative importance of in-stream biogeochemical processes under different flow regimes regulate P delivery in ways that may influence ecological impacts to downstream river reaches and reservoirs. These results are useful for quantifying the effects of nutrient management on watershed loading and for improving parameterization of water quality models.

Watershed Science and Technical Conference. September 2012. West Point, New York.

Mukundan, R.[1], E. Schneiderman[2], D. Davis[3], and E. Langendoen[4] 2012. ***Modeling the Evolution of Catskill Stream Channels- Preliminary Results***

[1] CUNY Institute of Sustainable Cities/DEP
[2] NYC DEP Bureau Water Supply
[3] NYC DEP Stream Management Program
[4] National Sediment Lab, USDA ARS, Mississippi

Abstract:

Catskill Mountain streams provide up to 90% of the municipal water supply for 9 million residents of NYC through a network of six reservoirs draining approximately 3885 km^2. High magnitude runoff events with flood frequency recurrence intervals greater than 10 years cause significant suspended sediment turbidity conditions limiting the use of up to 40% of this unfiltered water supply for drinking water. The Catskill Mountains were glaciated in the Pleistocene and the stream network has variably incised into the glacial "legacy" sediments which are enriched in fine sediment. When streams intersect clay-rich glacial till and/or glaciolacustrine silt and clay, fine sediment is entrained during high runoff giving the streams a characteristic red-brown turbidity with levels often exceeding 300 NTU (DEP 2006). A multi-phase research project has been initiated to investigate the processes that control erosion, entrainment and transport of fine sediment in the Catskill Mountain streams as well as developing conceptual and quantitative modeling tools capable of simulating the evolution of stream channels under a range of hydro-climatic and watershed physical conditions. Here we present results from a preliminary analysis using the CONservational Channel Evolution and Pollutant Transport System (CONCEPTS) for Stony Clove, a tributary of the Esopus Creek watershed that drains to the Ashokan reservoir. This deterministic, numerical model is unique in that it accounts for the hydraulic and geotechnical processes that control streambank erosion, in addition to bed processes and the routing of flow and sediment. The potential response of the Stony Clove (representing channels characteristic of those in the Ashokan Basin watershed) stream channels under a range of hydrologic events and an examination of the limitations to the current version of CONCEPTS applied in a glaciated mountain fluvial system will be presented and used to inform the development of subsequent conceptual and quantitative process-based models.

Wang, L., R.[1] Mukundan[2], M. Zion[3], and D. Pierson[3] 2012. ***Beyond Rating Curves: Time Series Models for In-Stream Turbidity Prediction***

[1] NOVA Consulting & Engineering, LLC.
[2] CUNY Institute of Sustainable Cities/DEP
[3] DEP Bureau Water Supply

Abstract:

Turbidity control is a critical function of utilities managing surface water supplies. For New York City's System, a logical strategy for turbidity control is to temporarily remove the Catskill System from service. While effective in limiting delivery of turbid water and reducing the need for alum treatment at Kensico, this strategy runs the risk of negatively impacting water supply reliability. Thus, it is advantageous for DEP to understand how long a particular turbidity event will affect their system. In order to understand the duration, intensity and total load of a turbidity event, predictions of future in-stream turbidity values are important. Traditionally, turbidity predictions have been carried out by applying streamflow observations/forecasts to a flow-turbidity rating curve. However, predictions from rating curves are often inaccurate because of inter-event and within event variability in flow-turbidity relations. Fortunately, predictions can be improved by applying an autoregressive moving average (ARMA) time series model on top of a rating curve. Like streamflow, turbidity time series are serially correlated in time. ARMA models condition predictions using the serial correlation in recent observations. For example, imagine a storm event has passed through a basin; in-stream turbidity spiked in response and now observed turbidity is slowly trending downward. Using a rating curve, predicted turbidity would increase during the storm, but would quickly decrease after flow returns to average hydrology. Using a rating curve supplemented with an ARMA model, the recent observations are taken into account and predictions are adjusted accordingly. As a result, predictions from this model will have a more accurate, gradual slope to ambient conditions. This presentation details the ARMA model selection/calibration procedure and compares its predictive skill to traditional rating curves. Models for Esopus Creek above Ashokan reservoir are provided as examples and will become part of DEP's Operations Support Tool.

Zion Mark S.[1], Donald C. Pierson[1], Elliot M. Schneiderman[1] and Adao Matonse[2] 2012. ***An Evaluation of Water Quality Modeling used to Inform Operational Decisions for the NYC Water Supply.***

[1] DEP Bureau Water Supply
[2] CUNY Institute of Sustainable Cities/DEP

Abstract:

Turbidity is a primary factor that potentially limits use of Catskill System portion of the New York City Water Supply. During the elevated turbidity events daily decisions are carefully taken to optimize system operations for turbidity control, while ensuring adequate water storage levels within the entire water system. To support these decisions, a combination of watershed, reservoir water quality and water system simulation models are used to evaluate alternative operational scenarios within a probabilistic framework. These simulation models form the basis for the Operational Support Tool (OST) currently under development by DEP.

The OST model predictions are based on future forecasts of meteorology, streamflows, and operations to better understand the implications of a given operating strategy on future water quality. Uncertainty in future forecasts is estimated using a range of possible futures scenarios that are judged to be representative of present conditions, but based on past history. A retrospective analysis of water quality data collected during the model forecast period measures the response that actually occurred during the model forecast period, and gives an indication of the accuracy of the forecast. This presentation compares the model forecasts to the data collected during the forecast period to better understand and evaluate the use of the modeling system in minimizing the impacts of turbidity within the water supply system.

9. References

Allen, P.M., J.G. Arnold and B.W. Byars, 1994. Downstream channel geometry for use in planning-level models. *Water Resources Bulletin*, **30**(4): 663–670.

Anandhi, A., A. Frei, D. C. Pierson, E. M. Schneiderman, M. S. Zion, D. Lounsbury, and A. H. Matonse. 2011a. Examination of change factor methodologies for climate change impact assessment. *Water Resources Research*, **47**:W03501. doi:10.1029/2010WR009104.

Anandhi, A., A. Frei, S.M. Pradhanang, M.S. Zion, D.C. Pierson, and E.M. Schneiderman, 2011b. AR4 climate model performance in simulating snow water equivalent over Catskill Mountain watersheds, New York, USA. *Hydrological Processes*, **25**:3302-3311.

Arnold, J.G., P.M. Allen, R. Muttiah and G. Bernhardt, 1995. Automated base flow separation and recession analysis techniques. *Ground Water*, **33**:1010-1018.

Arnold, J.G. and P.M. Allen, 1996. Simulating hydrologic budgets for three Illinois watersheds, *J.of Hydrology*, **176**: 55-77.

Arnold, J.G., R. Srinivasan, R.S. Mutiah and J.R. Williams, 1998. Large area hydrologic modeling and assessment-Part I: Model development. *J. Am. Water Resources Assoc.*, **34**(1) 73-89.

Ashley, S.T. and W.S. Ashley, 2008. The storm morphology of deadly flooding events in the United States. *Int. J. Climatol.*, **28**: 493-503. doi.:10.1002/joc.1554.

Auer, M.T. and B.E. Forrer, 1998. Development and parameterization of a kinetic framework for modelling light and phosphorus limited limited phytoplankton growth in Cannonsville Reservoir. *Lake and Reservoir Managment*, **14**: 290-300.

Avila, L.A. and J. Cangialosi, 2011. Tropical Cyclone Report: Hurricane Irene (AL092011) 21-28 August 2011; National Hurricane Center, National Oceanic and Atmospheric Administration.

Bagnold, R.A. 1966. An Approach to the Sediment Transport Problem from General Physics, USGS Professional Paper 422-I.

Bagnold, R.A., 1977. Bedload transport in natural rivers. *Water Resources Research*, **13**(2): 303−312.

Band, L., C. Tague, S. Brun, D. Tenenbaum and R. Fernandes, 2000. Modeling watersheds as spatial object hierarchies: Structure and dynamics. *Trans. Geogr. Info. Syst.*, **4**, 181–196.

Barker, D., D.M. Lawler, D.W. Knight, D.G. Morris, H.N. Davies and E.J. Stewart, 2009. Longitudinal distributions of river flood power: The combined automated flood, elevation and stream power (CAFES) methodology. *Earth Surface Processes and Landforms*, **34**(2): 280-290.

Barnett T.P., J.C. Adam and D.P. Lettenmaier, 2005. Potential impacts of a warming climate on water availability in snow-dominated regions. *Nature*, **438**: 303-309.

Barrett, A., 2003. National Operational Hydrologic Remote Sensing Center Snow Data Assimilation System (SNODAS) Products at NSIDC. NSIDC Special Report 11. Boulder, CO USA: National Snow and Ice Data Center. 19 pp.

Bartley, R., R.J. Keen, A.A. Hawdon, P.B. Hairsine, M.G. Disher and A.E. Kinsey-Henderson, 2008. Bank erosion and channel width change in a tropical catchment. *Earth Surface Processes and Landforms,* **33**(14): 2174–2200.

Bilotta, G.S. and R.E. Brazier, 2008. Understanding the influence of suspended solids on water quality and aquatic biota. *Water Research*, **42**: 2849-2861.

Blake, E.S., C.W. Landsea, E.J. Gibney, 2011. The deadliest, costliest, and most intense United States tropical cyclones from 1851 to 2010 (and other frequently requested hurricane facts); NOAA Technical Memorandum NWS NHC-6; National Weather Service: Miami, Florida.

Brach-Papa, C., P. Boyer, F. Ternat, M. Amielh and F. Anselmet, 2006. Settling classes for fine suspended particles. *C. R. Mecanique*, **334**: 560-567.

Buffam, I., J.N. Galloway, L.K. Blum and K.J. McGlathery, 2001. A stormflow/baseflow comparison of dissolved organic matter concentrations and bioavailability in an Appalachian stream. *Biogeochemistry,* **53** (3), 269-306.

Burns D.A., J. Klaus, and M.R. McHale. 2007. Recent climate trends and implications for water resources in the Catskill Mountain region, New York, USA, *Journal of Hydrology*, **336**, 155-170.

Carroll, T., D. Cline, G. Fall, A. Nilsson, L. Li and A. Rost, 2001. NOHRSC Operations and the Simulation of Snow Cover Properties for the Conterminous U.S. *Proceedings of the 69th Annual Meeting of the Western Snow Conference*, pp. 1-14.

Carroll, T., 2005. *Overview of the Center's Web Site and Products* . National Operational Hydrologic Remote Sensing Center, 15 pp.

Casamitjana, X. and G. Schladow, 1993. Vertical distribution of particles in stratified lake. *ASCE J. Environ. Eng.*, **119** (3): 443-462.

Catalan, J., 1992. Evolution of dissolved and particulate matter during the ice-covered period in a deep, high-moutain lake. *Canadian Journal of Fisheries and Aquatic Sciences*, **49**: 945-955. doi: 10.1139/f92-105.

Chakraborti, R.K., J.F. Atkinson and J. Kaur, 2009. Effect of mixing on suspended particle-size distribution. *ASCE J. Environ. Eng.,***135** (5): 306-316.

Chung, S.W., M.R. Hipsey and J. Imberger, 2009. Modelling the propagation of turbid density inflows into a stratified lake: Daecheong Reservoir, Korea. *Environmental Modelling & Software*, **24** (2009) 1467-1482.

Clow, D.W., L. Nanus, K.L. Verdin and J. Schmidt, 2012. Evaluation of SNODAS snow depth and snow water equivalent estimates for the Colorado Rocky Mountains, USA, *Hydrol. Process.*, **26**(17): 2583-2591. doi:10.1002/hyp.9385.

Cole, J.J., Y.T. Prairie, N.F. Caraco, W.H. McDowell, L.J. Tranvik, R.G. Striegl, C.M. Duarte, P. Kortelainen, J.A. Downing, J.J. Middelburg and J. Melack, 2007. Plumbing the global carbon cycle: Integrating inland waters into the terrestrial carbon budget. *Ecosystems,* **10** (1), 171-184.

Cole, T.M. and E.M. Buchak. 1995. CE-QUAL-W2: A Two-Dimensional, Laterally Averaged, Hydrodynamic and Water Quality Model, Version 2.0. U.S. Army Corps of Engineers, Vicksburg, MS.

Cole, T.M. and S.A. Wells, 2002. CE-QUAL-W2: A Two-Dimensional, Laterally Averaged, Hydrodynamicand Water Quality Model, Version 3.1." Instruction Report EL-2002-1. U.S. Army Engineering and Research Development Center, Vicksburg, MS.

Curriero, F.C., J.A. Patz, J.B. Rose and S. Lele, 2001. The association between extreme precipitation and waterborne disease outbreaks in the United States, 1948 – 1994. *American Journal of Public Health,* **91**(8):1194 – 1199.

D'Alonzo, K.T., 2004. The Johnson-Neyman procedure as an alternative to ANCOVA. *West. J. Nurs. Res.,* **26** (7), 804-812.

Davies-Colley, R.J., W.N. Vant and D.G. Smith, 2003. *Colour and Clarity of Natural Waters: Science and Management of Optical Water Quality*. Blackburn Press, Caldwell, NJ.

DeGaetano, A.T. and B.N. Belcher, 2007. Spatial interpolation of daily maximum and minimum air temperature based on meteorological model analyses and independent observations. *J. of Applied Meteorology and Climatology*, **46**:1981-1992.

DeGaetano, A.T. and D.S. Wilks, 2009. Radar-guided interpolation of climatological precipitation data. *Int. J. Climatol.,* **29**: 185-196.

DEP. 2004. Multi Tiered Water Quality Modeling Program Semi-Annual Status Report – EPA Filtration Avoidance Deliverable Report. New York City Department of Environmental Protection, Valhalla, New York. July 2004.

DEP, 2007. New York City Water Supply System Reference Guide, New York City Department of Environmental Protection, Valhalla, New York.

DEP. 2008a. Evaluation of Turbidity Reduction Potential through Watershed Management in the Ashokan Basin. Valhalla, New York. July 2008

DEP. 2008b. Climate Change Program: Assessment and Action Plan. New York, NY. May 2008.

DEP, 2011. New York City's Operations Support Tool (OST) White Paper. http://www.nyc.gov/html/dep/pdf/reports/ost_white_paper.pdf. Accessed 21st August 2012.

Doerr, S.M., E.M. Owens, R.K. Gelda, M.T. Auer and S.W. Effler. 1998. Development and testing of a nutrient-phytoplankton model for Cannonsville Reservoir. *Lake and Reservoir Management* **14**, 301-321.

Easterling, D.R., J.L. Evans, P. Ya. Groisman, T.R. Karl, K.E. Kunkel and P. Ambenje, 2000. Observed variability and trends in extreme climate events: A brief review. *Bulletin of the American Meteorological Society,* **81**(3): 417-425.

Effler, S.W. and D.A. Matthews, 2004. Sediment resuspension and drawdown in a water supply reservoir. *J. American Water Works Assoc.,* **40**:251-264.

Effler, S.W., D.A. Matthews, J. Kaser, A.R. Prestigiacomo and D.G. Smith, 2006a. Runoff event impacts on a water supply reservoir: Suspended sediment loading, turbid plume behavior, and sediment deposition. *J. Am. Water Resour. Assoc.*, **42**(6), 1697-1710.

Effler, S.W., A. Prestigiacomo, F. Peng, K.B. Bulygina and D.G. Smith, 2006b. Resolution of patterns of turbidity in a water supply reservoir from runoff events and the advantages of in situ beam attenuation measurements. *Lake and Reservoir Management*, **22**:79-93.

Effler, S.W., F. Peng and R.K. Gelda, 2007. Size distributions and light scattering features of minerogenic particles in a stream during runoff events. *ASCE J. Environ. Eng.,* **133**:931-940.

Effler, S.W., D.M. O'Donnell, D.A. Matthews, M.G. Perkins, S.M. O'Donnell, R.K. Gelda, A.R. Prestigiacomo, F.Peng, D.G. Smith, A.P. Bader and J.D. Mayfield, 2008. Insights for the structure of a reservoir turbidity model from monitoring and process studies. *Lake and Reservoir Management*, **24**:69-86.

El Adlouni, S. and T.B.M.J. Ouarda, 2010. Frequency analysis of extreme rainfall events. In: Testik, F.Y. and M. Gebremichael, (eds.), *Rainfall: State of the Science, Geophys. Monogr. Ser.* **191**: 171-188. American Geophysical Union, Washington. DC. doi: 10.1029/2010GM000976.

Evans, B.M., S.A. Sheeder and D.W. Lehning, 2003. A spatial technique for estimating streambank erosion based on watershed characteristics. *Journal of Spatial Hydrol.*, **3**: 1

Flores, A.N., C.O. Cuhaciyan, B.P. Bledsoe and E.E. Wohl, 2006. Channel-reach morphology dependence on energy, scale, and hydroclimatic processes with implications for prediction using geospatial data. *Water Resources Research*, **42** (6), W06412

Fontaine, T.A., T.S. Cruickshank, J.G. Arnold and R.H. Hotchkiss, 2002. Development of a snowfall-snowmelt routine for mountainous terrain for the soil water assessment tool (SWAT). *J. of Hydrology*, **262**: 209-223.

Frederick, R.H., V.A. Meyers and E.P. Auciello, 1977. Five- to 60-minute precipitation frequency for the eastern and central United States. *NOAA Tech. Mem. NWS HYDRO-35*. Washington D.C.

Frei, A., R.L. Armstrong, M.P. Clark and M.C. Serreze, 2000. Catskill mountain water resources: Vulnerability, hydroclimatology, and climate-change sensitivity. *Ann. Assoc. Am. Geographers*, **92** (2), 203–224.

Fuka, D.R., Z.M. Easton, E.S. Brooks, J. Boll, T.S. Steenhuis and M.T. Walter, 2012. A simple process-based snowmelt routine to model spatially distributed snow depth and snowmelt in the SWAT model. *J. of the American Water Resources Association*, in press. doi:10.1111/j.1752-1688.2012.00680.x.

Gannett Fleming & Hazen and Sawyer. 2007. Catskill turbidity control study: Phase III Final Report, Prepared for New York City Department of Environmental Protection, Bureau of Engineering Design and Construction.

Gannett Fleming & Hazen and Sawyer. 2008. Catskill turbidity control studies: Phase III Implementation Plan, Prepared for New York City Department of Environmental Protection, Bureau of Engineering Design and Construction

Gelda, R.K., E.M. Owens and S.W. Effler, 1998. Calibration, verification and an application of a two-dimensional hydrothermal model [CE-QUAL-W2(t)] for Cannonsville Reservoir. *Lake and Reservoir Management*,**14**,186-196.

Gelda, R.K. and S.W. Effler. 2007a. Modeling turbidity in a water supply reservoir: Advancements and issues. *ASCE J. Environ. Eng*, **133**: 139–148.

Gelda, R.K. and S.W. Effler, 2007b. Simulation of operations and water quality performance of reservoir multilevel intake configurations. *J. of Water Resources Planning and Management*, **133**:78-86.

Gelda, R.K. and S.W. Effler, 2007c. Testing and application of a two-dimensional hydrothermal model for a water supply reservoir: Implications of sedimentation. *J. of Environmental Engineering and Science*, **6**:73-84.

Gelda, R.K. and S.W. Effler, 2008. Probabilistic model for temperature and turbidity in a reservoir withdrawal. *Lake and Reservoir Management*, **24**:1-12.

Gelda, R.K., S.W. Effler, F. Peng, E.M. Owens, and D.C. Pierson. 2009. Turbidity model for Ashokan Reservoir, New York: Case study. *ASCE J. Environ. Eng.*, **135** (9): 885-895.

Gelda, R.K., S.W. Effler, F. Peng, 2012. Modeling turbidity and the effects of alum application for a water supply reservoir. *ASCE J. Environ. Eng.*,**138** (1): 38-47.

Graf, W.L., 1983. Downstream changes in stream power in the Henry Mountains, Utah. *Annals of the Association of American Geographers*, **73**: 373– 387.

Graybeal, D.Y. and D.J. Leathers, 2006. Snowmelt-related flood risk in Appalachia: First estimates from a historical snow climatology. *Journal of Applied Meteorology and Climatology*, **45**:178-193.

Groves, D. G., and R. J. Lempert. 2007. A new analytic method for finding policy-relevant scenarios, *Global Environ. Change*, **17**, 73– 85.

Haith, D.A. and L.L. Shoemaker, 1987. Generalized watershed loading functions for stream flow nutrients, *Water Resources Bull*., **23**(3):471-478.

Harr, R.D., 1981. Some characteristics and consequences of snowmelt during rainfall in western Oregon. *J. of Hydrology*, **53**:277-304.

Haupt, R.L. and S.E. Haupt. 2004. *Practical Genetic Algorithms*. John Wiley & Sons, Inc.

Havens, K. E., J.R. Beaver, D.A. Casamatta, T.L. East, R.T. James, P. McCormick, E.J. Phlips and A.J. Rodusky, 2011. Hurricane effects on the planktonic food web of a large subtropical lake. *J. Plankton Res.*, **33** (7), 1081-1094.

Hayhoe, K., C.P. Wake, T.G. Huntington, L. Luo, M.D. Schwartz, J. Sheffield, E. Wood, B. Anderson, J. Bradbury, A. DeGaetano, T.J. Troy and D. Wolfe, 2007. Past and Future Changes in Climate and Hydrological Indicators in the US Northeast. *Climate Dynamics*, **28**: 381–407.

Hayhoe, K., C. Wake, B. Anderson, X.-Z. Liang, E. Maurer, J. Zhu, J. Bradbury, A. DeGaetano, A. Stoner, and D. Wuebbles, 2008. Regional climate change projections for the northeast USA. *Mitigation and Adaptation Strategies for Global Change*, **13**:425-436.

Helsel, D.R. and R.M. Hirsch, 1992. *Statistical Methods in Water Resources.* Elsevier, NY.

Hershfield, D.M., 1961. *Rainfall Frequency Atlas of the United States for Durations from 30 Minutes to 24 Hours and Return Periods from 1 to 100 Years*. Tech. paper 40. U. S. Weather Bureau. Wachington, D. C.

Hewlett, J.D. and A.R. Hibbert, 1967. Factors affecting the response of small watersheds to precipitation in humid areas. p. 275-290 *in* W. E. Sopper and H. W. Lull, eds., *Forest Hydrology*, Pergamon Press, New York.

Hirsch, R. M., 1988. Statistical methods and sampling design for estimating step trends in surface-water quality. *J. of the American Water Resources Assoc.*, **24**: 493–503. doi: 10.1111/j.1752-1688.1988.tb00899.x.

Horn, H., L. Paul, W. Horn and T. Petzoldt, 2011. Long-term trends in the diatom composition of the spring bloom of a German reservoir: Is Aulacoseira subarctica favoured by warm winters? *Freshwater Biology*, **56**: 2483-2499. doi: 10.1111/j.1365-2427.2011.02674.x.

Houser, P.R., W.J. Shuttleworth, J.S. Famiglietti, H.V. Gupta, K.H. Syed and D.C. Goodrich, 1998. Integration of soil moisture remote sensing and hydrologic modeling using data assimilation, *Water Resour Res*, **34**(12): 3405-20.

Huang, Y.T. and L. Liu. 2008. A hybrid perturbation and Morris approach for identifying sensitive parameters in surface water quality models. *Journal of Environmental Informatics* **12**(2):150-159.

Huang, Y.T. and L. Liu 2010. Multiobjective water quality model calibration using a hybrid genetic algorithm and neural network–based approach. *ASCE J. Environ. Eng.*, **136**(10), 1020-1031.

HydroLogics, Inc. 2007 *User Manual for OASIS with OCL*, Columbia, MD

Idso, S.B., 1973. On the concept of lake stability. *Limnology and Oceanography*, 18 (4), 681-683.

Inamdar, S., S. Singh, S. Dutta, D. Levia, M. Mitchell, D. Scott, H. Bais and P. McHale, 2011. Fluorescence characteristics and sources of dissolved organic matter for stream water during storm events in a forested mid-Atlantic watershed. *J. Geophys. Res.*, **116**, G03043. doi: 03010.01029/02011JG001735.

Interagency Advisory Committee on Water Data, 1982. *Guidelines for Determining Flood Flow Frequency*. Bulletin 17B. U.S. Department of the Interior. U.S. Geological Survey, Office of Water Data Coordination. Reston, Va.

IPCC (Intergovernmental Panel on Climate Change), 2007. *IPCC Fourth Assessment Report: Climate Change 2007*. Cambridge University Press, Cambridge, United Kingdom and New York, NY, USA.

IPCC (Intergovernmental Panel on Climate Change), 2012. Summary for Policymakers. In: Field, C.B., V. Barros, T.F. Stocker, D. Qin, D.J. Dokken, K.L. Ebi, M.D. Mastrandrea, K.J. Mach, G. Plattner, K. Allen, M. Tignor and P.M. Midgley (eds.). *Managing the Risks of Extreme Events and disasters to advance climate change adaptation*. A Special Report of Working Groups I and II of the Intergovernmental Panel on Climate Change. Cambridge University Press; Cambridge. pp. 1-19.

Jain, V., N. Preston, K. Fryirs and G. Brierly, 2006. Comparative assessment of three approaches for deriving stream power plots along long profiles in the upper Hunter River catchment, New South Wales, Australia. *Geomorphology* **74**, 297–317.

Jennings, E., S. Jones, L. Arvola, P.A. Staehr, E. Gaiser, I.D. Jones, K.C. Weathers, G.A. Weyhenmeyer, C.-Y. Chiu and E.D. Eyto, 2012. Effects of weather-related episodic events in lakes: An analysis based on high-frequency data. *Freshwater Biol.*, **57** (3), 589–601.

Johannessen, M. and A. Henriksen, 1978. Chemistry of snow meltwater: Changes in concentration during melting. *Water Resour Res*, **14**: 615-619.

Karl, T.R. and D.R. Easterling, 1999. Climate extremes: Selected review and future research directions. *Climatic Change*, **42:** 309–325.

Kattelmann, R.C., 1985. Macropores in snowpacks of Sierra Nevada. *Annals of Glaciology*, **6**:272-273.

Kiili, M., M. Pulkkanen and K. Salonen, 2009. Distribution and development of under-ice phytoplankton in 90-m deep water column of Lake Paijanne (Finland) during spring convection. *Aquatic Ecology*, **43**: 707-713. doi: 10.1007/s10452-009-9262-7.

Knighton, A.D., 1999. Downstream Variation in Stream Power. *Geomorphology*, **29**: 293–306.

Knutson, T.R., J.L. McBride, J. Chan, K. Emanuel, G. Holland, C. Landsea, I. Held, J.P. Kossin, A.K. Srivastava and M. Sugi, 2010. Tropical cyclones and climate change. *Nature Geosci.*, **3**: 157-163.

Lane, L.J., M.H. Nichols, M. Hernandez, C. Manetsch and W.R. Osterkamp, 1994. Variability in discharge, stream power, and particle-size distributions in ephemeral-stream channel systems. In: Variability in Stream Erosion and Sediment Transport; Proceedings of the Canberra Symposium, December 1994. IAHS Publication 224: 335-342.

Langendoen, E. J., 2000. CONCEPTS – Conservational Channel Evolution and Pollutant Transport System. United States Department of Agriculture – Agricultural Research Service National Sedimentation Laboratory. Oxford, MS.

Lawler, D.M., 1992. Process dominance in bank erosion systems. In Lowland Floodplain Rivers: Geomorphological Perspectives, Carling PA, Petts GE (eds). Wiley: Chichester; 117–143.

Lawler, D.M., 1995. The Impact of Scale on the Processes of Channel Side Sediment Supply: A Conceptual Model. In Effects of Scale on the Interpretation and Management of Sediment and Water Quality, IAHS Publication 226, Osterkamp WR (ed.); 175–184.

Lawler, D.M., J.R. Grove, J.S. Couperthwaite and G.J.L. Leeks. 1999. Downstream change in river bank erosion rates in the Swale–Ouse system, Northern England. *Hydrol. Proc.*, **13**: 977–992.

Leathers, D.J., D.R. Kluck and S. Kroczynski, 1998. The severe flooding event of January 1996 across north-central Pennsylvania. *Bulletin of the American Meteorological Society*, **79**:785-797.

Leece, S.A., 1997. Nonlinear downstream changes in stream power on Wisconsin's Blue River. *Annals of the American Association of Geographers*, **87**: 471– 486.

Lehner, B. and P. Doll, 2004. Development and validation of a global data base of lakes, reservoirs and wetlands. *J . Hydrol.*, **296**: 1-22.

Lempert, R. J., S. W. Popper, and S. C. Bankes. 2003. *Shaping the Next One Hundred Ye ars: New Methods for Quantitative, Long-Term Policy Analysis*, 187 pp., RAND, Santa Monica, Calif.

Leopold, L.B., M.G.Wolman and J. P. Miller, 1964. *Fluvial Processes in Geomorphology*. Freeman, San Francisco. 522 pp.

Lou, J. and D.J. Schwab, 2000. A model of sediment resuspension and transport dynamics in southern Lake Michigan, *J. of Geophysical Res.*, **105** (C3): 6591-6610.

Lundquist, J.D., M.D. Dettinger and D.R. Cayan, 2005. Snow-fed streamflow timing at different basin scales: Case study of the Tuolumne River above Hetch Hetchy, Yosemite, California. *Water Resour Res*. **41**. W07005. doi:10.1029/2004WR003933.

MacIntyre S., J.P. Fram, P.J. Kushner, N.D. Bettez,W.J. O'Brien, J.E. Hobbie and G.W. Kling, 2009. Climate-related variations in mixing dynamics in an Alaskan arctic lake. *Limnology and Oceanography,* **54**, 2401-2417.

Mandapaka, P.V. and U. Germann, 2010. Radar-rainfall error models and ensemble generations, in Testik F.Y., and M. Gebremichael, Ed., *Rainfall: State of the Science, Geophys. Monogr. Ser.*, ***191****: 246-264* American Geophysical Union, Washington, DC. doi: 10.1029/2010GM001003.

Markensten, H. and D. Pierson. 2007. Weather driven influences on phytoplankton succession in a shallow lake during contrasting years: Application of PROTBAS. *Ecological Modelling*, **207**, 128-136.

Matonse, A.H., D.C. Pierson, A. Frei, M.S. Zion, E.M. Schneiderman, A. Anandhi, R. Mukundan, and S.M. Pradhanang, 2011. Effects of changes in snow pattern and the timing of runoff on NYC water supply system. *Hydrological Processes*, **25**:3278-3288.

Matonse A.H., D.C. Pierson, A. Frei, M. S. Zion, A. Anandhi, E. Schneiderman and B. Wright, 2012. Investigating the impact of climate change on New York City's primary water supply. *Climatic Change,* **113**. doi 10.1007/s10584-012-0515-4.

MacIntyre, S., K.M. Flynn,R. Jelliso and J.R. Romero, 1999. Boundary mixing and nutrient fluxes in Mono Lake, California. *Limnology and. Oceanography.*, **44**(3): 512-529.

McCabe, G.J., L.E. Hay and M.P. Clark, 2007. Rain-on-snow events in the western United States. *Bulletin of the American Meteorological Society*, **88**:319-328.

Miller, S.J. and D. Davis, 2003. Optimizing Catskill Mountain regional bankfull discharge and hydraulic geometry relationships: Proceedings of the American Water Resources Association, 2003 International Congress, Watershed management for water supply systems, New York City, N.Y., June 29-July 2, 2003, 10 p. http://www.catskillstreams.org/pdfs/catskillregionalcurves.pdf Accessed April 27, 2010

Morris, M.D., 1991. Factorial sampling plans for preliminary computational experiments. *Technometrics,* **33**(2): 161-74.

Mukundan, R., D.C. Pierson, E.S. Schneiderman, D. O'Donnell, A.H. Matonse and M.S. Zion, 2010. Suspended sediment transport dynamics in the Esopus Creek watershed, New York. *American Geophysical Union Annual Meeting 2010,* San Francisco, CA USA

Mukundan, R., S.M. Pradhanang, E.M. Schneiderman, D.C. Pierson, A. Anandhi, M.S. Zion, A.H. Matonse, D.G. Lounsbury, and T.S. Steenhuis. 2012. Suspended sediment source areas and future climate impact on soil erosion and sediment yield in a New York City water supply watershed, USA. *Geomorphology*, http://dx.doi.org/10.1016/j.geomorph.2012.06.021.

Muttiah, R.S., R. Srinivasan and P.M. Allen, 1997. Prediction of two-year peak stream discharges using neural networks. *J. of the American Water Resources Assoc.*, **33**: 625–630.

Nash, J. E., and J.V. Sutcliffe, 1970. River flow forecasting through conceptual models – Part I: A discussion of principles. *Journal of Hydrology,* **10**: 282–290.

Neitsch, S.L., J.G. Arnold, J.R. Kiniry and J.R. Williams, 2005. Soil and Water Assessment Tool: Theoretical Documentation – Version 2005. Grassland, Soil and Water Research Laboratory, Agricultural Research Service. January 2005

Nelder, J.A. and R. Mead. 1965. A simplex method for function minimization. *The Computer Journal*, 7: 308-313.

NOHRSC (National Operational Hydrologic Remote Sensing Center), 2010. Snow Data Assimilation System (SNODAS) Data Products at NSIDC. Boulder, Colorado USA: National Snow and Ice Data Center. Digital media.

O'Donnell, D.M. and S.W. Effler, 2006. Resolution of impacts of runoff events on a water supply reservoir with a robotic monitoring network. *J. of the American Water Resources Assoc.*, **42**:323-335.

O'Donnell, S.M., R.K. Gelda, S.W. Effler and D.C. Pierson, 2011. Testing and application of a transport model for runoff event inputs for a water supply reservoir. *ASCE J. Environ. Eng.*, **137**:678-688.

Owens, E.M. 1998. Development and testing of a one-dimensional hydrothermal models of Cannonsville Reservoir. *Lake and Reservoir Management,* **14**, 172-185.

Owens, E., 2009. Observation and simulation of surface waves in two water supply reservoirs. *ASCE J. of Hydraulic Eng.*, **135**:663-670.

Owens, E.M., R.K. Gelda, S.W. Effler, P.J. Rusello, E.C. Cowen and D.C. Pierson, 2011. Modeling resuspension in a dynamic water supply reservoir. *ASCE J. Environ. Eng.*, **137**:585-595.

Paerl, H. W., J.D. Bales, L.W. Ausley, C.P. Buzzelli, L.B. Crowder, L.A. Eby, J.M. Fear, M. Go, B.L. Peierls, T.L. Richardson and J.S. Ramus, 2001. Ecosystem impacts of three sequential hurricanes (Dennis, Floyd, and Irene) on the United States' largest lagoonal estuary, Pamlico Sound, NC. *Proc. Natl. Acad. Sci. USA*, **98** (10), 5655-5660.

Paerl, H.W., L.M. Valdes, A.R. Joyner, B.L. Peierls, M.F. Piehler, S.R. Riggs, R.R. Christian, L.A. Eby, L.B. Crowder, J.S. Ramus, E.J. Clesceri, C.P. Buzzelli and R.A. Luettich, 2006. Ecological response to hurricane events in the Pamlico Sound System, North Carolina, and implications for assessment and management in a regime of increased frequency. *Estuaries Coasts*, **29** (6A), 1033-1045.

Paniconi, C., M. Marrocu, M. Putti and M. Erbunt, 2003. Newtonian nudging for a Richards equation-based distributed hydrological model. *Advances in Water Resources* **26**: 161-178.

Pederson, N., A.R. Bell, E.R. Cook, U. Lall, N. Devineni, R. Seager, K. Eggleston and K.J. Vranes, 2012. Is an epic pluvial masking the water insecurity of the Greater New York City Region? *Journal of Climate*, in press.

Peeters, F., D.M. Livingstone, G.-H. Goudsmit, R. Kipfer and R. Forster, 2002. Modeling 50 years of historical temperature profiles in a large central European lake. *Limnology and Oceanography,* **47**, 186–197.

Peng, F. and S.W. Effler, 2007. Suspended minerogenic particles in a reservoir: Light-scattering features from individual particle analysis. *Limnology and Oceanography,* **52**:204-216.

Peng, F., S.W. Effler, D.C. Pierson, and D.G. Smith, 2009. Light-scattering features of turbidity-causing particles in interconnected reservoir basins and a connecting stream. *Water Research*, **34**(8): 2280-2292.

Peng, F. and S.W. Effler, 2012. Mass-specific scattering coefficient for natural minerogenic particle populations: particle size distribution effect and closure analyses. *Applied Optics*, **51**:2236-2249.

Perkins, M., S.W. Effler, F. Peng, D. Pierson, D.G. Smith and Y.C. Agrawal, 2007. Particle characterization and settling velocities for a water supply reservoir during a turbidity event. *ASCE J. Environ. Eng.*, **133**:800-808.

Pettersson, K., K. Grust, G. Weyhenmeyer, T. Blenckner, 2003. Seasonality of chlorophyll and nutrients in Lake Erken - effects of weather conditions. *Hydrobiologia*, **506**: 75-81. doi: 10.1023/b:hydr.0000008582.61851.76.

Phillips, K.A. and M.W. Fawley, 2002. Winter phytoplankton community structure in three shallow temperate lakes during ice cover. *Hydrobiologia*, **470**: 97-113. doi: 10.1023/a:1015667803372.

Pielke, R., Jr. and C. Landsea, 1998. Normalized Atlantic hurricane damage: 1925–1995. *Wea. Forecasting*, **12:** 621–631.

Pierson, D.C., H. Markensten, and N. Strombeck, 2003. Long and short term variations in suspended particulate material: the influence on light available to the phytoplankton community. *Hydrobiologia*, **494** (1-3), 299-304.

Pierson, D.C., N. Samal, E. Owens, E.M. Schneiderman and M.S. Zion, 2012. Changes in the timing of snowmelt, and the seasonality of nutrient loading: Can models simulate the impacts on freshwater trophic status? *Hydrological Processes* (submitted).

Pradhanang, S.M., A. Anandhi, R. Mukundan, M.S. Zion, D.C. Pierson, E.M. Schneiderman, A. Matonse, A. Frei. 2011. Application of SWAT model to assess snowpack development and streamflow in the Cannonsville watershed, New York, USA. *Hydrological Processes*, **25**:3268-3277. doi: 10.1002/hyp.8171.

Prestigiacomo, A.R., S.W. Effler, D.M. O'Donnell, D.G. Smith and D.C. Pierson, 2008. Turbidity and temperature patterns in a reservoir and its primary tributary from robotic monitoring: Implications for managing the quality of withdrawals. *Lake and Reservoir Management*, **24**:231-243.

Raymond, P.A. and J.E. Saiers, 2010. Event controlled DOC export from forested watersheds. *Biogeochemistry*, **100** (1-3), 197-209.

Read, J.S., D.P. Hamilton, I.D. Jones, K. Muraoka, L.A. Winslow, R. Kroiss, C.H. Wu, E. Gaiser, 2011. Derivation of lake mixing and stratification indices from high-resolution lake buoy data. *Environmental Modelling and Software*, **26** (11), 1325-1336.

Reed, R.E., D.A. Dickey, J.M. Burkholder, C.A. Kinder and C. Brownie, 2008. Water level variations in the Neuse and Pamlico Estuaries, North Carolina due to local and remote forcing. *Estuarine Coastal and Shelf Science*, **76**(2):431-446.

Reicosky, D.C., L.J. Winkelman, J.M. Baker and D.G. Baker, 1989. Accuracy of hourly air temperatures calculated from daily minima and maxima. *Agricultural and Forest Meteorology*, **46**: 193-209.

Reinfields, I., T. Cohen, P. Batten and G.J. Brierly, 2004. Assessment of downstream trends in channel gradient, total, and specific stream power: A GIS approach. *Geomorphology* **60**: 403–416.

Reitner, B., A. Herzig and G.J. Herndl, 1997. Microbial activity under the ice cover of the shallow Neusiedler See (Austria, Central Europe). *Hydrobiologia*, **357**: 173-184. doi: 10.1023/a:1003151323756.

Reynolds, C.S., A.E. Irish and J.A. Elliott. 2001. The ecological basis for simulating phytoplankton responses to environmental change (PROTECH). *Ecological Modelling*, **140**, 271-291.

Richards, R.P., D.B. Baker, J.P. Crumrine, J.W. Kramer, D.E. Ewing, and B.J. Merryfield, 2008. Thirty-year trends in suspended sediment in seven Lake Erie tributaries. *J. Environ. Qual.*, **37**, 1894–1908.

Riley, G.A., 1947. Factors controlling phytoplankton populations on Georges Bank. *J. Marine Res*, **6**: 54-73.

Rogers, M.W. and M.S. Allen, 2008. Hurricane impacts to Lake Okeechobee: Altered hydrology creates difficult management trade offs. *Fisheries*, **33**(1), 11-17.

Saltelli, A., Tarantola, S., Campolongo, F. and Ratto, R. 2004. *Sensitivity Analysis in Practice: a Guide to Assessing Scientific Models*. John Wiley & Sons Ltd, Chichester.

Samal, N.R., A. Mazumdar, K. D. J¨ohnk and F. Peeters, 2009. Assessment of ecosystem health of tropical shallow waterbodies in eastern India using turbulence model. *Journal of Aqua. Ecosys. Health & Manage*, Society (AEHMS), Canada. **12**(2), 215–225.

Samal, N.R., A.H. Matonse, R. Mukundan, D.C. Pierson, R. Gelda, M.S. Zion and E.M. Schneiderman, 2012a. Potential effects of climate change on winter turbidity loading in the Ashokan Reservoir, NY. *Hydrological Processes* (submitted).

Samal, N.R., D.C. Pierson, E. Schneiderman, Y. Huang, J.S. Read, A. Anandhi, and E.M. Owens, 2012b. Impact of climate change on Cannonsville Reservoir thermal structure in the New York City water supply. *Water Quality Research Journal of Canada*, in press.

SAS Institute, 2003. *SAS 9.1.3 Help and Documentation*. Cary, NC: SAS Institute Inc.

Schneiderman, E.M., D.C. Pierson, D.G. Lounsbury and M.S. Zion. 2002. Modeling the Hydrochemistry of the Cannonsville Watershed with Generalized Watershed Loading Functions (GWLF). *Journal of the American Water Resources Association*, **38**(5):1323-1347.

Schneiderman, E.M., T.S. Steenhuis, D.J. Thongs, Z.M. Easton, M.S. Zion, A.L. Neal, G.F. Mendoza and M.T. Walter, 2007. Incorporating variable source area hydrology into the curve number based Generalized Watershed Loading Function model. *Hydrol. Process*., **21**:3420-3430.

Seager, R., N. Pederson, Y. Kushnir, J. Nakamura and S. Jurburg, 2012. The 1960s drought and the subsequent shift to a wetter climate in the Catskill Mountains region of the New York City watershed. *Journal of Climate*, **25**(19): 6721-6742. http://dx.doi.org/10.1175/JCLI-D-11-00518.1.

Simanton, J.R. and H.B. Osborn, 1980. Reciprocal distance estimate of point rainfall, *Journal of the Hydraulics Division, ASCE* **106**: 1242-1246.

Simon, A., W. Dickerson and A. Heins, 2004. Suspended-sediment transport rates at the 1.5-year recurrence interval for ecoregions of the United States: Transport conditions at the bankfull and effective discharge? *Geomorphology*, **58**(1-4): 243-262.

Simon, A. and L. Klimetz, 2008. Relative magnitudes and sources of sediment in benchmark watersheds of the conservation effects assessment project. *J. of Soil and Water Conservation*, **63**(6): 504-522.

Smith, J.A., 1993. Precipitation. In: Maidment, D.R., *Handbook of Hydrology*. Chapter 3. McGraw-Hill Inc.: New York.

Sommer U.Z., M. Gliwcz, W. Lampert, and A. Duncan, 1986. The PEG model of seasonal succession of planktonic events in fresh waters. *Arch. Hydrolbiol.*, **106**: 433-471.

Stedinger, J.R., R.M. Vogel and E. Foufoula-Georgiou, 1993. Frequency analysis of extreme events. In: Maidment, D.R., *Handbook of Hydrology*. Chapter 18. McGraw-Hill Inc. New York.

Stewart, I.T., 2009. Changes in snowpack and snowmelt runoff for key mountain regions. *Hydrological Processes*, **23**: 78-94.

Stottlemyer, R. and D. Toczydlowski, 1999. Seasonal change in precipitation, snowpack, snowmelt, soil water and streamflow chemistry, northern Michigan. *Hydrol Process*. **13**: 2215-2231.

Suzuki, K., 2003. Chemistry of stream water in a snowy temperate catchment. *Hydrol Process*. **17**: 2795-2810. doi:10.1002/hyp.1434.

Tague, C.L. and L.E. Band, 2004. RHESSys: Regional hydro-ecologic simulation system – an object-oriented approach to spatially distributed modeling of carbon, water, and nutrient cycling. *Earth Interactions*, **8** (19): 1-42.

Thorne, C.R., R.D. Hey and M.D. Newson, 1997. *Applied Fluvial Geomorphology for River Engineering and Management*. John Wiley & Sons Inc., New York, USA.

Towler, E., B. Rajagopalan, E. Gilleland, R.S. Summers, D. Yates and R.W. Kats RW, 2010. Modeling hydrologic and water quality extremes in a changing climate: A statistical approach based on extreme value theory. *Water Resources Research*, **46**: W11504. doi:10.1029/2009WR008876.

Tsai, J.-W., T.K. Kratz, P.C. Hanson, J.-T. Wu, W.Y.B. Chang, P.W. Arzberger, B.-S. Lin, F.-P. Lin, H.-M. Chou and C.-Y. Chiu, 2008. Seasonal dynamics, typhoons and the regulation of lake metabolism in a subtropical humic lake,.*Freshwater Biology*, **53**: 1929–1941.

Tsai, J.W. T.K. Kratz, P.C. Hanson, N. Kimura, W.C. Liu, F.P. Lin, H.M. Chou, J.T. Wu and C.Y. Chiu, 2011. Metabolic changes and the resistance and resilience of a subtropical heterotrophic lake to typhoon disturbance. *Can. J. Fish. Aquat. Sci.*, **68** (5), 768-780.

Tulonen, T., P. Kankaala, A.Ojala and L. Arvola, 1994. Factors controlling production of phytoplankton and bacteria under ice in a humic, boreal lake.. *Journal of Plankton Research*, **16**: 1411-1432. doi: 10.1093/plankt/16.10.1411.

Twiss, M.R., R.M.L. McKay, R.A. Bourbonniere, G.S. Bullerjahn, H.J. Carrick, R.E.H. Smith, J.G. Winter, N.A. D'Souza, P.C. Furey, A.R. Lashaway, M.A. Saxton and S.W. Wilhelm, 2012. Diatoms abound in ice-covered Lake Erie: An investigation of offshore winter limnology in Lake Erie over the period 2007 to 2010. *Journal of Great Lakes Research*, **38**: 18-30. doi: 10.1016/j.jglr.2011.12.008.

UFI (Upstate Freshwater Institute). 2001. Calibration, Verification of a One-Dimensional Hydrothermal and Eutrophication Model for Catskill/Delaware Reservoirs.

USEPA (U. S. Environmental Protection Agency), 2006. Water Quality Assessment and Total Maximum Daily Loads (TMDL) information. Available at http://www.epa.gov/waters/ir/index.html verified (February 1, 2010).

USGS. 2006, Magnitude and Frequency of Floods in New York: U.S. Geological Survey Scientific Investigations Report 2006–5112, 152 p.

Valiela, I., P. Peckol, C. D'Avanzo, J. Kremer, D. Hersh, K. Foreman, K. Lajtha, B. Seely, W.R. Geyer, T. Isaji and R. Crawford, 1998. Ecological effects of major storms on coastal watersheds and coastal waters: Hurricane Bob on Cape Cod. *J. Coastal Res.*, **14** (1), 218-238.

Van de Bogert, M.C., S.R. Carpenter, J.J. Cole and M.L. Pace, 2007. Assessing pelagic and benthic metabolism using free water measurements. *Limnol. Oceanogr.: Methods*, **5**, 145-155.

Vicuna, S. and J.A. Dracup, 2007. The evolution of climate change impacts studies on hydrology and water resources in California, *Climatic Change*. **82**:327-350. doi:10.1007/s10584-006-9207-2.

Vocal-Ferencevic, M. and P. Ashmore, 2011. Creating and evaluating digital elevation model-based stream-power map as a stream assessment tool. *River Research and Applications*, **28**(9): 1394-1416. doi:10.1002/rra.1523.

Walker, J.T., J.M. Vose, J. Knoepp and C.D. Geron. 2009. Recovery of nitrogen pools and processes in degraded riparian zones in the southern Appalachians. *J. Environ. Qual.*, **38**(4): 1391-1399.

Walling, D. E. 2009. The Impact of Global Change on Erosion and Sediment Transport by Rivers: Current Progress and Future Challenges. UNESCO-IHP The United Nations World Water Development Report 3 Available at http://unesdoc.unesco.org/images/0018/001850/185078e.pdf (Accessed Sept 23, 2010)

Wang, L., R. Mukundan, M.S. Zion, and D.C. Pierson, 2012. Beyond rating curves: Time series models for in-stream turbidity prediction. *American Geophysical Union Annual Meeting 2012*, San Francisco, CA USA

Wankiewicz, A., 1978. Water pressure in ripe snowpacks. *Water Resour. Res.*, **14**:593-600.

Watson, B.M. and G. Putz, 2012. Comparison of temperature-index snowmelt models for use within an operational water quality model. *J. Environ. Qual*. doi:10.2134/jeq2011.0369

Weniger, B.G., M.J. Blaser, J. Gedrose, E.C. Lippy, D.D. Juranek, 1983. An outbreak of waterborne giardiasis associated with heavy water runoff due to warm weather and volcanic ashfall. *Am J Public Health*, **73**: 868–872.

Wetzel RG. 2001. *Limnology Lake and River Ecosystems.* 3rd Edn., Academic Press.

Wynn, T. and S. Mostaghimi, 2006. The effects of vegetation and soil type on streambank erosion, southwestern Virginia, USA. *J. of the American Water Resources Assoc.*, **42**(1): 69-82.

Yeates, P.S., J. Imberger and C. Dallimore, 2008. Thermistor chain data assimilation to improve hydrodynamic modeling skill in stratified lakes and reservoirs. *ASCE Journal of Hydraulic Engineering*, **134**(8), 1123-1135.

Zion, M. S., S. M. Pradhanang, D. C. Pierson, A. Anandhi, D. G. Lounsbury, A. H. Matonse, and E. M. Schneiderman. 2011. Investigation and Modeling of winter streamflow timing and magnitude under changing climate conditions for the Catskill Mountain region, New York, USA. *Hydrological Processes*, **25**:3289-3301.

Appendix A:

Journal Articles by members of Water Quality Modeling Section

Matonse, A.H., D.C. Pierson, A. Frei, M.S. Zion, A. Anandhi, B. Wright, and E. Schneiderman, 2012. Investigating the impact of Climate Change Impact on New York City's Primary Water Supply. *Climatic Change*, **113.** doi: 10.1007/s10584-012-0515-4.

Mukundan, R., S. Pradhanang, E. Schneiderman, D.C. Pierson, A. Anandhi, M. Zion, A. Matonse, D. Lounsbury, and T. Steenhuis, 2012. Suspended Sediment Source Areas and Future Climate Impact on Soil Erosion and Sediment Yield in a New York City Water Supply Watershed, USA. *Geomorphology*, (2012). doi: 10.1016/j.geomorph.2012.06.021.

Climatic Change
DOI 10.1007/s10584-012-0515-4

Investigating the impact of climate change on New York City's primary water supply

Adão H. Matonse · Donald C. Pierson · Allan Frei · Mark S. Zion · Aavudai Anandhi · Elliot Schneiderman · Ben Wright

Received: 7 October 2010 / Accepted: 4 June 2012

Abstract Future climate scenarios projected by three different General Circulation Models and a delta-change methodology are used as input to the Generalized Watershed Loading Functions – Variable Source Area (GWLF-VSA) watershed model to simulate future inflows to reservoirs that are part of the New York City water supply system (NYCWSS). These inflows are in turn used as part of the NYC OASIS model designed to simulate operations for the NYCWSS. In this study future demands and operation rules are assumed stationary and future climate variability is based on historical data to which change factors were applied in order to develop the future scenarios. Our results for the West of Hudson portion of the NYCWSS suggest that future climate change will impact regional hydrology on a seasonal basis. The combined effect of projected increases in winter air temperatures, increased winter rain, and earlier snowmelt results in more runoff occurring during winter and slightly less runoff in early spring, increased spring and summer evapotranspiration, and reduction in number of days the system is under drought conditions. At subsystem level reservoir storages, water releases and spills appear to be higher and less variable during the winter months and are slightly reduced during summer. Under the projected future climate and assumptions in this study the NYC reservoir system continues to show high resilience, high annual reliability and relatively low vulnerability.

1 Introduction

Projected twenty first century changes in air temperature and precipitation patterns due to climate change may alter the availability of water leading to new challenges for water supply

A. H. Matonse (✉) · A. Frei
City University of New York (CUNY) Institute for Sustainable Cities (CISC), New York City, NY 10065, USA
e-mail: amatonse@hunter.cuny.edu

D. C. Pierson · M. S. Zion · E. Schneiderman
New York City Department of Environmental Protection, Kingston, NY 12401, USA

A. Anandhi
Department of Agronomy, Kansas State University, Manhattan, KS 66506, USA

B. Wright
Hazen and Sawyer, P.C., Baltimore, MD 21202, USA

Published online: 28 June 2012

planning and management in many regions throughout the world (Bates et al. 2008; Hunt and Watkiss 2011; Vicuna and Dracup 2007; Gleckler et al. 2008) including the New York City (Rosenzweig and Solecki 2001). For mountainous regions of the northeastern U.S. these changes can reduce annual snowpack accumulation, accelerate snowmelt processes and increase water losses due to evapotranspiration (ET) which may lead to more winter flooding and reduced summer flows (Brekke et al. 2009; Milly et al. 2005; Seager et al. 2007; Burns et al. 2007; Blake et al. 2000; Vicuna and Dracup 2007; Frei et al. 2002; Matonse et al. 2011). The potential impact of climate change on the ability to meet future demands for high quality drinking water, and satisfy other competing goals for surface water supplies (Bates et al. 2008; Brekke et al. 2009), is an issue of importance in many regions in U.S. and around the world and of primary concern to New York City (NYC) (NYCDEP 2008). A thorough investigation of climate change impacts on the NYC water supply system (NYCWSS) should include, in addition to climatic variations, the operational constraints of the system and potential responses through adaptive management in order to meet demands and other day-to-day operational goals (NYCDEP 2008).

The NYCWSS is a system of nineteen reservoirs and connecting aqueducts that deliver more than 3.8×10^6 cubic meters of drinking water per day to approximately nine million people in NYC and four upstate counties (Matonse et al. 2011). The Catskill and Delaware watersheds that constitute the West of Hudson (WOH) portion of the NYCWSS cover an area of approximately 4100 square kilometers in the Catskill Mountain region and contribute more than 90 % of all water supplied to NYC. As illustrated in Fig. 1 the Delaware

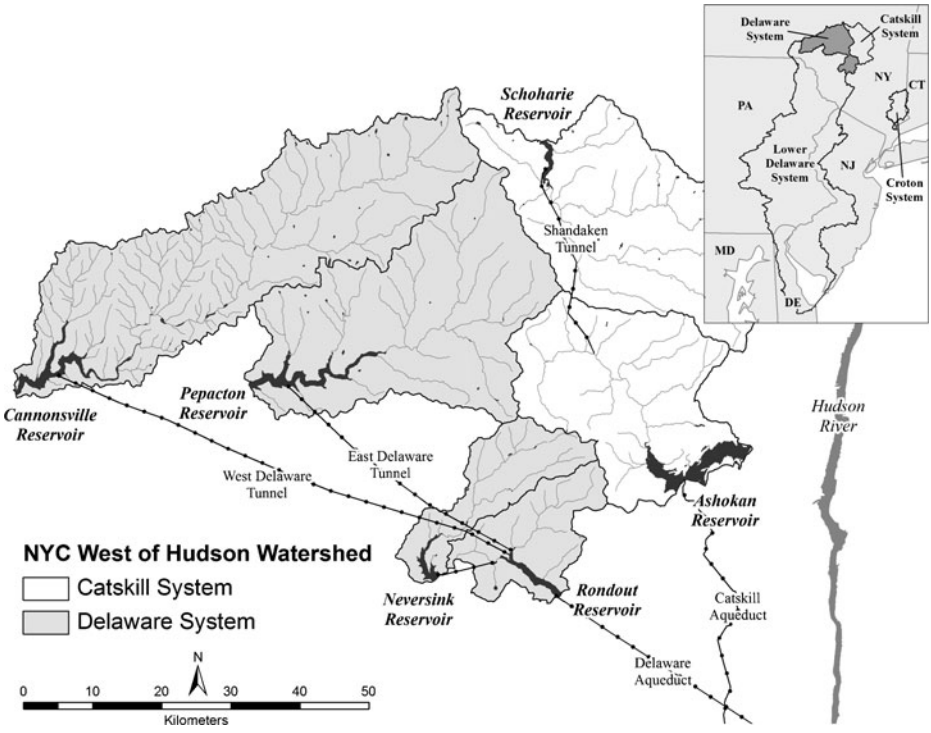

Fig. 1 NYC WOH Catskill and Delaware watersheds and aqueducts schematic. The NYC Croton and the Lower Delaware (LD) systems are represented in the location map on the top right corner. Regulatory rules requires NYC WOH system to deliver water to LD that serves New Jersey and Pensylvania (adapted from Matonse et al. 2011)

subsystem of the WOH water supply has a 2621 square kilometer drainage area that includes the Pepacton, Cannonsville, Rondout and Neversink reservoirs. The Ashokan and Schoharie reservoirs form the Catskill subsystem, which covers the remaining 1479 square kilometers. Table 1 summarizes major characteristics of the Delaware and Catskill subsystems.

The Catskill Mountain region is part of the Allegheny Plateau consisting mainly of sedimentary bedrock that rises approximately 1100 m in elevation from the Hudson River, its eastern boundary (Burns et al. 2007). The region is mostly rural and forested with some dairy farms in low-land areas, particularly in the western part of the mountains. About 70 % (2850 square km) of the WOH area is part of the New York State Catskill Forest Preserve. The climate of this region is humid continental with relatively cold winters and cool summers. The temperature is variable among locations in the region and is highly impacted by elevation. Annual average temperatures range between 5.2 °C at higher elevations (Slide Mountain, 807 m elevation) and 7.5 °C at valley locations (Walton, 450 m elevation). Regional hydrology in NYC WOH watersheds is strongly influenced by snowpack and snow melt particularly during March and April (Matonse et al. 2011).

Past studies addressing climate change impacts on the NYC water supply have projected changes in climatology and hydrology and found evidence to suggest that some of the projected changes are underway. Burns et al. (2007) applied a non-parametric Mann-Kendall test to study trends in air temperature, precipitation, streamflow and ET for the Catskill Mountain region during the period of 1952–2005. Over the course of their study they found a 0.6 °C increase in yearly air temperature with higher increases in daily minimum temperature during May through September and daily maximum temperature during February through April. Precipitation was observed to increase by 136 mm and ET by 19 mm per 50 years. Peak snowmelt showed a shift from early April to late March with a reduction in snowpack consistent with patterns in streamflow and monthly air temperature. Frei et al. (2002) arrived at similar results when applying a version of the Thornthwaite water-balance model to study inter-annual variations and sensitivity to climate change for the Cannonsville basin (Delaware subsystem). In addition, the results from Frei et al. (2002) indicated a change in mean annual streamflow of approximately 6 % per degree C change in average annual temperature and a 1.5–2 % change of annual streamflow for each percent change in annual precipitation. These changes in hydrology indicate that as a result of climate change more water will become streamflow during winter potentially filling the reservoirs earlier in the spring (Matonse et al. 2011), but also increasing the potential for regional flooding (Burns et al. 2007). These results also suggest that for the NYC WOH watersheds projected increases in precipitation generally surpass the effects of increased water loss due to higher ET rates associated with higher temperatures. Conversely as suggested by Blake et al. (2000), if increases in precipitation are not as large as expected,

Table 1 Major characteristics of the WOH watersheds. Historical dependable yield is the maximum withdrawal that can be continuously obtained during a period of years which represent the probable driest period (Joint Editorial Board 1969; Mays and Tung 1992)

Subsystem	Storage capacity (10^6 cu.m)*	Historical dependable yield (cms)*	Drainage area (sq. Km)	Annual average flow (cms)	Coefficient of variation (annual flow)
Delaware	1212	25.4	2621	51.7	0.27
Catskill	531	20.6	1479	28	0.3

* Source: New York City Department of Environmental Protection (NYCDEP) (2006) NYC water supply system Reference guide, Valhalla, NY

the resulting reduction in water availability from increased winter spill and summer ET could lead to a greater risk of drought and increased drought severity.

The management of large systems such as the NYC water supply system is complex as it depends on watershed hydroclimatologic characteristics, reservoir capacities, reservoir operating rules, and system demands (Vogel et al. 1995). Operational complexity is a consequence of the large number of interconnected reservoirs and a decision-making process that includes meeting oft-times competing goals to satisfy demands, balance storage in different parts of the system so as to maximize water availability and minimize spills, meet regulatory flow requirements, and maintain water quality standards imposed on the system (NYCDEP 2011). One important aspect in this process is the management of extreme events to mitigate peak flows and drought (Matonse et al. 2011; Yin et al. 2010; Chang and Chang 2001) through the use of control structures and system operations in order to maintain reliability.

A variety of variables or indicators can be used to describe the operational state of the system. These include measures of inflow, reservoir storage and probability of future refill, releases, spills and demands on a daily, weekly, monthly and yearly basis. Some indicators describe the state of the system or its components (e.g. reservoir, subsystem, or other element) at a given point in time and are therefore very important for managing operations on a short-term basis. Other indicators, such as safe yield (NYCDEP 2008; Mayer 1993), system reliability and resilience (Vogel et al. 1995; Vogel and Bolognese 1995; Vogel 1987), storage vulnerability, surface and ground water stress, coefficient of variation of annual inflow (Lane et al. 1999), and standardized net inflow (Vogel et al. 1999) can be used to evaluate the overall performance of the system on a seasonal and/or long-term basis. Most of these indicators have been used in the past in order to: (i) summarize the effectiveness of regional water supply systems to meet demands (Lane et al. 1999), (ii) compare the relative performance of proposed improvements to water supply infrastructure, (iii) evaluate the effectiveness of reservoir operation policies (Yin et al. 2010), (iv) study the impact of new regulatory procedures, and most recently (v) assess the impact of climate change on existing reservoir systems (Lane et al. 1999; Vogel et al. 1999).

Ongoing nationwide infrastructure and system reliability assessments in the United States highlight the importance of system indicators (Harberg 1997; Vogel et al. 1999). Globally, a growing importance is given to local and regional assessment of water systems in balancing water supply and ecological needs, or socio-economic and environmental objectives (Vogel et al. 2007; Lane et al. 1999; Rogers 1999; Gao et al. 2009; Richter et al. 1996) or characterizing the effects of regulation on flow regimes (Black et al. 2005). Vogel et al. (1995) studied the storage-reliability-resilience-yield relationship for four different water supply systems in the northeastern United States, including the NYCWSS. The objective was to integrate the effects of hydroclimatologic characteristics, reservoir system storage capacity, operating rules, and system yield in a systematic manner to answer questions about which water supply systems are most vulnerable to major water supply failure (i.e., inability to satisfy demands) in the region, and what characteristics make one water supply system more vulnerable or more resilient to drought than others. For this study we combined indicators that provide important information for daily operations with those that help evaluate overall reservoir system performance.

2 The OASIS model and the NYCWSS modeling framework

This evaluation relied on two primary modeling tools: a rainfall-runoff model serially coupled with a reservoir system model. The Operational Analysis and Simulation of

Integrated Systems (OASIS) is a reservoir system model, which simulates water supply system operations, accounting for both "human control and physical constraints on the system" (HydroLogics Inc. 2007). OASIS is a generalized program that has been customized to the NYCWSS (NYCDEP 2011) by specifying a system framework and rules that are specific to NYCWSS. Each of the reservoirs and conveyances of the system are represented as nodes and arcs that store and transfer water on a daily basis. System properties (e.g., reservoir storage capacities, flow capacities, elevations of control structures, etc.) represent the physical properties and constraints of the system components. A complex set of rules codify the day-to-day decision making process of actual operation of the system by weighing actions in relation to competing goals and constraints, while a linear programming (LP) routine determines the optimal set of actions on each day. The rules embody both empirical knowledge accumulated during years of operating the system and the current regulations and water quality requirements for the system. Examples of operating objectives represented in the OASIS model include:

- Meeting regulatory release requirements for NYC reservoirs;
- Balancing diversions from the Delaware, Catskill and Croton subsystems; and
- Meeting demands from both NYC and outside communities (OC).

The operating rules expressed in the OASIS model provide a robust simulation of NYC reservoir system operations under current operating protocols.

A modeling framework for the NYC water supply system includes OASIS linked to other models (Fig. 2). The NYC OASIS model has been linked to a calibrated set of CE-Qual-W2 (Cole and Wells 2002) reservoir models for modeling in-reservoir water quality processes. However, for this analysis, a simplified method based on empirical relationships between

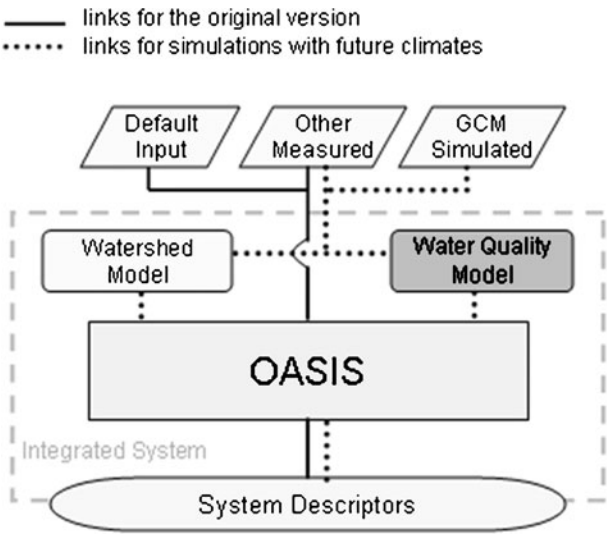

Fig. 2 OASIS modeling framework. The black lines show the model linkages using the historical flow inputs. The doted lines show the flow input linkages using the GWLF-VSA modeled inflows for current and future climate change scenarios. The Water Quality model box is shown in dark gray color to indicate that water quality inputs to OASIS can be obtained from either a fully coupled reservoir water quality model, or from simplified indices of water quality based on empirical relationships using reservoir stage and flow

turbidity and the storage/flow properties of the system was incorporated into OASIS. This method represents a faster alternative compared to running the linked OASIS- W2 model.

In its original form the NYC OASIS model was driven by historical stream flow inputs (Fig. 2 with links in black). As part of this study, the model was configured to use input derived from climate change scenario simulations. Future streamflow projections were obtained from simulations using the Generalized Watershed Loading Functions-Variable Source Area (GWLF-VSA) model (Schneiderman et al. 2007; Schneiderman et al. 2002; Haith and Shoemaker 1987). GWLF-VSA is a lumped-parameter continuous simulation model that simulates daily streamflow, nutrients, and sediment loads on a watershed scale. GWLF-VSA forcing inputs include daily air temperature, precipitation, incoming solar radiation, and daily average relative humidity. Both, the original GWLF (Haith and Shoemaker 1987) and GWLF-VSA treat the watershed as a system of different land areas (Hydrologic Response Units or HRUs) that produce surface runoff, and a single groundwater reservoir that supplies baseflow. GWLF-VSA differs from the original GWLF (Haith and Shoemaker, 1987) in that it simulates saturation-excess runoff on variable source areas, which is considered the primary runoff generation mechanism in WOH watersheds (Walter et al. 2003). To do so, GWLF-VSA simulates runoff volumes using the SCS Curve Number Method, as in the original GWLF model, but spatially-distributes the runoff response according to a soil wetness index, based on the TOPMODEL soils-topographic index (Schneiderman et al. 2007; Beven and Kirkby 1979). Potential evapotranspiration in GWLF-VSA is calculated using the Priestley-Taylor method (Priestley and Taylor 1972; Neitsch et al. 2005) with crop parameters varying between growing and dormant seasons. For this study GWLF-VSA is run over the entire reservoir basin area. As this area includes the reservoir surface itself, the model treats precipitation over the water surface as a direct inflow to the reservoir after subtracting potential evaporation.

Future scenarios of precipitation and air temperature derived from different GCM models using a delta-change methodology (Hay et al. 2000; Anandhi et al. 2011) were input into GWLF-VSA for all WOH reservoir watersheds (Fig. 2 with dotted links) to simulate inflows to the reservoir system. The complete integrated modeling framework including GWLF-VSA and OASIS accurately simulate the state of the system over time and provide data to evaluate the performance of the system under projected changes in climate.

3 Methods

In the following sub-sections we describe briefly each of the indicators used in this study to evaluate possible effects of climate change on the NYC water supply. These indicators were selected based on their importance (i) for the NYC water supply operation and (ii) for assessing system performance and subsequent comparison with other systems at a regional level.

3.1 Reservoirs storage, inflow, release, spill, and diversion

Comparing patterns of storage, inflow, release and spill helps describes how the system functions. We compare indicators for the baseline and future projections simulated using different GCM climate scenarios. Inflows are related to hydro-climatic conditions, while the relationship between inflow, storage, release, and spill are governed by the rules within OASIS. Releases (i.e., controlled outflows from the reservoirs outlets) in the Delaware subsystem, for example, are governed by minimum downstream flow objectives and, to a

lesser extent, peak flow mitigation and habitat protection. Delaware subsystem reservoirs are typically drawn down from November through March to create storage void equal to half the equivalent water volume in the snowpack and during this time diversions from the Catskill subsystem may be minimized. The Catskill subsystem includes rules to regulate water diversions from Schoharie reservoir through the Shandaken Tunnel to Esopus Creek. These rules account for allowable flow rates, temperature and turbidity limits for the tunnel discharges. Diversions of water from and between reservoirs are based on individual reservoir storage volumes, drought conditions, water quality, demands and local downstream requirements.

3.2 Drought occurrence

Drought occurrence is an indicator that is important for operations because it leads to temporary changes in the criteria for moving water from reservoirs and acts to trigger demand reductions. There are three drought levels in the NYCWSS: Watch, Warning, and Emergency. The classification and call for a particular drought level is executed by comparing the total storage of each subsystem with average yearly storage patterns associated with each drought level and each subsystem (Catskill and Delaware). The combination of the drought conditions in Delaware and Catskill subsystems determines the drought status for the entire NYCWSS.

3.3 Standardized net inflow and reservoir system resilience

The standardized net inflow (m) (Perrens and Howell 1972; Vogel et al. 1999) is a unitless index that indicates whether a reservoir system is likely to have within-year or over-year variations in storage. This indicator can be calculated as:

$$m = \frac{(1-\alpha)\mu}{\sigma} = \frac{(1-\alpha)}{C_v} \tag{1}$$

where μ is the mean annual inflow, α is the average annual system demand or yield as a fraction μ, σ is the standard deviation of the annual inflows, and $C_v=\sigma/\mu$ is the coefficient of variation of the annual inflows. Systems with higher values of m ($m>1$) are more likely to exhibit a within-year behavior whereas systems with $0\leq m\leq 1$ are normally dominated by over-year behavior with long multiyear drawdown periods (Vogel and Stedinger 1987; Vogel et al. 1999). Within-year systems are characterized by reservoirs that typically refill at the end of each year. These systems often exhibit a relatively high resilience index (see below, and Vogel and Bolognese 1995) but they appear to be more sensitive to seasonal, monthly and daily variations in demands and inflows to the system. Past studies (Vogel and Bolognese 1995; Vogel et al. 1999) have revealed that under the present conditions the NYC water supply system exhibits within-year behavior.

Hashimoto et al. (1982) define a resilience index (r) as a measure of the likelihood a particular system will recover after a failure has occurred, where failure or shortage is defined as inability of the reservoir system to supply its yield in a given year (Vogel et al. 1999). The resilience index for systems fed by lag-one autoregressive normally distributed inflows, as is the case in the northeastern United States (Vogel et al. 1995), can be estimated as

$$r = \Phi\left[\frac{m - \frac{\rho(2\pi)^{-1/2}}{\Phi(-m)\exp(m^2/2)}}{\sqrt{1-\rho^2}}\right] \tag{2}$$

where ρ is the lag-one serial correlation coefficient of the inflows (equal to zero for independent inflows), Φ denotes the cumulative probability distribution operator for the standardized normal random variable, and m is the standardized net inflow as defined above. Using goodness-of-fit tests on 166 watersheds in the northeastern United States Vogel et al. (1995) found that time-series of annual streamflow in this region are well approximated by a lag-one normally distributed autoregressive process with ρ=0.19, and C_v=0.25. The index r is one of the two parameters in a two-state Markov model of reservoir system states used for evaluating the conditional behavior of systems dominated by both within-year and over-year storage requirements, as shown by Vogel and Bolognese (1995) and Vogel et al. (1995). The resilience index is considered a better indicator (than m) of over-year and within-year behavior of a system, given the fact that it accounts for the serial correlation of inflows (Vogel and Bolognese 1995)

3.4 Storage ratio

The storage ratio (S/μ), where S is the reservoir storage capacity has been used in the past to characterize system operations. Vogel et al. (1999) analyzed storage-yield curves for different regions across the United States and found that storage-yield curves may lead to different values depending on whether mean annual or monthly flows are used in the computation. Monthly flow based curves will generally show a higher value of storage ratio compared to annual based curves except when $Cv \geq 0.3$ and $m<1$; when both annual and monthly flows based ratios provide similar (within 30 %) results of storage-yield curves. Though this indicator is less informative to system operations than other indicators (Vogel et al. 1999) it was included in order to compare this study with past reservoir system analyses.

3.5 Reservoir system reliability

For the design of hydraulic structures for flood control it is a standard practice to employ the average return period of a flood as the design event. Similarly, an index showing the average return period N of a reservoir system shortage can be used for the design of a water supply system (Vogel 1987). The corresponding probability that a reservoir will deliver a constant yield Y, without failure, over Nyears is known as no-failure reliability R_N (Vogel et al. 1999). A failure for any given year is defined as the inability (shortage) of a water system to supply the anticipated annual demand (Vogel et al. 1999; Vogel and Bolognese 1995). For reservoirs fed by AR(1) normal and lognormal inflows, the storage capacity S required to meet a constant yield Y over Nyears without failure follows a three-parameter lognormal distribution (Vogel 1985). Within-year systems fed by serially correlated normal and lognormal inflows can be accurately represented by a two-state Markov model (Vogel 1987; Vogel and Bolognese 1995; Vogel et al. 1995). Based on these assumptions the annual reliability R_a (the steady-state probability, in a given year, that the reservoir system will deliver Y without shortage) can be related to reliability R_N, resilience r and N using the following equation (Vogel et al. 1999)

$$r = R_a \left[\frac{1 - \left(\frac{R_N}{R_a}\right)^{1/(N-1)}}{1 - R_a} \right] \tag{3}$$

For this study this equation was solved to estimate R_a for N=50 and 100 years. As in Vogel et al. (1999) we assumed a no-failure reliability R_N=0.5. Although reservoirs in the system are interconnected, this assumption is reasonable since we considered the entire system as a unit.

3.6 Reservoir system vulnerability

Reservoir system vulnerability D, which can be defined as the average magnitude of a water supply failure as a fraction of the annual yield (Y) (Vogel et al. 1999) is an additional indicator used to measure the level of stress of water resources in a region. This indicator was introduced as a socio-economic indicator by Vogel et al. (1999) and can be calculated from the storage-yield ratio as

$$D = 0.452\left(\frac{S}{Y}\right)^{1.27} \tag{4}$$

where S represents the active reservoir storage capacity. Examples in the literature estimated regional storage vulnerability assuming each reservoir was operated individually (Vogel et al. 1999). In this analysis we focus on all reservoirs operated conjunctively (Hardison 1972; Lof and Hardison 1966), guided by rules and constraints inherent in the present system operations.

4 Data and modeling assumptions

4.1 Climate data

Observed climate and streamflow data for this study include historical measurements of daily air temperature and precipitation covering a period from 1927 to 2004. These data used to drive the GWLF-VSA watershed model were obtained from up to nineteen stations for precipitation and four stations for temperature distributed throughout the WOH watershed region.

To create historical daily precipitation time series for each reservoir's watershed that could be input into the GWLF-VSA model, individual station precipitation values were spatially averaged using Thiessen polygon weighting (Burrough 1987). For air temperature inverse distance weighting was used and lapse rates were applied to account for variations in temperature with elevation (Zion et al. 2011).

Sixteen projections of future air temperature and precipitation (Table 2) were calculated using the European Centre Hamburg Model (ECHAM), Goddard Institute for Space Studies (GISS), and the National Center for Atmospheric Research (NCAR) GCM model simulations for three scenarios, and two future time periods or time slices.

Future climate projections were constructed using a delta change method (e.g. Hay et al. 2000; Gleick 1986) also known as change factor methodology (Anandhi et al. 2011). In delta change method monthly factors are calculated from the difference between GCM baseline and future simulated using pooled monthly data for the two time slices (Anandhi et al. 2011). The calculated delta change factors were then combined with records of observed data

Table 2 List of GCM, emission scenarios and time slices used to develop climate change scenarios for this study. 20C3M represent the baseline (from the 20th century experiment model runs)

GCM	20C3M	Emission scenario	Future time slices
ECHAM	1981–2000	A2, A1B, B1	2046–2065, 2081–2100
GISS	1981–2000	A2, A1B, B1	2046–2065, 2081–2100
NCAR	1980–1999	A2, A1B	2046–2065, 2080–2099

(additively for air temperature and multiplicatively for precipitation) to generate future climate projections for each scenario. In this manuscript we will refer to the 2046–2065 and 2081–2100 periods as the 2055s and 2090s, respectively. The baseline scenario represents model runs using the observed forcing data.

Projected changes in average monthly air temperature indicate consistent air temperature increases throughout the year with larger increases for the later time slice (Fig. 3). Precipitation is generally projected to increase in most months, but this increase is accompanied by much greater variability. These increases appear to be somewhat greater and more variable in the 2055s time period.

4.2 Modeling assumptions

OASIS simulations were conducted for the entire NYCWSS, which includes the upper and lower Delaware, Catskill, and Croton subsystems (Fig. 1). However, only the WOH portion (the upper Delaware and Catskill basins) was simulated using both current and future modeled inflows. The remaining Croton (East of Hudson (EOH)) portion of NYCWSS and the lower Delaware (LD) were simulated using historical flow inputs for all baseline and future scenarios. Though these two portions have an impact on the water routing processes in WOH, we choose to maintain this assumption for this analysis because EOH contributes about 10 % of all NYCWSS requirements and the LD does not contribute any flow to NYC. NYC and OC average demand levels and system operation rules across the system were considered stationary and remained unchanged between baseline and future simulations.

5 Evapotranspiration, snow and reservoir inflows in the study area

Simulations with GWLF-VSA revealed increased growing season ET and decreased snowfall and snowpack as temperature increased (Fig. 4). Snowfall and snowpack are projected to

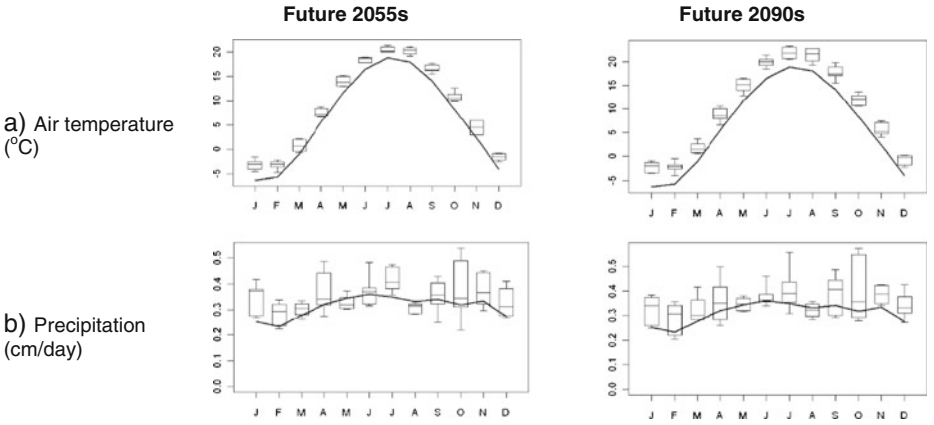

Fig. 3 Monthly average input precipitation and average daily air temperature for baseline and eight scenarios. Graphs are representative for the 2055s and 2090s future climate scenarios. Data consist of areal averages over all WOH watersheds. The solid lines on the graphs show the baseline scenario. The mid-way line in the boxes shows the median value of the monthly average for the climate scenarios, the extent of the boxes show the range of averages for the middle six scenarios, the whiskers show the range of all eight scenarios. Precipitation units are given in centimetres per day

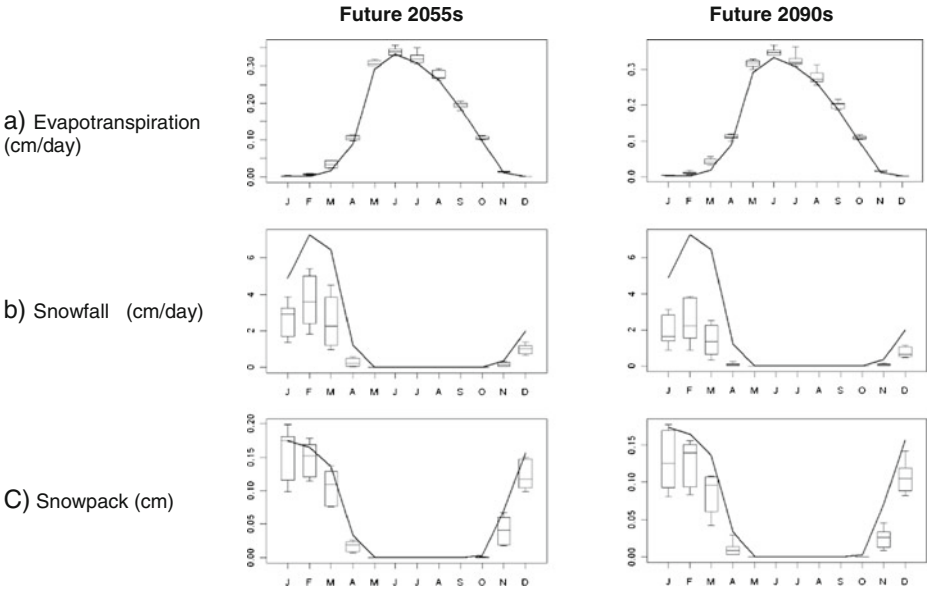

Fig. 4 Monthly mean evapotranspiration, snowfall and snowpack for baseline and future scenarios as areal averages for all WOH watersheds. The solid lines on the graphs show the baseline scenario. The mid-way line in the boxes shows the median value of the monthly average for the climate scenarios, the extent of the boxes show the range of averages for the middle six scenarios, the whiskers show the range of all eight scenarios. Boxplots represent simulated future 2055s and 2090s periods. The units are centimeters per day (cm/day) and centimeters (cm)

greatly decrease during the winter months, as increased temperature causes more of the precipitation to fall as rain and the snowpack that does develop to melt earlier in the year (Matonse et al. 2011).

Results from most future simulations show an increase in annual median inflow to Delaware and Caskill subsystems (Fig. 5). Though, the absolute magnitude is higher for

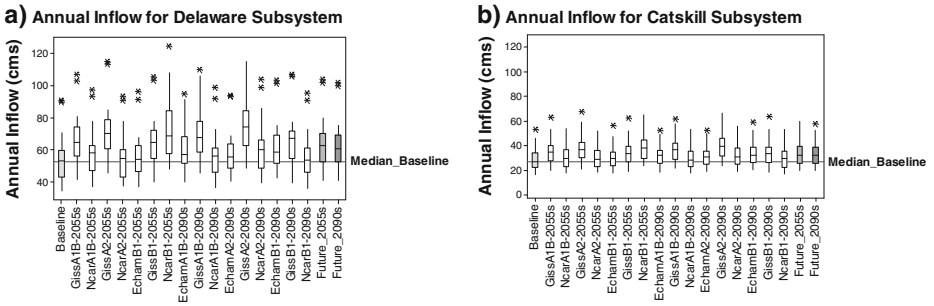

Fig. 5 Annual inflow for baseline (in light grey color) and for future GCMs climate simulations (white boxes). Medium dark gray boxes represent the combination of all future 2055s and dark gray all future 2090s simulations. The units are cubic meters per second (cms). For this and all subsequent figures box-plots show the bounds between the 25th (Q1) and 75th (Q3) quartiles, and the whiskers represent the lowest and highest data values within the lower (Q1-1.5*(Q3-Q1)) and upper (Q3+1.5*(Q3-Q1) limits. The stars represent outliers. The dark horizontal lines in the box-plots represent the median. All statistics are calculated using a 20 year period

the larger Delaware subsystem, variations in annual inflow simulated for future conditions are similar to baseline for both subsystems, as was expected given the dependence of the delta change method on historical data. Among the three GCMs the magnitudes of change are mixed but with GISS apparently exhibiting higher values, more often. For both subsystems, a test of significance comparing the two time slices at a type I error α=0.05, revealed insufficient evidence to reject the null hypothesis (H_o) that the mean inflows for the 2055s and 2090s are equal.

Monthly box-plots for the baseline (white), future 2055s (light gray) and future 2090s (dark gray) streamflow shown in Fig. 6 were created for baseline and future time periods using the combined monthly data from all GCM and emission scenarios. These show average flows to be higher during winter and early spring with the present day high flows of March and April shifting to earlier in the year and becoming more evenly distributed throughout the winter-spring period. Such changes in the seasonality of streamflow are consistent with the combined effects of a decrease in snow and an increase in precipitation falling as rain, as well as earlier snow melt associated with higher temperatures during winter and spring (Fig. 3 and Fig. 4, respectively). This results in more water being available earlier during winter and relatively less water being available during late spring, due to a loss of snowpack storage. Despite this, summer inflows do not decrease, but in fact increase slightly during June (Catskill subsystem) and July (Catskill and Delaware subsystems).

During the growing season, part of the increased precipitation is offset by increased ET, resulting in only a slight increase in the inflow to the reservoirs. It is interesting to note that even though there is little change in flow during the growing season period, the average unsaturated zone soil moisture (not shown here) decreases slightly during the spring months. This is because the soil has a limited storage, and the increased precipitation cannot increase the maximum soil moisture storage. The increased ET rate in the future climate simulations therefore tends to enhance the decline in soil moisture storage from its maximum value during inter-storm periods.

6 Results for system indicators

To describe the state of the water supply system and help assess performance a number of indicators were selected and evaluated in terms of their ability to capture and display system changes associated with projected future climate change.

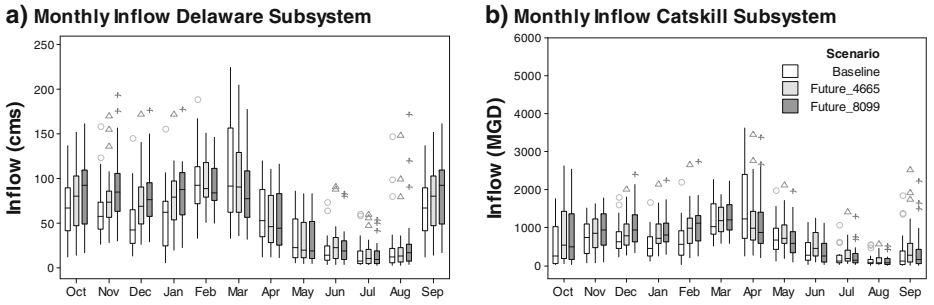

Fig. 6 Monthly inflow from baseline (white) and future simulated inflow for the 2055s (light gray) and 2090s (dark gray). Each box plot represents monthly variability derived from all 20 years for the specific time period. For future simulations that includes all combinations of GCMs and emission scenarios. Units are in cubic meters per second (cms)

6.1 Reservoirs storage, spill and release

Inflows for both Delaware and Catskill subsystems appear to peak in April under baseline conditions (white box-plots, Fig. 6a,b), while under future simulated climate inflows appear to peak earlier in winter and are more evenly distributed among the winter months due to more rainfall and earlier snowmelt. Slight increases in inflows during June and July and earlier increases in inflow during the September and October help slow drawdown through the summer and result in more rapid refill in the winter. These higher inflows are responsible for reservoirs becoming full earlier and for greater water storage during most of the year (Fig. 7a,b). The Catskill subsystem exhibits relatively higher storage throughout the entire summer, likely a result of generally higher inflows, and perhaps reflecting decreased diversions associated with turbidity events. Spill in both Delaware (Fig. 7c) and Catskill

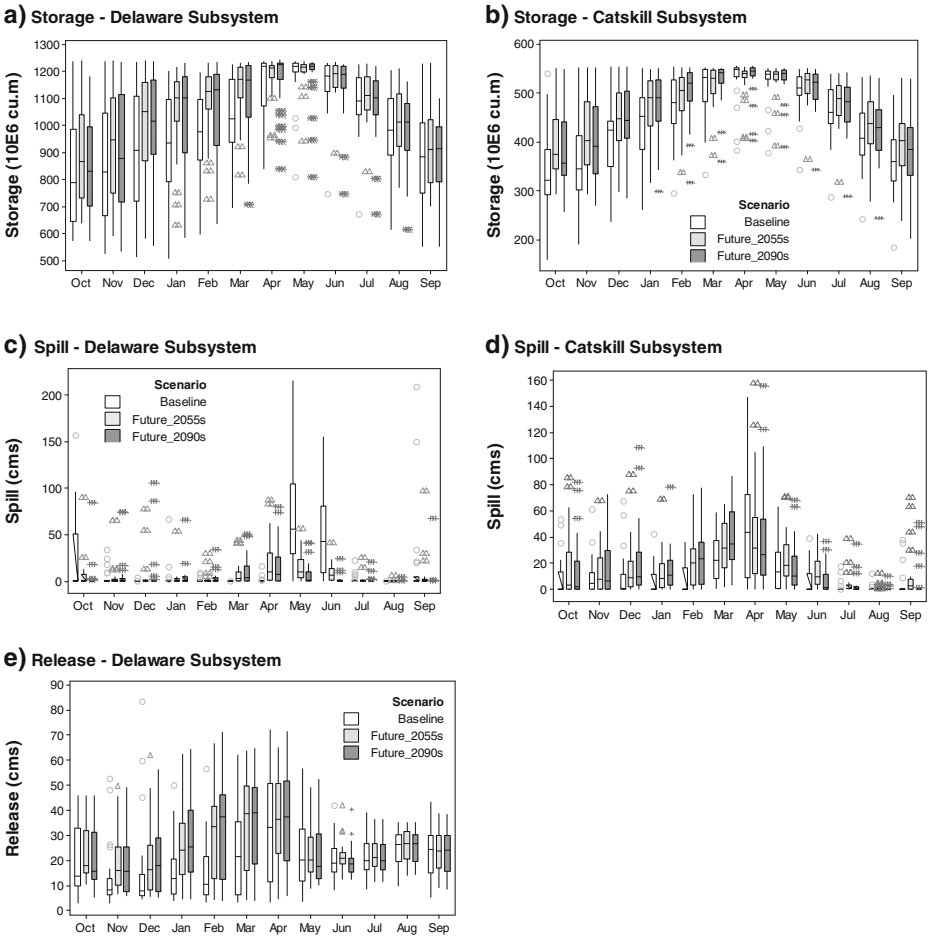

Fig. 7 Monthly storage, spill, and release patterns for Delaware and Catskill subsystems for the baseline (white), future 2055s (light gray) and future 2090s (dark gray) scenarios. Each box-plot represents monthly variability derived from all 20 years for the specific period. For future simulation that include all combinations of GCM models and emission scenarios. Units are in cubic meter (10^6 cu.m) and cubic meters per second (cms). The Catskill subsystem currently has no regulated releases

(Fig. 7d) subsystems and releases in Delaware (Fig. 7e) subsystem appear to follow inflow patterns, with future increases predicted for the winter-spring period. Releases in the Delaware subsystem are driven by rules that include habitat protection and flood mitigation. There are currently no regulated releases from the Catskill subsystem.

While differences in storage among the two projected future climate time periods are minimal, changes in spill and release appear more pronounced for the end of the century. It is important to note that, although the total volume of simulated future releases and spills during late fall and winter increase somewhat, the volumes of spill and release never reach the highest levels encountered in the baseline period during April.

6.2 Drought conditions occurrence

Results from most future simulations show a decrease in average number of days under watch, warning and emergency drought conditions in both the Catskill and Delaware subsystems (Fig. 8). Changes in inflow patterns, including an increase in total flow and the lower streamflow percentiles, contribute to these results. However, when comparing the results from individual projected simulations in Fig. 8 it becomes apparent that the results show large variability. Of all model simulations used in this study NCAR_A1B-4665 appears to be the only one projecting an increase in number of days under emergency for the Delaware subsystem. In terms of number of days under warning and watch drought conditions most scenarios indicate a decrease for both subsystems but again, with high variability in the size of the reduction.

6.3 Reservoir system performance

6.3.1 Demand ratio α, standardized net inflow, coefficient of variation and storage ratio

Results of standardized net inflow (m) (Fig. 9) indicate an increase under future climate simulations. All m values are above 1 (on average >1.65) indicating a continuing within-year behavior of the system. The interquantile range appears to be slightly higher for the 2055s period and a few scenario simulations in the box-plot for the 2090s show m values that are lower than the baseline scenario. As a consequence of the delta-change method, the coefficient of variation for baseline and future simulations are similar.

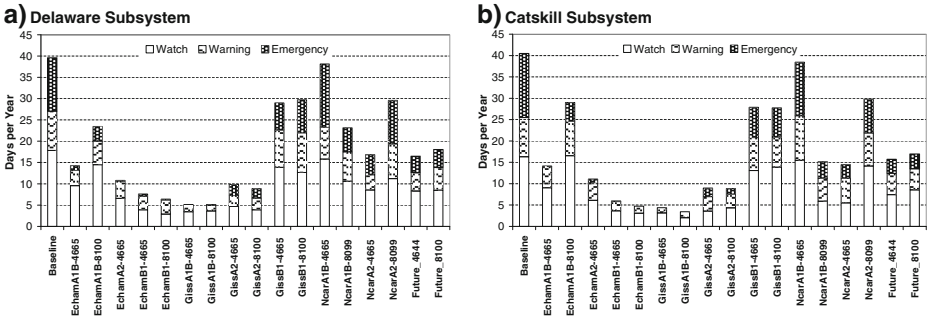

Fig. 8 Average number of days per year when the Delaware and Catskill subsystems are under emergency, warning, and watch drought conditions. The x-axis represents the different climate simulation scenarios. On each graph the bars to the left represent the baseline scenarios, the two bars on the right represent an average over all future 2055s and 2090s simulations, respectively

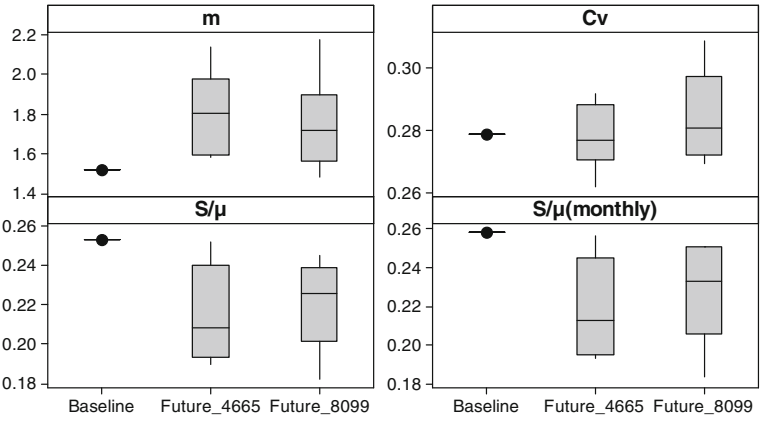

Fig. 9 Box-plots indicating standardized net flow (m), coefficient of variation of annual flow (C_v) and storage ratio using annual (S/μ) and monthly flow data ($S/\mu_{(monthly)}$). Box-plots for the simulated future 2055s and 2090s were developed using average values by each of the climate change scenario simulations for the WOH system. Baseline values are shown with dots

The coefficient of variation of annual inflow (C_v) remains below 0.3 for most future simulations except for a few in the 2090s, while the storage ratio shows a decrease under future simulated climate. These results are consistent with findings by Vogel et al. (1999) who found that systems showing pronounced within-year behavior are associated with $C_v<1$ and $C_v \leq m \leq (1/C_v)$. Also, Vogel et al. (1999) showed how for systems with C_v less than 0.3, the storage ratio based on annual flow differs from the storage ratio based on monthly inflows. Our results are consistent with those from Vogel et al. (1999) indicating slightly higher storage ratios when using monthly flows rather than annual flows; a sign of the impact of seasonality associated with monthly flows. Project changes in the coefficient of variation and storage ratios are within the range found by Vogel et al. (1999) for this region, while standardized net flow values are slightly higher, probably due to the fact that their estimations of yield and mean annual inflow were made at a larger regional scale.

6.3.2 System resilience, reliability and vulnerability

The impact of increased inflows is also reflected in Fig. 10 where future simulations indicate a more resilient reservoir system or a higher probability for the system to recover from a failure after one has occurred. Here again there is variability between calculations based on different future climate scenarios with a few simulations in both time slices showing a resilience lower than under baseline conditions.

Annual reliability of reservoirs across the United States is generally between 0.97 and 0.985 (Vogel et al. 1999), with annual reliability being the steady-state probability that a reservoir will deliver the required yield for a particular year without failure. Our baseline simulation (Fig. 10) suggests that WOH reservoirs are in the upper limit of this range and that future changes in climate will result in no substantial difference in annual reliability. The variability among the different model scenario simulations is less than 0.0015. A high positive correlation between resilience and reliability for the NYC reservoir system is not surprising; Vogel et al. (1999) arrived at similar results for reservoir systems in the eastern United States.

As under the present conditions projected D for future climate simulations indicate that the NYC reservoir system will continue showing high resilience and low vulnerability ($D \approx 0.1$). As

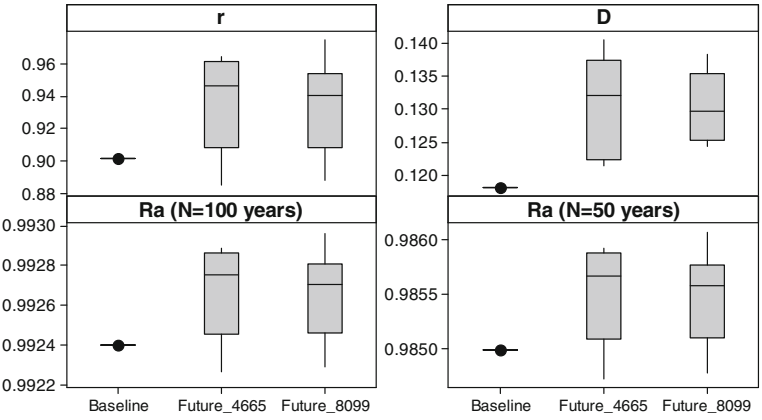

Fig. 10 Box-plots representative for system resilience (r), annual reliability (Ra), and reservoir vulnerability (D) for the WOH system. (N) represents the non-failure planning period for (Ra) calculation. The box-plots represent the simulated models average values for the future 2055s and 2090s

D is an indicator of average number of consecutive years a reservoir system fails to deliver an expected yield a unity vulnerability (D=1) can be interpreted as a failure state that will last one year on average (Vogel et al. 1999). This is important because based on our results any eventual failure in the NYC reservoir system will last for far less than a year. Our D, r, and R_a values are within the range found in previous studies for this region (e.g., Lane et al. 1999; Vogel et al. 1999).

7 Summary and conclusions

This study focuses on the potential impacts of climate change on NYC water supply with regards to reservoir operations and water supply system performance. An ensemble of three GCMs, three emission scenarios and two future time periods were used to simulate a present baseline and 16 different future climate change projections for the west of Hudson (WOH) region of the NYCWSS, which contributes more than 90 % of all water needed to meet NYC water demands. Air temperature and precipitation derived from these scenarios were used as inputs to the GWLF watershed model to simulate inflows required to run OASIS and simulate reservoir operations.

Results from this study comparing baseline inflow estimations with simulations for two future time slices representing the 2055s and 2090s suggest that the trend of increasing streamflow identified in historical records from Catskill basins (Burns et al. 2007) will continue so that on average annual streamflow will increase by approximately 97 mm in the next fifty year period. No statistically significant difference was detected in the annual streamflow between the future 2055s and 2090s.

On a seasonal basis monthly inflows will rise for almost all months with the greatest changes during winter and early spring due to a combined effect of more rainfall and snowmelt associated with higher temperatures (Matonse et al. 2011). Increases in winter inflows are more pronounced during the 2090s compared to 2055s. During summer projected changes in streamflow are relatively small suggesting that increased evapotranspiration (ET) rates associated with higher summer temperatures largely counteracts increased precipitation at this time. This result is not surprising; in the past Burns et al. (2007) and

Blake et al. (2000) suggested that higher ET rates will impact inflows in a warmer climate. Future summer flows remained basically unchanged as both ET and precipitation increased; effectively canceling the individual effects of each component. It should be noted that the uncertainty of future precipitation is much greater than that of future temperature. If the future precipitation estimates are over-predictions, then summer low flows could decrease more dramatically and annual inflow into the reservoir system will be less than expected.

To better gauge the impact of climate change on reservoir system operation, indicators such as reservoir inflow, storage, release, spill, and drought level were examined. Other indicators, such as the coefficient of variation of inflow, standardized net inflow, reservoir system resilience, reliability and vulnerability which have been used in the literature to measure and compare reservoir system performance were also examined.

Based on our results the combined effects of earlier snowmelt, higher rainfall and higher ET rates projected to occur during the two simulated future time slices will lead to:

1. Reservoirs filling earlier with inflows more evenly distributed during winter and early spring and a reduction in the historically observed April runoff peak. Under these conditions releases and spills will become higher during late fall and winter and less during April.
2. A decrease in the average number of days the Catskill and Delaware reservoirs will be under drought emergency, warning and watch conditions.
3. An increase in average standardized net inflow m ($m>1$). Average coefficients of variation C_v for future simulations that are similar to baseline and less than 0.3, and decreased average storage ratios ($D<1$), but with storage ratios based on monthly flows being slightly higher than storage ratios based on annual flows, indicating the effect of seasonality present in monthly flows. Our results support a previous regional analysis that characterizes reservoirs systems for the eastern United States region by $C_v<1$ and $C_v \leq m \leq (1/C_v)$ and are consistent with a reservoir system dominated by within-year variability; also found in previous studies to be characteristic for the eastern United States region.

Historical meteorology and model simulated baseline and future meteorology and streamflow were used in this study of the effects of climate change on NYC water supply. For this study only historical water demands and operational rules were available and these were considered stationary during future simulations. Maintaining current rules and demands helps evaluate the system effectiveness in responding to changes in climate alone (Matonse et al. 2011). However, population and other socio economic changes in the future may alter the current level of water demand (IPCC 2001). In addition historical data analysis indicates a positive correlation between water demands and high temperatures suggesting a potential direct impact of climate change on demands. These factors and any changes in regulatory flow requirements and water quality standards may have an impact on system operations and need to be accounted for in future studies. Also, the variability of inflows associated with future climate simulations are not directly obtained from the GCMs variability, but reflect the variability of the historic climate, a limitation of the delta change method. As water supply systems are sensitive to the frequency and magnitude of extreme hydrological events the use of model ensembles including other (dynamical and/or statistical) downscaling methods can potentially provide additional information that is important for the impact assessment and adaptation processes (Stainforth et al. 2007).

In conclusion, according to the climate models and scenarios applied in this study the NYC reservoir system will most likely continue to show high resilience, high annual reliability and relatively low vulnerability. As in previous studies reliability and resilience show a positive correlation. These conclusions will continue to be evaluated as updated climate model scenarios and future demand projections become available.

Acknowledgements The authors are grateful to New York City Department of Environmental Protection (NYC DEP) who provided funding for the research that led to this manuscript. This paper does not necessarily reflect the official views of NYC DEP, and no endorsement should be inferred; to Grantley W Pike for the valuable review; and to David Lounsbury and Donald Kent of the NYC DEP water quality modeling group for their inputs. Also, the authors want to thank the Columbia University Center for Climate Systems Research and the NASA Goddard Institute for Space Studies for providing the NCAR, GISS and ECHAM GCM data.

References

Anandhi A, Frei A, Pierson DC, Schneiderman EM, Zion MS, Lounsbury D, Matonse A (2011) Examination of change factor methodologies for climate change impact assessment. Water Resour Res 47:W03501. doi:10.1029/2010WR009104

Bates B, Kundzewicz C, Wu W, Palutikof P (eds) (2008) Climate change and water. Technical Paper of the Intergovernmental Panel on Climate Change. Geneva, Switzerland, IPCC Secretariat, p 210

Beven KJ, Kirkby MJ (1979) A physically-based, variable contributing area model of basin hydrology. Hydrolog Sci Bull 24:43–69

Black AR, Rowan JS, Duck RW, Bragg OM, Clelland BE (2005) DHRAM: a method for classifying river flow regime alterations for the EC water framework directive. Aquatic Conservation 15:427–446

Blake R, Khanbilvardi R, Rosenzweig C (2000) Climate change impacts on the New York City's water supply system. J Am Water Resour Assoc 36:279–292

Brekke LD, Maurer EP, Anderson JD, Dettinger MD, Townsley ES, Harrison A, Pruitt T (2009) Assessing reservoir operations risk under climate change. Water Resour Res 45:W04411. doi:10.1029/2008WR006941

Burns DA, Klaus J, McHale MR (2007) Recent climate trends and implications for water resources in the Catskill Mountain region, New York, USA. J Hydrol 336:155–170. doi:10.1016/j.jhydrol.2006.12.019

Burrough PA (1987) Principles of geographical information systems for land resources assessment. Clarendon, Oxford, 186

Chang LC, Chang FJ (2001) Intelligent control of modeling of real-time reservoir operation. Hydrol Process 15:1621–1634. doi:10.1002/hyp.226

Cole TT, Wells SA (2002) CE-QUAL-W2: a two-dimensional, laterally averaged, hydrodynamic and water quality model, version 3.1. Instruction Report EL-2002-1., U.S. Army Engineering and Research Development Center, Vicksburg, MS

Frei A, Armstrong RL, Clark MP, Serreze MC (2002) Catskill mountain water resources vulnerability, hydroclimatology, and climate-change sensitivity. Ann Assoc Am Geogr 92(2):203–224

Gao Y, Vogel RM, Kroll CN, Poff NL, Olden JD (2009) Development of representative indicators of hydrologic alteration. J Hydrol 374:136–147. doi:10.1016/j.jhydrol.2009.06.009

Gleckler PJ, Taylor KE, Doutriaux C (2008) Performance metrics for climate models. Water Resour Res 113: D06104. doi:10.1029/2007JD008972

Gleick PH (1986) Methods for evaluating the regional hydrologic effects of global climate changes. J Hydrol 88:97–116

Haith DA, Shoemaker LL (1987) Generalized watershed loading functions for stream flow nutrients. Water Resour Bull 23(3):471–478

Harberg RJ (1997) Planning and managing reliable urban water systems. American Water Works Association, Denver

Hardison CH (1972) Potential United States water-supply development. J Irrig Drain Div ASCE 98(3):479–492

Hay LE, Wilby RL, Leavesley GH (2000) A comparison of delta change and downscaled GCM scenarios for three mountainous basins in the United States. J Am Water Resour Assoc 36(2)

Hashimoto T, Stedinger JR, Loucks DP (1982) Reliability, resiliency, and vulnerability criteria for water resources system performance evaluation. Water Resour Res 18:14–20

HydroLogics Inc (2007) User manual for OASIS with OCL, Columbia, MD

Hunt A, Watkiss P (2011) Climate change impacts and adaptation in cities: a review of the literature. Clim Chang 104:13–49. doi:10.1007/s10584-010-9975-6

IPCC (2001) Climate Change 2001: the scientific basis. In: Houghton JT, Ding Y, Griggs DJ, Noguer M, van der Linden PJ, Dai X, Marskell K, Johnson CA (eds) Contribution of working group I to the third assessment report of the intergovernmental panel on climate change. Cambridge University Press, p 881

Joint Editorial Board Representing APHA, ASCE, AWWA, and WPCF (1969) Glossary: Water and Wastewater Control Engineering

Lane ME, Kirshen PH, Vogel RM (1999) Indicators of impacts of global climate change on U.S. water resources. J Water Resour Plan Manag, ASCE 125(4):194–204

Lof GOG, Hardison CH (1966) Storage requirements for water in the United States. Water Resour Res 2 (3):323–354

Mays LW, Tung Y-K (1992) Hydrosystems engineering and management. McGraw-Hill Inc, New York

Mayer RA (1993) Safe yield study of the New York City reservoir system. Progress report: Catskill/Delaware filtration. Strategic Services Division, NYC DEP

Milly PCD, Dunne KA, Vecchia AV (2005) Global pattern of trends in streamflow and water availability in a changing climate. Nature 438:347–350. doi:10.1038/nature04312

Matonse AH, Pierson DC, Frei A, Zion MS, Schneiderman EM, Anandhi A, Mukundan R, Pradhanang SM (2011) Effects of changes in snow pattern and the timing of runoff on NYC water supply system. Hydrol Process 25:3278–3288. doi:10.1002/hyp.8121

Neitsch SL, Arnold JG, Kiniry JR, Srinivasan R, Williams JR (2005) Soil and water assessment tool: theoretical documentation, version 2005. Agricultural Research Service, Temple, 476

New York City Department of Environmental Protection (NYCDEP) (2011) 2011 Watershed protection program summary and assessment. March 2011. http://www.nyc.gov/html/dep/pdf/reports/fad51_wmp_2011_fad_assessment_report_03-11.pdf. Accessed 27 April 2012

New York City Department of Environmental Protection (NYCDEP) (2008) Climate change program: assessment and action plan. May 2008. Report 1. A Report based on the ongoing work of the DEP climate change task force. http://www.nyc.gov/html/dep/pdf/climate/climate_complete.pdf. Accessed 27 April 2012

Perrens SJ, Howell DT (1972) Effects of serially correlated inflows on reservoir behavior. Water Resour Res 8:642–647

Priestley CHB, Taylor RJ (1972) On the assessment of surface heat flux and evaporation using large-scale parameters. Mon Weather Rev 100:81–92

Richter BD, Baumgartner JV, Powell J, Braun DP (1996) A method for assessing hydrologic alteration within ecosystems. Conserv Biol 10:1163–1174

Rogers PR (1999) Environmental indicators, *Journal of Water Resources Planning and Management*. ASCE 125(2):74–75

Rosenzweig C, Solecki WD (2001) Climate change and a global city: learning from New York. Environment 43(3):8–18

Schneiderman EM, Steenhuis TS, Thongs DJ, Easton ZM, Zion MS, Neal AL, Mendoza GF, Walter MT (2007) Incorporating variable source area hydrology into the curve number based Generalized Watershed Loading Function model. Hydrol Process 21:3420–3430

Schneiderman EM, Pierson DC, Lounsbury DG, Zion MS (2002) Modeling the Hydrochemistry of the Cannonsville Watershed with Generalized Watershed Loading Functions (GWLF). J Am Water Resour Assoc 38(5):1323–1347

Seager R et al (2007) Model projections of an imminent transition to a more arid climate in southwestern North America. Science 316:1181–1184. doi:10.1126/Science.1139601

Stainforth DA, Downing TE, Washington R, Lopez A, New M (2007) Issues in the interpretation of climate model ensembles to inform decisions. Phil Trans R Soc 365:2163–2177. doi:10.1098/rsta.2007.2073

Vicuna S, Dracup JA (2007) The evolution of climate change impact studies on hydrology and water resources in California. Clim Chang 82:327–350. doi:10.1007/s10584-006-9207-2

Vogel RM (1985) The variability of reservoir storage estimates, Ph.D. thesis, Cornell University, Ithaca, NY

Vogel RM (1987) Reliability indices for water supply systems, ASCE. J Water Resour Plan Manag Division 113(4):563–579

Vogel RM, Fennessey NM, Bolognese RA (1995) Storage-reliability-resilience-yield relations for Northeastern United States, ASCE. J Water Resour Plan Manag Division 121(5):365–374

Vogel RM, Sieber J, Archfield SA, Smith MP, Apse CD, Huber-Lee A (2007) Relations among storage, yield and instream flow. Water Resour Res 43. doi:10.1029/2006WR005226

Vogel RM, Lane M, Ravindiran RS, Kirshen P (1999) Storage reservoir in the United States, Journal of Water Resources Planning and Management. ASCE 125(5):245–254

Vogel RM, Bolognese RA (1995) Storage-reliability-resilience-yield relations for over-year water supply systems. Water Resour Res, 31(3):645–654

Vogel RM, Stedinger JR (1987) Generalized storage reliability yield relationships. J Hydrol 89:303–327

Walter MT, Mehta VK, Marrone AM, Boll J, Gerard-Merchant P, Steenhuis TS, Walter MF (2003) A simple estimation of the prevalence of Hortonian flow in New York City's watersheds. ASCE J Hydrolog Eng 8 (4):214–218

Yin X, Yang Z, Yang W, Zhao Y, Chen H (2010) Optimized reservoir operation to balance human and riverine ecosystem needs: model development, and a case study for the Tanghe reservoir, Tang river basin, China. Hydrol Process 24:461–471. doi:10.1002/hyp.7498

Zion MS, Pradhanang SM, Pierson DC, Anandhi A, Lounsbury DG, Matonse AH, Schneiderman EM (2011) Investigation and modeling os winter streamflow timing and magnitude under changing climate conditions for the Catskill Mountain region, New York, USA. Hydrol Process 25:3289–3301. doi:10.1002/hyp.8174

Geomorphology xxx (2012) xxx–xxx

Contents lists available at SciVerse ScienceDirect

Geomorphology

journal homepage: www.elsevier.com/locate/geomorph

Suspended sediment source areas and future climate impact on soil erosion and sediment yield in a New York City water supply watershed, USA

Rajith Mukundan [a,*], Soni M. Pradhanang [a], Elliot M. Schneiderman [b], Donald C. Pierson [b], Aavudai Anandhi [c], Mark S. Zion [b], Adão H. Matonse [a], David G. Lounsbury [b], Tammo S. Steenhuis [d]

[a] Institute for Sustainable Cities, City University of New York New York City, NY, USA
[b] New York City Department of Environmental Protection, Kingston, NY, USA
[c] Department of Agronomy, Kansas State University, Manhattan, KS, USA
[d] Department of Biological and Environmental Engineering, Cornell University, Ithaca, NY, USA

ARTICLE INFO

Article history:
Received 2 June 2011
Received in revised form 2 February 2012
Accepted 22 June 2012
Available online xxxx

Keywords:
Suspended sediment
Climate change
SWAT-WB
Saturation excess
New York City water supply

ABSTRACT

High suspended sediment loads and the resulting turbidity can impact the use of surface waters for water supply and other designated uses. Changes in fluvial sediment loads influence material fluxes, aquatic geochemistry, water quality, channel morphology, and aquatic habitats. Therefore, quantifying spatial and temporal patterns in sediment loads is important both for understanding and predicting soil erosion and sediment transport processes as well as watershed-scale management of sediment and associated pollutants. A case study from the 891 km^2 Cannonsville watershed, one of the major watersheds in the New York City water supply system is presented. The objective of this study was to apply Soil and Water Assessment Tool-Water Balance (SWAT-WB), a physically based semi-distributed model to identify suspended sediment generating source areas under current conditions and to simulate potential climate change impacts on soil erosion and suspended sediment yield in the study watershed for a set of future climate scenarios representative of the period 2081–2100. Future scenarios developed using nine global climate model (GCM) simulations indicate a sharp increase in the annual rates of soil erosion although a similar result in sediment yield at the watershed outlet was not evident. Future climate related changes in soil erosion and sediment yield appeared more significant in the winter due to a shift in the timing of snowmelt and also due to a decrease in the proportion of precipitation received as snow. Although an increase in future summer precipitation was predicted, soil erosion and sediment yield appeared to decrease owing to an increase in soil moisture deficit and a decrease in water yield due to increased evapotranspiration.

1. Introduction

Many recent studies have focused on the potential effects of climate change on water resources including water quality, hydrology, water demand, and socio-economic changes (Aber et al., 1995; Christensen et al., 2004; Parry et al., 2004; Bates et al., 2008). However, little research has been undertaken on the potential impact of climate change on sediment loads of streams and rivers (IPCC, 2007). High sediment loads and the resulting turbidity can impact the sustained use of rivers for water supply and other designated uses. Changes in fluvial sediment loads influence material fluxes, aquatic geochemistry, water quality, channel morphology, and aquatic habitats. Therefore, quantifying spatial and temporal patterns in sediment loads under present and future conditions will be valuable in both understanding and predicting sediment transport processes as well as watershed-scale management of sediment for maintaining high water quality.

Although it is impossible to predict the exact climate of the future, past climate trends combined with improved knowledge of global climatology, atmospheric processes and socio-economic changes have been used to develop future climate scenarios. The climate change scenarios recognized by the Intergovernmental Panel for Climate Change (IPCC) are widely used for modeling purposes. A limited number of studies have reported on the potential impact of climate change on soil erosion (Nearing, 2001; Yang et al., 2003; Nearing et al., 2004; O'Neal et al., 2005; Zhang and Nearing, 2005; Zhang, 2007; Nunes et al., 2009; Maeda et al., 2010; Nunes et al., 2011). While there is a general consensus that increasing rainfall intensity will increase watershed sediment loads (Kostaschuk et al., 2002; Bouraoui et al., 2004) through hillslope erosion (due to high rainfall erosivity) and channel erosion (due to high stream velocity), the regional impacts of future climate on erosion and sediment transport need further attention. Watershed sediment transport in response to changes in precipitation depends on the dominant sediment

* Corresponding author.
E-mail address: Rajith.Mukundan@hunter.cuny.edu (R. Mukundan).

0169-555X/$ – see front matter © 2012 Elsevier B.V. All rights reserved.
doi:10.1016/j.geomorph.2012.06.021

generation process. Soil erosion is closely linked to watershed sediment transport as it is a dominant process in watersheds where hillslope erosion is the primary source of sediment. The rate and magnitude of sediment transport are dependent on flow velocity in the channel, erodibility of the channel material as well as sediment delivery from upstream. A decrease in sediment supply combined with increased peak stream discharges can create imbalance between sediment supply and sediment transport capacity leading to channel instability (Rakovan and Renwick, 2011). Nunes and Nearing (2011) discuss the impact of climate change on erosion using multiple case studies. Knowledge gaps identified in their analysis include fewer studies at the watershed scale, uncertainty in climate change impact estimates, and links and feedbacks between erosion and land use/land cover.

Asselman et al. (2003) used UK Hadley Centre's high-resolution atmospheric general circulation model (UKHI) climate change scenario, in combination with land use changes to evaluate changes in sediment yield in the Rhine basin of the Dutch–German border. Although erosion rates were predicted to increase by 12% they found no significant effect on sediment yield at the basin outlet due to insufficient sediment delivery. Lawler et al. (2003) conducted a study in three catchments in Iceland and concluded that in response to climate change there was a decline in sediment yield in all catchments predominantly in the spring and in autumn. This decline in sediment yield was related to river flow reductions driven by significant cooling in spring and decreases in heavy daily precipitation events in autumn. Zhu et al. (2008) performed a climate change sensitivity analysis on measured sediment flux during the period 1960–1990 in a tributary of the Upper Yangtze River in China. They concluded that a combination of rainfall and temperature changes resulted in changes in the sediment flux of the river. Higher sediment flux is expected to appear under wetter and warmer climate, when higher transport capacity is accompanied by a higher erosion rate. Thodsen et al. (2008) used the HIRHAM regional climate model to study the influence of climate change on suspended sediment transport in Danish Rivers. Model simulations incorporating projected changes in land use/land cover scenarios for the period 2071–2100 suggested an increase in suspended sediment transport in the winter months as a result of the increase in river discharge caused by increase in precipitation, and decreases during summer and early autumn months. Li et al. (2011) based on Soil and Water Assessment Tool (SWAT) model simulations in the lower Pearl River Basin, South China concluded that a 3 °C increase in average annual air temperature would increase the sediment load by about 13%. Warming climate can reduce vegetation and slow plant growth resulting in increased soil loss.

Models such as ANSWERS (Beasley et al., 1980); AGNPS (Young et al., 1987); WEPP (Nearing et al., 1989); EuroSEM (Morgan et al., 1990); HSPF (Bicknell et al., 1993); RUSLE (Renard et al., 1997); and SWAT (Neitsch et al., 2005) are often used in combination with geographic information systems (GIS) in sediment transport studies. In the SWAT model sediment is generated by hillslope and stream channel erosion and routed through the stream which is explicitly characterized as a network of connected reaches. The model has been shown to simulate sediment loads at the outlet of the watershed fairly well for a variety of catchment types (Santhi et al., 2001; Cerucci and Conrad, 2003; Cotter et al., 2003; Arabi et al., 2006; Jha et al., 2007; Tolson and Shoemaker, 2007). Previous studies using SWAT model to simulate the impact of climate change on sediment transport have shown both increases as well as decreases in sediment transport rates depending on characteristics of the location of study (Hanratty and Stefan, 1998; Varanou et al., 2002; Nearing et al., 2005).

In this paper we apply the Soil and Water Assessment Tool-Water Balance (SWAT-WB) model (White et al., 2011) to simulate sediment transport and quantify the potential impact of climate change on soil erosion and sediment yield in the Cannonsville watershed. The watershed drains into the Cannonsville Reservoir, one of the drinking water supply reservoirs for New York City (NYC), USA. This catchment was chosen because a SWAT-2005 model application has been developed that simulates hydrology at the catchment outlet fairly well (Pradhanang et al., 2011), and a long term record of stream water suspended sediment data was available. An examination of historical data and results of model simulations for this region have both shown an increasing trend in precipitation and streamflow over the past fifty years (Burns et al., 2007; Zion et al., 2011). Our goal in this study is to examine how changes in precipitation and streamflow translate into changes in soil erosion and sediment transport in the Cannonsville catchment using a physically based semi-distributed model. Our study assumes stationary land use/cover for the study region. The specific objectives of this study are:

(1) To identify the major sediment source areas within the Cannonsville watershed
(2) To quantify the impact of future climate on long-term soil erosion and sediment yields at the watershed outlet

2. Study site

The Cannonsville watershed, one of the major NYC water supply watersheds is located in the Catskill region of New York State (Fig. 1). The watershed drains an area of 891 km^2 above the USGS gauging station at Walton and is predominantly forested (67%). Other major land uses include agriculture (23%) and brush lands (6%). Agricultural land use in this watershed consists primarily of dairy farms and includes hay lands, pastures, and Corn row crops. The elevation of the watershed ranges from about 300 m near the watershed outlet to about 1100 m near the headwaters. The mean annual rainfall in this region is about 1100 mm (Pradhanang et al., 2011) and the mean annual streamflow is about 601 mm of which 64% can be considered baseflow and 36% as surface runoff based on standard hydrograph separation techniques (Arnold and Allen, 1999). Saturation excess is the dominant runoff generation mechanism in NYC water supply watersheds (Walter et al., 2000; Schneiderman et al., 2007; Easton et al., 2008).

Previous studies in this watershed concluded that majority (95–100%) of the stream sediment in this watershed originated from surface erosion of hillslopes and agricultural fields (Nagle et al., 2007; Tolson and Shoemaker, 2007). The Catskill region has shown changes in regional water balance in recent years (Burns et al., 2007). An increasing trend in mean air temperature during 1952–2005 has caused an increase in potential evapotranspiration (PET) as a result of which one would expect decreases in watershed water yield. However, an increasing trend in precipitation has nullified this effect and actually resulted in a net increase in water yield. Such changes in water balance are expected to have a direct impact on soil erosion and sediment yield.

3. Methods

3.1. SWAT-water balance model

The SWAT-WB (White et al., 2011) is a modified version of the SWAT-2005 model (Neitsch et al., 2005). The original SWAT model uses Hydrologic Response Units (HRU) to define the scale at which precipitation is partitioned into runoff and infiltration. Each HRU is defined based on land use and soil, while the runoff curve number method is used to partition precipitation into runoff and infiltration. In SWAT-WB each HRU is defined based on land use and topographic location which define surface soil moisture pattern, and the partitioning of precipitation into runoff and infiltration is calculated based on daily soil water balance for the HRU. The modified version (SWAT-WB) has been found to perform well in simulating streamflow and sediment

Please cite this article as: Mukundan, R., et al., Suspended sediment source areas and future climate impact on soil erosion and sediment yield in a New York City water supply water..., Geomorphology (2012), doi:10.1016/j.geomorph.2012.06.021

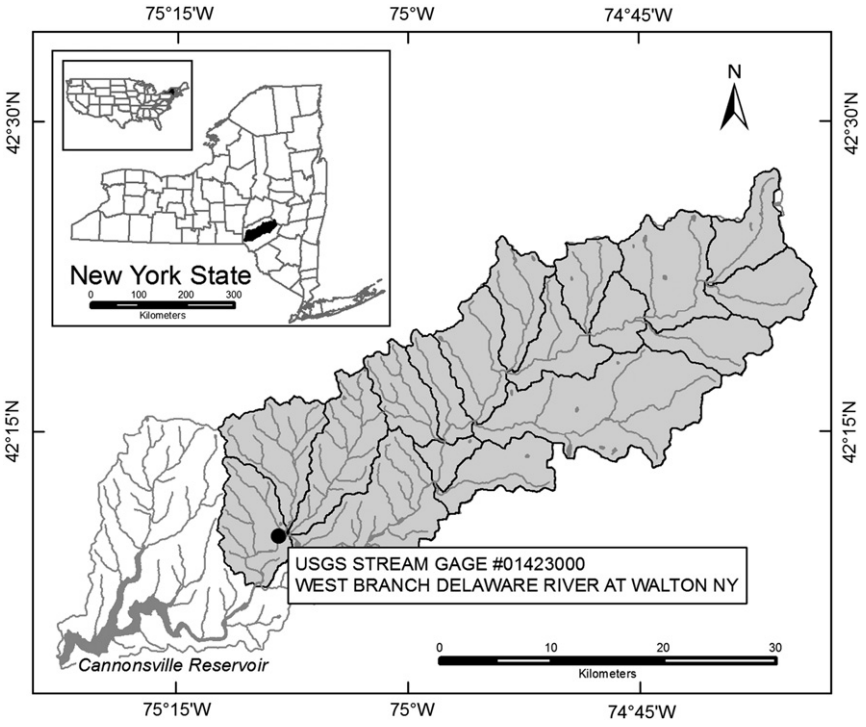

Fig. 1. Location of Cannonsville watershed in New York State, USA.

yield in watersheds, where saturation excess runoff process is dominant runoff generation mechanism (Easton et al., 2010; White et al., 2011).

SWAT's existing soil moisture routines are used by SWAT-WB to determine the degree of saturation-deficit for each soil profile for each day of simulation. This saturation-deficit (in mm of water) is termed the available soil storage, τ_i and is a function of soil properties and watershed soil moisture status (White et al., 2011).

$$\tau_i = (EDC_i \varepsilon_i - \Theta i, t) d_i \quad (1)$$

where EDC_i is the effective depth of a given soil profile i, (unitless), ε_i is the soil porosity (unitless) of a given soil i, $\theta_{i,t}$ is the volumetric soil moisture of a given soil i, for each day, t, (unitless), and d_i is the soil profile depth of soil i (mm). The porosity, ε_i, is a constant value for each soil type, whereas $\theta_{i,t}$ varies in time and is determined by SWAT's soil moisture routines. The effective depth coefficient, EDC_i, a parameter ranging from zero to one, is used to partition soil moisture in excess of ε_i into infiltrating (groundwater) and runoff fractions (including rapid shallow interflow). EDC_i is spatially varied based on a saturation probability defined by a soil wetness index (Easton et al., 2008). This spatially adjusted available storage is then used to partition rainfall into infiltration and runoff, q_i (mm):

$$q_i = \begin{cases} 0 & if\ P < \tau_i \\ P - \tau_i & if\ P > \tau_i \end{cases}. \quad (2)$$

The available soil storage, τ_i, is calculated each day and once precipitation starts, a portion of the rain, equal in volume to τ_i, will infiltrate the soil. If the rainfall event is larger in volume than τ_i, the soil profile will saturate and surface runoff will occur. If the rainfall is less than τ_i, the soil will remain unsaturated and there will be no surface runoff and SWAT's internal soil moisture routing will calculate the flux.

3.2. HRU definition

HRUs are defined in SWAT as unique combinations of soil type, land cover, and slope class. However, in basins dominated by variable source area (VSA) hydrology this HRU definition has been insufficient for describing the spatial variations in runoff generating areas (Schneiderman et al., 2007; Easton et al., 2008). Runoff-generating areas are likely to occur in portions of the landscape with shallow, low conductive soils, large upslope contributing areas, mild slopes, or any combination of the three. To include upslope contributing area while defining HRUs, a topographic index was integrated with existing soil data to create a soil topographic index (*STI*), which is then used in the SWAT-WB HRU definition process (Easton et al., 2008). The *STI* is defined as (Beven, 1986):

$$\lambda = \ln\left(\frac{\alpha}{T_0 \tan\beta}\right). \quad (3)$$

The upslope contributing area, α, and the slope, $\tan(\beta)$, were both obtained from a DEM, while the lateral transmissivity (L^2T^{-1}) of the soil profile, T_0, when water table intersects the soil surface (Beven, 1986) is a function of the soil layer depth, D_0, and soil layer saturated hydraulic conductivity, K_{s0}, ($T_0 = K_{s0} \cdot D_0$), and are obtained from the SSURGO database (USDA-NRCS, 2000). The *STI* values relate to a location's likelihood of saturation, and therefore the likelihood to contribute surface runoff. Values of STI are used to create wetness classes and are used to represent a location's likelihood to saturate. This wetness class map is then substituted for the soil map in the HRU definition process. While the wetness classes were used in HRU delineation instead of a soil type, SWAT still requires specific soil properties. Thus, in SWAT-WB soil properties obtained from the SSURGO database were areally weighted and averaged for each wetness class.

3.3. Sediment transport in SWAT

The SWAT model simulates soil erosion and sediment export from hillslopes as well as in-stream channel processes (Neitsch et al.,

Please cite this article as: Mukundan, R., et al., Suspended sediment source areas and future climate impact on soil erosion and sediment yield in a New York City water supply water..., Geomorphology (2012), doi:10.1016/j.geomorph.2012.06.021

2005). Erosion caused by rainfall and runoff is calculated with the Modified Universal Soil Loss Equation (MUSLE) as:

$$sed = 11.8 \cdot \left(Q_{surf} \cdot q_{peak} \cdot area_{hru}\right)^{0.56} \cdot K \cdot C \cdot P \cdot LS \cdot CFRG \quad (4)$$

where *sed* is the sediment exported from a HRU to the channel on a given day (metric tons), Q_{surf} is the surface runoff volume (mm ha^{-1}), q_{peak} is the peak surface runoff rate (m^3 s^{-1}), $area_{hru}$ is the area of the HRU (ha), *K* is the USLE soil erodibility factor (T h MJ^{-1} mm^{-1}), *C* is the USLE cover and management factor (dimensionless), *P* is the USLE support practice factor (dimensionless), *LS* is the USLE topographic factor (dimensionless) and *CFRG* is the coarse fragment factor (dimensionless). The use of a runoff term in the equation avoids the use of a sediment delivery ratio.

Watershed models widely used in sediment source assessment use various forms of the Universal Soil Loss Equation (USLE) for soil loss and sediment yield estimates. The use of these algorithms, developed from field scale evaluations, in watershed scale models has been cautioned by several researchers (Wischmeier and Smith, 1978; Risse et al., 1993; Kinnell, 2004). This is because of the need for validating these empirically derived equations at the watershed scale. However, a physically based hydrology model such as the SWAT-WB when coupled with the MUSLE may reduce uncertainty in soil erosion and sediment yield prediction when compared to the original USLE based calculations of long term sediment yields that are highly sensitive to topographic factors. Given the episodic nature of erosion and its variability in space, it is important to develop deterministic models capable of predicting the location and extent of sediment source areas. In many cases the eroded sediment originates from a small fraction of the landscape. Such information is required by watershed managers for effective implementation of sediment control practices.

Deposition and degradation are the dominant channel processes influencing sediment yield at the basin outlet. These channel processes are determined by the upland sediment loads and also the transport capacity of the channel network. The transport capacity of the channel segment is determined by the simplified Bagnold's equation (Bagnold, 1977):

$$T_{ch} = a \cdot v^b \quad (5)$$

where T_{ch} (T m^{-3}) is the transport capacity of a channel segment, *a* and *b* are user defined coefficients, and *v* (m s^{-1}) is the peak channel velocity. In addition parameters related to channel cover and channel erodibility that have a linear influence on channel contribution of sediment can be adjusted in SWAT.

3.4. SWAT model set up and calibration

A digital elevation model (DEM) of the basin obtained from the New York City Department of Environmental Protection (NYCDEP) with 10 m horizontal and 0.1 m vertical resolutions was used to delineate the watershed into 19 sub-basins. The sub-basins were further divided into 554 HRUs based on the method outlined above. A land use map derived by supervised classification of 2001 Landsat Enhanced Thematic Mapper Plus (ETM+) imagery was obtained from NYCDEP. Samples for each land use class were selected from the classification. An equalized random sampling approach was used, with 150 samples specified for each class. The sample pixels were compared with the original Landsat image and the reference 2001 orthoimagery to visually interpret their true land cover type. The generated land use map had an overall classification accuracy of 57%. SWAT simulations require daily meteorological data including precipitation, temperature, wind, humidity and solar radiation. Daily precipitation data were obtained from cooperator stations recognized by the National Climate Data Center (NCDC) and through the Northeast Regional Climate Center (NRCC). Minimum and maximum daily air temperatures for model input were derived from four stations in the NRCC data set. All other regional weather parameters were simulated by the model using a weather generator encoded within SWAT.

The model was calibrated for streamflow and sediment yield at the watershed outlet for the 1991–1995 water years and validated for the 2000–2002 water years. Measured daily streamflow data was obtained from the USGS gauging station (#01423000) located at the watershed outlet near Walton. Daily time series of total suspended solids (TSS) collected near the Walton stream monitoring station using a sampling protocol that allowed accurate estimation of both baseflow and storm event sediment loads (Longabucco and Rafferty, 1998). The calibrated streamflow and sediment models were used to simulate a historical baseline scenario (1965–2008) of sediment yield using measured meteorological forcing.

3.5. Future climate scenarios

The potential effect of climate change on soil erosion and sediment yield was evaluated using scenarios derived from a suite of nine Global Climate Model (GCMs) that represent a wide range of future climate conditions, during the 2081–2100 future period (Table 1). In this study, the A1B scenario from the Special Report on Emission Scenarios (SRES) in the IPCC Fourth Assessment Report (AR4) was used. This greenhouse gas emission scenario represents rapid economic growth with balanced emphasis on all energy sources. Data from the selected GCMs for the region surrounding the NYC water supply were extracted and interpolated to a common 2.5° grid using bilinear interpolation for baseline scenario (20C3M) for the period 1960–2000 and a future A1B emission scenario for the period 2081–2100. Climate scenarios were downscaled using change factor methodology described in Anandhi et al., 2011. Monthly change factors (CFs) were calculated from the difference between baseline (20C3M) and future GCM simulations. These monthly CFs were used to adjust the same local meteorological data used for the baseline simulation to represent the future climate conditions associated with a given GCM. Use of long term observed data in generating future climate scenarios ensured that the scenarios were representative of the observed climate patterns in the region. The nine GCMs selected in this study have high skill in simulating the observed precipitation or temperatures (Anandhi et al., in review).

4. Results and discussion

4.1. Model calibration for hydrology and sediment

Both hydrology and sediment calibration used the goal of maximizing the coefficient of determination (R^2), maximizing Nash–Sutcliffe efficiency (NSE) (Nash and Sutcliffe, 1970), and minimizing percent bias. In addition, hydrology calibration was optimized so that the runoff and baseflow components of streamflow were simulated reasonably well compared to values derived from measured

Table 1
GCMs used in this study.

GCM ID[a]	Acronym used
CGCM3.1 (T47)	CC4
CGCM3.1 (T63)	CC6
CSIRO-MK 3.0	CS0
GISS-AOM	GAO
GFDL-CM 2.0	GF0
IPSL-CM4	IPS
MIROC3.2 (HIRES)	MIH
ECHAM5/MPI-OM	MPI
MRI-CGCM 2.3.2	MRI

[a] As provided by Lawrence Livermore National Laboratory's Program for Coupled Model Diagnosis and Intercomparison (PCMDI): http://www-pcmdi.llnl.gov/ipcc/model_documentation/ipcc_model_documentation.php.

Please cite this article as: Mukundan, R., et al., Suspended sediment source areas and future climate impact on soil erosion and sediment yield in a New York City water supply water..., Geomorphology (2012), doi:10.1016/j.geomorph.2012.06.021

Table 2
Monthly model calibration statistics.

	Calibration 1991–1995	Validation 2000–2002
Streamflow		
R^2	0.76	0.71
NSE	0.76	0.68
% bias	+2.0%	−2.0%
Sediment		
R^2	0.62	0.70
NSE	0.61	0.70
% bias	−6.0%	−4.0%

data using standard baseflow separation techniques (Arnold and Allen, 1999).

In addition to the *EDC*, twenty parameters were calibrated which controls the hydrologic processes involved in streamflow generation including partitioning precipitation into infiltration and runoff, baseflow recession, and the rates of snowpack development and depletion. The calibrated model simulated streamflow reasonably well as evident from the monthly statistics for the calibration and validation period (Table 2). Predicted and measured monthly streamflow for the calibration and validation periods are presented in Fig. 2. Although the model was able to capture most peaks, it underestimated the measured streamflow during certain periods.

Soil erodibility, cover and management factors in the MUSLE equation, parameters related to sediment transport capacity (Eq. (5)), the channel cover parameter and the channel erodibility parameter were calibrated to optimize sediment yield results. The simulated contribution of stream channel processes to total sediment yield was only about 6% which is consistent with previous studies in the same watershed (Nagle et al., 2007; Tolson and Shoemaker, 2007). The calibrated model simulated suspended sediment load at the watershed outlet with acceptable model performance (Table 2). Predicted and measured sediment loads for the calibration and validation periods are presented in Fig. 3. Any discrepancy observed between measured and simulated sediment loads were either related to error in stream flow prediction or due to some inherent deficiency in the model especially during winter months.

4.2. Spatial variability in runoff and sediment source areas

Figs. 4 and 5 show the spatial variability in runoff and sediment generating areas across the watershed. The sub-basins generating maximum runoff were also found to generate maximum sediment through surface/hillslope erosion. The model computes the sediment generated from each HRU and thereby enabling identification of the actual location of erosion within a sub-basin. The high sediment generating areas would be a combination of relatively high surface runoff and erosive land cover (e.g.; agricultural field). The HRU maps of the highest sediment generating sub-basins were visualized to locate the sites of maximum erosion.

The long-term (1965–2008) average annual sediment export (transport of eroded sediment from hillslopes to stream channels) from each combination of wetness index class and major land use is presented in Table 3. The highest sediment export rate was from a combination of wetness class one and agricultural land use and progressively decreasing to higher wetness classes. In our classification scheme wetness class one has the highest probability of getting saturated followed by two, three and so on. As expected forests and brush lands produced less erosion than agricultural land use in addition to following the same pattern for the wetness index classes. Erosion from the last four wetness classes was minimal. A combination of wetness class seven with agricultural or brush land did not exist anywhere in the watershed.

4.3. Model evaluation of future climate impact on soil erosion and sediment yield

Simulated future changes in watershed water balance that may influence soil erosion and sediment yield are presented in Fig. 6. Our analysis of future climate impact on sediment included changes in basin wide average annual sediment export from HRUs as well as changes in average annual sediment yield (sediment exiting the watershed outlet) (Table 4). Future sediment export from HRUs based on the wide range of future climate conditions represented by the GCMs showed wide variability. The ensemble mean showed a net increase in future sediment export by 49% from average historical values indicating the possibility of higher rates of soil erosion in the future (2081–2100). The results are biased by one of the GCMs (MIH) without which the increase in future sediment export dropped to 27%. Such increasing rates of sediment export due to soil erosion are comparable with Nearing et al. (2004) who predicted similar rates of increase to occur in multiple sites across the U.S., based on two GCMs. In comparison, the sediment yield from the watershed outlet showed only a 3.9% increase in the ensemble mean compared to average historical values. Sediment export from HRUs is influenced by precipitation and surface runoff while sediment yield at the watershed outlet is primarily influenced by stream flow. Decreased sediment yield at the watershed outlet relative to the soil erosion rates predicted by the model under simulated future climate could be due to the inability of the model to account for sediment deposited in the channel. The model works on daily time steps and sediment deposited in the channel is not considered in subsequent time steps.

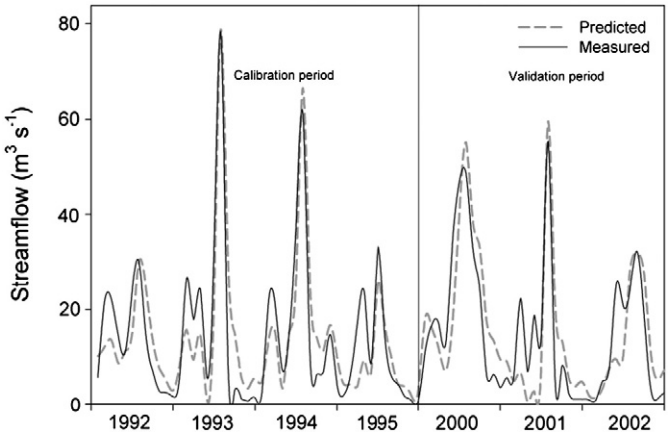

Fig. 2. Predicted vs measured streamflow.

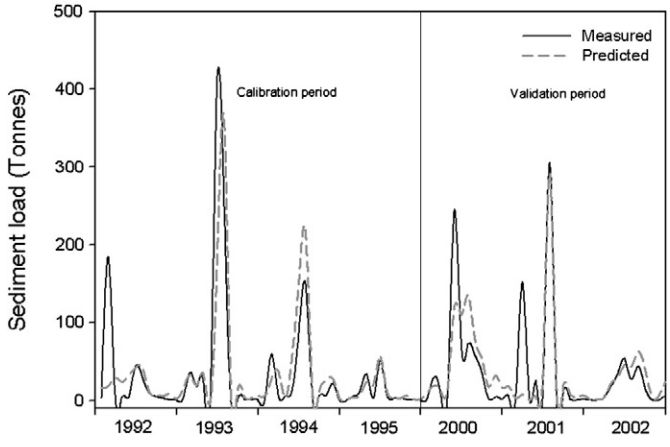

Fig. 3. Predicted vs measured sediment load.

Please cite this article as: Mukundan, R., et al., Suspended sediment source areas and future climate impact on soil erosion and sediment yield in a New York City water supply water..., Geomorphology (2012), doi:10.1016/j.geomorph.2012.06.021

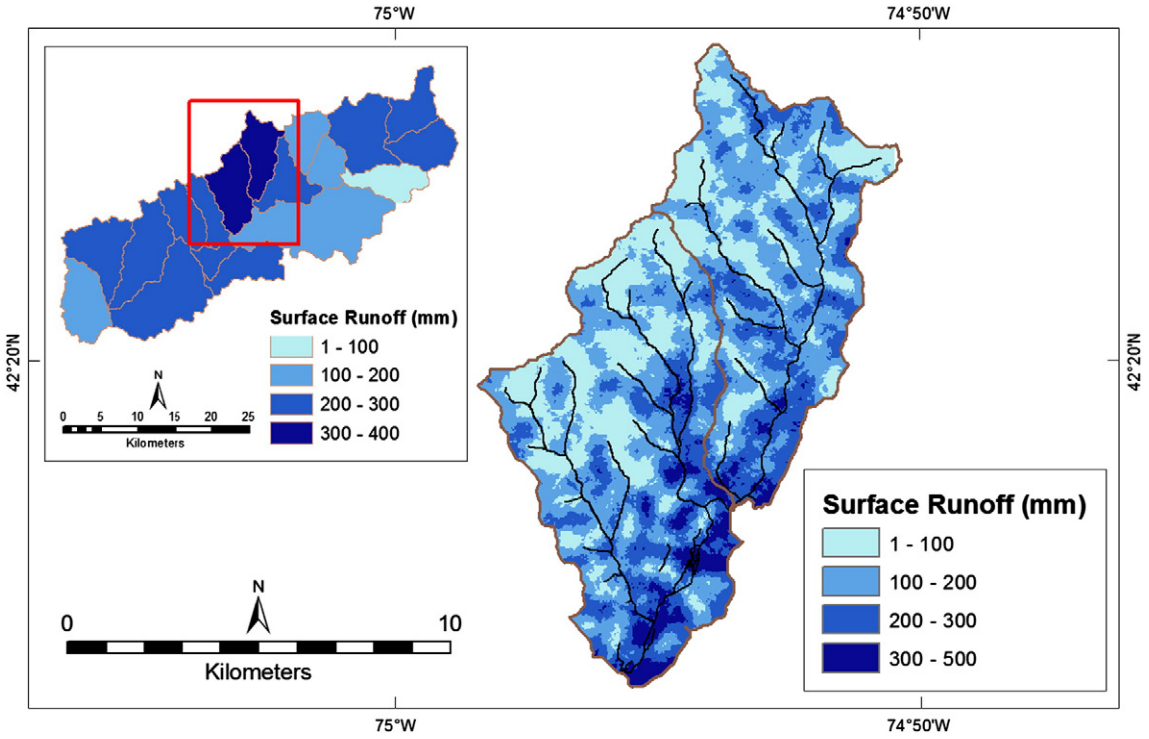

Fig. 4. Map showing spatial distribution of runoff generating areas at sub-basin level (inset) and HRUs from the dominant runoff generating region. Values are average annual estimates.

Analysis of seasonal changes in basin wide sediment export from HRUs showed increases in the winter and in the early spring and decreases in the summer and in early fall season (Fig. 7). The increase was much higher in magnitude compared to the decrease. This increase is due to the combined effect of increase in precipitation (Fig. 6a) and also the decrease in precipitation falling as snow. The existence of this phenomenon has already been detected in northeast U.S. catchments over the past fifty years (Hodgkins et al., 2003; Burns et al., 2007). The SWAT model predicts less erosion in the presence of snow. A comparison of the cumulative annual proportion of precipitation received as snow predicted by the model between the historical and future scenarios showed a sharp decline by 46% in the ensemble

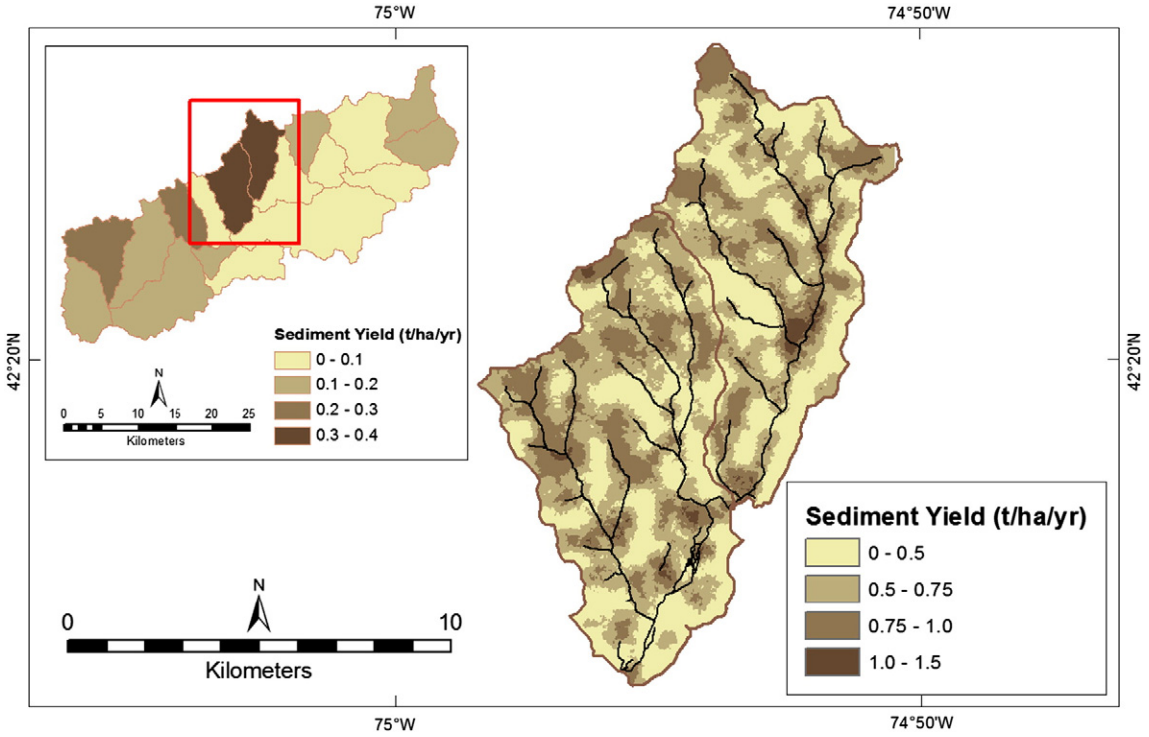

Fig. 5. Map showing spatial variability in average annual sediment export from sub-basins (inset) and HRUs expressed as sediment yield to stream channels from the dominant sediment generating region.

Please cite this article as: Mukundan, R., et al., Suspended sediment source areas and future climate impact on soil erosion and sediment yield in a New York City water supply water..., Geomorphology (2012), doi:10.1016/j.geomorph.2012.06.021

Table 3
Average annual sediment export from land use wetness index combinations. Wetness class one indicates the wettest conditions and class ten indicates the driest conditions.

Land use	Sediment export from wetness index class (t ha^{-1} year^{-1})									
	One	Two	Three	Four	Five	Six	Seven	Eight	Nine	Ten
Forest	0.04	0.05	0.02	0.02	0.02	0.02	0.00	0.00	0.00	0.00
Agriculture	1.03	0.74	0.43	0.37	0.34	0.46	–	0.00	0.00	0.00
Brush land	0.10	0.09	0.04	0.04	0.02	0.02	–	0.00	0.00	0.00

Table 4
Table showing average annual sediment export from HRUs and watershed outlet.

Scenario	Sediment export (t ha^{-1} year^{-1}) (2081–2100)	% change from baseline	Sediment yield (t ha^{-1} year^{-1}) (2081–2100)	% change from baseline
CC4	0.143	+6	0.085	−2.1
CC6	0.158	+18	0.106	+22.6
CS0	0.076	−43	0.069	−20.7
GAO	0.079	−41	0.085	−2.6
GFO	0.214	+59	0.091	+5.4
IPS	0.311	+131	0.081	−6.5
MIH	0.445	+231	0.100	+15.3
MPI	0.287	+113	0.109	+25.5
MRI	0.093	−31	0.085	−1.6
Average	0.194	+49	0.090	+3.9

mean with a range of 38–62% decline predicted by the nine GCMs (Fig. 6c).

Decrease in erosion during summer and early fall period may be related to the changes in antecedent soil water content during rainfall events under future conditions. Although an increase in summer rainfall was predicted by the GCMs (Fig. 6b) increases in evapotranspiration (Fig. 6d) can cause reduction in soil water content which may result in increased saturation deficit (τ_i in Eq. (1)). This means that more rainfall is required to bring the soil to saturation and generate equal amount of runoff as the current conditions. The importance of antecedent soil moisture on erosion from saturation excess dominated landscapes has been previously reported (Fitzjohn et al., 1998). Analysis of one of the HRUs under agricultural land use and soil wetness class one revealed an increase in crop biomass productivity during the months July and August by 19% and 29% respectively suggesting an earlier onset of growing season due to warmer climate. Such phenological changes are expected to affect the amount and timing of residue going back to the soil and thus soil erosion. These results are consistent with the finding of Nunes et al. (2011) using a SWAT model application for climate change assessment of soil erosion in two Mediterranean watersheds.

Future trends in sediment yield at the watershed outlet followed the soil erosion trends for most months except for March and April

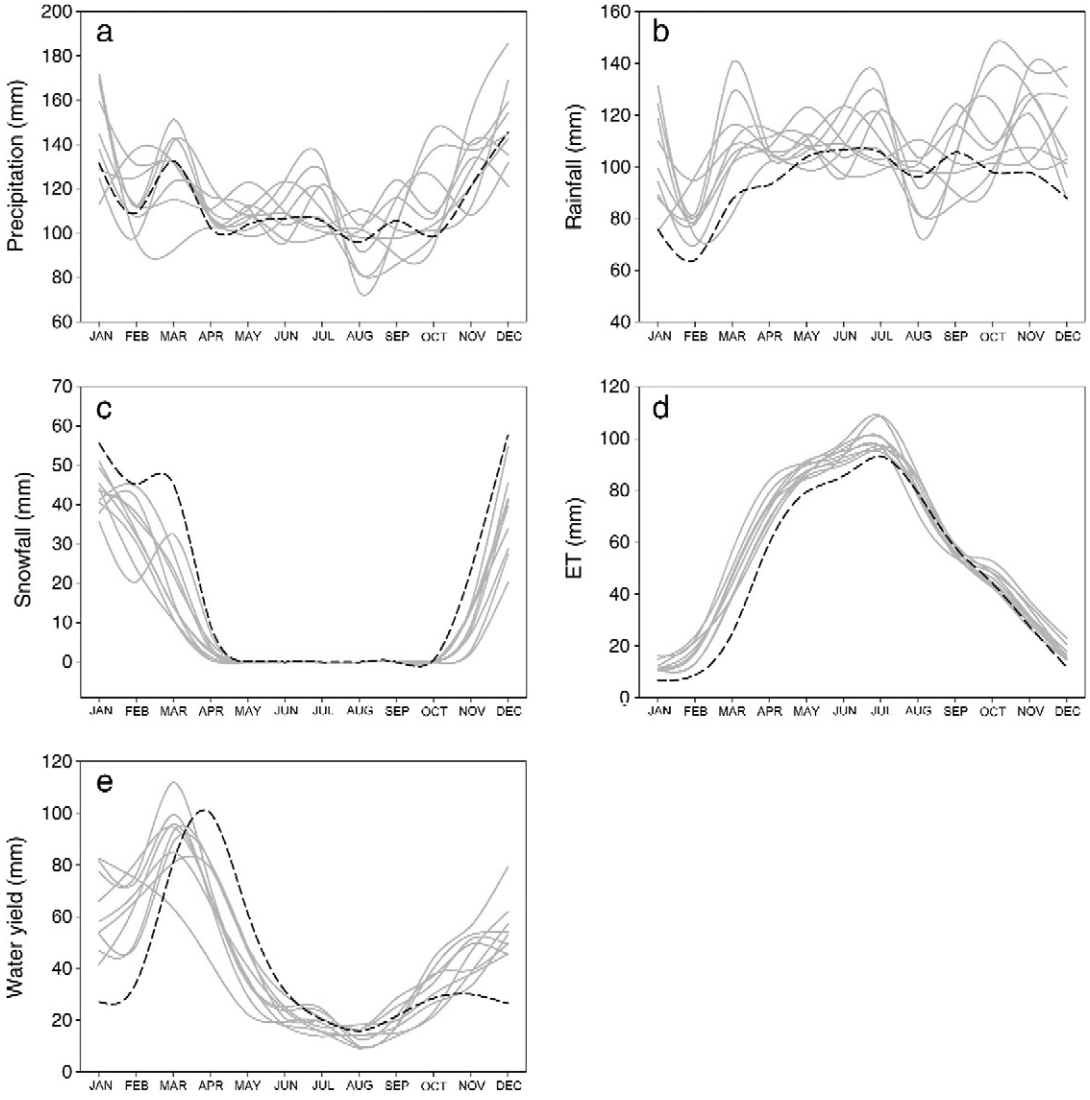

Fig. 6. Monthly simulated components of the watershed water balance, Historical (1965–2008) in dark dotted lines versus Future (2081–2100) in gray lines.

Please cite this article as: Mukundan, R., et al., Suspended sediment source areas and future climate impact on soil erosion and sediment yield in a New York City water supply water..., Geomorphology (2012), doi:10.1016/j.geomorph.2012.06.021

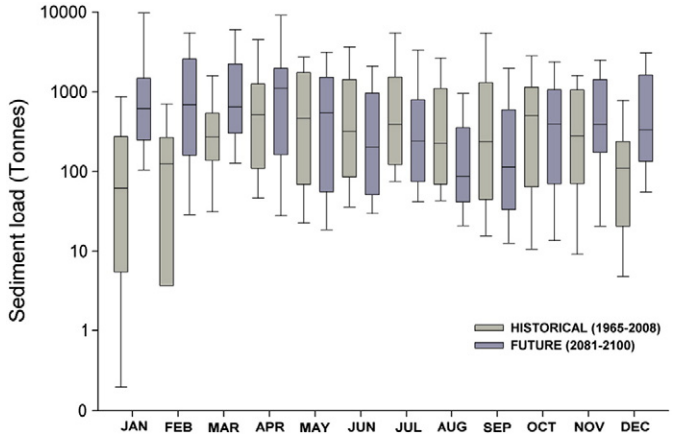

Fig. 7. Boxplot of average monthly basin wide sediment export from HRUs expressed as sediment load to stream channels. Boxes represent the 25th and the 75th percentile and whiskers represent the 10th and 90th percentile values.

(Fig. 8). These two months transported the maximum amount of sediment through the watershed outlet as seen in the historical scenario. Decline in sediment yield in these months during future periods explains to a certain extent the relatively small increase in average annual sediment yield at the watershed outlet (Table 3). The decrease in sediment yield is related to the decrease in basin wide streamflow during this period. This decrease in sediment yield predicted is consistent with the findings of Burns et al. (2007) who found a sharp decreasing trend in streamflow during April in the same region although a similar trend in precipitation was not evident. The decrease in April streamflow results from early snowmelt being observed in the region (Burns et al., 2007; Matonse et al., 2011; Zion et al., 2011). Although summer precipitation appeared to increase in the future scenarios, a decrease in water yield resulting from an increase in saturation deficit (described above) predicted by the model (Fig. 6d and e) coupled with a decrease in erosion resulted in less sediment yield at the watershed outlet in the summer.

4.4. What to expect in the future?

The results of this study indicate that under future climate scenarios the rate of surface erosion from fields and hillslopes may increase; however there may not be a significant increase in sediment yield at the watershed outlet. This conclusion depends on a number of assumptions within the modeling scheme. Our modeling indicated that majority of the stream sediment yield originated from surface erosion of hillslopes. This finding was consistent with the conclusions drawn by Nagle et al. (2007) and Tolson and Shoemaker (2007) for the same watershed. Other factors related to the fraction of sediment yield at the outlet due to stream channel sources versus landscape erosion sources may alter the quantitative results presented here.

We analyzed long term records of measured flow and stream water sediment concentration (1991–2008). For low flow (days when base flow was >90% of total flow) the median base flow TSS value was consistently below 3.0 mg L^{-1} between 1991 and 2005; however, in recent years (2007–2008) a relatively high median TSS value of 4.4 mg L^{-1} has occurred (Fig. 9). This increase might be attributed to an extreme event that occurred in June 27 of 2006 that generated the highest streamflow in a record that goes back to the early 1950s. This event created major changes in the watershed landscape in the form of hillslope erosion and mass wasting of tributaries and subsequent deposition of sediment in the main stem of the watershed (Eskeli, *Personal communication*). The long-term memory in stream TSS during low flows could be the result of re-suspension and subsequent transport of sediment that was deposited in the channel bed during this extreme event. A non-parametric Wilcoxon test on low flow TSS values two years prior ($n=355$) and two years ($n=327$) after 2006 indicated that this change in low flow TSS was statistically significant ($P<0.0001$). These results are indicative of the existence of a geomorphic threshold capable of altering the sediment transport rates and sediment supply in the fluvial system. Such thresholds could be either intrinsic (related to the geomorphic structure of the system such as critical shear stress of the stream banks) or extrinsic (related to changes in climate forcing) (Phillips, 2006).

Although the SWAT-WB model is capable of providing a general sensitivity on the effect of future climate, it is not developed to capture the subtle changes in the rate of sediment transport resulting from events such as the one in 2006. Depending on the frequency of such extreme events, the major sediment source in the Cannonsville watershed might shift in the future with eroding stream channels becoming the primary source. Such geomorphic changes could lead to non-stationarity in sediment transport rates, which is not represented in the SWAT-WB model.

Another area for improvement deals with the implications of the methods of producing future climate scenarios. Our study examines the effect of changes in magnitude of precipitation and air temperature on sediment loads; however the climate scenarios do not change the frequency of storm events and its effect on sediment loads are not represented here. In order to assume a one-to-one correlation between environmental forcing and sediment response, it is required that the sedimentary system remains in equilibrium or respond to the forcing in a linear fashion (Swenson, 2005). However, in reality potential changes in intensity and frequency of storm events as a

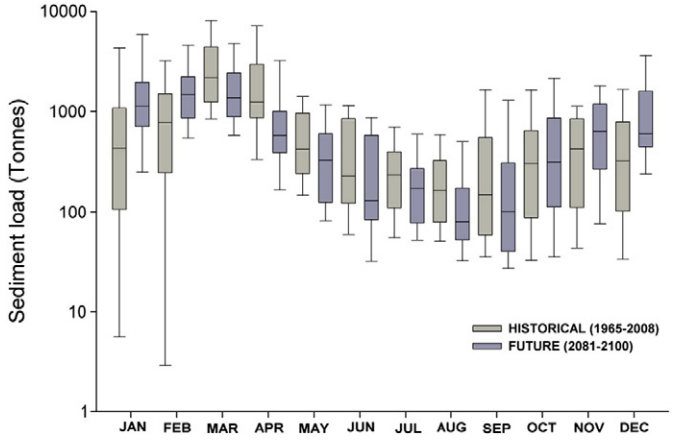

Fig. 8. Boxplot of average monthly sediment yield from watershed outlet. Boxes represent the 25th and the 75th percentile and whiskers represent the 10th and 90th percentile values.

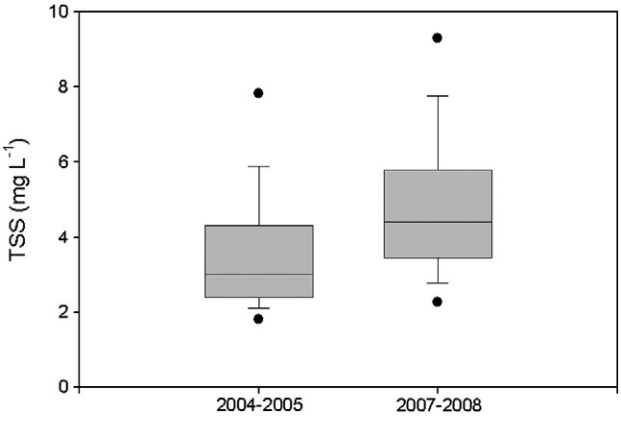

Fig. 9. Box plot showing shift in low flow suspended sediment concentration due to an extreme event in 2006.

result of global climate change may have varying impact on suspended sediment transport and the resulting turbidity. Increased precipitation following prolonged period of low flows are projected to exacerbate many forms of water pollution including sediment (Bates et al., 2008). However, one could argue that the impact of storm frequency on turbidity is influenced by several independent hydrological processes such as wetness/saturation of soils in watersheds with relatively high hillslope erosion or baseflow dilution and sediment supply in channel erosion dominated watersheds. Therefore, future changes in storm event frequency will make turbidity prediction difficult especially in channel erosion dominant watersheds.

5. Summary and conclusions

A physically based watershed model was used to identify the location of major sediment generating areas in a NYC water supply watershed. To evaluate the effect of future climate on soil erosion and sediment yield, the model output was compared using historical (1965–2008) and future (2081–2100) climate scenarios. The predictions presented here should be viewed as qualitative trends, rather than as absolute numerical predictions, given the uncertainty in future climate predictions, particularly since potential changes in extreme events are not completely captured by GCMs and downscaling method used in this study. Results indicate a sharp increase in the annual rates of soil erosion although a similar result in sediment yield at the watershed outlet was not evident. Analysis of seasonal changes in basin wide soil erosion and sediment export from HRUs showed an increase in the winter and in the early spring and a decrease in the summer and early fall seasons. Future simulated sediment yield at the watershed outlet followed the soil erosion results for most months except for March and April. Future climate related changes in soil erosion and sediment yield were more significant in the winter due to a shift in the timing of snowmelt and also due to a decrease in the proportion of precipitation received as snow. Although an increase in future summer precipitation was predicted, soil erosion and sediment yield appeared to decrease owing to an increase in soil moisture deficit and a decrease in water yield due to increased evapotranspiration.

Acknowledgment

We thank Dr. Allan Frei (Hunter College, City University of New York) for his support in this research project.

References

Aber, J.D., Ollinger, S.V., Federer, C.A., Kicklighter, D.W., Melillo, J.M., Lathrop Jr., R.G., Ellis, J.M., 1995. Predicting the effects of climate change on water yield and forest production in the Northeastern U.S. Climate Research 5, 207–222.

Anandhi, A., Frei, A., Pierson, D.C., Schneiderman, E.M., Zion, M.S., Lounsbury, D., Matonse, A.H., 2011. Examination of change factor methodologies for climate change impact assessment. Water Resources Research 47, W03501, http://dx.doi.org/10.1029/2010WR009104.

Arabi, M., Govindaraju, R.S., Hantush, M.M., Engel, B.A., 2006. Role of watershed subdivision on modeling the effectiveness of best management practices with SWAT. Journal of the American Water Resources Association 42, 513–528.

Arnold, J.G., Allen, P.M., 1999. Methods for estimating baseflow and groundwater recharge from streamflow. Journal of the American Water Resources Association 35, 411–424.

Asselman, N.E.M., Middelkoop, H., van Dijk, P.M., 2003. The impact of changes in climate and land use on soil erosion, transport and deposition of suspended sediment in the River Rhine. Hydrological Processes 17, 3225–3244.

Bagnold, R.A., 1977. Bedload transport in natural rivers. Water Resources Research 13, 303–312.

Bates, B.C., Kundzewicz, Z.W., Wu, S., Palutikof, J.P., 2008. Climate change and water. Technical Paper of the Intergovernmental Panel on Climate Change. Geneva, 210 pp.

Beasley, D.B., Huggins, L.F., Monke, E.J., 1980. ANSWERS: a model for watershed planning. Transactions of ASAE 23, 938–944.

Beven, K.J., 1986. Runoff production and flood frequency in catchments of order n: an alternative approach. In: Gupta, V.K., Rodriguez-Iturbe, I. (Eds.), Scale Problems in Hydrology. Reidel, Dordrecht, pp. 107–131.

Bicknell, B.R., Imhoff, J.C., Kittle Jr., J.L., Donigian Jr., A.S., Johanson, R.C., 1993. Hydrologic Simulation Program — FORTRAN (HSPF) User's Manual for Release 10. Report No. EPA/600/R-93/174. U.S. EPA Environmental Research Lab., Athens, GA.

Bouraoui, F., Grizzetti, B., Granlund, K., Rekolainen, S., Bidoglio, G., 2004. Impact of climate change on the water cycle and nutrient losses in a Finnish catchment. Climatic Change 66, 109–126.

Burns, D.A., Klaus, J., McHale, M.R., 2007. Recent climate trends and implications for water resources in the Catskill Mountain region, New York, USA. Journal of Hydrology 336, 155–170.

Cerucci, M., Conrad, J.M., 2003. The use of binary optimization and hydrologic models to form riparian buffers. Journal of the American Water Resources Association 39, 1167–1180.

Christensen, N.S., Wood, A.W., Lettenmaier, D.P., Palmer, R.N., 2004. Effects of climate change on the hydrology and water resources of the Colorado River Basin. Climatic Change 62, 337–363.

Cotter, A.S., Chaubey, I., Costello, T.A., Soerens, T.S., Nelson, M.A., 2003. Water quality model output uncertainty as affected by spatial resolution of input data. Journal of the American Water Resources Association 39, 977–986.

Easton, Z.M., Fuka, D.R., Walter, M.T., Cowan, D.M., Schneiderman, E.M., Steenhuis, T.S., 2008. Re-conceptualizing the Soil and Water Assessment Tool (SWAT) model to predict runoff from variable source areas. Journal of Hydrology 348, 279–291.

Easton, Z.M., Fuka, D.R., White, E.D., Collick, A.S., Biruk Asharge, B., McCartney, M., Awulachew, S.B., Ahmed, A.A., Steenhuis, T.S., 2010. A multi basin SWAT model analysis of runoff and sedimentation in the Blue Nile, Ethiopia. Hydrology and Earth System Sciences 7, 3837–3878.

Fitzjohn, C., Ternan, J.L., Williams, A.G., 1998. Soil moisture variability in a semi-arid gully catchment: implications for runoff and erosion control. Catena 32, 55–70.

Hanratty, M.P., Stefan, H.G., 1998. Simulating climate change effects in a Minnesota agricultural watershed. Journal of Environmental Quality 27, 1524–1532.

Hodgkins, G.A., Dudley, R.W., Huntington, T.G., 2003. Changes in the timing of high river flows in New England over the 20th Century. Journal of Hydrology 278, 244–252.

IPCC (Intergovernmental Panel on Climate Change), 2007. Climate change: impacts, adaptation and vulnerability. Contribution of Working Group II to the Fourth Assessment Report of IPCC. Cambridge, United Kingdom and New York, USA, 976 pp.

Jha, M., Gassman, P.W., Arnold, J.G., 2007. Water quality modeling for the Raccoon River Watershed using SWAT. Transactions of the ASABE 50, 479–493.

Kinnell, P.I.A., 2004. Letter to the editor on the mathematical integrity of some universal soil loss variants. Soil Science Society of America Journal 68, 336–337.

Kostaschuk, R., Terry, J., Raj, R., 2002. Suspended sediment transport during tropical-cyclone floods in Fiji. Hydrological Processes 17, 1149–1164.

Lawler, D.M., McGregor, G.R., Phillips, I.D., 2003. Influence of atmospheric circulation changes and regional climate variability on river flow and suspended sediment fluxes in southern Iceland. Hydrological Processes 17, 195–223.

Li, Y., Chen, B.M., Wang, Z.G., Peng, S.L., 2011. Effects of temperature change on water discharge, and sediment and nutrient loading in the lower Pearl River basin based on SWAT modelling. Hydrological Sciences Journal 56, 68–83.

Longabucco, P., Rafferty, M.R., 1998. Analysis of material loading to Cannonsville Reservoir: advantages of event-based sampling. Lake and Reservoir Management 14, 197–212.

Maeda, E.E., Pellikka, P.K.E., Siljander, M., Clark, B.J.F., 2010. Potential impacts of agricultural expansion and climate change on soil erosion in the Eastern Arc Mountains of Kenya. Geomorphology 123, 279–289.

Matonse, A.H., Pierson, D.C., Frei, A., Zion, M.S., Schneiderman, E.S., Anandhi, A., Mukundan, R., Pradhanang, S.M., 2011. Effects of changes in snow pattern and the timing of runoff on NYC water supply system. Hydrological Processes 25, 3278–3288.

Morgan, R.P.C., Quinton, J.N., Rickson, R.J., 1990. Structure of the soil erosion prediction model for the European community. Proceedings of International Symposium on Water Erosion, Sedimentation and Resource Conservation, 9–13 Oct 1990, Dehradun, India. Central Soil and Water Conservation Research and Training Institute, CSWCRTI, Dehradun, India, pp. 49–59.

Nagle, G.N., Fahey, T.J., Ritchie, J.C., Woodbury, P.B., 2007. Variations in sediment sources and yields in the Finger Lakes and Catskills Regions of New York. Hydrological Processes 21, 828–838.

Nash, J.E., Sutcliffe, J.V., 1970. River flow forecasting through conceptual models — part I: a discussion of principles. Journal of Hydrology 10, 282–290.

Nearing, M.A., 2001. Potential changes in rainfall erosivity in the United States with climate change during the 21st century. Journal of Soil and Water Conservation 56, 229–232.

Nearing, M.A., Foster, G.R., Lane, L.J., 1989. A process-based soil erosion model for USDA water erosion prediction project. Transactions of ASAE 32, 1587–1593.

Nearing, M.A., Pruski, F.F., O'Neal, M.R., 2004. Expected climate change impacts on soil erosion rates: a review. Journal of Soil and Water Conservation 59, 43–50.

Nearing, M.A., Jetten, V., Baffaut, C., Cerdan, O., Couturier, A., Hernandez, M., Le Bissonais, Y., Nichols, M.H., Nunes, J.P., Renschler, C.S., Souchère, V., Van Oost, K., 2005. Modelling response of soil erosion and runoff to changes in precipitation and cover. Catena 61, 131–154.

Neitsch, S.L., Arnold, J.G., Kiniry, J.R., Williams, J.R., 2005. Soil and water assessment tool: theoretical documentation — version 2005. Grassland, Soil and Water Research Laboratory, Agricultural Research Service. January 2005, 494 pp.

Nunes, J.P., Nearing, M.A., 2011. Modelling impacts of climatic change. In: Morgan, R.P.C., Nearing, M.A. (Eds.), Handbook of Erosion Modelling. Wiley-Blackwell, Oxford, pp. 289–312.

Nunes, J.P., Seixas, J., Keizer, J.J., Ferreira, A.J.D., 2009. Sensitivity of runoff and soil erosion to climate change in two Mediterranean watersheds. Part II: assessing impacts from changes in storm rainfall, soil moisture and vegetation cover. Hydrological Processes 23, 1212–1220.

Please cite this article as: Mukundan, R., et al., Suspended sediment source areas and future climate impact on soil erosion and sediment yield in a New York City water supply water..., Geomorphology (2012), doi:10.1016/j.geomorph.2012.06.021

Nunes, J.P., Seixas, J., Keizer, J.J., 2011. Modeling the response of within-storm runoff and erosion dynamics to climate change in two Mediterranean watersheds: a multi-model, multi-scale approach to scenario design and analysis. Catena, http://dx.doi.org/10.1016/j.catena.2011.04.001.

O'Neal, M.R., Nearing, M.A., Vining, R.C., Southworth, J., Pfeifer, R.A., 2005. Climate change impacts on soil erosion in Midwest United States with changes in crop management. Catena 61, 165–184.

Parry, M.L., Rosenzweig, C., Iglesias, A., Livermore, M., Fischer, G., 2004. Effects of climate change on global food production under SRES emissions and socioeconomic scenarios. Global Environmental Change 14, 53–67.

Phillips, J.D., 2006. Evolutionary geomorphology: thresholds and nonlinearity in landform response to environmental change. Hydrology and Earth System Sciences 10, 731–742.

Pradhanang, S.M., Anandhi, A., Mukundan, R., Zion, M.S., Pierson, D.C., Schneiderman, E.S., Matonse, A.H., Frei, A., 2011. Application of SWAT model to assess snowpack development and streamflow in the Cannonsville watershed, New York, USA. Hydrological Processes 25, 3268–3277.

Rakovan, M.T., Renwick, W.H., 2011. The role of sediment supply in channel instability and stream restoration. Journal of Soil and Water Conservation 60, 40–50.

Renard, K.G., Foster, G.R., Weesies, G.A., McCool, D.K., Yoder, D.C., 1997. Predicting soil erosion by water: a guide to conservation planning with the Revised Universal Soil Loss Equation (RUSLE). Agriculture Handbook N.703. U.S. Department of Agriculture Research Service, Washington, DC, USA. 348 pp.

Risse, L.M., Nearing, M.A., Nicks, A.D., Laflen, J.M., 1993. Error assessment in the universal soil loss equation. Soil Science Society of America Journal 57, 825–833.

Santhi, C., Arnold, J.G., Williams, J.R., Dugas, W.A., Hauck, L., 2001. Validation of the SWAT Model on a large river basin with point and nonpoint sources. Journal of the American Water Resources Association 37, 1169–1188.

Schneiderman, E.M., Steenhuis, T.S., Thongs, D.J., Easton, Z.M., Zion, M.S., Neal, A.L., Mendoza, G.F., Walter, M.T., 2007. Incorporating variable source area hydrology into a curve-number-based watershed model. Hydrological Processes 21, 3420–3430.

Swenson, J.B., 2005. Fluviodeltaic response to sea level perturbations: amplitude and timing of shoreline translation and coastal onlap. Journal of Geophysical Research 110, F03007, http://dx.doi.org/10.1029/2004JF000208.

Thodsen, H., Hasholt, B., Kjærsgaard, J.H., 2008. The influence of climate change on suspended sediment transport in Danish rivers. Hydrological Processes 22, 764–774.

Tolson, B.A., Shoemaker, C.A., 2007. Cannonsville Reservoir Watershed SWAT2000 model development, calibration and validation. Journal of Hydrology 337, 68–86.

USDA-NRCS, 2000. Soil Survey Geographic (SSURGO) Database for Delaware County, New York.

Varanou, E., Gkouvatsou, E., Baltas, E., Mimikou, M., 2002. Quantity and quality integrated catchment modeling under climate change with use of soil and water assessment tool model. Journal of Hydrologic Engineering 7, 228–244.

Walter, M.T., Walter, M.F., Brooks, E.S., Steenhuis, T.S., Boll, J., Weiler, K.R., 2000. Hydrologically sensitive areas: variable source area hydrology implications for water quality risk assessment. Journal of Soil and Water Conservation 3, 277–284.

White, E.D., Easton, Z.M., Fuka, D.R., Collick, A.S., Adgo, E., McCartney, M., Awulachew, S.B., Selassie, Y.G., Steenhuis, T.S., 2011. Development and application of a physically based landscape water balance in the SWAT model. Hydrological Processes 25, 915–925.

Wischmeier, W.H., Smith, D.D., 1978. Predicting rainfall erosion losses; a guide to conservation planning, U.S. Department of Agriculture, Agricultural Handbook No. 537. 58 pp.

Yang, D., Kanae, S., Oki, T., Koike, T., Musiake, K., 2003. Global potential soil erosion with reference to land use and climate changes. Hydrological Processes 17, 2913–2928.

Young, R.A., Onstad, C.A., Bosch, D.D., Anderson, W.P., 1987. AGNPS, agricultural nonpoint source pollution model: a watershed analytical tool. U.S. Department of Agriculture Conservation Research Report, 35.

Zhang, X.C., 2007. A comparison of explicit and implicit spatial downscaling of GCM output for soil erosion and crop production assessments. Climate Change 84, 337–363.

Zhang, X.C., Nearing, M.A., 2005. Impact of climate change on soil erosion, runoff, and wheat productivity in Central Oklahoma. Catena 61, 185–195.

Zhu, Y.M., Lu, X.X., Zhou, Y., 2008. Sediment flux sensitivity to climate change: a case study in the Longchuanjiang catchment of the upper Yangtze River, China. Global and Planetary Change 60, 429–442.

Zion, M.S., Pradhanang, S.M., Pierson, D.C., Anandhi, A., Lounsbury, D., Matonse, A.H., Schneiderman, E.S., 2011. Investigation and modelling of winter streamflow and timing and magnitude under changing climate conditions for the Catskill mountain region, New York, USA. Hydrological Processes 25, 3289–3301.

Please cite this article as: Mukundan, R., et al., Suspended sediment source areas and future climate impact on soil erosion and sediment yield in a New York City water supply water..., Geomorphology (2012), doi:10.1016/j.geomorph.2012.06.021